GENERATION OF EMIGRATING MEMORY B CELLS AND THEIR MIGRATORY BEHAVIOURS

by

CAMERON JOSEPH MADOC BURNETT

A thesis submitted to the University of Birmingham for the degree of
DOCTOR OF PHILOSOPHY

Institute of Immunology and Immunotherapy
College of Medical and Dental Sciences
University of Birmingham
February 2023

UNIVERSITY OF
BIRMINGHAM

University of Birmingham Research Archive

e-theses repository

This unpublished thesis/dissertation is copyright of the author and/or third parties. The intellectual property rights of the author or third parties in respect of this work are as defined by The Copyright Designs and Patents Act 1988 or as modified by any successor legislation.

Any use made of information contained in this thesis/dissertation must be in accordance with that legislation and must be properly acknowledged. Further distribution or reproduction in any format is prohibited without the permission of the copyright holder.

Abstract

The germinal centre (GC) reaction is a site of extensive B cell proliferation and somatic hypermutation of Ig variable region genes. Its outputs are plasma cells (PCs), selected from high affinity B cells, and memory B cells (mBCs), which are less stringently selected for affinity. Movements of lymphocytes within secondary lymphoid organs are dependent on an array of chemotactic cues. These play a role in lymphocyte entry, activation, and egress from the tissue.

A group of memory-like B cells migrating from GCs (BEMs) and entering the lymph node subcapsular sinus (SCS) were discovered in reactive lymph nodes (LNs). Some of these recycled between the SCS and back into the B cell follicles. S1PR1-blockade prevented migration of BEMs into the SCS, and deletion of ACKR4 prevented CCR7-ligand dependent recycling of BEMs back into the follicle. RNA-sequencing showed that BEMs shared some phenotypical characteristics with GC B cells but were a distinct subset of B cells. Cell surface markers were uncovered from RNA-sequencing to distinguish BEMs from GC B cells and naïve B cells at the peak of the GC response in the LN and spleen. ACKR4-mediated recycling of BEMs supported humoral responses to antigenic variants of chemical haptens as well as dengue virus envelope proteins.

Entry of circulating mBCs (BCMs) to distant lymphoid tissues was affected by CCR7 ligands. CCL21 was important for entry into non-reactive LNs and CCL19 may be directing entry into the spleen. ACKR4-deficient BCMs showed improved entry into distant lymphoid tissues, whereas CCR7-deficiency tended towards reduced entry.

Re-challenge experiments showed that mBCs were pre-disposed to a PC fate when re-exposed to antigen in an antigen-experienced LN. Conversely, BCMs in distant LNs that had no direct contact with antigen preferred GC B cell fates.

Acknowledgements

Thank you so much to my supervisor Dr. Kai-Michael Toellner for providing me with this opportunity, and all the support he has given me throughout my PhD. Thank you to Dr Graham Anderson, my co-supervisor. I would also like to thank past and present members of the Toellner lab: Dr Yang Zhang, Dr Juan-Carlos Yam-Puc and Dr Lingling Zhang for your infinite patience with me and helping to show me the ropes when I first joined the lab. I need to thank my fellow lab mates, past and present especially Rebecca Boston, Ashley Hudson, Fernanda Escobar Riquelme and Mike Price. You all helped to make my time in the lab a pleasant one and offered a great sounding board for ideas.

I would like to thank the members of the 4th Floor IBR for all your help, for offering me advice and helping to provide me with reagents. Thank you to the BMSU for all their help. Thank you to the UoBFC and the Microscopy Facilities for their training and advice. Anyone not mentioned please know that I am still grateful for all the help you have provided me.

I would like to thank my friends and family for all their advice and support. Particularly to my good friend Anthony, you helped to keep me calm and focused during the pandemic, I am very grateful for your support.

This PhD has been quite the experience, I have enjoyed the challenges and the opportunities.

Abbreviations

Abbreviation	Full name
ABC	adenosine trisphosphate-binding cassette
ACKR4	atypical chemokine receptor 4
AID	activation-induced cytidine deaminase
AKT	Ak strain transforming
AP	alkaline phosphatase
APRIL	A proliferation-inducing ligand
ASC	antibody-secreting cell
BACH2	BTB domain and CNC homolog 2
BAFF	B cell activating factor
BAFF-R	B cell activating factor receptor
BALT	bronchus-associated lymphoid tissue
BCL2	B cell lymphoma 2
BCL6	B cell lymphoma 6
BCM	circulating memory B cell
BCR	B cell receptor
BEM	emigrating memory B cell
BLIMP-1	B-lymphocyte-induced maturation protein 1
BM	bone marrow
BrdU	5-bromo-2-deoxyuridine
BSA	bovine serum albumin
BtK	Bruton's tyrosine kinase
CCL19	C-C motif chemokine ligand 19
CCL20	C-C motif chemokine ligand 20
CCL21	C-C motif chemokine ligand 21
CCL25	C-C motif chemokine ligand 25
CCR6	C-C motif chemokine receptor 6
CCR7	C-C motif chemokine receptor 7
Cg1	immunoglobulin gamma constant region 1
CGG	chicken gamma globulin
CLP	common lymphoid progenitor
CR1	complement receptor 1
CR2	complement receptor 2
Cre	Cre recombinase
CSR	class switch recombination
CXCL12	C-X-C motif chemokine ligand 12
CXCL13	C-X-C motif chemokine ligand 13
CXCR3	C-X-C motif chemokine receptor 3
CXCR4	C-X-C motif chemokine receptor 4
CXCR5	C-X-C motif chemokine receptor 5
DC	dendritic cell
DEG	differentially expressed gene
Denv-1	dengue virus serotype 1
Denv-4	dengue virus serotype 4
distLN	distant lymph node
DNP	2,4-dinitrophenyl hapten
drLN	draining lymph node
DZ	dark zone
E1	Dengue virus serotype 1 envelope protein
E2A	transcription factor 3
E4	Dengue virus serotype 4 envelope protein
EBF-1	early B cell factor 1
EBI2	Epstein-Barr virus-induced molecule 2
ECM	extracellular membrane
EDTA	ethylenediaminetetraacetic acid
EdU	5-ethynyl-2-deoxyuridine
EF	extrafollicular
ELISA	enzyme linked immunosorbent assay
ERT2	mutant estrogen ligand binding domain
eYFP	enhanced yellow fluorescent protein
FACS	fluorescence associated cell sorting
FDC	follicular dendritic cell
FDR	false discovery rate
GC	germinal centre

GFP	green fluorescent protein
GL7	lymphocyte antigen 77
GPCR	G-protein-coupled receptor
GRK	G-protein-coupled receptor kinase
GSEA	gene set enrichment analysis
HEV	high-endothelial venule
HSC	haematopoietic stem cell
i.p.	intraperitoneal
i.v.	intravenous
iDTR	inducible diphtheria receptor
IFN	interferon
IgH	heavy chain immunoglobulin
IL-2	interleukin 2
IL-2R	interleukin 2 receptor
KLH	keyhole limpet hemocyanin
KO	knockout
LEC	lymphatic endothelial cell
LEF1	lymphoid enhancer binding factor
LIF	leukaemia inhibitory factor
LN	lymph node
LZ	light zone
MAPK	mitogen-activated protein kinase
mBC	memory B cell
MEF2C	MADS box transcription enhancer factor 2
MHC	major histocompatibility complex
MRC	marginal reticular cell
mTmG	mTomato/mGFP
MZ	marginal zone
nBC	naïve B cell
NFkB	nuclear factor kappa B
NiP	4-hydroxy-3-iodo-5-nitrophenylacetyl
NP	4-hydroxy-3-nitrophenylacetyl hapten
PALS	periarteriolar lymphoid sheath
PB	plasmablast
PBS	phosphate buffered saline
PC	plasma cell
PCA	principle component analysis
PD-L2	programmed death ligand 2
PFA	paraformaldehyde
PI3K	phosphoinositide 3-kinase
QC	quality control
QM	quasi-monoclonal
RAG	recombination activation gene
Ras	Rat sarcoma virus GTPase
RFP	red fluorescent protein
S1P	sphingosine-1-phosphate
S1PR1	sphingosine-1-phosphate receptor 1
S1PR2	sphingosine-1-phosphate receptor 2
S1PR3	sphingosine-1-phosphate receptor 3
S1PR4	sphingosine-1-phosphate receptor 4
S1PR5	sphingosine-1-phosphate receptor 5
SAP	SLAM associated protein
SCS	subcapsular sinus
SHM	somatic hypermutation
SLAM	signalling lymphatic activation molecule
SLO	secondary lymphoid organ
STAT3	signal transducer and activator of transcription 3
STAT5	signal transducer and activator of transcription 5
TCF	T cell factor
TD	T cell-dependent
Tfh	follicular T helper cell
Tfr	follicular T regulatory cell
TI	T cell-independent
TLR	toll-like receptor
TNP	2,4,6-trinitrophenyl hapten
TRC	T cell zone reticular cell
VDJ	variable-diversity-joining
WNT	wingless-related integration site
WNV	West Nile virus
WT	wild-type

Table of Contents

Abstract ii

Acknowledgements iv

Abbreviations v

1 Introduction 1

1.1 B cell development 1

1.2 Secondary Lymphoid Organs 5

1.2.1 Spleen 5

1.2.1 Lymph Node 7

1.3 Chemokines and Chemotaxis 10

1.3.1 CCR7 12

1.3.2 ACKR4 12

1.4 B Cell Activation 13

1.4.1 Extrafollicular response 14

1.4.2 Germinal Centre Reaction 16

1.5 Memory B cells 22

1.5.1 Memory B Cell Subtypes 25

1.6 Lymphocyte patrol of SCS and marginal sinus 28

1.7 Objectives and Aims 30

2 Materials and Methods 32

2.1 Animals and Immunisations 32

2.2 Flow Cytometry 35

2.3 Indirect ELISA 40

2.4 Histology 41

2.5 Light Sheet Microscopy 42

2.6 RNA Sequencing 42

2.7 Antigenic Drift 44

2.8 Data Analysis 44

2.9 Materials Lists 45

3 Emigrating memory B cells within the draining lymph node 49

3.1 Introduction and Objectives 49

3.2 Results 50

3.2.1 The dynamics of memory B cell development in the draining lymph node over time 50

3.2.2 Emigrating memory B cells make contact with subcapsular sinus macrophages 55

3.2.3 RNA-sequencing analysis of B cells in the draining lymph node and distant lymph node 60
3.2.3.1 Definition of B cell subsets from bulk RNA sequencing data 60
3.2.3.1.1 GSEA of BEMs and GC B cells 62
3.2.3.1.2 GSEA of BEMs and BCMs 63
3.2.3.1.3 GSEA of BCMs and GC B cells 64
3.2.3.1.4 GSEA of BCMs and nBCs 65
3.2.3.2 Differential gene expression analysis revealed similarities and differences between BEMs and GC B cells 73
3.2.4 CD55 and CD24 as markers to identify BEMs 84
3.2.5 NP-specific B cell response in the spleen 100
3.2.5.1 NP-specific response in the spleen over time showed a peak GC response at day 5 post-immunisation 100
3.2.5.2 BEM marker expression in the spleen changed over time 108
3.3 Discussion 113
4 Emigrating memory B cells within the draining lymph node 119
4.1 Introduction and Objectives 119
4.2 Results 121
4.2.1 Investigating the role of ACKR4 and expression of CCL21 in draining lymph nodes 121
4.2.2 S1PR1-blockade impaired egress of emigrating memory B cells from the drLN 136
4.2.3 The role of ACKR4-mediated BEM recycling in response to antigenic variants 151
4.2.3.1 ACKR4-defiency resulted in impaired antibody response to hapten antigenic variants 152
4.2.3.2 Reduced generation of Dengue virus envelope protein variant specific antibodies in ACKR4-deficient mice 153
4.3 Discussion 162
5 Circulating memory B cells in distant tissues 168
5.1 Introduction and Objectives 168
5.2 Results 172
5.2.1 ACKR4-deficiency resulted in decreased levels of BCM in distLN but not blood and spleen 172
5.2.2 Generation of BEMs is unchanged but fewer BCMs detected in distant lymphoid tissues in CCL19-deficient mice 176
5.2.3 Response and migration of ACKR4-KO and CCR7-KO B cells in CCL19-KO mice 182
5.2.3.1 In an adoptive cell co-transfer ACKR4-KO B cells outcompete CCR7-KO in drLN and in distant lymphoid tissues in both CCL19-WT and CCL19-KO mice 182

5.2.3.2 CCR7-deficient B cells were decreased in distant lymph node and fewer circulating CCR7-deficient memory B cells were detected in CCL19-KO spleen 189
5.2.4 Increased BEM generation in drLN and fewer BCM detected in distant lymphoid tissues of CCL21-deficient mice 197
5.2.5 Differences in GC-derived memory B cell recall responses in drLN and distLN 205
5.3 Discussion 213
6 Conclusions 220
7 References 229

Lists of Tables and Figures

Figure 1. 1. B cell development in bone marrow 4
Figure 1. 2. Schematic of the murine spleen 6
Figure 1. 3. Schematic of the murine lymph node 9
Figure 1. 4. B cell and T cell interactions during B cell activation 16
Figure 1. 5. Schematic of the germinal centre reaction 18
Figure 1. 6. Summary of characteristics of memory B cell subsets 27

Table 2. 1. List of genetically modified mouse strains. 35
Table 2. 2. List of antibodies used for FACS staining including the dilution factor used. 39
Table 2. 3. List of materials used in the experiments described in this thesis. 47
Table 2. 4. List of equipment used for data acquisition. 48
Table 2. 5. List of software used for data processing and analysis. 48

Figure 3. 1. In the drLN peak levels of B cells and PCs was at 7 days post-immunisation 53
Figure 3. 2. Peak GCs and BEM production at 7 days post-immunisation in drLN 54
Figure 3. 3. BEMs detected in SCS in contact with antigen 57
Figure 3. 4. BEMs detected in SCS proximal to SCS macrophages and collect antigen 59
Figure 3. 5. BEMs were cell sorted and underwent RNA sequencing 67
Figure 3. 6. Sorted cells passed quality control tests 68
Figure 3. 7. Sorted BEMs are a distinct group from GC B cells, naive B cells and BCMs 69
Figure 3. 8. GC B cells were more enriched for gene sets associated with proliferation than BEMs 70
Figure 3. 9. BEMs enriched for proliferation-associated gene sets over BCMs 71
Figure 3. 10. GC B cell gene set enrichment showed that they were more proliferative than BCMs 72
Figure 3. 11. BCMs were enriched for gene sets for antigen processing and presentation, inflammatory response and cell signalling over naïve B cells 73
Figure 3. 12. BEMs have differentially expressed genes distinguishing them from BCMs and GC B cells 79
Figure 3. 13. Volcano plots show that BEMs have differentially expressed genes from GC B cells, BCMs and naive B cells 80
Figure 3. 14. Differentially expressed genes encoding cell surface proteins may distinguish BEMs from other B cell subsets 81
Figure 3. 15. BEM gene expression profile was similar to pre-memory B cells 83

Figure 3. 16. Identification of potential flow cytometry markers to detect BEMs from RNA-sequencing data 93
Figure 3. 17. Expression of CD24 and CD55 in BEMs from adoptively transferred cells assists distinguishing them from naive B cells and GC B cells 94
Figure 3. 18. Gating naive B cells, GC B cells and BEMs by CD24/CD55 expression detected cells from both endogenous and adoptively transferred populations 96
Figure 3. 19. BEMs were detected in WT mice using CD24/CD55 staining 99
Figure 3. 20. Among EdU+ cells GC B cells and BEMs detected by CD24/CD55 staining were increased 99
Figure 3. 21. Marginal zone B cells detected in an immunised spleen by flow cytometry over 14 days 103
Figure 3. 22. MZ B cells reached a peak at 10 days post-immunisation in the spleen 104
Figure 3. 23. Peak GC response and BEM levels at 5 days post-immunisation in the spleen 105
Figure 3. 24. Peak level of IgG1+ GC B cells and BEMs was at 5 days post-immunisation 108
Figure 3. 25. Markers distinguishing BEM from GC B cells and naive B cells were detected in the immunised spleen and BEM marker expression was tracked over time 112

Figure 4. 1. No significant effect on size of GC response and BEM production in ACKR4-deficient drLNs 126
Figure 4. 2. Light sheet microscopy of ACKR4-WT drLN with adoptively transferred QM mTmG cells showed BEM in the SCS 129
Figure 4. 3. BEM were detected in the SCS of ACKR4-KO drLN by light sheet microscopy 131
Figure 4. 4. CCL21 expressing MRCs and TRCs detected in the draining and non-immunised LNs 132
Figure 4. 5. CCL21-RFP expression detected in the SCS floor of non-immunised popliteal LN 134
Figure 4. 6. CCL21-expression detected in the SCS floor of immunised popliteal LN 135
Figure 4. 7. FTY720 treated drLNs were evaluated by flow cytometry 141
Figure 4. 8. Fewer B cells and GC B cells in FTY720-treated drLNs but no effect on production of BEMs 141
Figure 4. 9. Fewer BCMs in distant lymphoid tissues of FTY720-treated mice 143
Figure 4. 10. Fewer circulating B cells and T cells in blood of FTY720-treated mice 145
Figure 4. 11. At least as few BCMs in distant lymphoid tissues after BAF312 treatment as after FTY720-treatment 146
Figure 4. 12. BEMs detected in SCS of FTY720-untreated drLNs 149
Figure 4. 13. Fewer BCMs present in FTY720-treated drLN SCS 151
Figure 4. 14. Hapten-based model to simulate antigenic drift 156
Figure 4. 15. Affinity maturation to TNP was impaired in ACKR4-KO mice that could not recycle BEMs between SCS and follicles 159
Figure 4. 16. Characterisation of dengue virus envelope proteins 161
Figure 4. 17. E4-specific serum IgG1 as a ratio to E1-specific serum IgG1 increased in WT but not ACKR4-KO mice after boosting with E4 161
Figure 4. 18. Representative diagram of the migratory behaviours of BEM in the drLN 166

Figure 5. 1. Fewer BCM detected in distLN of ACKR4-deficient mice 175
Figure 5. 2. Fewer GC B cells in CCL19-KO drLN but levels of BEMs were unaffected 180
Figure 5. 3. Reduced levels of BCMs in distant lymphoid tissues of CCL19-deficient mice 181

Figure 5. 4. CCR7-KO, ACKR4-KO and WT adoptive cell co-transfer and gating strategy 186
Figure 5. 5. CCR7-KO B cells were outcompeted by WT and ACKR4-KO B cells in WT and CCL19-KO drLN.....186
Figure 5. 6. Gating strategy to detect adoptive cell co-transfer BCM in distant lymphoid tissues 188
Figure 5. 7. More ACKR4-deficient BCMs detected in distant lymphoid tissues than WT and CCR7-KO BCMs 188
Figure 5. 8. WT and CCR7-KO B cells were detected in WT and CCL19-KO drLN by flow cytometry ..193
Figure 5. 9. GC response and BEM production in drLN was minimally affected by CCL19-deficiency 194
Figure 5. 10. No differences in IgM and NP expression in WT and CCR7-KO GC B cells and BEMs of WT and CCL19-KO drLNs.....195
Figure 5. 11. A trend was detected towards fewer adoptively transferred BCM in the CCL19-KO spleen and fewer CCR7-KO BCM in the distLN 197
Figure 5. 12. B cell responses were measured in WT and CCL21-KO drLNs by flow cytometry 201
Figure 5. 13. Fewer GFP- B cells present in CCL21-KO drLN compared with WT drLN.....202
Figure 5. 14. Increased frequency of GFP+ B cells, PCs, GC B cells and BEMs in CCL21-KO mice 203
Figure 5. 15. BCM detected in WT and CCL21-KO distant lymphoid tissues by flow cytometry 204
Figure 5. 16. Fewer BCM detected in CCL21-KO distant lymphoid tissues 205
Figure 5. 17. Fewer BCM detected in CCL21-KO distant lymphoid tissues 205
Figure 5. 18. GC-derived mBCs become PCs in a recall response in the drLN 211
Figure 5. 19. Boosting distLNs increased dTomato+ mBCs and dTomato+ GC B cells but not PCs 213
Figure 5. 20. CCR7 and its ligands direct migration of BCMs to distant lymphoid tissues 217

Figure 6. 1. Schematic of generation and migration of BEM in the draining LN and migration of BCM to distant LN and spleen 224
Figure 6. 2. A proposed model for the role of mBCs in secondary responses to antigen: re-exposure to primary antigen or exposure to a variant of the primary antigen 227

Appendix 1: Baseline input data detecting NP+B220+ splenocytes for adoptive cell transfers.....245
Appendix 2: Gating scheme for qRT-PCR, RNA-sequencing library preparation.....247
Appendix 3: Table of BEM Markers with available antibody 250
Appendix 4: BCM in the distant LN after removal of samples containing GCs 251

1 Introduction

1.1 B cell development

The immune system can be divided into two features: innate immunity and adaptive immunity. Innate immunity offers non-specific protection against all antigens, this involves barriers to prevent entry of pathogens into the body. Innate immunity also includes innate humoral features such as the complement system and interferons. Adaptive immunity grants the capacity to recognise and develop a specific response to a pathogen.

Immune cells originate from haematopoietic stem cells (HSCs) produced in the bone marrow (BM), which is a primary lymphoid organ. HSCs can differentiate into myeloid cells which develop into cells that participate in the innate immune system such as basophils, mast cells, monocytes/macrophages, and neutrophils. Erythrocytes are also derived from myeloid cells. T cells are lymphocytes derived from HSCs that migrate from the BM to another primary lymphoid organ known as the thymus. Here thymocytes complete their development and maturation into CD4+ and CD8+ T cells.

HSCs can also differentiate into common lymphoid progenitors (CLPs) and develop into B cells. Approximately 10-20 million B cells are produced in the murine BM daily, however, only ~10% of these make it to the periphery. During embryonic and neonatal stages of life HSCs from the foetal liver seed the BM, these are recognisable due to expression of high levels of c-Kit (Hardy and Hayakawa, 2001). These HSCs develop into CLPs which lack the B cell lineage marker B220 but can be distinguished based on their expression of IL-7Ra and intermediate levels of c-Kit (Hardy and Hayakawa, 2001). CLPs then mature into B cells, recognisable by the B cell lineage marker, B220.

The first immature B cell fraction that CLPs become are pre-pro-B cells which express B220 and CD43 but lack expression of CD24 and CD19 (Rolink et al., 1996)(Fig. 1.1). During this stage these cells undergo D-J IgH rearrangement (Van Zelm et al., 2007). This requires expression of high levels of re-arrangement genes RAG1, RAG2 (Oettinger et al., 1990) and TdT (Komori et al., 1993). IKAROS encodes the transcription factors that activated Rag1 and TdT (Kirstetter et al., 2002), as such it is crucial to B cell development as IgH rearrangement is impaired without it. E2A encodes E12 and E47 which are helix-loop-helix transcription factors crucial in early stages of B cell lineage, as they are required for D-J IgH rearrangement (Bain et al., 1997).

Pre-Pro-B cells progress to the IgH rearranged pro-B cells which are distinguished by their increased expression of CD19 and higher levels of B220 expression (Hardy, 2013). EBF-1 is required for this stage, which in turn is directed by positive feedback loops involving IL-7Ra, E2A and Pax5, among others (Singh et al., 2005). These are irreversibly committed to the B cell lineage due to expression of Pax5 (Nutt et al., 1999). During the pro-B cell stage these cells undergo V-DJ IgH rearrangement. These cells begin to express the rearranged IgH μ pre-B cell receptor with surrogate light chain made up of VpreB and λ5 peptides to become pre-B cells. These pre-B cell receptors (BCRs) associate with Igα and Igβ to facilitate signal transduction (Hardy, 2013).

Signalling of the pre-BCR is thought to induce allelic exclusion in these early pre-B cells (Xu et al., 2000), also known as large pre-B cells, and can also promote proliferation mediated by expression of Sox-4 and Lef-1 (Schilham et al., 1996, Reya et al., 2000). After proliferation, small pre-B cells re-express RAG1/2 and undergo rearrangement of κ light chain V-J genes

(Schlissel and Baltimore, 1989). Successful assembly terminates RAG expression (Hardy, 2013). If κ assembly fails, λ V-J rearrangement and assembly occurs (Derudder et al., 2009).

When pre-B cells express this rearranged μ chain BCR they are defined as immature B cells. These differ from mature B cells as they have a very short lifespan and are more sensitive to calcium flux, but BCR cross-linking will not induce proliferation; instead, it induces apoptosis or anergy. Negative selection occurs at this stage (Melamed et al., 1998).

In the BM when immature B cells express IgM but not IgD BCRs binding to self-antigen can lead to clonal deletion or anergy (Healy and Goodnow, 1998, Allman et al., 1992, Hertz and Nemazee, 1997). Self-reactive B cells can also undergo receptor editing in which they reassemble light chain variable genes in order to alter specificity to not recognise self-antigen (Hertz and Nemazee, 1997).

Newly formed immature B cells that are not negatively selected become transitional B cells that migrate to the spleen, and once in the spleen they become mature B cells (Hardy, 2013). Fate decisions to become MZ B cells are NFkB-dependent, the decision is promoted by signalling through BCRs, Notch2 and B cell activating factor receptor (BAFF-R); conditions of APRIL and BAFF-R deficiency reduce MZ B cell numbers (Rauch et al., 2009, Tull et al., 2021). MZ B cells can differentiate from transitional B cells but sufficiently high levels of Notch2 can drive differentiation of follicular B cells to MZ B cells (Lechner et al., 2021). Notch2 binds its ligand Dll1 and is cleaved by ADAM family metalloproteases that frees the Notch2 intracellular domain to traffic to the nucleus (Radtke et al., 2010). In the nucleus, the freed intracellular Notch2 domain forms a transcription complex with DNA-binding transcription factor CSL which recruits other co-activators, such as MAML1, resulting in a

transcriptional program that contributes to MZ B cell differentiation (Radtke et al., 2010, Tanigaki et al., 2002, Wu et al., 2007, Oyama et al., 2007). In type 1 transitional B cells BCR signalling can regulate activation of the serine/threonine kinase Taok3 which in turn activates the metalloproteinase ADAM10 (Hammad et al., 2017). ADAM10 cleavage frees the intracellular domain of Notch2 after Notch2 ligation with Dll1 resulting in MZ B cell differentiation (Radtke et al., 2010). This BCR signalling appears to be modulated by integrins as β1 modulates BCR signalling, restricts downstream PI3K signalling and facilitates differentiation to MZ B cells (Andreani et al., 2023). This suggests that there are many contributing factors, such as the co-signalling of NFkB and Notch2, that drive the differentiation to MZ B cells.

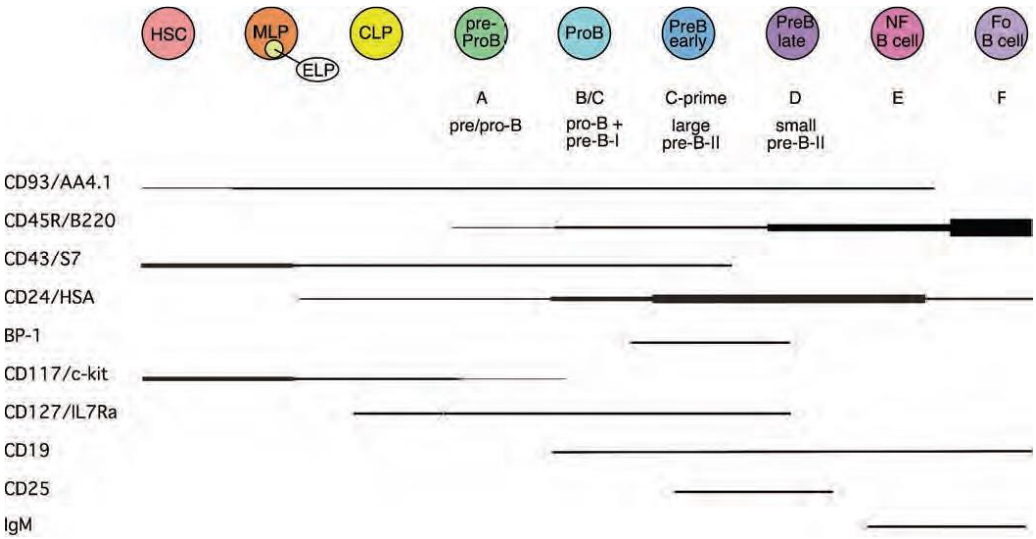


Figure 1. 1. B cell development in bone marrow

Summary of B cell developmental stages in the bone marrow, this diagram shows the expression of markers distinguishing each developmental stage as HSCs differentiate into mature B cells. CD43+ c-kit+ HSCs differentiate into multilymphoid progenitors (MLPs) that further upregulate expression of AA4.1. MLPs can differentiate into CLPs which upregulate CD24 and IL7Ra. CLPs can then differentiate into pre-pro-B cells that begin expression of B220. These mature to become pro-B cells that downregulate c-kit and begin expression of CD19 while further upregulating B220 and CD24. Pro-B cells mature into early and late pre-B

cells that lose expression of CD43 by the time they become late pre-B cells, pre-B cells express BP-1 and CD25. Pre-B cells differentiate into immature B cells that begin expression of IgM and cease expression of BP-1, c-kit and CD25. These then become mature B cells that cease expression of AA4.1, upregulate B220 and downregulate CD43 (Hardy, 2013).

1.2 Secondary Lymphoid Organs

15% of murine peripheral leukocytes are B cells, which are a feature of the adaptive immune system. Mature B cells can be found in the secondary lymphoid organs (SLOs) which include the spleen and the lymph nodes (LNs). Mature T cells can also be found in the SLOs.

1.2.1 Spleen

The spleen functions as a filter for blood, it is comprised of the red pulp and white pulp. Blood enters the spleen from the splenic artery via the hilum and is carried through the red pulp via arterioles which are carried through the white pulp via central arterioles, branches of this terminate at the marginal zone (MZ) surrounding the white pulp (Mueller and Germain, 2009). The red pulp removes old erythrocytes and recycles iron and platelets. The white pulp consists of peri-arterial lymphatic sheaths (PALS) where arterioles can facilitate entry of lymphocytes, and this region is the T cell zone of the spleen (Förster et al., 1999). Adjacent to PALS are B cell-rich follicles which in turn are surrounded by the MZ. The MZ is adjacent to the marginal sinus, this is a region where the red pulp and white pulp meet, it contains many blood vessels (Fig. 1.2). Until recently it has been reported that lymphocyte entry to the splenic PALS is via the marginal sinus to the PALS using bridging channels (Bajenoff et al., 2008). However, recent evidence suggested that entry of lymphocytes instead occurs directly through peri-vascular stroma of bridging channels connecting red pulp to the PALS (Chauveau et al., 2020). Further work identified a layer of vasculature

separate from the red pulp and white pulp with shunts connecting to special bridging channels to the PALS (Werth et al., 2021). T cells enter the spleen using CCR7 ligands but can follow CXCR4 ligands if CCR7 expression is modulated (Okada et al., 2002). Expression of CCR7 by B cells is also required for movement through the T cell zones of the spleen (Pereira et al., 2010). The MZ acts as an antigen transit area as MZ B cells can screen systemic circulating antigen and play a role in antigen processing (Mebius and Kraal, 2005).

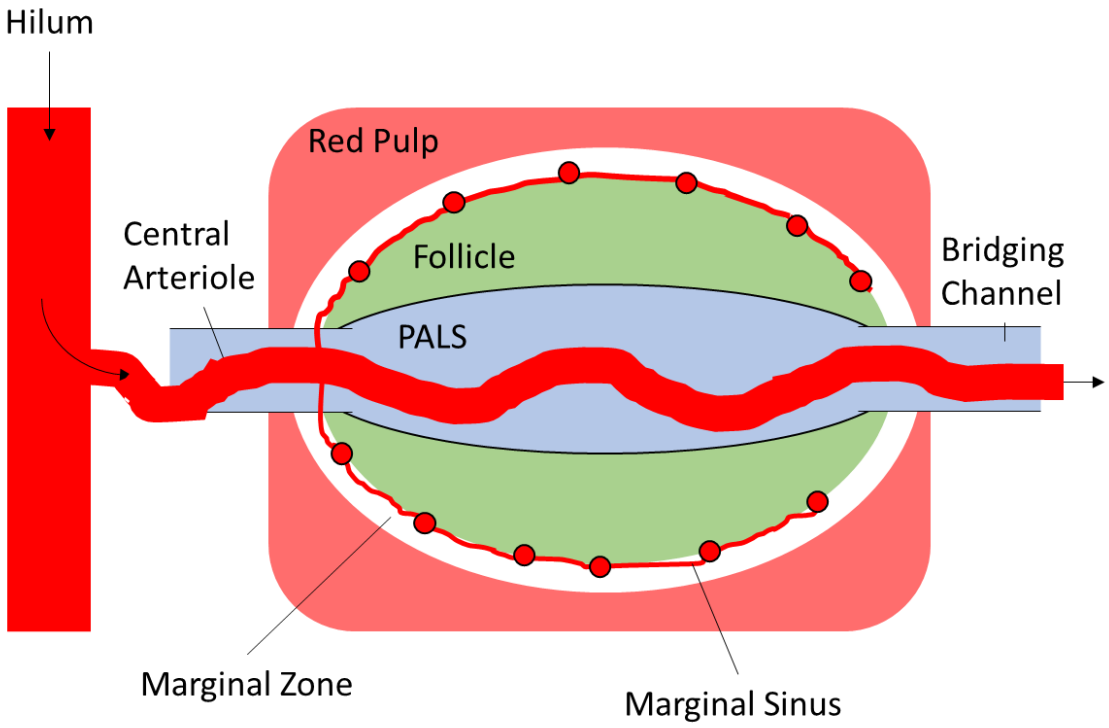


Figure 1. 2. Schematic of the murine spleen

Arrows show blood entering the spleen from the hilum via the central arteriole, which passes through the white pulp through the PALS. Bridging channels connect red pulp and white pulp. Branching off from the central arteriole are smaller blood vessels which comprise the marginal sinus. Red circles represent blood vessels of the marginal sinus running perpendicular to the other blood vessels in this overview. The marginal sinus sits between the marginal zone and the B cell-containing follicle.

Circulating B cells in the spleen are retained in the B cell follicle for up to a day, after this point they begin to move towards the marginal sinus. This was due to the increased sensitivity of S1PR1 allowing migration following S1P gradients leading to the marginal sinus (Ramos-Perez et al., 2015, Pereira et al., 2010). As these follicular B cells lack the cell adhesion molecules of MZ B cells, they are unable to withstand the shear forces of the marginal sinus and re-enter circulation (Pereira et al., 2010).

1.2.1 Lymph Node

The LN is comprised of cortical, paracortical and medullary regions which are surrounded in sinuses carrying circulating antigens from lymphatics (Fig. 1.3). B cells may enter the LN via high endothelial venules (HEVs) due to expression of CCR7 and CXCR4 following chemotaxis towards CCL19, CCL21 and CXCL12 produced by HEVs (Steen et al., 2014). Expression of CXCR5 allows lymphocyte homing to the CXCL13-rich B cell follicles of the LN cortex (Ansel et al., 2000). This is facilitated by the expression of CXCL13 produced by CD21/35+ follicular dendritic cells (FDCs) and follicular stroma cells (Mueller and Germain, 2009). CCR7+ T cells are drawn to the T zone in the LN cortex due to expression of CCL19/21 by stromal cells in the T zone (Förster et al., 1999).

Entry of leukocytes into via venules involves a process known as the multi-step cascade that ends with trans-endothelial migration (Butcher, 1991, Springer, 1994, Ley et al., 2007). Inflammatory signals such as TNF, IL-1 and IFN promote expression of P- and E-selectins, ICAM-1, VCAM-1 and chemokines of endothelial cells that co-ordinate the recruitment of leukocytes (Liu et al., 2004, Dunon et al., 1996, Ed Rainger et al., 2015). Selectins, VCAM-1 and ICAM-1 promote capture and rolling of leukocytes on the endothelium by binding

integrins, VLA-4 and LFA-1 respectively expressed by leukocytes, leukocytes also express L-selectin (Kansas, 1996, Lawrence and Springer, 1991, Ley et al., 2007, Ebisuno et al., 2010). Chemokine receptor signalling promotes activation of integrins leading to stronger leukocyte adhesion resulting in leukocyte arrest on the endothelium (Luu et al., 2000, Ley et al., 2007). Leukocytes then undergo cytoskeleton remodelling and crawl across the endothelial wall until they reach a preferred site of transmigration (Ley et al., 2007). The leukocytes can then migrate through the endothelial wall endothelium following the paracellular pathway and the transcellular pathway to enter the tissue (Ley et al., 2007). Transcellular migration is the major pathway for lymphocyte trans-endothelial migration and involves movement directly through transcellular pores formed in endothelial cells (Küppers et al., 2013, Millán et al., 2006, Schimmel et al., 2017). This process reflects how lymphocytes enter the SLOs via HEVs (Mackay, 1995, Gunn et al., 1998)

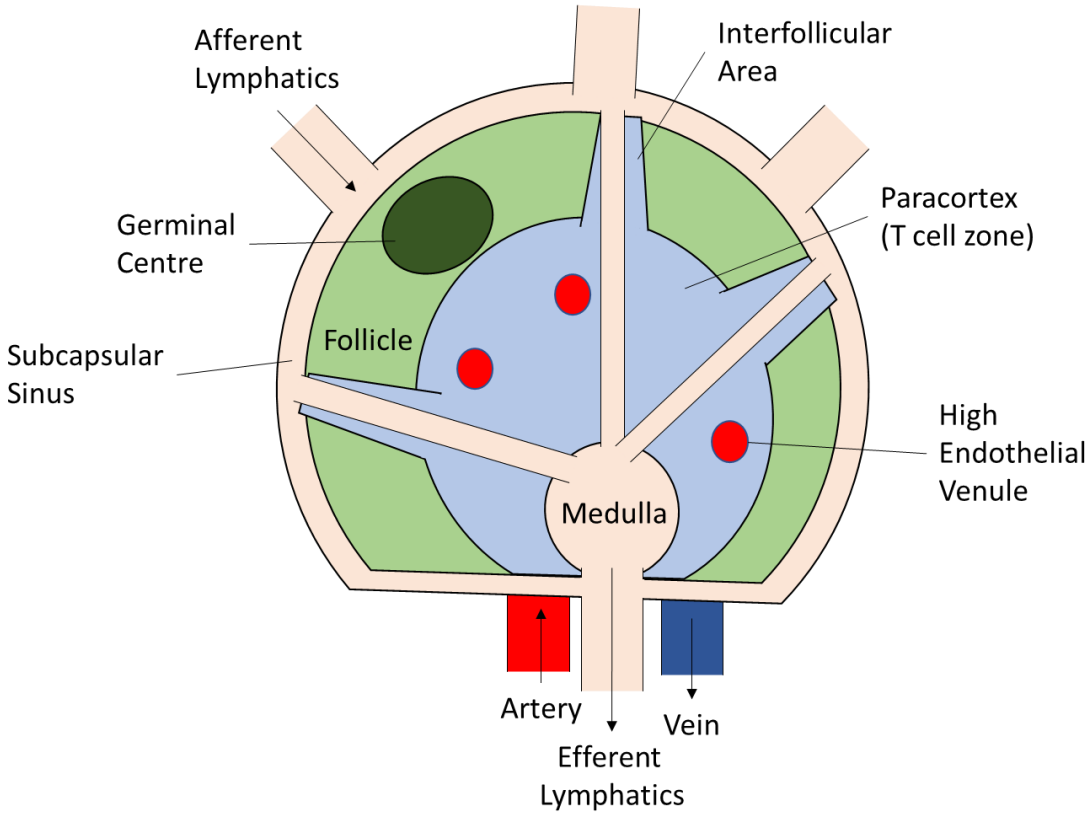


Figure 1. 3. Schematic of the murine lymph node

The lymph node is encapsulated in a subcapsular sinus which allows flow of lymph from the afferent lymphatics. Below the capsule are the follicles, these are B cell areas, activated B cells form germinal centres in the follicles. Deeper in the tissues is the paracortex, this is T cell area but also contains high endothelial venules. Arrows show the flow of lymph through the lymph node from afferent lymphatics to subcapsular sinus and cortical sinuses to the efferent lymphatics. Blood flows through arterioles to high endothelial venules.

B cells in the follicle of the LN follow a similar pattern as those described in the spleen. Naïve B cells are retained in the LN follicle for around 24 hours before they begin to migrate towards the outer follicles and the cortical sinus, followed by egressing the LN via efferent lymphatics (Schwab and Cyster, 2007, Smith and Ford, 1983, Westermann et al., 1988, Pereira et al., 2010, Sinha et al., 2009). Lymphocyte movement towards the cortical sinuses in the LN and subsequent egress involves the S1PR1 ligand S1P, one source of S1P is Lyve-1+

lymphatic endothelial cells (LECs) (Pham et al., 2010). EBI2 (also known as GPR183) is a chemokine receptor that follows the concentration gradient of its oxysterol ligand 7a,25-dihydroxycholesterol produced by FRCs of the outer follicles to direct migration of B cells to the outer follicular regions, including the SCS of the lymph node (Yi et al., 2012, Gatto and Brink, 2013).

Desensitisation of CCR7, CXCR4 and CXCR5 of B cells occurs in the LN over time. This compounded by increasing expression of S1PR1 ensured that these B cells are less able to respond to signals retaining them in the LN and more able to respond to signals encouraging egress from the LN (Park et al., 2012). Once these lymphocytes reach the blood the sensitivity of CCR7, CXCR4 and CXCR5 is replenished allowing them to start the process again (Park et al., 2012).

1.3 Chemokines and Chemotaxis

Migration of lymphocytes within SLOs are facilitated by chemokines. Chemokines signal through G-protein coupled receptors (GPCRs). Chemokines are of relatively small size (between 8-14 kDa) and are comprised of a monomeric structure (Baggiolini et al., 1997). A chemokine is made up of an NH2 terminal loop followed by 3 anti-parallel β-strands and ending with a C-terminal α-helix (Baggiolini et al., 1997). Chemokines are named based on the number of residues between cysteines in the NH2-terminal loop. CXC are α-chemokines with one residue between cysteines, CC are β-chemokines with no residues between cysteines and CX_3C are γ-chemokines with 3 residues between the cysteines (Zlotnik and Yoshie, 2000).

A GPCR contains 7 transmembrane domains and has two conserved cysteines, one in its N-terminal loop and one in the third extracellular loop. One important motif of the GPCR is its conserved DRYLAIVHA on TM3 that acts as NH2 and COOH terminal extensions. This motif is required for coupling with Ga proteins that are used for phosphorylation and subsequent downstream signalling (Ulvmar et al., 2011). Atypical chemokine receptors (ACKRs) are homologous to GPCRs, except they lack a Ga protein-binding DRYLAIVHA motif, and as such, they are incapable signal transduction (Ulvmar et al., 2011). After binding its chemokine, an ACKR then undergoes internalisation and subcellular localisation. They can move to the lysosome to degrade the chemokine, and subsequently the receptor is recycled back to the cell surface (Comerford et al., 2006). ACKRs can also transcytose chemokines to facilitate traversal of biological barriers resulting in increased chemokine concentrations in microanatomical domains (Nibbs and Graham, 2013). There are 4 known ACKRs, ACKR1-ACKR4, these can dimerise into homo- and heterodimers. The present study will focus on ACKR4 (also known as CCRL1). In the human context, ACKR4 has been observed to recruit G protein-coupled receptor kinases (GRKs) after ligation with chemokines which in turn recruit β-arrestins. These β-arrestins enhance but are dispensable for ligand uptake into the cell by ACKR4 (Matti et al., 2020b).

Many stromal cells within SLOs, such as LECs, some fibroblastic reticular cells (particularly those in T cell areas) and peri-HEV cells, can produce chemokines CCL19 and CCL21, which bind CCR7 (Johnson and Jackson, 2010, Manzo et al., 2007). CCL19 and CCL21 share only 25% homology in amino acid sequence, but there are several conserved tertiary structures between them (Comerford et al., 2013): a disordered N-terminus, followed by a core domain containing an N-loop, a 3-stranded β-sheet and then a C-terminal helix. CCL21 differs from

CCL19 by containing a unique negatively charged 30 aa length carboxyl-terminal extension with 2 extra cysteine residues, and 12 of these residues are basic (Ott et al., 2006, Nagira et al., 1997). Mice possess 2 isoforms of CCL21: CCL21a containing a Serine at residue 65 and CCL21b containing a leucine at residue 65 (Comerford et al., 2013).

1.3.1 CCR7

Upon binding of CCR7 with its ligands (CCL19 and CCL21) it recruits β-arrestins and GRKs, such as GRK6, leading to signal transduction and the promotion of migration of the cell, through means such as actin polymerisation and polarisation of the cell in the direction of the ligand concentration gradient (Zidar et al., 2009). CCL19 induces a slightly different response when binding CCR7, in CCR7-CCL19 interactions there is the additional recruitment of GRK3 which promotes the internalisation of CCR7 leading to desensitisation of the cell towards CCR7 ligands (Zidar et al., 2009). CCL19 and CCL21 also differ in another respect, at shallower concentration gradient CCL19 had a stronger chemotactic index (a measure of how efficiently cell migration follows the chemokine gradient) than CCL21, whereas at steeper concentration gradients CCL21 had a stronger chemotactic index (Ricart et al., 2011). This may reflect greater desensitisation of CCR7 at higher CCL19 concentrations, impairing the response to this chemokine at steep concentration gradients, allowing CCL21 to outpace CCL19 with its potency to induce chemotaxis without impairing its receptor.

1.3.2 ACKR4

Among the ligands of ACKR4 are CCL19, CCL21, CCL25. CCL20 has also been observed as another ligand for ACKR4 which also induces recruitment of β-arrestins to ACKR4. SCS

endothelial cells in murine popliteal LN were observed to take in CCL20 by ACKR4 (Matti et al., 2020a).

ACKR4 creates micro-gradients of its ligands (Nibbs and Graham, 2013). This may increase sensitivity to the chemokine gradient. ACKR4 is thought to play a role in maintenance of CCL19 and CCL21 chemokine gradients by scavenging these CCR7 ligands and internalisation (Ulvmar et al., 2014). ACKR4 is expressed by ceiling LECs in the SCS; this allows entry of CCR7 expressing cells, such as DCs, from the lymphatics into the LN (Ulvmar et al., 2014).

1.4 B Cell Activation

After B cells migrate to SLOs they can become activated, there are chemotactic cues involved in the process of B cell activation. B cells can become activated in one of two processes: thymic independent (TI) and thymic dependent (TD) activation. TI activation does not require the involvement of T cells, whereas TD activation requires T cell help. After activation B cells can develop into antibody-secreting plasma cells (PCs) or memory B cells (mBCs) that can be activated upon re-encounter with antigen. PCs and mBCs can be produced from a an extrafollicular (EF) response or a germinal centre (GC) reaction.

B cells can be categorised into two groups: B1 cells and B2 cells. B1 Cells ($IgM^{hi}B220^{lo}IgD^{lo}CD23^{-}$) are derived from foetal liver cells and are primarily located in the peritoneal cavity. B1 cells are rare in LNs and the spleen. “Classical” B2 cells ($CD23^{hi}B220^{hi}IgD^{hi}IgM^{lo}$) are constantly recirculating throughout the body; these include follicular B cells and the $CD1d^{hi}CD21^{hi}$ MZ B cells. Splenic MZ B cells can respond to T-

independent antigens by differentiating into plasmablasts (PBs) that produce high quantities of IgM, additionally they can also produce class-switched IgA and IgG (Cerutti et al., 2013).

1.4.1 Extrafollicular response

TI antigens induce EF responses. TI-1 responses involve cognate ligation of toll-like receptors (TLRs) on the B cell. This does not induce Bruton's Tyrosine Kinase (BtK) signalling. The TI-1 response is faster than the thymic-dependent (TD) response and can lead to the production of extrafollicular (EF) PCs and a few mBCs, B1 cells and MZ B cells were better able to become PCs than follicular B cells (Martin et al., 2001, Genestier et al., 2007). TI-2 response involves BCR cross-linking by multi-epitope antigens leading to persistent BtK signalling, CD5+ B1 cells were particularly important to produce TI-2 antigen-specific antibodies (Sidorova et al., 2003). There is a robust extrafollicular PC response, and a few mBCs are produced (de Vinuesa et al., 2000). The TI extrafollicular response involves the extrafollicular activation of B cells which can result in autoreactive B cell activation (Herlands et al., 2008, Weisel et al., 2007).

TD EF responses have also been observed. TD EF responses require CD40-CD40L interaction of B cell blasts with activated CD4 T cells and IL-21 signals from T cells at the T-B border for initiation, this can result in the activation of autoreactive B cells (Sweet et al., 2011). EF primed B blasts then exit the T-B border and enter the extrafollicular site and associate with $CD11c^{hi}$ DCs (MacLennan et al., 2003). These B blasts undergo class-switch recombination prior to differentiation into PBs (Marshall et al., 2011). miR182 is upregulated in these extrafollicular activated B cells and is required for the antibody response (Li et al., 2016). This occurs in EF regions and involves B cell proliferation, resulting in the production of antibody

secreting PBs. This canonical EF response often requires a T-dependent antigen and occurs approximately 2 days post-immunisation. The peak of this canonical EF response is usually 4-6 days post-immunisation (Elsner and Shlomchik, 2020).

Affinity selection during the EF response in the early stages of TD B cell activation results in a low affinity response (Dal Porto et al., 1998, Jacob and Kelsoe, 1992). These EF responses result in lower affinity antibody responses and less robust memory compared with the GC response (Elsner and Shlomchik, 2020). HIV patients responding to COVID-19 had more EF responses and fewer GC responses, resulting in lower affinity antibodies and impaired long-term memory (Krause et al., 2022). However, there is still some evidence of affinity maturation in Salmonella infection, in which the GC response was impaired but with a strong EF response, due to high affinity clones at EF sites that underwent SHM (Roberto et al., 2015).

The EF response is important as it can contribute to an early protection from infection by adaptive immunity. The EF response produces short-lived PCs that produce antibodies which offer an initial, weaker, protection before the GC reaction can provide antibodies from high affinity clones to better target the antigen.

1.4.2 Germinal Centre Reaction

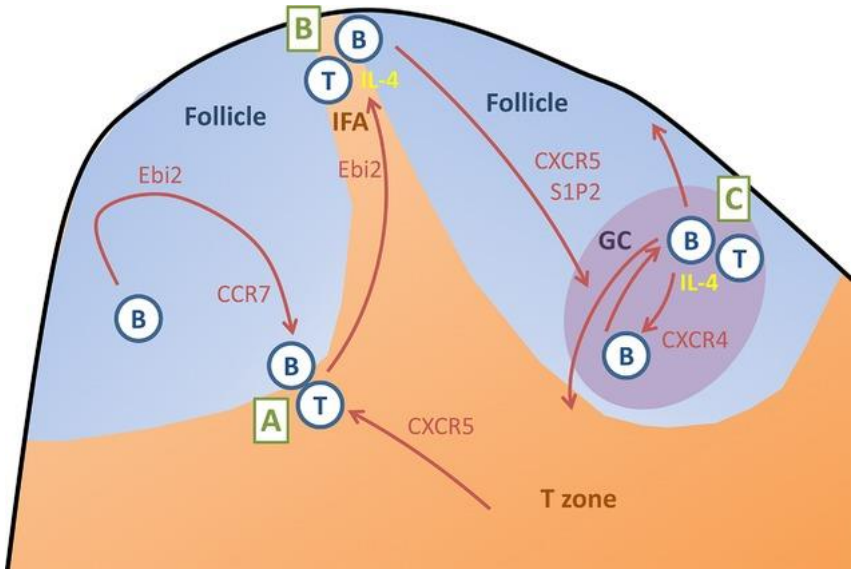


Figure 1. 4. B cell and T cell interactions during B cell activation

Schematic of chemotactic cues involved in the interactions between B cells and T cells during activation in the lymph node. (A) Upon activation B cell expression of CCR7 is upregulated which overpowers EBI2 and promoting migration to the T cell zone-B cell zone border where B cells interact with T cell that upregulated CXCR5. (B) Cognate interactions between B and T cells at the T-B border promotes EBI2 expression promoting migration of B cells to the interfollicular areas where they may further interact with T cells in the context of IL-4. (C) This results in the upregulation of CXCR5 and S1PR2 which promote restriction of B cells within the follicle allowing them to cluster together to form a germinal centre. The germinal centre consists of a light zone and a dark zone, in the light zone GC B cells can interact with T follicular helper cells. Germinal centre B cells upregulate CXCR4 to enter the DZ. The germinal centre outputs are plasma cells, which leave the germinal centre from the germinal centre-T zone interface near the dark zone, and memory B cells, which exit the germinal centre near the light zone (Toellner, 2014).

Follicular B cells that recognise antigen on their BCRs upregulate the chemokine receptors EBI2 and CCR7 (Fig. 1.4). 1-2 days after antigen encounter, CCR7 allows migration to the B-T interface where they interact with CXCR5+ CD4+ T cells to receive co-stimulatory signals and begin to proliferate (Garside et al., 1998, Okada et al., 2005). The B cell presents antigen in the context of class II major histocompatibility complex (MHCII) recognised by CD4+ T cells in

the T zone. During this interaction CD40-CD40L ligation, in synergy with BCR signalling causes B cell upregulation of Myc (Luo et al., 2018). SAP-CD84 interactions facilitate cell-cell adhesion maintaining B cell-T cell contact (Cannons et al., 2010). Subsequent CCR7 downregulation and increased EBI2 sensitivity to oxysterol ligands on activated B cells facilitates migration to the interfollicular area (Kelly et al., 2011). Prolonged interactions with T cells in the IL-4 and IL-21 rich environment of the interfollicular area induces B cell lymphoma 6 (Bcl-6) (Chevrier et al., 2017, Toellner, 2014). CXCR5 and S1PR2 are upregulated and EBI2 is downregulated causing the B cell migration to the follicle and cluster together with other B cells to form a GC (Toellner, 2014). Bcl-6-mediated transcriptional repression of *Ebi2* and *S1pr1* causes confinement to the GC niche (Huang et al., 2014). These GC B cells are formed from B cell blasts. After B cell activation but prior to commitment to either EF or GC pathways B cells may commence class-switch recombination (CSR) (Roco et al., 2019, Marshall et al., 2011, Toellner et al., 1996, Toellner et al., 1998).

The GC forms within 3 days after primary antigen exposure to ovalbumin conjugated to hen egg lysozyme (HEL-OVA) (Garside et al., 1998), and GC B cells reach peak levels by 7 days post-exposure to 4-hydroxy-3-nitrophenylacetyl (NP) hapten conjugated to chicken gamma globulin (CGG) (Zhang et al., 2018), but the timing of this peak varies dependent on antigen. Proliferation and strong selection pressures on the GC B cell make the GC highly mitotic and apoptotic. Tingible body macrophages in the GC are involved in clearance of these apoptotic cells and may have a role in regulation of the GC (Rahman et al., 2010). The metabolism of the GC B cells is mainly oxidative phosphorylation of fatty acids (Weisel et al., 2020).

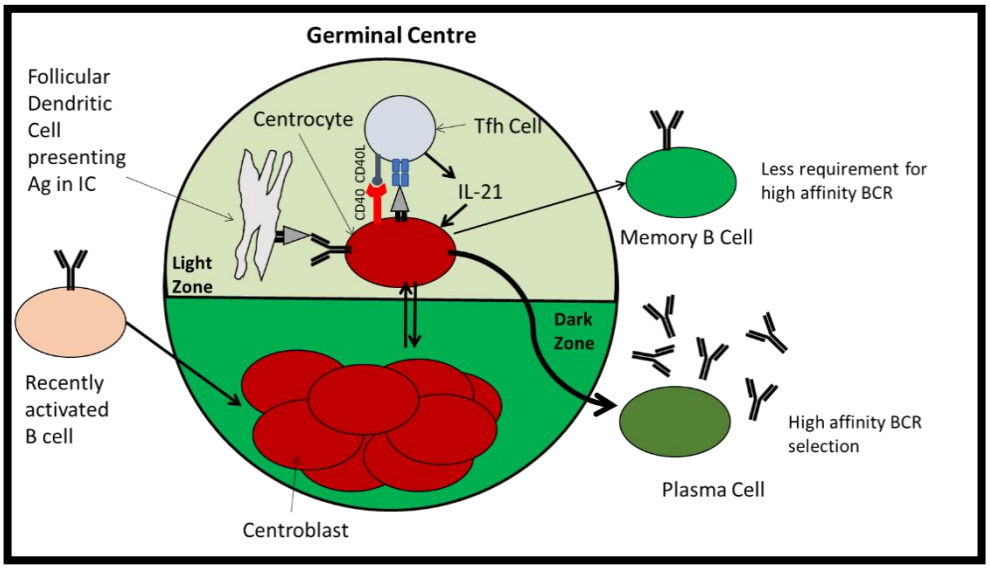


Figure 1. 5. Schematic of the germinal centre reaction

The germinal centre reaction involves proliferation and mutation in DZ. In the LZ GC B cells compete to collect antigen presented in immune complexes (IC) by FDCs and then present it to Tfh cells to receive T cell help in a process known as positive selection. The GC produces PCs and mBCs.

The GC is comprised of the dark zone (DZ) and the light zone (LZ), which are home to CXCR4+ DZ B cells and CXCR4^{low} LZ B cells, respectively (Fig. 1.5). DZ B cells undergo proliferation and somatic hypermutation (SHM). LZ B cells express BCRs and undergo positive selection (MacLennan, 1994). LZ B cells compete to collect antigen in immune complex (IC) presented by FDCs by their BCRs. LZ B cells then compete to present antigen to the Tfh cells in the context of MHCII to receive T cell help by CD40L and IL-21 signals in a process known as positive selection (Victora and Nussenzweig, 2012).

CSR and SHM relies on activation-induced deaminase (AID). AID facilitates CSR by deaminating cytidine residues of switch (S) regions of the IgH locus resulting in double strand DNA breakage which is followed by intrachromosomal deletion of IgH genes between the

affected S regions (Stavnezer et al., 2008). AID is involved in SHM by deaminating cytosine to deoxy-uracil at the Ig variable region locus, which induces DNA-repair mechanisms in an error prone manner resulting in mutation (Pilzecker and Jacobs, 2019). Upregulation of CXCR4 by LZ B cells allows them to follow CXCL12 gradients generated by a network Cxcl12-expressing reticular cells in the DZ driving migration to the DZ (Bannard et al., 2013, Rodda et al., 2015). GC B cells in the DZ proliferate extensively and undergo SHM. They have the options to re-enter S phase for another round of cell division, or downregulate CXCR4 allowing them to follow CXCR5 ligands for entry into the LZ or undergo apoptosis (Stewart et al., 2018). In the LZ GC B cells receive positive selection by T cell help from Tfh cells, inducing c-Myc, which stimulates B cell differentiation and amplifies calcium signalling, followed by migration into the DZ which is enriched for cells in the G2/M phase (Gitlin et al., 2015, Habib et al., 2007, Victora et al., 2010).

The GC B cell is programmed to undergo apoptosis unless it receives positive selection signals due to lack of expression of BCL2, an anti-apoptotic signalling molecule (Liu et al., 1989, Liu et al., 1991). Apoptosis can also occur as the result of accumulation deleterious mutations of BCRs by DZ GC B cells (Stewart et al., 2018). Under these conditions affinity maturation occurs due to a slow but consistent increase in selection stringency. GC B cells undergo rounds of SHM and affinity selection moving back and forth between the GC LZ and DZ leading to affinity maturation. PBs are selected from GC B cells that receive strong positive selection signals from Tfh cells (Ise et al., 2018). These exit the GC via the DZ to enter the APRIL-rich GC-T zone interface (Zhang et al., 2018). Long-lived mBCs are not so stringently selected for high BCR affinity (Suan et al., 2017).

Tfh cells are crucial for the GC reaction. The TI-2 response (with BCR cross-linking) can result in the formation of non-productive GCs when induced by high antigen concentrations. These GC B cells were aborted at the LZ B cell stage due to an absence of T cell help from Tfh cells (de Vinuesa et al., 2000). Additionally, there was an impaired SHM of GC B cells without T cell help (Toellner et al., 2002).

There are many cytokines that influence B cell activation by regulating Tfh cell and T cell function. IL-12 is produced by dendritic cells which can inhibit Tfh differentiation and induces generation of IFNγ and IL-21-secreting non-Th1/Tfh cells (Elsner and Shlomchik, 2020, Elsner and Shlomchik, 2019). Therefore, IL-12 limits humoral response towards a T-independent EF response due to a lack of T cell help to support GCs. IL-21 promotes both GC and T-dependent EF responses by promoting T cell expression of BCL-6 and promoting maintenance of the IL-21R expressing GC B cells (Linterman et al., 2010, Lee et al., 2011). In responses to malaria IFNγ along with TNFα and ANKA suppress Tfh differentiation but do not completely inhibit GCs (Ryg-Cornejo et al., 2016). IL-2 suppresses Tfh differentiation by signal transducer and activator of transcription 5 (STAT5)-mediated induction of Blimp1 which antagonises Bcl-6 (Johnston et al., 2012).

There are some mechanisms of peripheral tolerance in the GC reaction. Self-reactive B cells are removed from GC reactions by failing to receive positive selection signals upon presenting antigen to Tfh cells. In the GC response the expression of Fas does not prevent the production of self-reactive GC B cells, but it does prevent the development of a population of rogue IgE-secreting PCs that produce autoantibodies (Butt et al., 2015). There is also an emerging role for a group of T follicular regulatory (Tfr) cells in this process. These

are defined as FOXP3+ CXCR5+ CD4 T cells in the GC (Linterman et al., 2011, Wollenberg et al., 2011, Chung et al., 2011). They have been observed to exert suppression on both Tfh and GC B cells. In Tfh cells they reduced expression of Bcl-6 and impaired cell cycling. They also impaired the secretion of IL-21 which is important in the maintenance of GC B cells (Sage et al., 2014). Tfr cells suppressed CSR in GC B cells and suppressed metabolism, however this was negated by IL-21 which both impaired Tfr cell function and restored GC B cell function (Sage et al., 2016). This Tfr-mediated suppression of Tfh expression of IL-21 may work to prevent both a suppression of Tfr cell function and promotion of GC B cell activity by Tfh cells. It is unclear whether Tfr cells directly interact with GC B cells or act through impairing the capacity of Tfh cells to support GC, however, this process is thought to involve CTLA4 (Peter et al., 2014). This can be broken when a GC B cell specific to a foreign antigen has some cross-reactivity with a self-antigen and receives positive selection signals (Chan et al., 2012).

BCR signalling is also important for GC B cells selection. LZ B cells must compete to bind antigen in IC present on FDCs to receive positive selection. Antibody feedback occurs as a means of negative regulation of the GC reaction. Antibody feedback can be demonstrated by immunisation along with antigen-specific immune complex that results in a limitation on the strength of the response (Song et al., 1998). High affinity antibodies likely secreted from GC-derived PCs enter the GC and limit antigen access (Zhang et al., 2013). During early GC activation, the lower affinity antibodies produced in the EF response preceding GC may provide a baseline selection threshold in the response to novel antigen. In secondary response to a previously encountered antigen, antibodies produced from mBCs induced to become PCs may provide a higher selection threshold driving the secondary GC response.

Increasing affinity of antibodies resultant from an ongoing GC reaction raises the threshold of BCR affinity required for positive selection (Tarlinton and Smith, 2000). Due to their smaller size antibodies are more mobile than GC B cells and better able to permeate the stromal network of the GC, which may enhance competition for antigen. These antibodies can bind antigen presented on FDCs in immune complexes ensuring that BCRs on LZ GC B cells must compete to collect antigen (Zhang et al., 2013). This may imply that the GC reaction has an upper limit to the strength of its response after which cessation begins to occur due to an inability of GC B cells to outcompete secreted antibodies and receive positive selection signals.

1.5 Memory B cells

Activation of B cells results in the production of mBCs, these facilitate a strong response to previously encountered antigens. Exploitation of immune memory is an important facet behind vaccination. MBCs persist in the body in a quiescent state. They can mount a rapid, high affinity response to antigen upon a secondary exposure far greater than that of naïve B cells (Takemori et al., 2014). Upon antigen recognition mBCs can differentiate into PCs and GC B cells, IgG+ mBCs have a preference for differentiation into PBs and produce recall antigen-specific antibodies rapidly after exposure, whereas IgM+ mBCs tend to become GC B cells (Dogan et al., 2009).

Niches and residency of memory B cells is not fully elucidated (Palm and Henry, 2019). Some mBCs may be spleen resident, for example CD11c+ T-bet+ age-associated mBCs are spleen resident and provide responses to influenza hemagglutinin (Johnson et al., 2020). The spleen

is also a reservoir for circulating mBCs as vaccinia and smallpox specific mBCs are specifically enriched in the spleen and fewer of these mBCs are detected in the blood after splenectomy (Mamani-Matsuda et al., 2008). Some mBCs can also be found in the BM associating with VCAM1+ stromal cells (Riedel et al., 2020). MBCs are positioned at sites where they are likely to encounter antigen, which is why they can be found in the spleen and lymph node SCS (Palm and Henry, 2019, Mamani-Matsuda et al., 2008, Moran et al., 2018).

MBCs may not be strictly necessary for secondary GC response to antigen. A study using confetti labelled mice indicated that only a small proportion of the GC B cells in the secondary response are derived from mBCs produced in the primary response (Mesin et al., 2020). MBCs in culture have been observed to readily differentiate into PCs rather than GC B cells (Arpin et al., 1997). MBC differentiation into PCs is likely not entirely dependent on T cell interactions. Upon re-exposure to antigen in the lung during blockade of CD40-CD40L interactions, lung resident mBCs could still differentiate into PCs (Maclean et al., 2022). GCs produced in a recall response to antigen were mainly derived from naïve B cells (nBCs) rather than mBCs (Kuraoka et al., 2022).

MBC-derived PCs produce high affinity antibodies (Dogan et al., 2009). This may increase the selection threshold against the recall antigen in the GC by antibody feedback (Zhang et al., 2013). This would imply a more indirect role for mBCs rather than directly seeding a new GC but instead facilitating production of high affinity clones upon re-exposure by directing SHM. Resident mBCs in lung were observed after re-exposure to influenza antigen to home towards foci of infection, this was directed by alveolar macrophages due to expression of CXCL9 and CXCL10 which are ligands for CXCR3 expressed on lung resident mBCs. This was

followed by rapid differentiation of resident mBCs into PCs which secreted influenza specific antibodies (Maclean et al., 2022). Maclean et al., (2022) proposed that these PCs produced antibodies to assist with neutralisation of the virus as they appeared close to sites of viral replication. In the context of LN mBCs are observed to cluster towards the outer follicle and SCS but retain motility likely allowing them to seek out antigen. Upon activation these mBCs in the SCS readily differentiated into short-lived PCs that lacked motility and remained in SCS (Moran et al., 2018).

PC BCRs are of higher affinity towards the primary antigen than mBCs, however, mBCs are more able to bind antigenic variants of the primary antigen. PCs from mice immunised with West Nile virus (WNV) produced high affinity and strongly neutralising antibodies to primary antigen. Conversely, antibodies in supernatant from cultured WNV-stimulated mBCs displayed greater affinity and neutralisation of WNV mutant variant antigen than PCs (Purtha et al., 2011). The primary function of the mBC may be to grant the capacity for effective response to antigenic drift variants rather than a direct secondary response towards the same antigen. IgM+ mBCs are more prone to become GC B cells (Dogan et al., 2009). IgM BCRs tend to have fewer SHMs than IgG, IgA and IgE BCRs (Kitaura et al., 2017). This combined with the previously described cross-reactivity of mBCs with other antigens may imply a role for these IgM+ mBCs in a GC response to antigenic variants compared with IgG+ mBCs that have affinity matured to the primary antigen. The minority of mBC-derived GC-B cells described by Mesin et al. may have originated as IgM+ mBCs. MBC re-exposure to antigen can differ between whether re-exposed locally to or distant from the site of primary exposure (Kuraoka et al., 2022). Although distant or local re-exposure does not affect the magnitude of the antibody response, local exposures had greater levels of antigen-specific

antibodies, more SHM mutations and a greater participation of mBCs and persistent GC B cells in the secondary GC. Additionally, local re-exposure led to the production of more cross-reactive BCRs (Kuraoka et al., 2022).

The lower selection threshold for mBC fate (Suan et al., 2017) may facilitate a broader diversity of BCR specificities. This would allow them to rapidly mount a response upon encounter with an antigen variant of the primary exposure as described earlier (Purtha et al., 2011).

1.5.1 Memory B Cell Subtypes

There are many types of mBCs. Some are in circulation around the body and others have been found to be tissue resident. Lung-resident mBCs facilitate protection from exposure to inhaled pathogens such as influenza and locally produce early PBs in response to infection (Allie et al., 2019). mBCs can seed peripheral organs prone to exposure to pathogens (Palm and Henry, 2019). mBCs can be produced in the extrafollicular response these comprise the majority of IgM+ mBCs (Takemori et al., 2014). Naïve B cells and mBCs both exist in a state of quiescence until they encounter antigen. Upon activation they are fated for one of four outcomes: EF response to become EF PBs or EF mBCs or GC reaction to become PCs or mBCs. In mice, mBCs are distinguished from naïve B cells due to their activation resulting in CSR and the presence of mutations of the Ig V region conferring higher affinity specificity to antigen. mBCs can be defined as antigen-specific, non-PC CD38+ activated B cells. CD38 promotes internal signalling leading to Calcium influx mediated Bruton's tyrosine kinase activation (Kikuchi et al., 1995), ensuring that these cells are readily activated upon antigen encounter.

CD27 is frequently used as a marker for mBCs in humans. However, CD27 is not an appropriate marker of murine mBCs as in mice it is not upregulated in response to BCR ligation but is expressed to facilitate CD27-CD70 interactions of T cells with DCs (Tesselaar et al., 2003). In the case of CD8+ T cells this interaction induces proliferation (Keller et al., 2009). CD70 can activate a population of CD27+ T cells to negatively regulate CD70 expressing GC B cells (Beishuizen et al., 2009). Studies in mice can overcome this issue using several different methods.

NP-specific B cells after immunisation against NP-CGG can be used to distinguish mBCs. NP predominantly provokes an IgG1 response so IgG1-isotype BCRs can be used to help identify GC-derived mBCs (McHeyzer-Williams et al., 1991). Response to NP-CGG is well documented. mBCs produced from this response can persist for the entirety of the mouse's life. NP-CGG immunisation leads to the emergence of V186.2 clones in C57BL/6 mice (Bothwell et al., 1981). These clones can develop various mutations as their affinity changes, particularly at residues 33 and 95. Common point mutations include Trp33 to Leu and accumulation of Gly95 or Tyr95. Tyr95 W33L mutants confer an immediate higher affinity to NP-CGG by a factor of 10-fold, but over time these high affinity mBCs gradually became Gly95-type (Nishimura et al., 2011). Reporter mice can be used to distinguish mBCs. The Aicda-Cre reporter has been used to identify AID experienced B cells, this can delineate GC-derived mBCs (Crouch et al., 2007). Additionally, the Cg1-Cre reporter can also be used to identify activated B cells that have received cell signals from IL-4 and CD40L. This identifies GC B cells, PCs and mBCs that can be readily distinguished from one another using other markers (Casola et al., 2006). Another way to identify mBCs is by using the S1PR2$^{Cre/Ert2}$ Rosa26$^{fl\text{-}Stp\text{-}fl\text{-}dTomato}$ mouse (Shinnakasu et al., 2016). S1PR2 is an inhibitory receptor

expressed by activated B cells that plays a role in allowing them to cluster together to form a GC (Green et al., 2011). As such this reporter demarcates GC-derived B cells, and from this we can detect mBCs.

	IgM+ mBCs		IgG1+ mBCs
Abundance and Retention:	High		Low
	CD73+ represent antigen experienced		
PNA binding:	PNA+ GC-like	PNA+ and PNA- in both compartments	PNA- Located outside follicles
	IgM+ mBCs		**IgG1+ mBCs**
Preferential differentiation fate:	GC fate		Plasmablast fate
	CD80- PD-L2-	**CD80+ PD-L2-**	**CD80+ PD-L2+**
	Preferential GC fate	No preference for either fate	Preferential plasmablast fate
	Predominantly IgM+ mBCs		Predominantly IgG1+ mBCs

Figure 1. 6. Summary of characteristics of memory B cell subsets

Characteristics of mBC subsets based on expression of IgM, IgG1, CD80 and PD-L2. IgM+ mBCs are highly abundant and antigen experienced IgM+ mBCs are CD73+. IgG1+ mBCs are less abundant than IgM+ mBCs. While both IgM+ and IgG1+ mBC pools contain both PNA+ and PNA- cells the IgM+ mBCs were predominantly PNA+ which indicated that they were more GC-like, whereas IgG1+ mBCs were predominantly PNA- and were located outside of the follicles. During a recall response IgM+ mBCs preferred the GC fate and IgG1+ mBCs preferred the PB fate. The CD80 PD-L2 double negative mBC pool was predominantly IgM+ and in recall responses they preferred the GC fate, whereas double positive mBCs were predominantly IgG1+ and preferred the PB fate in recall responses. CD80+ PD-L2- mBCs had no preference either for GC or PB fates.

Mature mBCs can be differentiated into multiple subsets with distinct functions and behaviours. IgM+ mBCs are more abundant than IgG1+ mBCs and retain these larger

numbers for longer (Dogan et al., 2009). CD73+ mBCs represent antigen experienced IgM+ mBCs induced by CD40-CD40L interactions with Tfh cells (D'Souza et al., 2017, Tomayko et al., 2010). IgM+ and IgG1+ mBC compartments both contain both PNA+ and PNA- populations: PNA+ populations are very GC-like, whereas PNA- populations were located outside follicles. IgG1+ PNA- mBCs are found in splenic red pulp. IgM+ and IgG1+ mBCs had two distinct fates: IgM+ mBCs preferentially became GC B cells and IgG1+ mBCs were predisposed to become plasmacytes (Dogan et al., 2009). These IgG1+ mBCs had reduced expression of BTB domain and CNC homolog 2 (Bach2) ensuring less inhibition of Blimp-1, promoting differentiation to PC (Kometani et al., 2013). Expression of CD80 and PD-L2 can determine mBC function, CD80+ PD-L2+ mBCs are predisposed towards PB fate; IgG1+ mBCs are predominantly CD80+ PD-L2+. CD80- PD-L2- mBCs are predisposed to GC fate; these are predominantly IgM+. CD80- PD-L2+ mBCs had moderate preference to either fate (Zuccarino-Catania et al., 2014) (Fig. 1.6). High CD80 expression is the result of strong CD40-CD40L signalling in the GC B cell (Koike et al., 2019). This suggests that there is more nuance in selection of mBCs in the GC reaction than just affinity for antigen.

1.6 Lymphocyte patrol of SCS and marginal sinus

Many innate-like lymphocytes have been observed to migrate to the SCS in LNs and marginal sinus in the spleen. MZ B cells were positioned in the marginal sinus due to their expression of S1PR1 and S1PR3 allowing them to follow S1P chemokine gradients. MZ B cells were able to migrate to the GC follicle due to their expression of CXCR5. Through CD21-PE-labelling these cells were observed to shuttle antigen independent of BCR specificity to the follicle to

deposit on FDCs and then return to marginal sinus depending on a careful balance between CXCR5 and S1PR1/3 expression (Cinamon et al., 2008).

In the LN IL7-Rα^{hi}CCR6^{+} lymphocytes were observed in the SCS, this consisted of a mix of T cells and non-T cells, which rapidly produced IL-17 in response to challenge, however this was dependent on the presence of SCS macrophages. These IL7-Rα^{hi}CCR6^{+} shuttled back and forth between the SCS and parenchyma. SCS macrophages also maintained their presence in the SCS. Positioning of these cells in the SCS was dependent upon S1PR1. They found that the return of these cells to LN parenchyma was dependent on LFA-1-ICAM-1 interactions, as when these were deficient fewer IL7-Rα^{hi}CCR6^{+} were observed in the parenchyma and more could be found in the blood (Zhang et al., 2016).

The “flypaper” hypothesis describes SCS macrophages capturing antigen from the lymphatics, they can then transport antigen to the LN to facilitate the activation of an immune response (Junt et al., 2007, Bellomo et al., 2018). This is supported by the observation of SCS macrophages scavenging PE-immune complexes from the lymph to present back to the LN (Phan et al., 2009).

SCS macrophages are associated with follicles in the LN because they are dependent on B cell-derived lymphotoxin for survival, they are diminished in B cell deficient or lymphotoxin deficient conditions, whereas SCS macrophages were raised when lymphotoxin was over expressed (Phan et al., 2009). B cells can migrate to the SCS where they can obtain particulate antigen from SCS macrophages (Carrasco and Batista, 2007). Additionally, under conditions of CR1/2 (CD21/35)-deficiency among B cells and FDCs, antigen-specific B cells were found not to be transport competent and affinity maturation appeared to be impaired

(Phan et al., 2009). This suggests that B cells play a role in GC reaction by collecting antigen from SCS macrophages to drive affinity maturation and maintain SCS macrophages.

B cell movement to the SCS to interact with SCS macrophages includes mBCs. Intravital microscopy revealed that as mBCs move into the SCS they interact with CD169+ SCS macrophages before either exiting the LN via efferent lymphatics or returning into the follicle (Zhang et al., 2022). ACKR4 plays a role in migration of mBCs back from the SCS to the LN, likely following CCR7 ligand gradients. Intravital microscopy of ACKR4-deficient murine draining LN (drLNs) revealed that mBCs produced from the GC move to the SCS as normal (Zhang et al., 2022), but there was a failure to return to the LN and mBCs were retained in the SCS.

Lymphocytes have been observed in SCS of LN and marginal sinus of spleen and likely play a role in initial immune response as they encounter antigen arriving from the lymph or blood respectively.

1.7 Objectives and Aims

The general aim of this thesis is to improve the understanding of the migratory behaviours of GC-derived mBCs and how they participate in the response to antigen. Recent work is making great strides in uncovering how mBCs become reactivated upon re-exposure to antigen how they differentiate to respond directly to antigen as PBs or the measure in which they participate in the secondary GC reaction.

Chapter 3 will focus on the characterisation of early mBCs that emerged from GCs (BEMs), how they are produced in the drLN by examining the dynamics of generation and the gene

expression profile of BEM. Chapter 4 will investigate factors directing migration of BEMs in the drLN and discern the role BEMs play in response to antigenic variants. This is achieved and exploring the effect of ACKR4-KO mice and blockade of S1PR1. Chapter 5 will study the migration of BCMs to distant tissues and the role that CCR7 and its ligands play in this process.

2 Materials and Methods

2.1 Animals and Immunisations

Sex matched C57BL/6J (wild type, WT) mice (Wallace, 1950) at 6 to 12 weeks old, obtained from Harlan Laboratories, and were kept under specific pathogen free conditions in the Biomedical Services Unit, University of Birmingham. The University of Birmingham Ethics Committee AWERB (Animal Welfare Ethical Review Board) approved all procedures. Procedures were performed under the UK Home Office licenses PP8702596 and PEAE5FA92.

Igh-J$^{tm1(VDJ-17.2.25)Wabl}$ and Igk^{tm1Dhu} mice were crossed to produce quasimonoclonal (QM) mice with NP-specific BCRs when kappa light chains were not expressed (Cascalho et al., 1996). Crossing Igh-J$^{tm1(VDJ-17.2.25)Wabl}$ and Igk^{tm1Dhu} mice normally produces heterozygous mice at both loci, but these mice were made homozygous by further inbreeding (genotype: IgH$^{NP/NP}$ x k$^{-/-}$). QM mice were crossed with C.129P2(Cg)-Ighg1$^{tm1(cre)Cgn/J}$ (Casola et al., 2006) and Gt(ROSA)26Sor$^{tm4(ACTB-tdTomato,-EGFP)Luo}$ (Muzumdar et al., 2007) to produce QM Cg1cre mTmG mice (genotype: IgH$^{NP/Cre}$ x k$^{-/-}$ x mTmG), these have NP-specific B cells and are reporters for activation by switching from expression of membrane-bound tdTomato to GFP. QM and Gt(ROSA)26Sor$^{tm4(ACTB-tdTomato,-EGFP)Luo}$ (Muzumdar et al., 2007) mice were crossed to produce QM mTmG mice (genotype: IgH$^{NP/NP}$ x k$^{-/-}$ x mTmG). S1PR2$^{Ert2-Cre}$ were crossed with Rosa26$^{STOP-tdTomato}$ mice (Shinnakasu et al., 2016, Madisen et al., 2010) (genotype: S1PR2$^{Cre/wt}$ x Ai14-dTomato$^{+/wt}$). This produced a reporter mouse for GC-derived B cells: S1PR2-expressing cells began expressing tdTomato induced by tamoxifen. S1PR2cre x Ai14dT mice received oral gavage of tamoxifen in 200 µl corn oil (20 mg/mL) 48 hours prior to tissue collection. CCR7^{tm1Rfor} (Höpken et al., 2004) and Ackr4$^{tm1.1Rjbn}$ (Comerford et al., 2010) mice

were crossed with QM mice to produce QM CCR7-KO (genotype: $IgH^{NP/NP}$ x $k^{-/-}$ x $CCR7^{-/-}$) and QM ACKR4-KO mice (genotype: $IgH^{NP/NP}$ x $k^{-/-}$ x $ACKR4^{-/-}$), respectively. Additional mouse strains used include $Ccl19^{tm1Cys}$ CCL19-KO (Link et al., 2007), CCL21 $Ccl21^{tdTom}$ (Kozai et al., 2017) and C57BL/6J (WT) (Wallace, 1950). All strains were crossed at least 10 times with to C57BL/6 mice. See table 2.1 for summary.

For adoptive cell transfers 10^5 NP-binding B220+ splenocytes in 200 µl PBS from QM Cg1-Cre mTmG, QM mTmG mice, CCR7-KO x QM mTmG, CCR7-KO x QM Cg1-cre mTmG or ACKR4-KO x QM mTmG were transferred into recipients by i.v. These B cells possess a V_HDJH 17.2.25 segment, a targeted deletion of the k light chain allele, resulting in expression of a BCR specific for the NP hapten.

The appropriate level of splenocytes to transfer was calculated after fluorescence associated cell sorting (FACS) staining to determine the proportion of NP+B220+ splenocytes. Concentration of cell suspension was then adjusted to $5x10^5$ NP+B220+ cells per ml. Contaminating non-specific B cells and T cells were not removed from the cell suspension as it was assumed that they would not impact the response of the host, which had a complete and WT B and T cell repertoire. Additionally, non-antigen specific transferred B cells would not survive for long. Recipients were immunised within 24 hours of cell transfer unless otherwise specified.

Mice were immunised with alum precipitated or soluble (in PBS) NP_{31}-CGG, 4-hydroxy-3-iodo-5-nitrophenylacetyl $(NiP)_{25}$-keyhole limpet hemocyanin (KLH), NP_{23}-KLH, 2,4-dinitrophenylacetyl $(DNP)_5$-KLH, 2,4-dinitrophenylacetyl 2,4,6-trinitrophenylacetyl $(TNP)_{13}$-KLH (Biosearch Technologies, USA), Dengue envelope protein E1, Dengue envelope protein

E4 (Biorbyt, UK) or Rabbit IgG (Bio-Rad, USA) on plantar surface of hind foot. Some mice also received immunisation with alum precipitated KLH by i.p. injection and a booster injection of soluble NP-KLH by i.p. NP-CGG immunisations were provided with $1x10^5$ heat-inactivated *Bordetella pertussis* adjuvant (LEE Laboratories, USA) (Sze et al., 2000). Briefly, the alum precipitation protocol involved mixing together antigen in 1x PBS with an equal volume of 9% aluminium potassium sulphate (in ddH_2O), the pH was adjusted to 6.5-7.0 by adding 10 M NaOH. The mixture of antigen was left in dark on rotator for 1 hour at room temperature to allow precipitate to form. The precipitated antigen was washed in PBS 3 times and resuspended to the desired volume for doses.

To downmodulate S1PR1, mice received i.p. injections of FTY720 (Cayman Chemical) or BAF312 (APExBio) in PBS at a concentration of 1 mg/kg bodyweight at 48 hours and/or 24 hours prior to tissue collection.

For mice that were treated with goat anti-LIF (R&D Systems) or goat isotype control (Abcam), they received i.p. injections of 10 µg antibody in 200 µl PBS.

To explore the role of LIF mice received prime/boost immunisations. LIF was blocked by administration of 10 µg of goat anti-LIF (R&D Systems) or goat isotype control (Abcam) by i.p. injection on days 1 and 3 after boost. Tissues were collected at day 4 after boost as this is the expected peak of PCs (Sze et al., 2000).

Popliteal LN were analysed as reactive LN draining the site of injection (drLN), and axillary and brachial LNs were analysed as distant LN (distLN).

Strain Name	MGI Symbol	Supplied by	Reference
S1PR2-Cre	Tg(S1pr2-cre/ERT)#Kuro	Gift from Tomohiro Kurosaki (Osaka University)	(Shinnakasu et al., 2016)
Ai14dTomato	Gt(ROSA)26Sor$^{tm14(CAG-tdTomato)Hze}$	Jackson Labs (Stock: 007908)	(Madisen et al., 2010)
Cg1-Cre	Ighg1$^{tm1(cre)Cgn}$	Gift from Stefano Casola (Istituto FIRC di Oncologia Molecolare, Milan)	(Casola et al., 2006)
QM IgHNP	Igh-J$^{tm1(VDJ-17.2.25)Wabl}$ and Igk^{tm1Dhu}	Gift from Mathias Wabl (University of California, San Francisco, USA)	(Cascalho et al., 1996)
mTmG	Gt(ROSA)26Sor$^{tm4(ACTB-tdTomato, -EGFP)Luo}$	Jackson Labs (Stock: 007914)	(Muzumdar et al., 2007)
CCL21-KO	Ccl21a^{tm1Yout}	Gift from Graham Anderson (University of Birmingham)	(Kozai et al., 2017)
CCL19-KO	Ccl19^{tm1Cys}	Gift from Graham Anderson (University of Birmingham)	(Link et al., 2007)
ACKR4-KO	Ackr4$^{tm1.1Rjbn}$	Gift from Robert Nibbs (University of Glasgow)	(Comerford et al., 2010)
CCR7-KO	CCR7^{tm1Rfor}	Gift from Graham Anderson (University of Birmingham)	(Förster et al., 1999)
WT	C57BL/6J	Harlan Laboratories (Stock: 632c57bl/6j)	(Wallace, 1950)

Table 2. 1. List of genetically modified mouse strains.

2.2 Flow Cytometry

For examination of stromal cells and SCS macrophages LNs underwent digestion. Briefly, digestion involved teasing apart of LNs with a needle and placing them in a mix in a 2 mL tube containing 1 mL of digestion media (1 mL of 10% FBS in RPMI 1640, 25 µL Collagenase D 10 mg/ml (Sigma) and 4 µL DNase I 10 mg/ml (Sigma)). This was incubated in a heat block at

36 °C with shaking at 700 RPM for 20 minutes. Solution was mixed by aspiration with a pipette and placed back on the heat block for a further 25 minutes. If not fully digested the solution was mixed by aspiration with a pipette and place back on heat block for another 10 minutes. Then 15 µL EDTA (500 mM) was added, and the digested solution was on ice for 5-10 minutes. Digested solution was then filtered into 15 mL tubes and 5 mL FACS buffer (1x PBS with 1% FCS and 2 mM EDTA) was added. Digested solution was prepared for FACS as normal.

Tissues were macerated into single cell suspensions and transferred to 250 µl 96-well V-bottom plate. Single cell suspensions received anti-mouse CD16/32 (93) at 2.5 µg/ml (eBioscience) as blocking buffer for 25 minutes. Single cell suspensions were then stained with biotinylated antibodies where applicable followed by staining with the antibody cocktail including streptavidin conjugated fluorophore. Finally, they received fixable Near-IR Live/Dead staining (Invitrogen) as per manufacturer's instructions. Fixation was avoided in most cases where possible but when required BD Cytofix (BD Biosciences) was used as per manufacturer's instructions. In between each step, cells were washed twice in FACS Buffer and centrifuged at 150 x g for 5 minutes.

For EdU staining, the protocol provided in the Click-iT EdU Alexa Fluor 647 Flow Cytometry Assay Kit (Invitrogen) was used. Briefly, Fc block was used as normal, extracellular staining did not include PE or PE-tandem dyes, viability stain applied as normal. Washed in 1X PBS with 1% BSA, resuspended in Click-iT fixative and incubated for 15 minutes at room temperature in the dark, then washed again. Pellet was resuspended in 1x Click-iT saponin-based permeabilization/wash buffer (wash buffer), incubated for 15 minutes at room

temperature in the dark. Washed in wash buffer and resuspended in the reaction cocktail (in 60 µL for each sample: 43.8 µL PBS, 1 µL $CuSO_4$, 0.25 µL Click-iT Alexa Fluor 647, 5 µL 1x Click-iT EdU buffer and 10 µL wash buffer), incubated for 30 minutes at room temperature in the dark, then washed in wash buffer. Stain PE and PE-tandem dyes in FACS buffer were added as normal, then washed in FACS buffer. Samples were transferred to FACS tubes and analysed as normal.

Samples were acquired by flow cytometry on LSR Fortessa and LSR Fortessa X-20 (BD Biosciences). Please see table 2.2 below for detailed list of antibodies used. FACS data was analysed using FlowJo v10 (BD).

Specificity	Fluorophore/Conjugate	Clone	Supplier	Catalogue No	Dilution
B220	APC-Cy7	RA3-6B2	BioLegend	103224	1/1000
B220	BUV395	RA3-6B2	BD	563793	1/800
B220	BV510	RA3-6B2	BioLegend	103247	1/200
BAFF-R (CD268)	APC	7H22-E16	BioLegend	134105	1/300
BCL-6	PE-Cy7	K112-91	BD	563582	1/300
Biotin	Streptavidin-AlexaFluor647	-	eBioscience	554067	1/500
Biotin	Streptavidin-BV421	-	BioLegend	405226	1/300
Biotin	Streptavidin-PE-Cy7	-	BioLegend	405206	1/750
CCR6	BV785	29-2L17	BioLegend	129823	1/200
CCR7	AlexaFluor647	4B12	Serotec	MCA2367A647	1/100
CD11a	Biotin	M17/4	BD	557455	1/200
CD11b	PerCP-Cy5.5	M1/70	BD	550993	1/500
CD11b	BV510	M1/70	BioLegend	101245	1/200
CD11c	PE	HL3	BD	553802	1/500
CD138	BV711	281-2	BioLegend	142519	1/500
CD157 (BP3)	APC	BP3	BioLegend	140208	1/400
CD16/32	-	93	eBioscience	14-0161-86	1/200
CD169	Alexa Fluor 647	3D6.112	BioLegend	142408	1/400
CD19	BUV737	1D3	BD	612781	1/800
CD24	Biotin	30-F1	BD	555296	1/500
CD3	BV510	17A2	BioLegend	100233	1/400
CD3	PE-Cy7	145-2C11	BioLegend	560591	1/300
CD31	BV605	390	BioLegend	102427	1/200
CD38	AlexaFluor647	90	BioLegend	102715	1/1000
CD38	AlexaFluor700	90	eBioscience	56-0381-82	1/600
CD38	Biotin	90	BD	553762	1/200
CD38	BUV737	90	BD	553762	1/1000
CD38	eFluor450	90	eBioscience	741748	1/500
CD38	PerCP	90	BioLegend	102722	1/300
CD38	FITC	90	BioLegend	102705	1/1000
CD4	BV711	GK1.5	BD	563050	1/400
CD4	AlexaFluor700	GK1.5	Invitrogen	56-0041-82	1/500
CD4	BV421	GK1.5	BioLegend	100438	1/400
CD45	PerCP-Cy5.5	30-F11	BioLegend	103132	1/200
CD55 (DAF)	APC	REA300	Miltenyi Biotec	130-104-056	1/100
CD55 (DAF)	PE-Vio770	REA300	Miltenyi Biotec	130-104-054	1/100
CD62L	BV510	MEL-14	BioLegend	104441	1/200
CD62L	PE-Cy7	MEL-14	eBioscience	25-0621-82	1/200
CD69	FITC	H1.2F3	eBioscience	11-0691-82	1/200
CD69	PE-Cy7	H1.2F3	eBioscience	25-0691-82	1/200
CD73	PE-Cy7	TY/11.8	eBioscience	25-0731-82	1/500
CD80	BUV737	16-10A1	BD	612773	1/100
CD80	FITC	16-10A1	eBioscience	11-0801-81	1/100

CD80	PE-Cy5	16-10A1	eBioscience	15-0801-82	1/200
CD86	PE-Cy7	GL1	eBioscience	25-0862-82	1/500
CD86	PE	GL1	eBioscience	12-0862-81	1/200
Cell Viability	Near Infrared	-	Invitrogen	L10119	1/1000
CXCR3	BV421	174	BioLegend	126521	1/200
CXCR4	Biotin	2B11	BD	13-9991-82	1/300
EpCAM-1	PE-Cy7	G8.8	eBioscience	25-5791-80	1/100
Ephrin B1	Biotin	Polyclonal	R&D Systems	BAF473	1/100
F4/80	FITC	BM8	eBioscience	11-4801-82	1/400
Fas	BV605	Jo2	BD	740367	1/300
Fas	PE-Cy7	Jo2	BD	557653	1/200
FCRL5 (CD307)	APC	Polyclonal	R&D Systems	FAB6757A	1/10
GL7	eFluor450	GL-7	eBioscience	48-5902-82	1/100
GL-7	eFluor450	GL-7	eBioscience	48-5902-82	1/200
Gp38 (Podoplanin)	Alexa Fluor 488	8.1.1	eBioscience	53-5381-82	1/100
IgD	BV421	11-26c.2a	BioLegend	405725	1/200
IgD	BV510	11-26c.2a	BioLegend	405723	1/200
IgD	FITC	11-26c.2a	BD	553439	1/300
IgD	eFluor450	11-26c	eBioscience	48-5993-82	1/200
IgG1	APC	X56	BD	550874	1/1000
IgG1	PerCP-Cy5.5	RMG1-1	BioLegend	406612	1/200
IgM	PE-Cy7	RMM-1	BioLegend	406514	1/200
IgM	PE-Cy7	II/41	eBioscience	25-5790-82	1/500
IgM	BV510	II/41	BD	743324	1/300
MadCAM-1	Biotin	MECA367	BioLegend	120706	1/200
NP-specific	NP-APC	-	In House	-	1/600
NP-specific	NP-PE	-	Biosearch Technologies	N-5070-1	1/100
NP-specific	NP-FITC	-	Biosearch Technologies	N-1030-1	1/200
NP-specific	NP-CGG-FITC	-	Biosearch Technologies	N-5055F-1	1/200
PD-L2	BV421	TY25	BioLegend	107219	1/100
PD-L2	Biotin	TY25	BioLegend	107203	1/200
PE	Biotin	PE001	BioLegend	408104	1/200
PECAM-1 (CD31)	APC	390	Miltenyi Biotec	130-123-813	1/100
PECAM-1 (CD31)	PE-Vio770	390	Miltenyi Biotec	130-104-054	1/100
Rat IgG2a	Biotin	MRG2a-83	BioLegend	407503	1/100
S1PR1	-	713412	R&D Systems	MAB7089-SP	1/10
SLAMF7 (CD319)	APC	4G2	BioLegend	152003	1/300
Ter119	PerCP-Cy5.5	TER-119	BioLegend	116228	1/200

Table 2. 2. List of antibodies used for FACS staining including the dilution factor used.

2.3 Indirect ELISA

Blood from cardiac punctures were incubated at 37°C for 1 hour and centrifuged in Heraeus Biofuge Fresco at 21,100 x g for 10 minutes. Serum was aspirated from supernatant and stored in a freezer at -20°C.

Plates were coated with 5 µg/ml of protein/antigen in 100µl per well using coating buffer at pH 9.6 (15 mM Na_2CO_3 and 35 mM $NaHCO_3$). In between steps, ELISA plates were washed in Wash Buffer (1x PBS and 0.05% Tween 20). Plates were blocked in Blocking Buffer (1% BSA in 1x PBS) for 1-1.5 hours at 37°C or overnight at 4°C. Serum was diluted in dilution buffer (1% BSA in 1x PBS and 0.05% Tween 20) to a starting dilution of between 1:50 to 1:200 depending on the experiment. This was followed by a serial dilution of 1 in 3 across the plate. Serum from a non-immunised mouse used a negative control and serum from one immunised mouse was consistently used as the positive control. Serum was incubated for 1.5 hours at 37°C. Alkaline Phosphatase-conjugated antibody was used at the following dilutions:

Goat anti-IgG, Human ads-AP (Southern Biotech), 1/1000

Goat anti-IgG1, Human ads-AP (Southern Biotech), 1/2000

This was incubated for 1 hour at 37°C.

Finally, alkaline phosphatase substrate was added (Sigma) and incubated for 20 to 60 minutes. At the endpoint, the reaction was quenched with 1.5 M NaOH. Plates were read at 405 nm using SpectraMax ABS Plus (Molecular Devices) microplate reader.

To investigate serum antibody titres for Denv-4 serum was either directly incubated to Denv-4 or previously exposed to Denv-1-coated plate to cause adherence of Denv-1 specific and cross-reactive antibodies before incubating with Denv-4 coated plate.

2.4 Histology

LNs were fixed in 1% PFA for 8 hours or overnight in the fridge, followed by rehydration in 30% sucrose overnight before being flash frozen with dry ice. LNs were sectioned at 6 µm using the OTF5000 Cryostat (Bright Instruments). Sections were stored in a -20°C freezer. Immunostaining of LNs took place in a humid chamber in darkness at room temperature. First slides were removed from the freezer and allowed to air dry for 10-20 minutes. The borders were drawn around tissues with a hydrophobic pen. Slides were washed in wash buffer (1x PBS containing 0.5 % Saponin) for 10 minutes. Staining antibodies were prepared in dilution buffer (1X PBS and 2% BSA). Primary unconjugated and Biotin-conjugated antibodies were added and incubated for 1 hour. Slides were washed in wash buffer for 10 minutes, then fluorophore-labelled secondary antibodies, fluorophore-conjugated streptavidin and fluorophore-labelled primary antibodies were added and incubated for 45 minutes. Slides were washed in wash buffer for 10 minutes. Sides were mounted with ProLong Diamond anti-fade mountant (Thermo Fisher) and left to dry in dark at room temperature overnight.

Images were taken of the immunostained slides by using a ZEISS Axioscan 7 slide scanning fluorescence microscope (Zeiss). Images were analysed using Zen Blue software (Zeiss).

2.5 Light Sheet Microscopy

Zeiss Lightsheet Z.1 (Zeiss) was used to image popliteal lymph nodes. These were stained *in vivo* by injection of fluorescently labelled antibodies on plantar surface of foot 30 minutes prior to collection. Imaging took within 30 minutes after collection:

1 µg Alexa647 anti-mouse CD169 (3D6.112) (BioLegend) was used to label SCS macrophages. Draining popliteal LNs were freshly harvested and then embedded in 1% agarose in 1X PBS.

To image transfer of immune complex into the GC, S1PR2-Cre Ai14dTomato mice were injected with 10 µg of rabbit IgG in alum precipitate. On day 8 post-immunisation 2 µg of fluorescently labelled immune complex was administered by plantar surface injection on the rear foot 2 hours prior to tissue collection.

Alexa488 Rabbit IgG Immune Complex was composed of equal amounts of purified Rabbit IgG (Bio-Rad; Cat no: PRABP01) and Alexa488 labelled anti-rabbit IgG (Jackson Immunoresearch; Cat no: 211-545-109). This was mixed well 30 minutes before the injection.

Tissues were imaged with 20x and 40x objective lens. Light sheet data was analysed using Vision4D (Arivis).

2.6 RNA Sequencing

B cells from QM Cg1-Cre mTmG were adoptive transferred into C57BL/6 recipients. These recipients were immunised with NP-CGG in alum precipitate on hind feet. B cell subsets were cell sorted from these mice at day 8 post-immunisation using FACS Aria Fusion (BD

Biosciences). Single cell suspensions from lymph nodes were stained with propidium iodide (Invitrogen) live/dead marker and respective antibodies in FACS buffer (1x PBS with EDTA and FCS). Cells were directly sorted into 500 µl of TRIzol (Invitrogen). The total RNA was purified using the RNeasy Plus Micro kit (QIAGEN) according to the manufacturer's instructions. GC B cells and emigrating mBCs were sorted from drLN 8 days post-immunisation (LN from 4 mice were pooled together). Non-activated naïve B cells (nBCs) and circulating mBCs in distLN were also sorted. GC B cells were defined as GFP+B220+CD38-Fas+, mBCs in drLN as GFP+B220+CD38+Fas^{low}CD138-, mBCs in distLN as GFP+B220+CD38+CD138- and naïve B cells in distLN as GFP-Tomato+B220+. Un-stranded, non-rRNA, non-polyA+ selected libraries were prepared by SMARTer Ultra Low Input RNA kit for Sequencing v3 (Clontech Laboratories). The libraries were sequenced using Illumina HiSeq 2000 platform (Illumina, Crick advanced sequencing) at 75 base pair end runs.

Reads were aligned against the GRCm38 (mm10) genome assembly with Ensembl release 86 transcript annotations. Expected gene-level counts were calculated using STAR v2.7.3a (Dobin et al., 2013) or Partek Flow v8.0.19 (Partek Inc., St. Louis, MO, USA). RNA-sequencing data was then analysed using R version 4.2.0 hosted by RStudio (2022.02.02+485) and its associated packages (RStudioTeam, 2020, R-Core-Team, 2022).

Read counts were denoised using the package noisyR (Moutsopoulos et al., 2021). RNA sequencing data was normalised by regularised log transformation and differential gene expression calculated using DESeq2 (Love et al., 2014). Graphs were produced using ggplot2 (Wickham, 2016). Gene set enrichment analysis was performed using GSEA v7.4 (MSigDB).

2.7 Antigenic Drift

Antigenic drift was modelled using haptens with gradually decreasing similarity to the hapten that has the highest affinity to the canonical VDJ recombination that emerges after immunisation if C57BL/6 mice with NP-protein. Mice were immunised with 10µg alum precipitated NiP_{25}-KLH followed by injections of 1 µg soluble NP_{23}-KLH in PBS on day 8 post-immunisation, followed by 1 µg of soluble DNP_5-KLH on day 10, and 1 µg of soluble TNP_{13}-KLH on day 12 (antigens from Biosearch Technologies), vein bleeds were collected prior to boosting injections.

To study antigenic drift in the context of Dengue viral proteins mice were immunised with 1 µg alum precipitated recombinant Denv-1 nuclear protein (E1) (Biorbyt) and a boost injection of 1 µg soluble recombinant Denv-1 or Denv-4 (E4) nuclear protein (Biorbyt) in PBS.

2.8 Data Analysis

Graph were produced and statistical tests conducted using Prism 9 (GraphPad). Data from multiple experiments were combined after normalising to the ratio of the median of the control sample as specified using the formula:

$$Normalised\ Ratio = \frac{sample\ frequency}{Median\ frequency\ of\ control\ samples}$$

2.9 Materials Lists

Item	Description	Supplier	Cat No
1x DPBS w/ Ca and Mg	Dulbecco's Phosphate Buffered Saline with CaCl2 and MgCl2	GibCo	14040-091
1x DPBS w/o Ca and Mg	Dulbecco's Phosphate Buffered Saline without CaCl2 and MgCl2	GibCo	14190-094
1x RPMI	RPMI 1640 Medium	GibCo	21875-034
PBS tablets	1 tablet in 500 mL dH2O produces 1x PBS	GibCo	18912-014
BD Cytofix Fixation Buffer	4.2% PFA	BD Biosciences	554655
Rat Serum	Normal Rat Serum	Sigma	R9759-5ML
FBS	Fetal Bovine Serum	Sigma	F7524-500ML
Tamoxifen	Dissolved in Corn Oil to 30 mg/ml. 200 ul per dose	Sigma	T5648-1G
BAF312 (Siponimod)	S1P1 receptor agonist	APExBio	B3225
FTY720 (Fingolimod)	S1P receptor agonist (Batch no: 0476039-22)	Cayman Chemicals	10006292
DMSO	Dimethyl Sulfoxide	Sigma	D8418-100ML
EDTA	Ethylenediaminetetraacetic acid	Sigma	E7889-100ML
ACK Lysing Buffer	Lysis of red blood cells	GibCo	A1049201
BSA	Bovine Serum Albumin	Sigma	A7906-100G
Tween20	Nonionic detergent	Sigma	P1379-500ML
B. Pertussis	Heat-inactivated *bordetella pertussis*	LEE Laboratories	9042741
Denv-1 (E1)	Dengue virus serotype 1 recombinant envelope Protein (45 kDa)	Biorbyt Ltd	orb81818
Denv-2 (E2)	Dengue virus serotype 4 recombinant envelope Protein (45 kDa)	Biorbyt Ltd	orb81821
NP-CGG	4-Hydroxy-3-nitrophenylacetyl hapten conjugated to CGG (Lot No: 139439-05)	Biosearch Technologies	N-50550-5

NP-KLH	4-Hydroxy-3-nitrophenylacetyl hapten conjugated to KLH (Lot No: 016720-06)	Biosearch Technologies	N-5060-5
NiP-KLH	4-Hydroxy-3-iodo-5-nitrophenylacetyl hapten conjugated to KLH (Lot No: 018910-01)	Biosearch Technologies	N-5042-5
DNP-KLH	2,4-Dinitrophenyl hapten conjugated to KLH (Lot No: 052223-13)	Biosearch Technologies	D-5060-5
TNP-KLH	2,4,6, Trinitrophenyl hapten conjugated to KLH (Lot No: 104635-02)	Biosearch Technologies	T-5060-5
NP2-BSA	4-Hydroxy-3-nitrophenylacetyl hapten conjugated to BSA in house	In House	-
NP14-BSA	4-Hydroxy-3-nitrophenylacetyl hapten conjugated to BSA, Ratio 14 (06639-12)	Biosearch Technologies	N-5050M-10
TNP2-BSA	2,4,6-Trinitrophenyl hapten conjugated to BSA, Ratio 2 (052048-07)	Biosearch Technologies	T-5050-10
TNP35-BSA	2,4,6-Trinitrophenyl hapten conjugated to BSA, Ratio 35 (116384-01)	Biosearch Technologies	T-5050-10
IgG-AP	Goat Anti-Mouse IgG, Human ads-AP (Polyclonal). Used at a dilution of 1/1000.	Southern Biotech	1030-04
IgG1-AP	Goat Anti-Mouse IgG1, Human ads-AP (Polyclonal). Used at a dilution of 1/2000.	Southern Biotech	1070-04
AP Substrate	SIGMAFAST p-Nitrophenyl phosphate Tablets	Sigma	N2770-50SET
NaOH	Sodium Hydroxide	Sigma	55881-1KG
Click-iT EdU Alexa Fluor 647 Flow Cytometry Assay Kit	Contains EdU, Alexa Fluor 647 azide, DMSO, Click-iT fixative, Click-iT saponin-based permeabalisation and wash buffer, CuSO4 and Click-iT EdU buffer additive	Invitrogen	C10424

MaxiSorp Flat-Bottom Immuno Nonsterile 96-Well Plates		Thermo Fisher	442404
Histology Slides	Epredia SuperFrost Plus Slides	Fisher Scientific	J1800AMNZ
Low-Melting Agarose	Agarose, low gelling temperature	Sigma	A9414-25G
10x TBE	UltraPure 10x TBE buffer	Invitrogen	15581-044
THF	Tetrahydrafuran, anhydrous	Sigma	186562-100ML
DBE	Dibenzyl ether	Sigma	33630-250ML
DCM	Dichloromethane, anhydrous	Sigma	270997-100ML
Ethyl Cinnamate		Merck	8.00238.0250
BD Brilliant Stain Buffer		BD Biosciences	563794
GFP BrightComp eBeads	GFP Compensation Beads	Invitrogen	A10514
Penicillin Streptomycin		GibCo	15140-122
ProLong™ Gold Antifade Mountant	Slide Mounting Media	Thermo Fisher	P10144
Aluminium Potassium Sulphate	Aluminium Potassium Sulfate, Extra Pure, SLR, Fisher Chemical	Fisher Scientific	11443713
DNAse I	Bovine pancreatic deoxyribonuclease I	Sigma	DN25-100MG
Collagenase D		Sigma	11088866001
Saponin		Sigma	84510-100G
Alexa Fluor 488 AffiniPure Mouse Anti-Rabbit IgG	Polyclonal	Jackson Immunoresearch	211-545-109
Purified Rabbit IgG	Polyclonal	Bio-Rad	PRABP01
Goat anti-LIF antibody	Polyclonal, Goat. Leukaemia inhibitory factor specific	Biolegend	674702
Purified Goat IgG, Isotype Control	Polyclonal	Abcam	ab37373
Diphtheria Toxin from Corynebacterium diphtheriae		Sigma	D0564

Table 2. 3. List of materials used in the experiments described in this thesis.

Equipment Name	Supplier	Description
OTF5000 Cryostat	Bright Instruments	Cryosectioning tissues
LSRFortessa X-20 Cell Analyser	BD Biosciences	Flow Cytometer
LSRFortessa Cell Analyser	BD Biosciences	Flow Cytometer
ZEISS Lightsheet Z.1	Zeiss	Light Sheet Microscope
UltraMicroscope II	LaVision BioTec	Light Sheet Microscope
SpectraMax ABS Plus	Molecular Devices	Absorbance ELISA Microplate Reader
ZEISS Axioscan 7	Zeiss	Slide Scanner

Table 2. 4. List of equipment used for data acquisition.

Software Name	Version	Company	Description
FlowJo	10.8	BD Biosciences	Analysis of flow cytometry data
Vision4D	3.5	Arivis	Analysis of light sheet images
Prism	9	GraphPad	Data presentation and statistical analysis
Zen Blue	1.1.2.0	Carl Zeiss Microscopy	Analysis of microscopy images
Rstudio	2022.02.02+485	R Foundation for Statistical Computing	Interface hosting R v4.2.0.

Table 2. 5. List of software used for data processing and analysis.

3 Emigrating memory B cells within the draining lymph node

3.1 Introduction and Objectives

The outputs of the GC response are PCs and mBCs. In the spleen, the B cell response mainly occurs in the B cell areas or follicles of the PALS. The peak of the primary GC response in the spleen and the LN to NP-protein has been previously recorded to peak at around 8 days post-immunisation (Jacob et al., 1991). The response to NP-protein is largely IgG1+ (Toellner et al., 1998). Understanding the dynamics of the GC response can help in identifying optimal times to examine the response, as flow cytometry shows a snapshot of the response at the time of sample collection. Resting mBCs have been seen in the LN SCS by light sheet microscopy (Moran et al., 2018). Recently we showed that early GC-derived mBCs could migrate out from GC LZ through follicles into the SCS. Some of these mBCs moved back to the GC and others egressed the LN via the SCS (Zhang et al., 2022). In the present study mBCs undergoing migration within the drLN are referred to as BEM, and GC-derived mBCs that were observed outside of the reactive LN are referred to as BCMs.

Laidlaw et al. (2017) described a group of GC B cells that were S1PR2^{low} and Ephrin B1+ cells, that also express high levels of CD38 and were defined as pre-memory B cells. These cells also expressed high levels of CCR6, CCR7, S1PR1, CXCR3, GPR183 (EBI2) and SELL (CD62L) (Laidlaw et al., 2017). BACH2 expression in low affinity LZ GC B cells marked out a group of GC B cells pre-disposed to differentiate into mBCs. These cells upregulated CCR6, CD38, CD72 and PECAM1, amongst others (Shinnakasu et al., 2016). Suan and colleagues also observed CCR6-expressing low affinity LZ GC B cells that readily differentiated into mBCs (Suan et al., 2017). These memory B cells or pre-cursor mBCs have been observed during the primary GC response. Evaluation of the gene expression profiles of these can help to reveal

the cell subset, signals regulating cell differentiation and migration, and provide hints to the functions and behaviours of these memory B cells.

This chapter aims to investigate the timings and dynamics of the GC response in the popliteal LN (as drLN) and in the spleen, and mBCs in distant lymphatic tissues e.g., non-reactive distLN and spleen. RNA-sequencing analysis of nBCs, GC B cells, BEMs and BCMs was performed to determine the similarities and differences of gene expression between these groups. This RNA-sequencing data was used to inform the selection of markers to distinguish BEMs from GC B cells.

This chapter investigated the following hypotheses:

1. The dynamics of the GC response to NP and generation of BEMs in the spleen differs from the dynamics in the drLN.
2. BEMs have a distinct gene expression profile from nBCs, GC B cells and BCMs.
3. Cell surface markers can be used to distinguish BEMs from GC B cells and nBCs in the drLN and spleen.

3.2 Results

3.2.1 The dynamics of memory B cell development in the draining lymph node over time

During the immune response it is important to understand the dynamics and timings of the mBCs developed from GCs. This assists determining the optimum time to investigate the development of mBCs in future experiments. The dynamics of the mBC development was investigated using the QM IgHNP Cg1-Cre mTmG adoptive cell transfer system. These NP-

specific B cells are reporters for activation of B cells by expression of Cre under the IgG1 germline transcript. Ig heavy chain germ line transcripts are induced by signals like CD40 ligation and IL-4. These are generated after cognate interactions with activated CD4 T cells after immunisation with the NP antigen (Toellner et al., 1996). Resultantly, antigen-activated B cells change from constitutively expressing membrane-bound tdTomato to membrane-bound GFP. Class switching mainly occurs prior to the formation of the GC (Roco et al., 2019, Toellner et al., 1998, Marshall et al., 2011). Therefore, this reporter model did not just label GC-derived B cells but also labelled B cells activated after cognate interactions with CD4+ T cells. The peak response of the IgG1+ B cells occurred at 8 days post-immunisation. Furthermore, levels of Cg1 germline transcript increased rapidly between 3 and 5 days post-immunisation before reaching a peak at 8 days post-immunisation (Toellner et al., 1998). Therefore, the QM IgHNP Cg1-Cre mTmG mouse strain can be used as a tool to track mBCs and PCs produced in response to NP antigen.

Wild-type mice received adoptive cell transfer with QM IgHNP Cg1-Cre mTmG splenocytes followed by foot immunisation with NP-CGG. Popliteal drLN, spleen and distLN were collected on 4-, 7-, 10- and 14-days post-immunisation (Fig. 3.1A). The DrLN was examined by flow cytometry to quantify GFP+ B cells, PCs, GC B cells and a population of CD38+ activated B cells referred to as BEMs (Fig. 3.1B). Firstly, in the drLN, adoptively transferred GFP+ B cells and PCs were examined between 4-14 days post-immunisation (Fig. 3.1C). GFP+ B cells in drLN were detectable only at low levels until 7 days post-immunisation when numbers peaked. GFP+ B cells decreased 8-fold by 10 days post-immunisation and reduced a further 18-fold by 14 days post-immunisation (Fig. 3.1D). When observing GFP+ B cells measured as proportion of all adoptively transferred cells (GFP+/Tomato+), some were

detected at 4-days and reached peak levels at 7 days post-immunisation. They decreased 7-fold by 10 days and reduced a further 7.5-fold at 14 days post-immunisation (Fig. 3.1E). GFP+ PCs in the drLN followed a similar trend with a peak at 7 days, reduced 52-fold by 10 days and were not detectable, except for a very low number in one sample at 14 days post-immunisation (Fig. 3.1F). This pattern was also seen among the GFP+ PCs measured as a proportion of GFP+/Tomato+ cells, with a peak at 7 days post-immunisation, by 10 days post-immunisation there was a 32-fold reduction, and few were detectable at 14 days post-immunisation (Fig. 3.1G). There was a PC response that peaked at 8 days post-immunisation, these likely share similarities to previous studies in which there was a strong IgG+ PB response at 8 days post-immunisation in the drLN (Toellner et al., 1998). It is likely that most of these PCs that arose in response to NP are also IgG1+.

The dynamics of GFP-expressing transferred MBCs and GC B cells were detected by flow cytometry (Fig. 3.2A). GFP+ GC B cells were at very low levels at 4 days post-immunisation, and then reached a peak at 7 days. They decreased 8-fold by 10 days post-immunisation and decreased a further 15-fold by 14 days post-immunisation (Fig. 3.2B). MBCs (identified as GFP+B220+CD138-CD38+) in drLN followed the same pattern as GC B cells with a peak at 7 days post-immunisation, decreased 6-fold by 10 days and a further 70-fold by 14 days post-immunisation (Fig. 3.2C). We have shown that these early GC-derived mBCs are different from mBCs in the distLN, therefore these mBCs in drLN are described as mBCs emerging from GC (BEMs) (Zhang et al., 2022).

The expression of NP-specific BCRs ensured that the majority of GFP+ cells were antigen specific; this confirmed that these cells were GC B cells, PCs or mBCs produced in response

to immunisation. These experiments showed that the peak of the antigen specific GC response was at around 7 days post-immunisation.

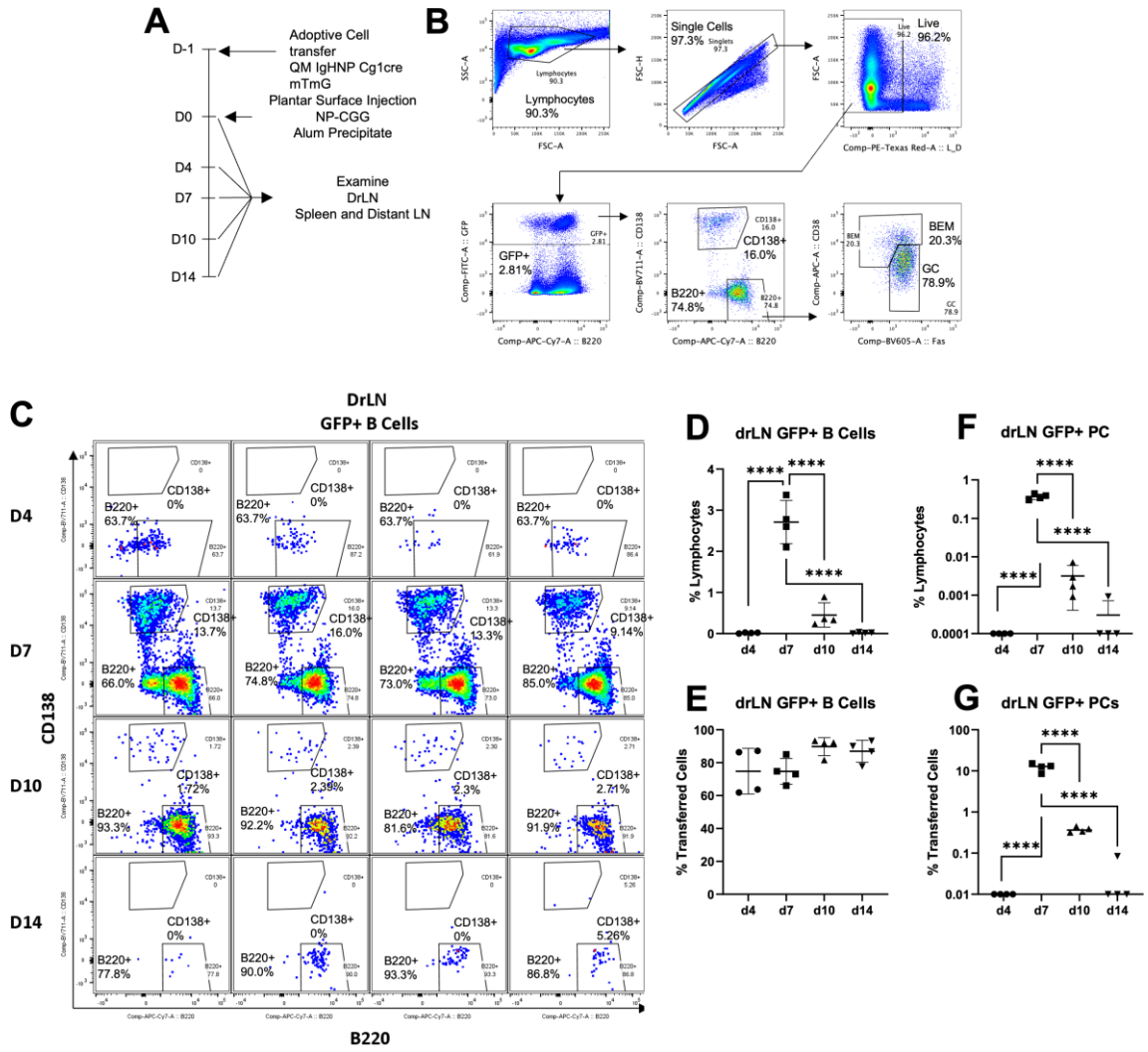


Figure 3. 1. In the drLN peak levels of B cells and PCs was at 7 days post-immunisation

(A) Experiment schematic to measure response of GCs and PCs in the drLN over time. See Appendix 1A for baseline adoptive cell transfer input data. (B) Gating strategy to identify B cells, PCs, GC B cells and BEMs in the drLN. (C) Flow cytometry raw data for GFP+ B cells and GFP+ PCs from total GFP+ live cells in the drLN. Summary of total B cells (GFP+B220+CD138-) in the drLN measured as (D) % live lymphocytes and (E) % transferred cells (GFP+ and/or dTomato+). Summary of GFP+ PCs (GFP+CD138+) in the drLN measured as (F) % live lymphocytes and (G) % transferred cells (GFP+ and/or dTomato+). Data presented are from one experiment (n=4). One-way ANOVA, **** $P < 0.0001$. Symbols represent individual mice. Horizontal bars show means. In this experiment mice were given adoptive cell transfers, immunised and tissues collected by Yang Zhang.

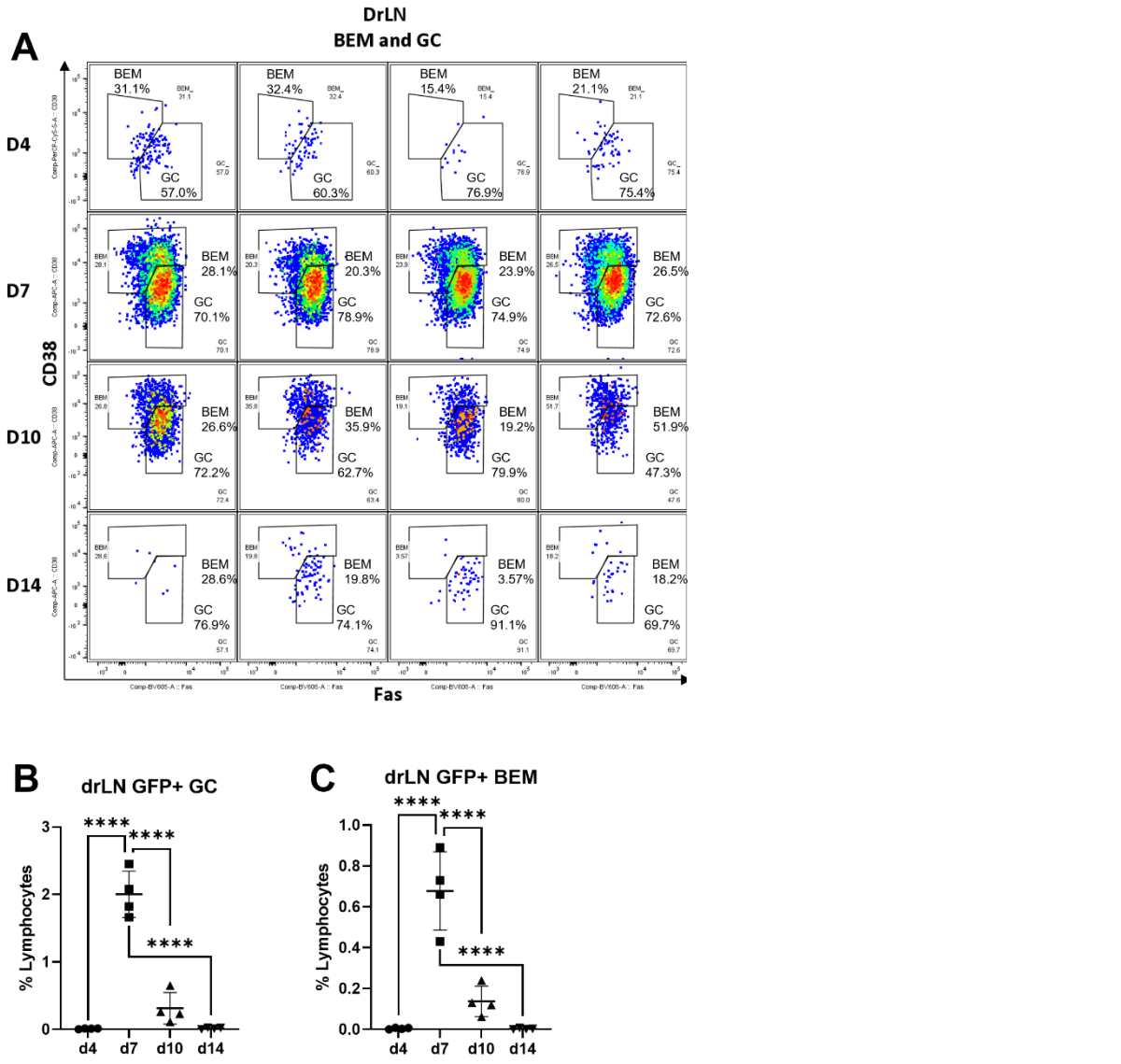


Figure 3. 2. Peak GCs and BEM production at 7 days post-immunisation in drLN

(A) Flow cytometry plots of BEMs (CD38+) and GC B cells (CD38-Fas+) gated from GFP+B220+CD138- cells in the drLN at days 4, 7, 10 and 14 post-immunisation. The GC gate on day 4 was larger due to a weaker voltage setting. (B) Summaries of GC B cells in the drLN measured as % lymphocytes. (C) Graphical summaries of BEMs in the drLN measured as % lymphocytes. Data presented are from one experiment (n=4). One-way ANOVA, **** P < 0.0001. Symbols represent individual mice. Horizontal bars show means. In this experiment mice were given adoptive cell transfers, immunised and tissues collected by Yang Zhang.

3.2.2 Emigrating memory B cells make contact with subcapsular sinus macrophages

The previous data showed that the peak of the GC-derived BEMs production was around 7 days post-immunisation. To gain spatial information about BEMs migration the location of BEMs was detected at this time using light sheet microscopy. Previous studies have shown that immunoglobulin heavy chain germline transcription occurs prior to differentiation into GC B cells (Toellner et al., 1996, Marshall et al., 2011, Roco et al., 2019). To detect GC-derived BEMs S1PR2-ERT2-Cre x Ai14dTomato mice were used to detect GC-derived mBCs. These mice were immunised with rabbit IgG. At 6 days post-immunisation they received tamoxifen to release Cre sequestered to the cytoplasm by associating with HSP90, allowing translocation to the nucleus in S1PR2-expressing cells (Feil et al., 1997, Shinnakasu et al., 2016). This labelled GC-derived B cells by activating continuous expression of dTomato in the ROSA26 locus. On 8 days post-immunisation, mice received injections on plantar surface with labelled immune complex 30 minutes before drLNs were collected. This provided antigen via afferent lymphatics to be captured by SCS macrophages to allow investigation of transfer and transport by BEMs (Fig. 3.3A). DrLNs were imaged by light sheet microscopy. 3D scans showed that Tomato+ GC-derived cells (that are defined as BEMs) were present between GC and SCS and within the SCS which contained the fluorescently labelled antigen (Fig. 3.3B-C). To better identify SCS macrophages, CD169-Alexa647 was co-injected with fluorescently labelled immune complex (Fig. 3.4A). This successfully labelled macrophages in the SCS floor. BEMs were again present between SCS and GC. Furthermore, many BEMs were seen in close proximity with SCS macrophages, and some were found in the SCS (Fig. 3.4B-C). This indicated a possible interaction between immune complex carrying macrophages and BEMs. BEMs were also seen making contact with antigen in the SCS and

carrying antigen during migration between the SCS and GC (Fig. 3.4D). This suggested that BEMs collected antigen from SCS macrophages before transporting it back towards the GC.

Light sheet microscopy detected dTomato+ cells indicating the presence of GC-derived B cells between the GC and SCS and in the SCS, this suggested that of GC-derived B cells migrate between the GC and the SCS. BEMs were proximal to antigen carrying SCS macrophages. It is important to note that while dTomato+ cells in the SCS were not formally shown to be B cells, it is likely that they are as Moran et al. (2018) previously showed the presence of mBCs near the SCS (Moran et al., 2018). These cells are likely to be BEMs that circulate between the SCS and the GC LZ, shown by intravital microscopy (Zhang et al., 2022). A group of precursor mBCs produced during the GC response have been observed in the LZ of the GC (Laidlaw et al., 2017). This may be because BEMs observed here emerged from the LZ and from there migrated towards the SCS. These BEMs may then collect antigen from SCS macrophages before migrating back towards the GC (Zhang et al., 2022).

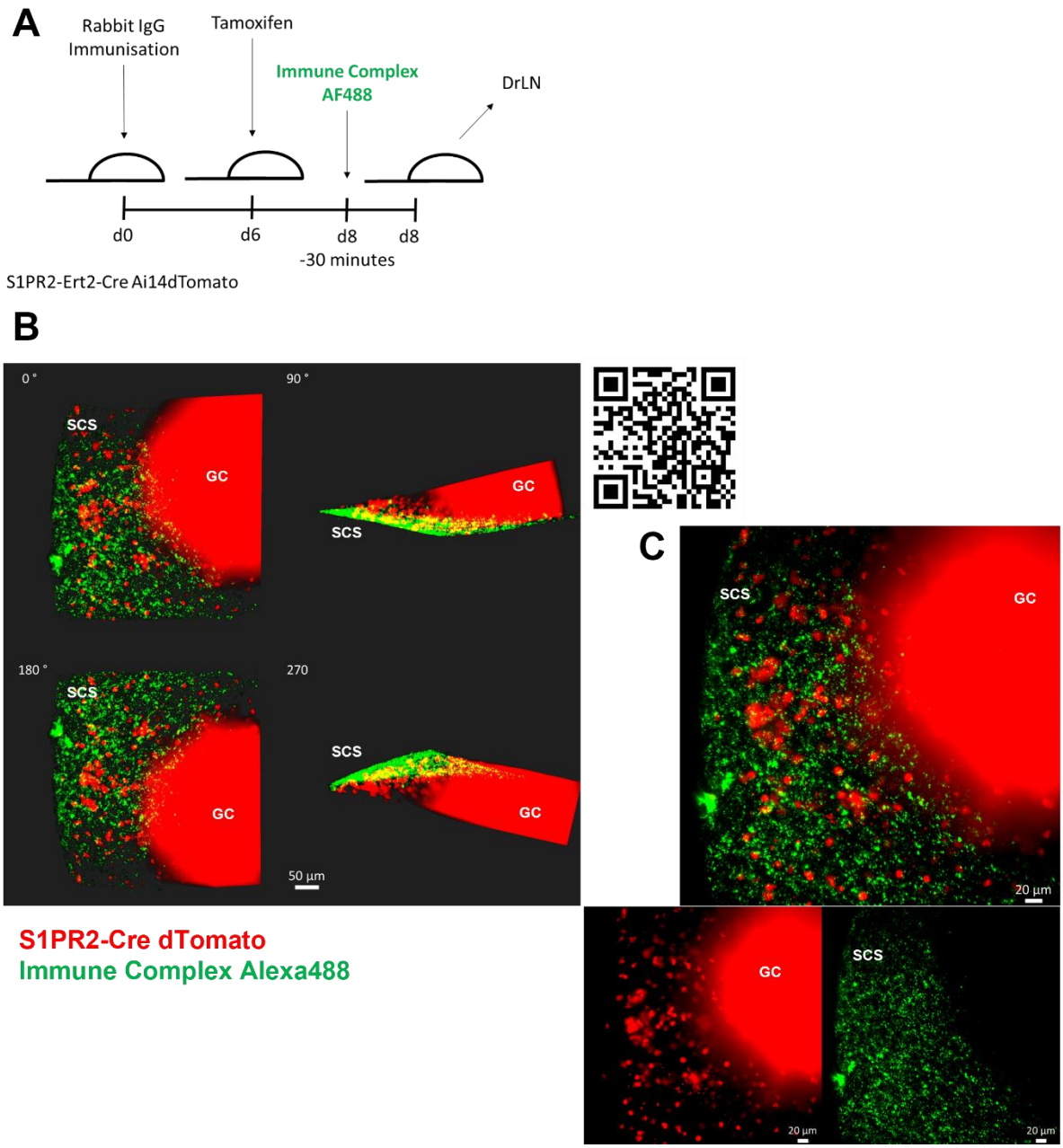


Figure 3. 3. BEMs detected in SCS in contact with antigen

(A) Experimental protocol: S1PR2-ERT2-Cre Ai14dTomato mice were immunised with rabbit IgG. 6 days post-immunisation mice received tamoxifen. At day 8 post-immunisation they received *in vivo* injections on plantar surface with Alexa488-labelled immune complex 30 minutes before collection of drLN. (B) Snapshots of light sheet microscopy image data of GC and SCS taken at 0°, 90°, 180° and 270° rotated along the X-axis. Migrating BEMs are visible between the GC and the SCS. QR code links to video of light sheet image in the URL: https://youtu.be/NdrfNtT82yM/ . (C) Maximum intensity projection of light sheet microscopy image (top), with dTomato (bottom left) and Alexa488-immune complex (bottom right) shown separately. Immune complex co-localised with BEMs showing they are

transported by BEMs. In this experiment mice were immunised, given tamoxifen and tissues collected by Yang Zhang.

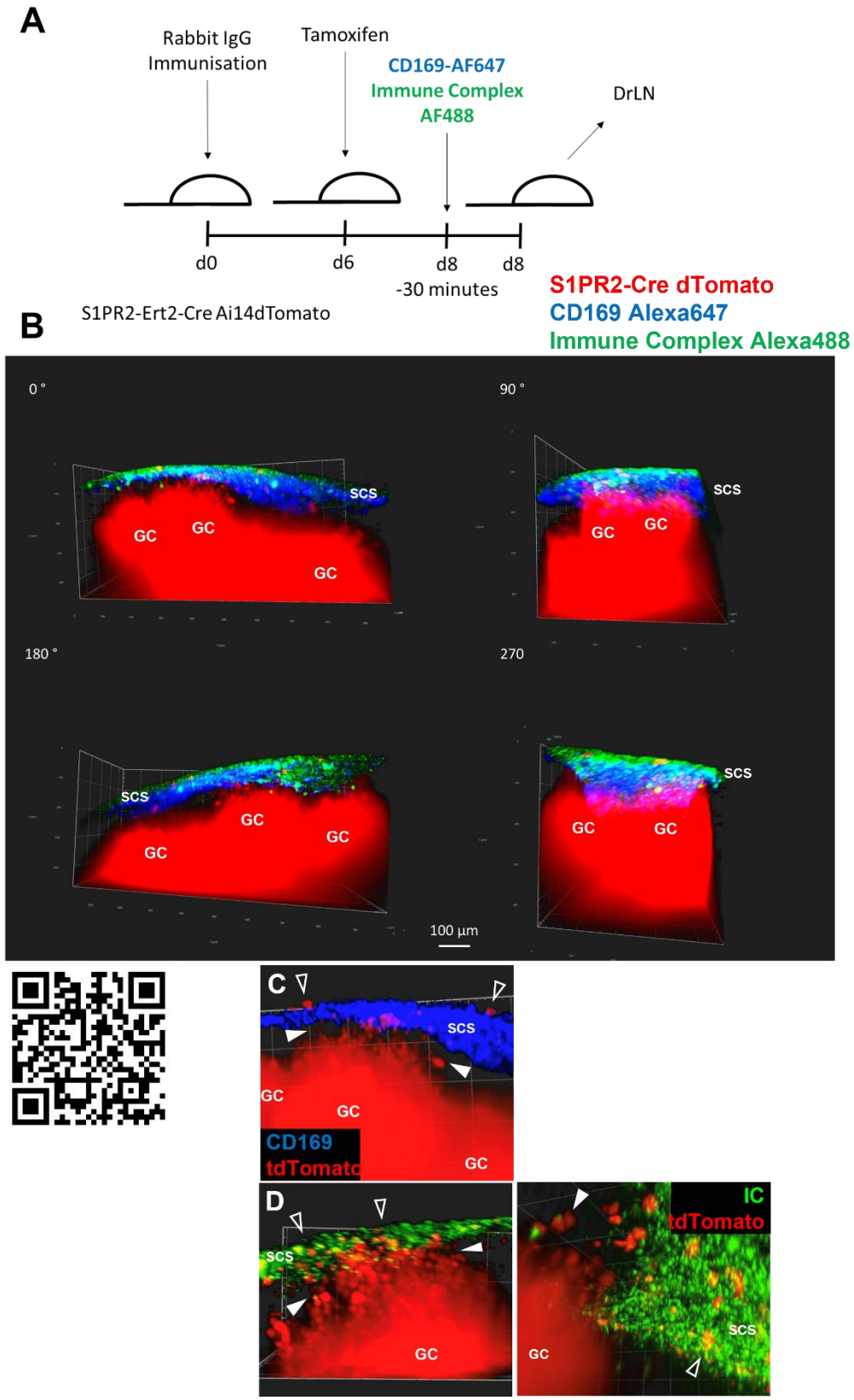


Figure 3. 4. BEMs detected in SCS proximal to SCS macrophages and collect antigen

(A) S1PR2-ERT2-Cre Ai14dTomato mice were immunised with rabbit IgG, 48 hours before collection these mice received tamoxifen. At day 8 post-immunisation they received *in vivo* injections with Alexa488-labelled immune complex and CD169-Alexa647 30 minutes before collection of drLN. (B) Snapshots of light sheet microscopy image of live explanted drLN showing GC and SCS taken at 0°, 90°, 180° and 270° rotated along the Y-axis. QR code links to video of light sheet image in the URL: https://youtu.be/NZ0QFUExpLE/ . (C) 3D scans of live drLNs showing BEMs (red) located between the GC and SCS (closed arrowheads). SCS macrophages (blue). Some BEMs were located in SCS above the SCS layer (open arrowheads). (D) Same as (C) showing Alexa488 labelled immune complex in the SCS and S1pr2-tdTom BEMs (red) between GC and SCS (closed arrowheads) or making contact with immune complex in SCS (open arrowheads). In this experiment mice were immunised, given tamoxifen and tissues collected by Yang Zhang.

3.2.3 RNA-sequencing analysis of B cells in the draining lymph node and distant lymph node

3.2.3.1 Definition of B cell subsets from bulk RNA sequencing data

We defined BEMs as $CD38^{hi}$ B cells that express variable levels of Fas. Fas expression may be residual because BEMs have recently emerged from GC. It is also possible that some BEMs are in the process of transitioning back into GC B cells. Furthermore, resting mBCs and nBCs are both in a quiescent state and share a similar transcriptional profile. This makes it challenging to distinguish between mBCs and nBCs based on RNA sequencing (Bhattacharya et al., 2007). The key differences between resting mBCs and nBCs are that mBCs are better able to respond to antigen and have enhanced survival due to expression of anti-apoptotic genes such as Bcl-2 (Good et al., 2009). As such, the population described as BEMs are likely to be a more heterogenous population than implied by the bulk RNA-sequencing data, they may consist of different activated B cells but will be referred to as BEMs throughout this thesis. GC B cells, BEMs, BCMs and nBCs were characterised by RNA-sequencing with the

goal of characterising gene expression profiles and uncovering the similarities and differences between each group.

Adoptive cell transfer recipients of B cells from IgHNP Cg1-Cre mTmG mice were immunised with NP-CGG in alum onto the foot. At 8 days post-immunisation GC B cells and BEMs in drLN and nBCs and BCMs in distLN were isolated by FACS (Fig. 3.5A and Appendix 2) followed by RNA sequencing by collaborators in the Francis Crick Institute. Samples of RNA-sequencing raw data were from STAR aligned read counts that were evaluated using R packages as described in Chapter 2.6. Reads were denoised for batch error using noisyR followed by dimensional reduction and differential gene expression analysis using the DESeq package (Fig. 3.5B). Samples underwent a series of quality control (QC) tests before analysis. Based on the mean quality scores all samples passed QC tests (Fig. 3.6A). However, a few samples had elevated sequence duplication levels (Fig. 3.6B) which suggested that there were some over-represented genes. There were some samples with very high guanine-cytosine content (Fig. 3.6C). These high guanine-cytosine samples would have under-represented gene counts within their lanes compared to the other samples, making direct comparison to other samples inaccurate as these samples had higher denaturing and annealing temperatures. When accounting for the results of these QC tests and the PCA plot of all samples, 2 samples (BEM1 and BEM4) were removed from analysis.

After removal of samples that failed QC tests, PCA plots were produced to show distance between samples and how well each group clustered (Fig. 3.7A). GC B cells and nBCs clustered into distinct groups with a large distance between them. BCMs clustered around the nBCs showing that they are very similar groups. BEMs clustered somewhere between the GC B cells and the BCM/nBC cluster. The heatmap with unsupervised clustering of the top

2000 most variant genes showed that GC B cells clustered separately from the other samples. BEMs clustered closely with BCMs, and BCMs clustered closely with nBCs (Fig. 3.7B).

Gene set enrichment analysis (GSEA) was performed using the gene sets in the Hallmark, KEGG and Reactome databases. Four comparisons were made using this process to provide clues into differing functions between B cell subsets. BEMs were compared against GC B cells because these subsets clustered closely together by PCA. The goal was to find ways in which they differed (Fig. 3.8A-C). BEMs was compared with BCMs as BEMs may eventually become BCMs, therefore, determining how they change would be informative (Fig. 3.9A-C). BCMs were compared against GC B cells to determine if BCMs differed from GC B cells in the same way they differed from BEMs (Fig. 3.10A-C). BCMs were compared against nBCs because they clustered closely by PCA; the goal was to see how they differed (Fig. 3.11A-C). Significantly enriched gene sets were defined as those with false discovery rate (FDR) scores < 0.1 (-log10(FDR)>1).

3.2.3.1.1 GSEA of BEMs and GC B cells

BEMs and GC B cells may be very similar as few gene sets from GSEA had an FDR < 0.1 (Fig. 3.8A-C). This may be because on a more general scale there were few differences between GC B cells and BEMs. Despite the high FDR scores, GC B cells were enriched for the datasets of mesenchymal epithelial transition and for the G2M Checkpoint. G2M checkpoint (FDR = 0.488) enrichment was expected, as GC B cells are known for being highly proliferative (Fig. 3.8A). The epithelial mesenchymal transition gene set also had a high FDR score (0.305).

BEMs were enriched for p53 pathway, IL-2 STAT5 signalling, IFN-α response and wingless-related integration site (WNT) β-catenin signalling, albeit all with a high FDR score (>0.1). The master regulator of damage and cell stress-induced apoptosis, p53, plays a role in B cells as it is downregulated by BCL-6 (Phan and Dalla-Favera, 2004). Surprisingly, BEMs may be more apoptotic than GC B cells which are already known for being prone to apoptosis.

From the Reactome database GC B cells were significantly enriched in the gene set - Signalling by WNT in cancer (Fig. 3.8C). The WNT signalling may play a role in proliferation of developing B cells, but WNT signalling by B-catenin is dispensable in B cell proliferation (Reya et al., 2000, Yu et al., 2008). However, this would concur with the highly proliferative nature of GC B cells.

Although GSEA failed to find many significant differences between BEMs and GC B cells in expression of whole pathways, this should not be used as evidence that these groups are indistinguishable. It is probably more of a reflection that BEMs are differentiated directly from GC B cells. As BEMs are in active migration from the GC, and BEMs and GC B cells were isolated from the same lymph node, it is likely that these BEMs have differentiated from GC B cells within hours before they were isolated. Therefore, they still shared many similarities with GC B cells.

3.2.3.1.2 GSEA of BEMs and BCMs

Comparing BEMs and BCMs there were more gene sets with an FDR <0.1. In the comparison of BEMs and BCMs using the Hallmark database, E2F targets and G2M checkpoint gene sets were significantly enriched in BEMs, showing that BEMs were more proliferative than BCMs

(Fig. 3.9A). This was also seen in the small distance between BEMs and GC B cells according to the PCA plot and Euclidean distance measure (Fig. 3.7).

In the KEGG database, BCMs were significantly enriched for the gene sets: Thyroid cancer; vasopressin regulated water reabsorption; arrhythmogenic right ventricular cardiomyopathy (ARVC); antigen processing and presentation; ABC transporters; prion diseases and ECM receptor interaction (Fig. 3.9B). Enrichment of vasopressin regulated water reabsorption may indicate that BCMs were undergoing migration as water reabsorption might play a role in actin polarisation of T cells during migration (De Boer et al., 2022).

In GSEA comparing BEMs and BCMs using the Reactome database, BCMs were significantly enriched for the gene sets: ECM proteoglycans; non-integrin membrane ECM interactions; and signalling by WNT in cancer (Fig. 3.9C). BCM enrichment for proteoglycan gene sets may imply that BCMs were more migratory as they interact more with the ECM.

3.2.3.1.3 GSEA of BCMs and GC B cells

In the comparison of BCMs and GC B cells by GSEA, GC B cells were significantly enriched for the G2M checkpoint, E2F targets and mitotic spindle, whereas BCMs were significantly enriched for the inflammatory response gene set (Fig. 3.10A). E2F is also involved in GC B cell proliferation by silencing Cdkn1a through EZh2 to promote cell cycle progression (Béguelin et al., 2017). BCM enrichment for inflammatory response suggested that they may have greater capacity to respond to stimulus.

In the KEGG database the BCMs were significantly enriched for haematopoietic cells lineage and ECM receptor interaction, whereas GC B cells were significantly enriched for DNA

replication (Fig. 3.10B). ECM receptor interaction gene set suggested that BCMs are more mobile than GC B cells. GC B cells were enriched for DNA replication indicating S phase during proliferation.

GSEA of BCMs compared to GC B cells in the Reactome database revealed that GC B cells were significantly enriched for gene sets involved with cell cycle and proliferation: Cyclin A B1 B2 associated events during G2M transition; mitotic spindle checkpoint; resolution of D loop structures through synthesis dependent strand annealing (SDSA); APC CDC20 mediated degradation of NEK2a; and activation of the pre-replicative complex (Fig. 3.10C). This reiterated that the GC B cells are more proliferative.

3.2.3.1.4 GSEA of BCMs and nBCs

BCMs and nBCs were compared by GSEA. Gene set enrichments were only found in the BCM group. In the hallmark database BCMs were significantly enriched for Kras signalling Upregulated; Inflammatory Response TGF-β signalling; allograft rejection apoptosis; and IL6 JAK STAT3 signalling (Fig. 3.11A). Kras is a GTPase transductor protein that plays a role in regulating cell division by controlling signal transduction; Kras is upstream of AKT phosphorylation (Jančík et al., 2010). IL6 is important in B cell responses and promotes antibody production (Maeda et al., 2010). STAT3 plays a role in B cell proliferation and maturation (Ding et al., 2016). These enrichments indicate that BCMs differ from nBCs due to having previously undergone activation and may be better placed to respond to antigen.

In the KEGG database BCM enrichments were not significant (FDR > 0.1). BCMs enriched for the complement and coagulation cascades (FDR = 0.288) gene set (Fig. 3.11B). Complement

is involved in B cell activation (Dunkelberger and Song, 2010, Cumpelik et al., 2021). This indicated that BCMs might be better placed to respond to stimulus than nBCs.

In the Reactome database, BCMs were significantly enriched in the following gene sets: antigen processing and cross presentation; RHOH GTPase cycle; and stabilisation of p53 (Fig. 3.11C). RHOH plays a role in the downregulation of cell cycle progression (Fueller and Kubatzky, 2008) and may facilitate the resting state of BCMs but not nBCs. These enrichments may also indicate that BCMs are primed to respond to antigen stimulus better than nBCs.

B cell subsets were compared at a more general scale to uncover gene expression pathways in which they differed. This suggested that GC B cells and BEMs were proliferative and that BCMs were more motile and primed to respond to stimulus. The next stage was to look at the subsets in a more detailed scale to identify specific genes.

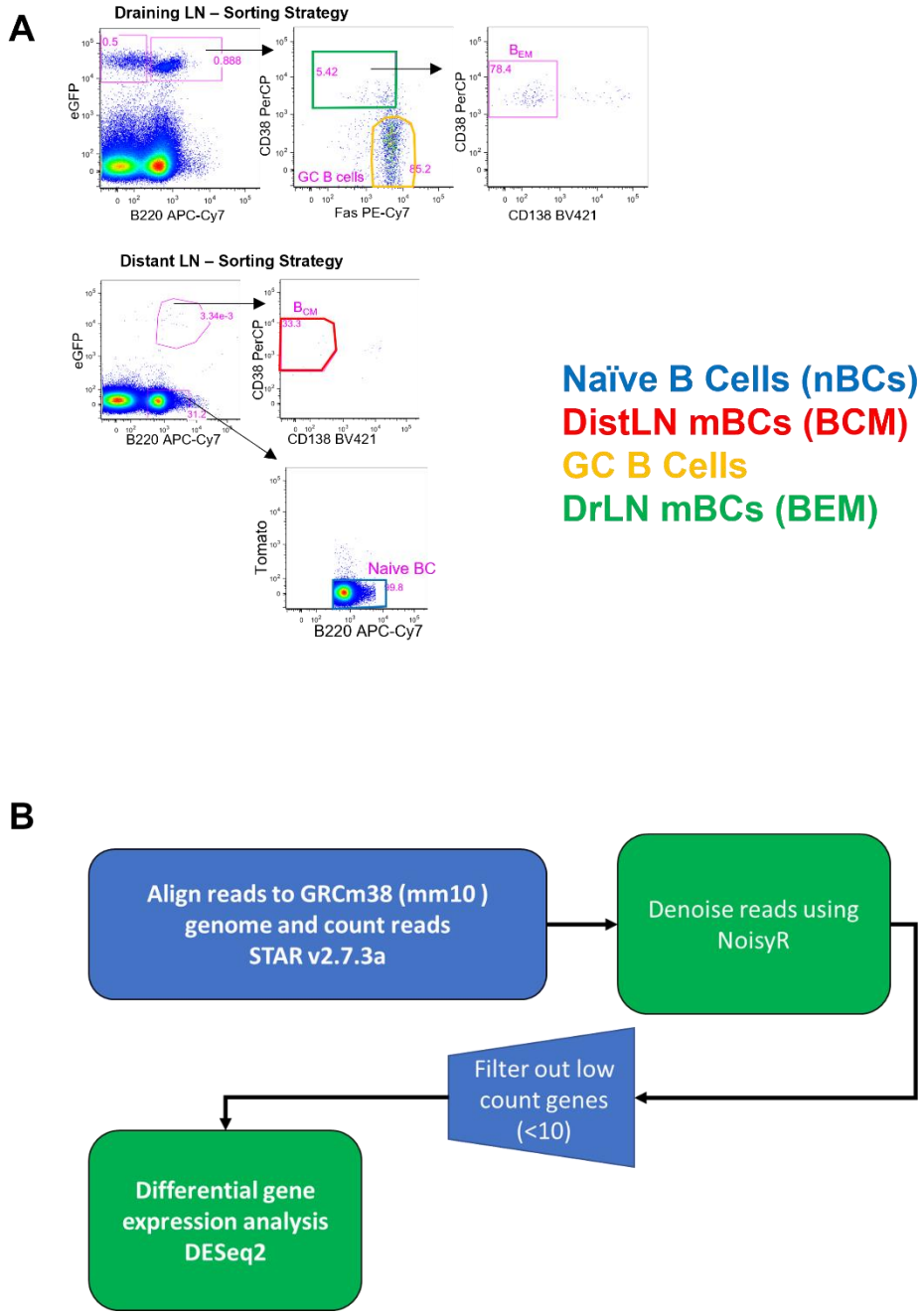


Figure 3. 5. BEMs were cell sorted and underwent RNA sequencing

(A) Representative sorting strategy from one experiment to isolate GC B cells (Fas+CD38-) and BEMs (CD38+) from GFP+B220+ cells in drLN, and BCMs (GFP+B220+CD38+CD138-) and naïve B cells (B220+GFP-dTomato-) from distLN of WT mice that received B cells from IgHNP Cg1cre mTmG mice at day 8 after NP-CGG foot injection (Zhang et al., 2022). These data are from 2 independent experiments with 4 samples and each sample consists of pooled popliteal and distant (axillary and brachial) LNs from 3 mice. (B) Analysis pipeline of bulk RNA-sequencing data from the sorted populations. Samples were produced by Yang Zhang and cell sorting was performed by University of Birmingham Flow Cytometry facility. Yang

Zhang extracted RNA and sequencing was performed by Jennifer Mueller-Winkler at the Francis Crick Institute.

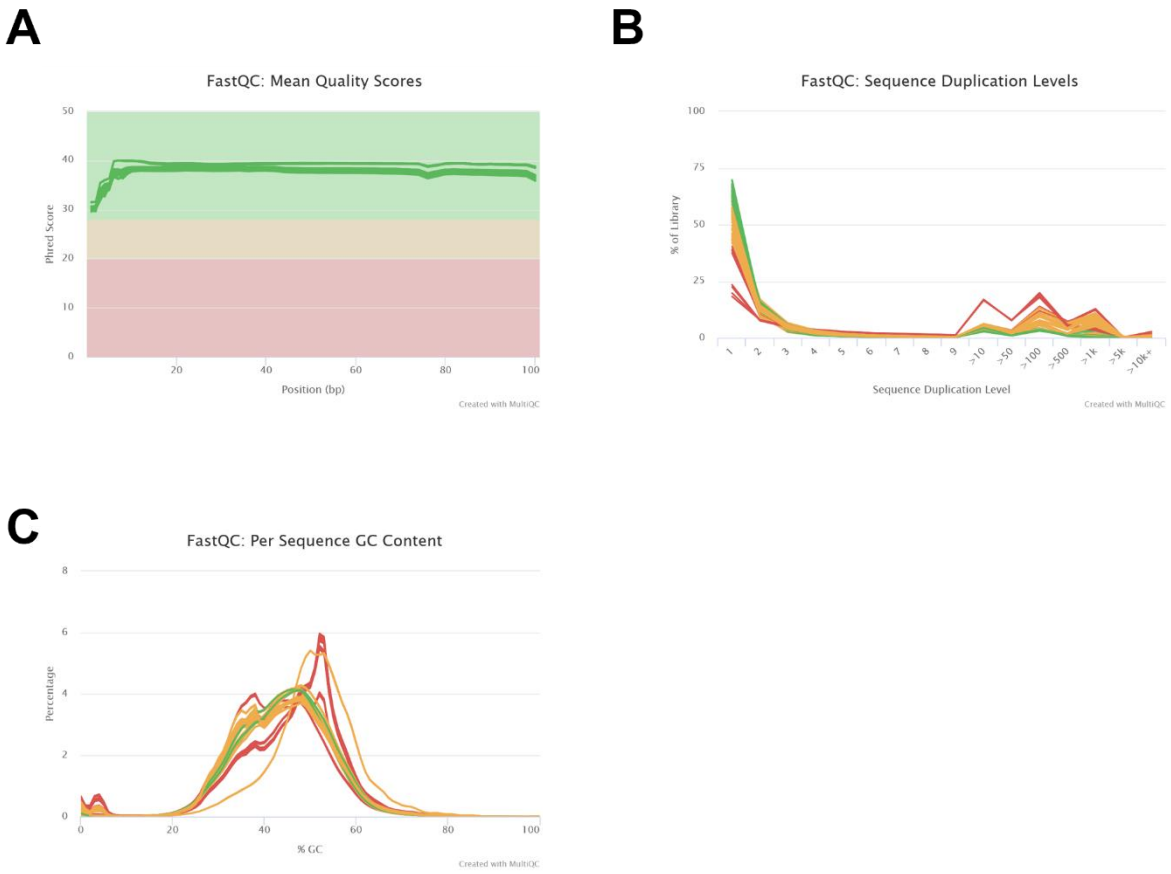


Figure 3. 6. Sorted cells passed quality control tests

Summaries of quality control tests of bulk RNA-sequencing data using Star. Represented are (A) Mean Quality scores per sample, (B) sequence duplication levels and (C) per sequence GC content. Green lines represent samples that passed quality control test, orange lines passed but with a warning and red lines failed quality control tests.

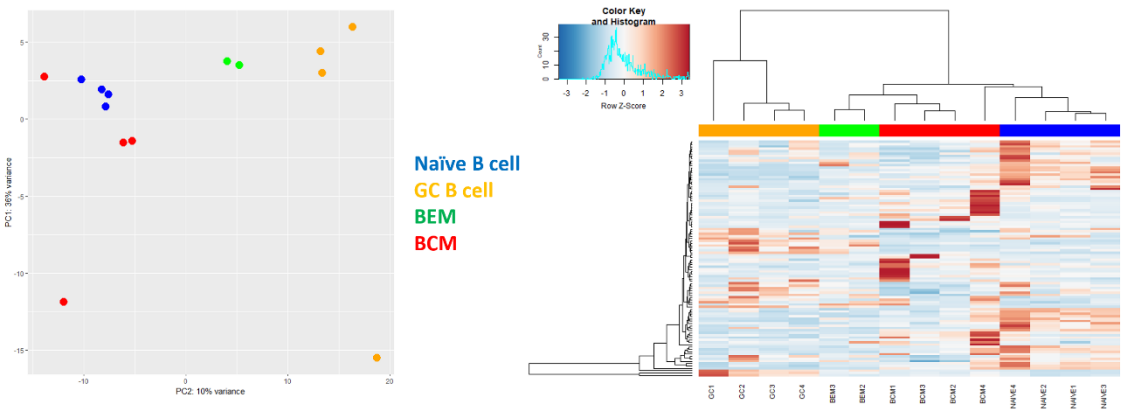


Figure 3. 7. Sorted BEMs are a distinct group from GC B cells, naive B cells and BCMs

(A) PCA plot of samples after removal of samples that failed QC tests and count data normalised by the Rlog method using the DESeq package. PCA was calculated based on the top 2000 genes based ranked by row variance. (B) Heatmap with unsupervised clustering of genes and samples using Euclidean distance measure. Heatmap was produced from normalised count data from DESeq package using ggplot2 package. Displayed are top 2000 genes ranked by row variance after filtering out genes in a differential gene expression analysis with a P-value <0.05.

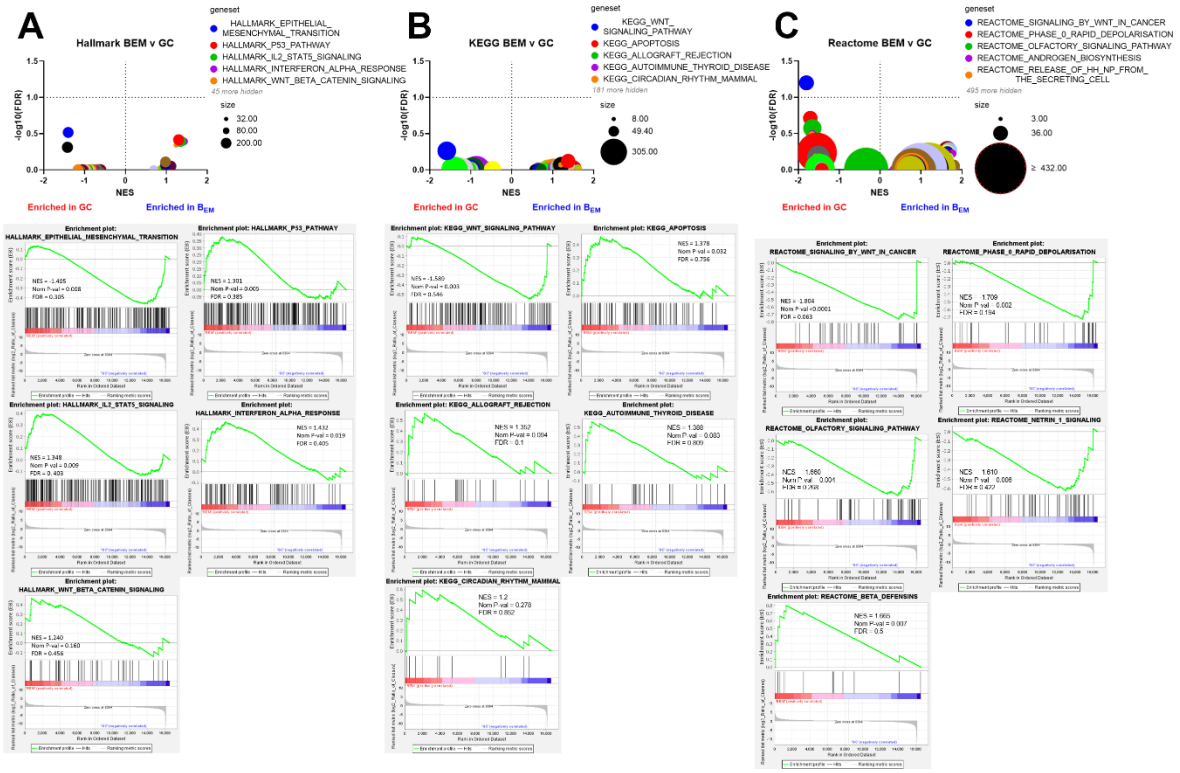


Figure 3. 8. GC B cells were more enriched for gene sets associated with proliferation than BEMs

GSEA was performed comparing BEMs and GC B cells, results are summarised in bubble plots figure legends and enrichment plots below display the 5 most significantly enriched gene sets. Threshold for significantly enriched gene sets was FDR <0.1 displayed on bubble plot as -log10(FDR)>1. Bubble plot and enrichment plots from GSEA using the (A) Hallmark data base, (B) KEGG database (C) and Reactome database.

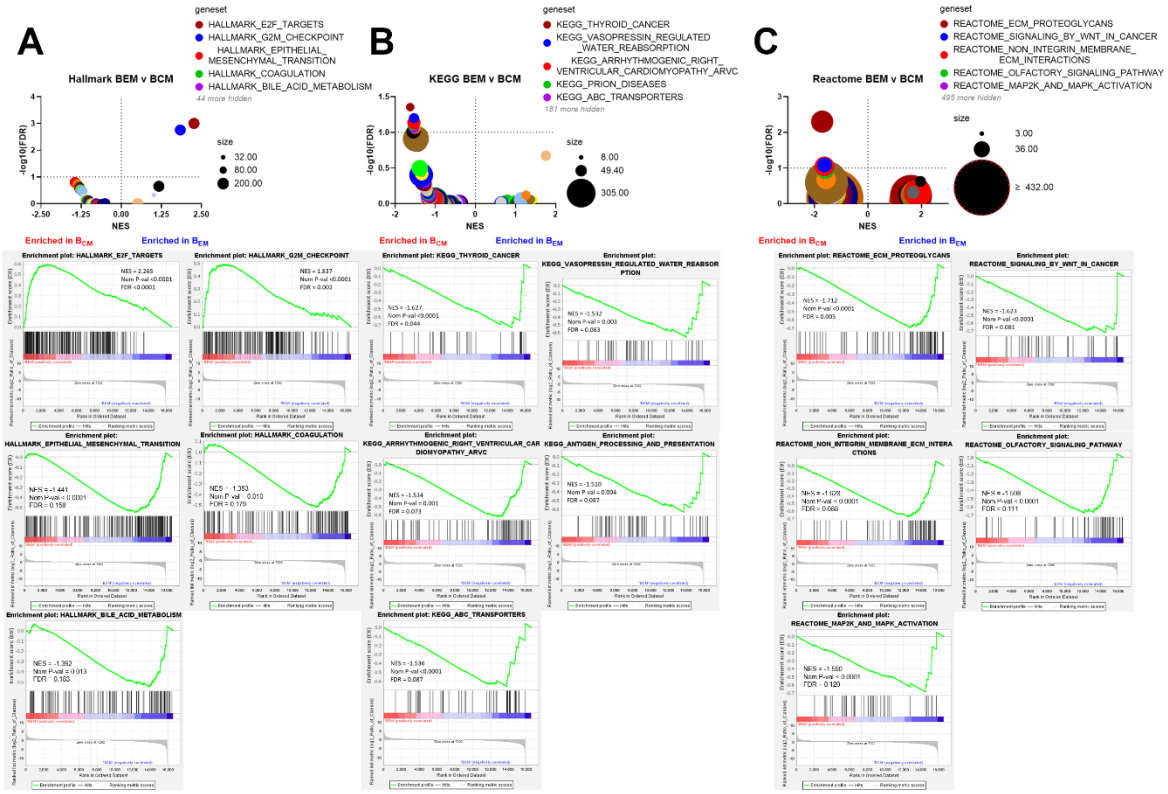


Figure 3. 9. BEMs enriched for proliferation-associated gene sets over BCMs

GSEA was performed comparing BEMs and BCMs, results are summarised in bubble plots figure legends and enrichment plots below display the 5 most significantly enriched gene sets. Threshold for significantly enriched gene sets was FDR <0.1 displayed on bubble plot as -log10(FDR)>1. Bubble plot and enrichment plots from GSEA using the (A) Hallmark data base, (B) KEGG database (C) and Reactome database.

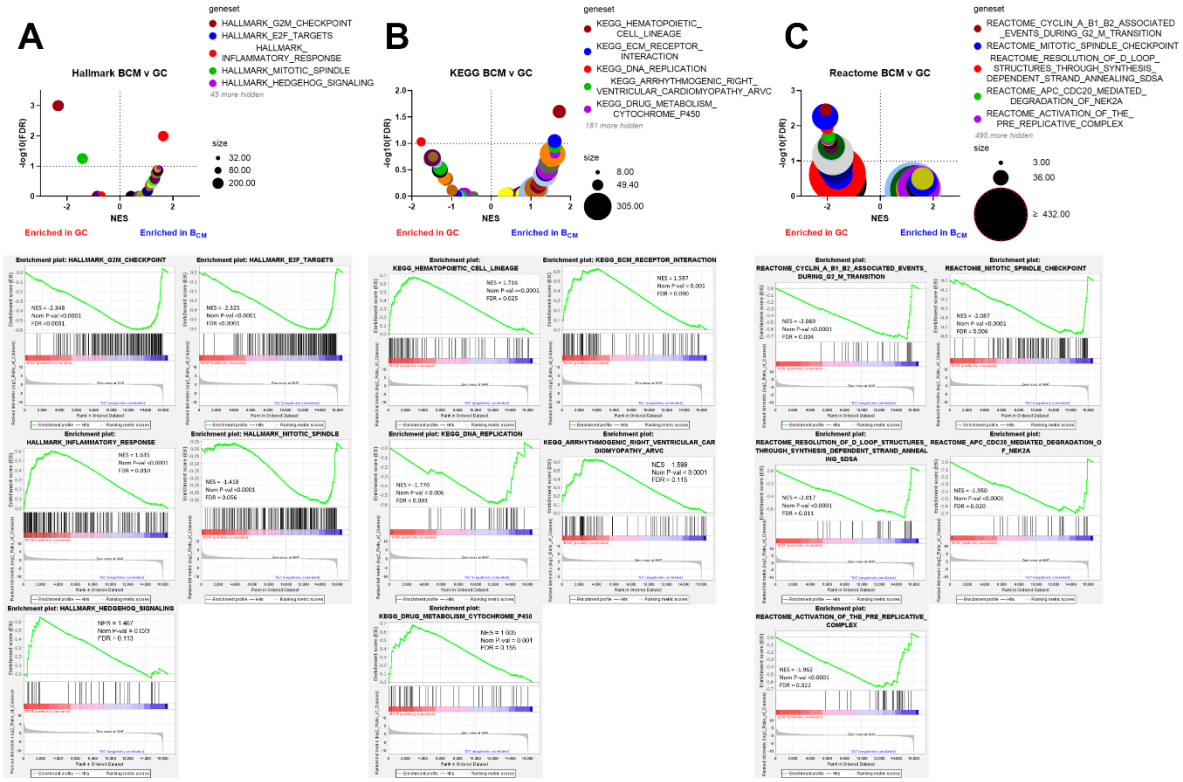


Figure 3. 10. GC B cell gene set enrichment showed that they were more proliferative than BCMs

GSEA was performed comparing groups BCMs and GC B cells, results are summarised in bubble plots figure legends and enrichment plots below display the 5 most significantly enriched gene sets. Threshold for significantly enriched gene sets was FDR <0.1 displayed on bubble plot as -log10(FDR)>1. Bubble plot and enrichment plots from GSEA using the (A) Hallmark data base, (B) KEGG database (C) and Reactome database.

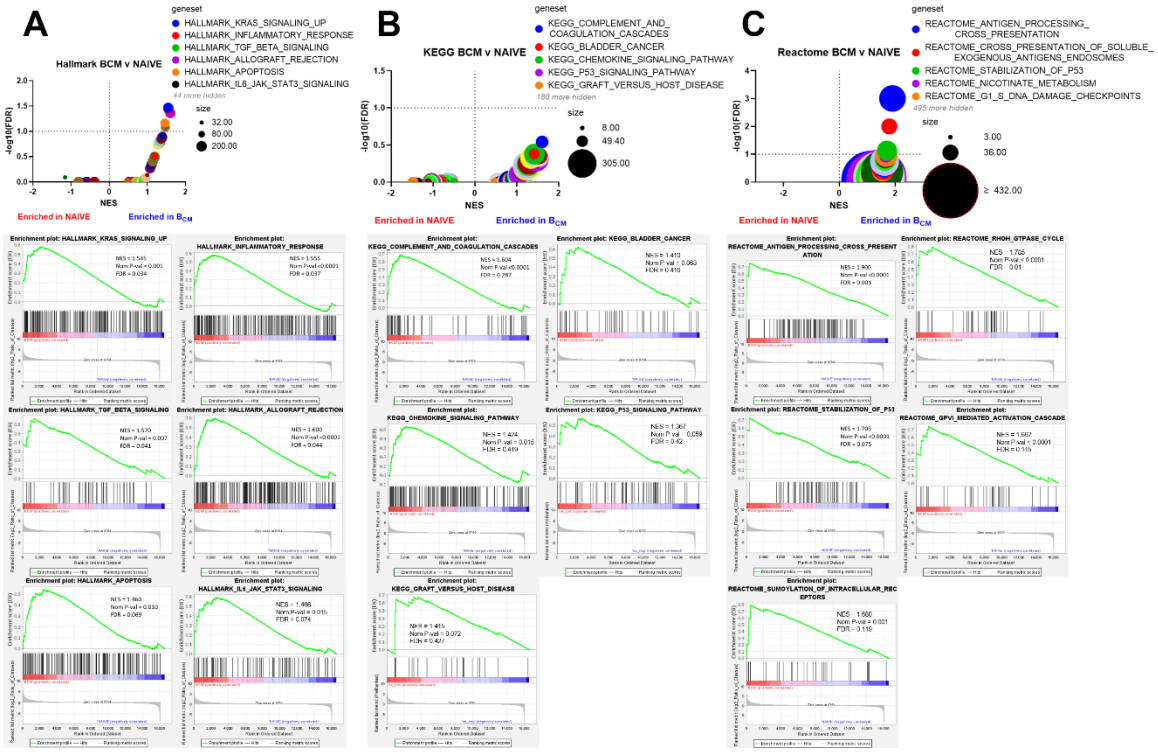


Figure 3. 11. BCMs were enriched for gene sets for antigen processing and presentation, inflammatory response and cell signalling over naïve B cells

GSEA was performed comparing groups BCMs and naïve B cells, results are summarised in bubble plots figure legends and enrichment plots below display the 6 most significantly enriched gene sets in the Hallmark database and 5 most significantly enriched gene sets in the KEGG and Reactome databases. Threshold for significantly enriched gene sets was FDR <0.1 displayed on bubble plot as -log10(FDR)>1. Bubble plot and enrichment plots from GSEA using the (A) Hallmark data base, (B) KEGG database (C) and Reactome database.

3.2.3.2 Differential gene expression analysis revealed similarities and differences between BEMs and GC B cells

Differentially expressed genes between B cell subsets were analysed to uncover clues to genes regulating the differing functions of each B cell subset. Significantly differentially expressed genes of each B cell subset were plotted against genes expressed in nBCs (Fig. 3.12A). In terms of upregulated genes GC B cells, BEMs and BCMs had distinct collections of

DEGs, with 77 of these genes shared between BEMs and GC. However, GC B cells shared only 2 genes with BCMs, and BEMs shared only 1 gene with BCMs (Fig. 3.12A). When downregulated genes are plotted, GC had many distinct DEGs, BEMs had far fewer distinct DEGs and shared the majority with GC B cells. There were very few downregulated DEGs for BCMs and the majority were shared with GC B cells and BEMs (Fig. 3.12B). A heatmap was produced from a selected group of chemokine receptors to directly compare expression of these genes of interest between groups. GC B cells had upregulated *S1pr2* and downregulated *S1pr1*, *Gpr183*, *Ccr6* and *Ccr7*; these genes were expressed at higher levels among BEMs. nBCs and BCMs had raised expression of *Cxcr5*, *S1pr1*, *Cxcr4*, *Ccr7* and *Cd69* compared with BEMs and GC B cells (Fig. 3.12C). The chemokine receptors S1PR1 (which binds S1P), GPR183 (EBI2) (which binds 25-dihydroxy-cholesterol) and CCR6 (which binds CCL20) can facilitate migration of lymphocytes towards the SCS in the LN (Pereira et al., 2010, Zhang et al., 2016, Grasso et al., 2021). Expression of these in BEMs may allow migration to the SCS. *Ccr7* is also expressed at raised levels in BEMs compared with GC B cells, but they do have a lower expression compared with BCMs and nBCs. We have shown that this may facilitate return of BEMs from the SCS back towards the follicle following CCL19/21 gradients regulated by ACKR4 (Ulvmar et al., 2014). S1PR2 works against migration following S1P gradients and has been shown to be chemo-repulsive in osteoclast precursors, which allows GC B cells to cluster together in the centres of the follicles (Ishii et al., 2010, Green and Cyster, 2012). CD69 plays a role in regulation of S1PR1 by promoting its internalisation (Bankovich et al., 2010), thus increased expression of CD69 in nBCs and BCMs may reduce their capacity to respond to S1P gradients.

Direct comparisons between populations were made by differential gene expression. BEMs had some genes differentially expressed in relation to GC B cells including *Ighd*, *Ccr6*, *Cd38* and *Cd62l* (*Sell*) (Fig. 3.13A). CD38 was used to distinguish BEMs from GC B cells so its increased expression is expected. CCR6 is expressed by a group of pre-memory B cells and remains expressed in mBCs (Suan et al., 2017). The BEM population may include pre-memory B cells (Fig. 3.13B). Comparing BCMs with GC B cells produced far more DEGs, which was expected from the principal component analysis (Fig. 3.7A). There was also a larger spatiotemporal distance of BCMs from GC B cells (Fig. 3.13B). BCMs expressed genes included *Sell* (*Cd62l*), *Cd38*, *Ighm* and *Cd55*, whereas GC B cells overexpressed genes for *Ighg1*, *Mki67*, *Aicda* and *S1pr2* (Fig. 3.13B). BEMs expressed high levels of *Mybl1*, *Mki67*, *Aicda* and *Iglc1* whereas, BCMs expressed *Igkc* and *Lyz2*, encoding the lysozyme 2 gene (Fig. 3.13C). GC B cells compared with nBCs upregulated *Mki67* and *Aicda*, whereas nBCs upregulated *Sell* (*Cd62l*), *S1pr1* and *Cd55* compared with GC B cells (Fig. 3.13D). BEMs also upregulated *Mybl1*, *Mki67*, *Aicda* and *Adam6b* compared with nBCs (Fig. 3.13E). BCMs had few genes upregulated compared with nBCs, among them was *Lyz2* (Fig. 3.13F).

RNA-sequencing data were also screened for potential surface markers that can be used to identify BEMs. Genes of cell surface proteins were filtered from DEGs by using the gene ontology term for cell surface GO:0009986. Comparing DEGs between BEMs v GC B cells, upregulated genes were mainly found in BEMs (Fig. 3.14A). These included *Ighd*, *Ccr6*, *Cd38*, *Sell*, *Cd55*, *Pecam1*, *Plaur* (*Cd87*) and *S1pr1*. There was a significant upregulation of any genes in GC B cells (Fig. 3.14A). Comparing BCMs and GC B cells there were significantly upregulated DEGs in both BCMs and GC B cells (Fig. 3.14B). BCMs upregulated *Sell*, *Ighm*, *Cd55*, *Cd38*, *S1pr1*, *Plaur* (*Cd87*), *Ccr7*, *Ccr6* and *Cd69*. GC B cells upregulated *Fas*, *Iglc*,

Adam6b and *Ighg2b*. BEMs and BCMs were also compared with a small number of DEGs in both BEMs and BCMs (Fig. 3.14C). BEMs upregulated *Iglc1*, *Ighg2b*, *Fas*, *F2* and *Ccr6*. BCMs upregulated *Igkc*, *Clec2i* and *Cd69*.

Cell surface genes of GC B cells were also compared with nBC cell surface genes (Fig. 3.14D). Most overexpressed DEGs were found in nBCs. These included *Sell*, *Ighm*, *Cd55*, *Clec2i*, *S1pr1*, *Dpp4*, *Cd38*, *Adam19* and *Cd87*. Far fewer genes were induced in GC B cells, these included *Adam6b* and *Fas*. In BEMs compared with nBCs BEMs upregulated *Iglc1*, *F2*, *Adam6b*, *Timd2* and *Fas*. Whereas nBCs upregulated *Igkc*, *Clec2i*, *Cd69*, *Ighd* and *Adgre5* (Fig. 3.14E). In the comparison between BCMs and nBCs there were very few DEGs, the majority of these were upregulated in BCMs (Fig. 3.14F). BCMs upregulated *Siglech*, *Fcer1g*, *Csf1rm*, *Cd4* and *C3*, whereas nBCs had higher expression of *Igha*. This was unexpected as nBCs would not have undergone CSR. This may be a result of contamination of the sorted population of nBCs with other B cell subsets. The top 40 most variable cell surface genes between the 4 groups were examined. These were presented in a heatmap with unsupervised clustering by Euclidean distance measure (Fig. 3.14G). GC B cells, BEMs, BCMs and nBCs clustered separately in the same manner as described in Fig. 3B. GC B cells and BEMs clustered closely together, but distant from BCMs and nBCs. BCMs and nBCs clustered closely together. This revealed cell surface markers that could be used to distinguish BEMs that may be explored further by flow cytometry.

Due to expression of *S1pr1*, *Cd38* and *Ccr6* it appeared that BEMs may share similar characteristics to a B cell subset described as pre-memory B cells (Suan et al., 2017, Laidlaw et al., 2017). To determine the similarity between BEMs and pre-memory B cells, publicly

available normalised gene counts from pre-memory B cells compared with GC B cells were extracted (Laidlaw et al., 2017). DEGs were then determined from these data to produce custom gene sets of pre-memory vs GC B cells (upregulated in pre-memory), pre-memory v memory B cells (upregulated in pre-memory) and pre-memory vs GC B cells and memory B cells (upregulated in pre-memory). These were then used for GSEA of a pre-ranked list of BEMs v GC B cells, ranked by log2 fold change (Fig. 3.15A). BEMs were enriched strongly with genes found in pre-memory B cells compared with GC and mBCs (Fig. 3.15B-C). This suggested that BEMs were phenotypically similar to pre-memory B cells.

Many of the characteristics ascribed to BEMs by these findings by bulk RNA-sequencing data concurred with data uncovered by other groups. For example, Shinnakasu et al., (2016) described a group of Bach2 expressing B cells as predisposed to differentiation into mBCs. Pre-memory B cells were defined as a group of CCR6-expressing cells that upon stimulation became mBCs (Suan at al., 2017). Pre-memory B cells were also described as Ephrin B1 expressing cells that were distinct from other GC B cells (Laidlaw et al., 2017). As BEMs and pre-memory B cells defined by Laidlaw et al. (2017) shared expression of *Ccr7*, *S1pr1*, *Ccr6*, *Gpr183* and *Sell* (*Cd62l*), they were compared. This was achieved by taking DEGs from the comparison of BEMs v GC B cells and performing a GSEA using a custom gene set defined as the Pre-Memory B cells v GC B cells Upregulated. These genes were pre-ranked by fold change and an enrichment score was calculated using the weighted statistic and permutations were calculated by phenotype. In this comparison it was found that BEMs were strongly enriched for pre-memory B cell genes. This provides strong evidence that the group defined here as BEMs are very similar to the pre-memory B cells. Thus, it is possible that identical groups or groups at very close stages of differentiation are being examined.

The main genes with similarly increased expression were *Pml*, *Sell*, *Cd38, Ccr6*, *S1pr1*, *Cd55*, *Plaur* (*Cd87*), *Lef1*, *Ccr7*, *Pecam1* and *Bcl2*. These were identified at the leading edge of the GSEA. This list concurs with data shown previously (Fig. 3.12C and 3.14A) that shows genes distinctly upregulated BEMs compared with GC B cells.

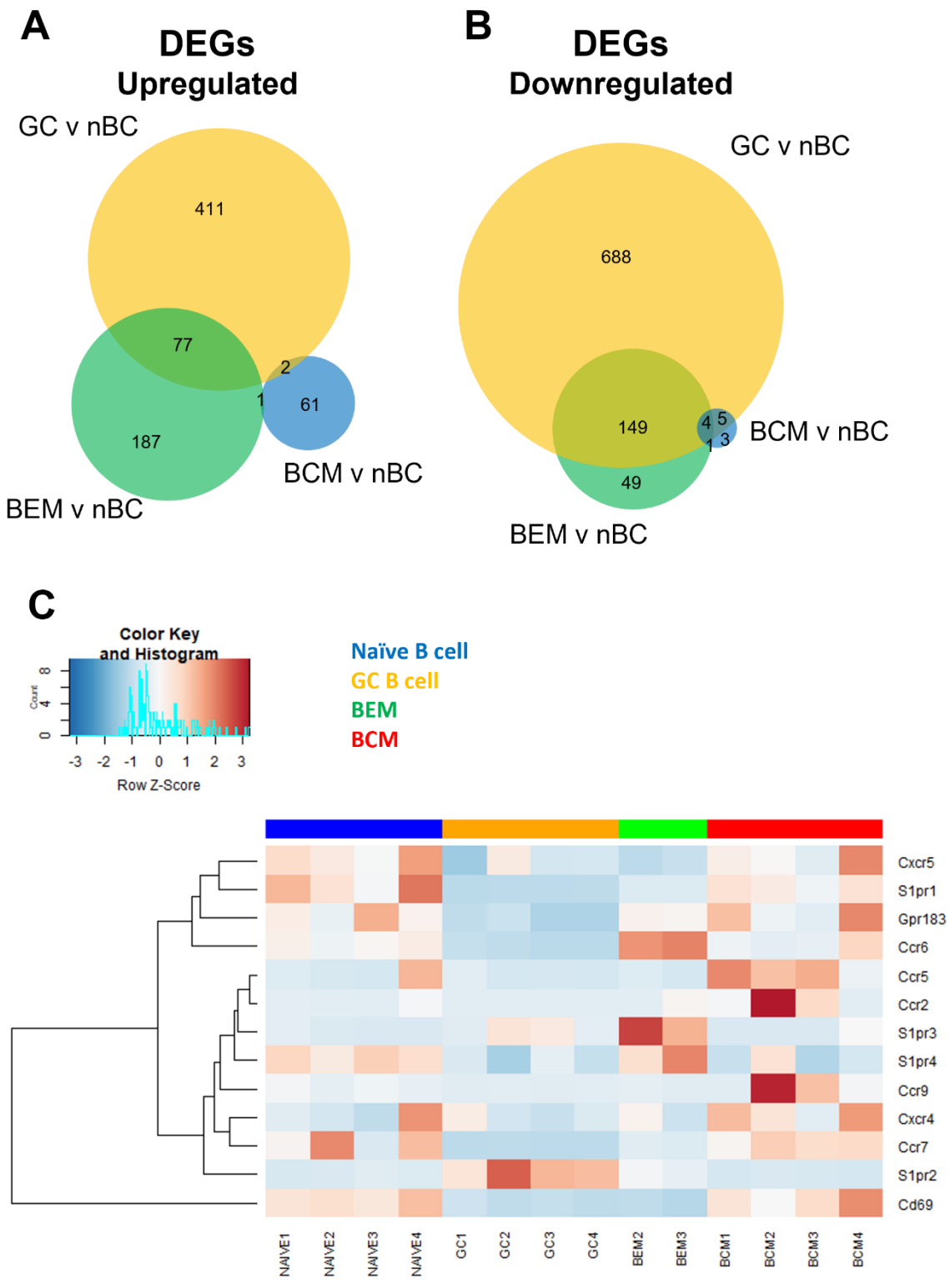


Figure 3. 12. BEMs have differentially expressed genes distinguishing them from BCMs and GC B cells

(A) Differentially expressed genes of GC B cells, BEMs and BCMs compared with nBCs with adjusted P-value <0.05 plotted into Venn diagrams of upregulated genes (left) and downregulated genes (right). (B) Heatmap showing gene expression of a list of selected chemokine receptors and related markers.

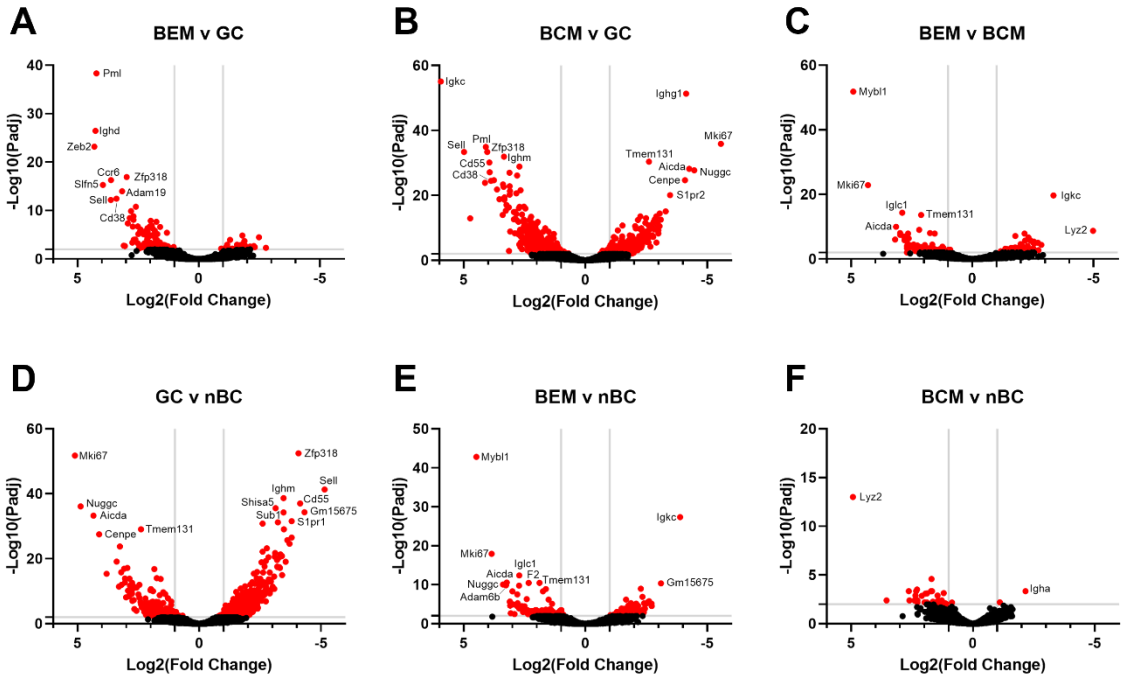


Figure 3. 13. Volcano plots show that BEMs have differentially expressed genes from GC B cells, BCMs and naive B cells

Volcano plots of differentially expressed genes, each dot represents a gene, with genes of interest labelled. Genes differentially expressed with a p-value <0.05 (-Log10(p-values) >1) are represented by red dots. Differentially gene expression comparisons shown are: (A) BEM v GC B cells, (B) BCM v GC B cells, (C) BEM v BCM, (D) GC v nBC, (E) BEM v nBC and (F) BCM v nBC. Symbols represent individual genes.

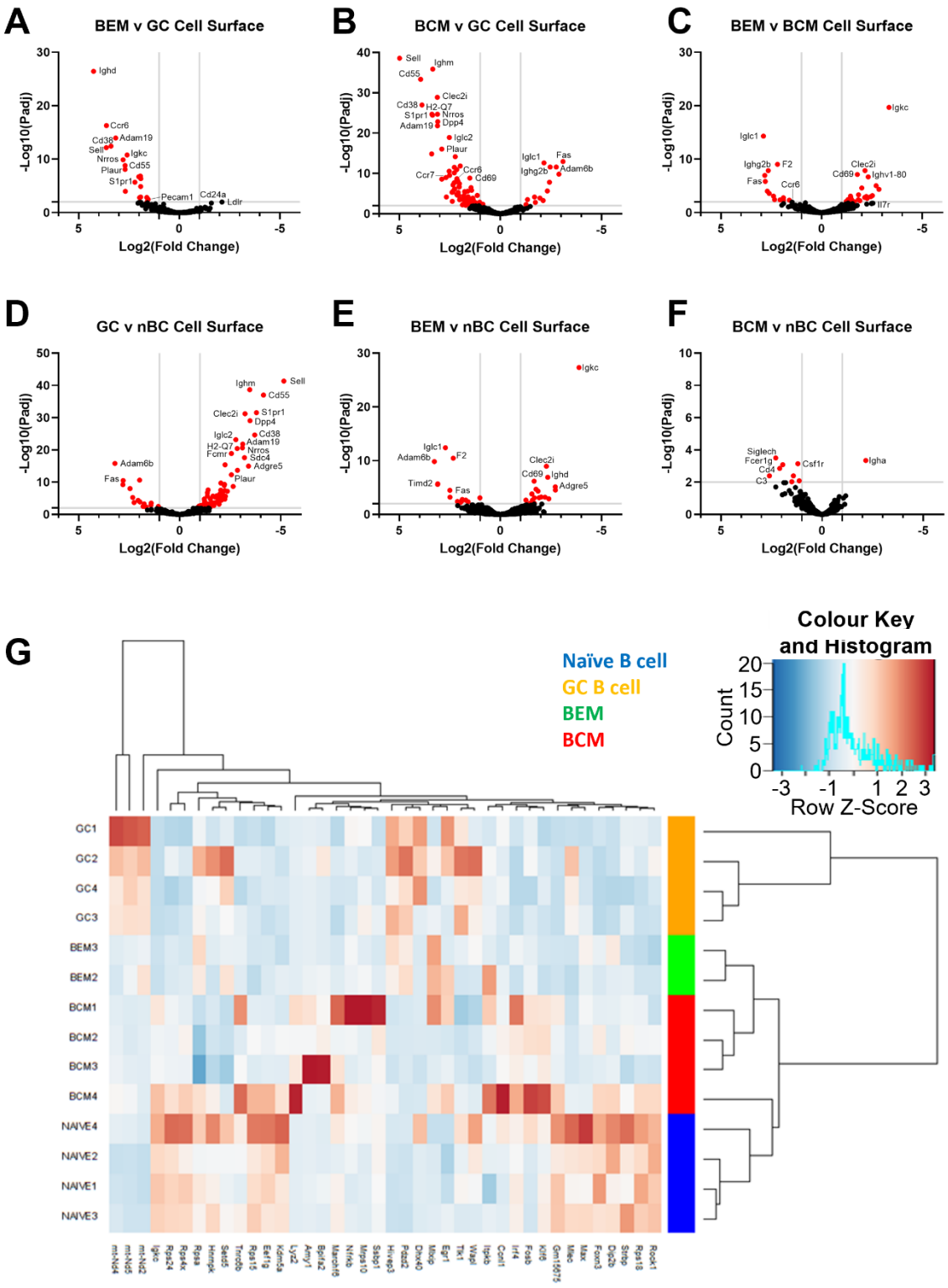


Figure 3. 14. Differentially expressed genes encoding cell surface proteins may distinguish BEMs from other B cell subsets

Volcano plots of differentially expressed genes of cell surface expressed markers filtered from gene ontology term cell surface (GO:0009986), each dot represents a gene, with genes

of interest labelled. Genes differentially expressed with a p-value <0.05 (-Log10(p-values) >1) are represented by red dots. Differentially gene expression comparisons shown are: (A) BEM v GC B cells, (B) BCM v GC B cells, (C) BEM v BCM, (D) GC v nBC, (E) BEM v nBC and (F) BCM v nBC. Symbols represent individual genes. (G) Heatmap of the top 40 cells surface expressed genes ranked by row variance, samples and genes underwent unsupervised clustering by Euclidean Distance measure.

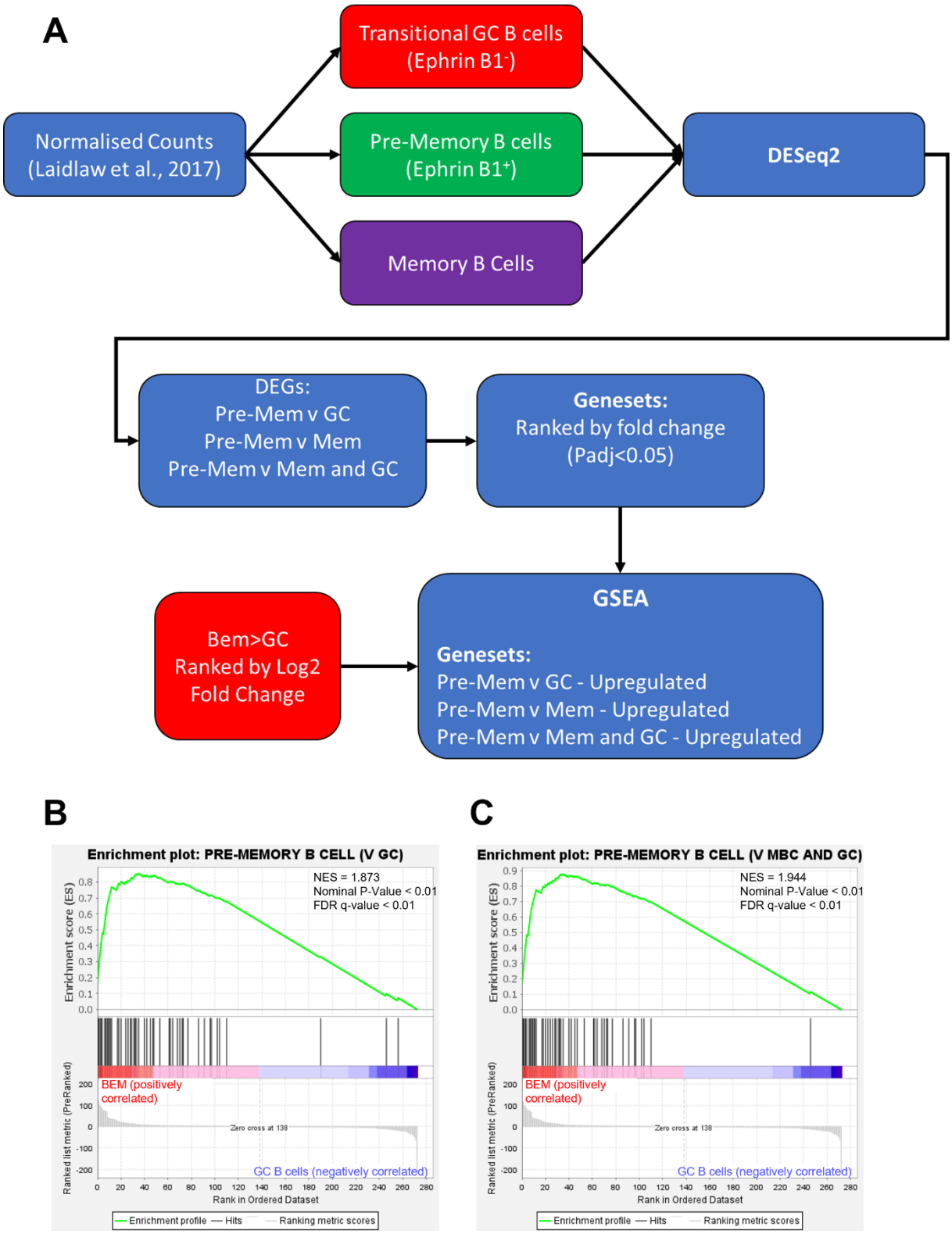


Figure 3. 15. BEM gene expression profile was similar to pre-memory B cells

(A) Pre-ranked dataset isolated from gene specific analysis of BEM v GC with P-value<0.05 and ranked by fold change. GSEA was performed using this pre-ranked list against a Pre-Memory B cell gene expression profile. Pre-Memory B cell profile defined from Laidlaw et al.

as genes upregulated in Pre-Memory B cells in their differential gene expression comparison between Pre-Memory B cells and GC B cells (Laidlaw et al., 2017). Raw counts data accessed from gene expression omnibus from GSE89897. Pre-Memory B cells were defined as Ephrin-B1^{+} S1PR2-Venus^{-} B cells in draining lymph node and GC B cells were defined as Ephrin-B1^{+} S1PR2-Venus^{+} B cells in draining lymph node.

Results of GSEA are presented in enrichment plots showing the enrichment for Pre-Memory B cell (v GC) – Upregulated (B) and Pre-Memory B cell (v MBC and GC) – Upregulated (C). Genes upregulated by BEMs were overrepresented among genes upregulated by pre-memory B cells.

3.2.4 CD55 and CD24 as markers to identify BEMs

The gene expression profiles of GC B cells and BEMs are very similar. The BEMs studied here represent a transient population emerging from the GC at the early peak of the GC reaction. RNA-sequencing data revealed DEGs expressed by BEMs and BCMs compared with GC B cells. The cell surface protein expression of some of these genes was examined by flow cytometry.

BEMs had many characteristics in common with pre-memory B cells (Laidlaw et al., 2017). RNA-sequencing results uncovered cell surface expressed genes that may be used as markers to distinguish mBCs such as BEMs from GC B cells and naïve B cells. These potential BEM markers were generated by taking DEGs that were differentially expressed from one of 2 comparisons for each gene: BEM vs GC B cells and BCM vs GC B cells. The comparison which had the smallest absolute difference was selected and filtered for adjusted P-value <0.05. These were then filtered by the gene ontology term “cell surface” (GO:009986). Amongst these genes, the ones with commercially available antibodies to detect cell surface expression were selected (Fig. 3.16A). The full list of BEM markers with available antibodies at the time of study is presented in Appendix 3. Expression of BEM markers are presented in

the heatmap (Fig. 3.16B). *Slamf7* and *Cd24a* showed increased expression by GC B cells and BEMs compared to lower expression by nBCs. Whereas *Pecam1*, *S1pr1*, *Ccr7*, *Cd55*, *Sell* (*Cd62l*) and *Cd47* were upregulated on BEMs compared to GC B cells.

Markers were tested by flow cytometry in mice that received adoptive cell transfers of $1x10^5$ NP-specific QM IgHNP mTmG splenocytes, immunised with NP-KLH and specificity of staining and levels of protein expression in nBCs (B220+CD138-dTomato-CD38+Fas-), GC B cells (B220+CD138-dTomato+CD38-Fas+) and BEMs (B220+CD138-dTomato+CD38+) from pooled popliteal LNs at 8 days post-immunisation (Fig. 3.16C). Expression in BCMs was not analysed as there were too few BCMs detected to accurately determine expression of markers. CD69 is a marker for cell activation and CXCR3 is expressed by mBCs, therefore their expression in BEMs was investigated (Muehlinghaus et al., 2005). Histograms show that BEMs upregulated CD69 and CXCR3 compared with nBCs and GC B cells, however, distribution of CD69 expressing BEMs was bimodal and only a minority of BEMs upregulated CXCR3 (Fig. 3.16D). MFIs imply that BEMs and GC B cells upregulated CD69 and CXCR3 compared with nBCs, and that BEMs expressed higher levels than GC B cells (Fig. 3.16E). There was no unstained control sample with which to compare them but, based on histograms, it appeared that CXCR3 and CD69 were not highly specific to BEMs. Histograms showed that CCR6 cell surface expression by BEMs was slightly upregulated compared with nBCs and much more upregulated compared with GC B cells. There was a lot of overlap between GC B cells and the unstained control sample (Fig. 3.16F). This was reflected by the MFIs showing that BEMs had increased expression of CCR6 compared with nBCs and GC B cells (Fig. 3.16G). The remaining markers were examined by flow cytometry by serial antibody dilutions as these antibodies had not previously been titrated. Histograms show staining at a dilution factor of

1:100. Expression BAFF-R was investigated as it is involved in the survival and maintenance of mBCs (Müller-Winkler et al., 2021). There was no major difference in the surface expression of BAFF-R, CD47 and CD49d (Fig. 3.16H-I). CD24a was expressed at high levels in BEMs and GC B cells but not in nBCs; the histogram showed a tail of $CD24^{lo}$ BEMs (Fig. 3.16H-I). SLAMF7 was upregulated in GC B cells and BEMs compared with nBCs, but the histogram showed a tail of $SLAMF7^{lo}$ BEMs (Fig. 3.16I). CD55 was downregulated in GC B cells compared with BEMs and nBCs. GC B cell expression of CD55 overlapped with the unstained control and BEMs also showed a tail of $CD55^{lo}$ cells (Fig. 3.16H). PECAM1 was downregulated in GC B cells compared with nBCs and BEMs (Fig. 3.16H-I). This shows that CD24 and SLAMF7 may be usable as markers for the activated B cell subsets: BEMs and GC B cells. CD55 and PECAM1 may be usable as markers for non-GC B cells. Dilution factor of 1:100 was used to detect these markers in the subsequent experiments. This suggested a potential strategy of co-staining to isolate BEMs by marking activated B cells by CD24a or SLAMF7 and non-GC B cells by CD55 or PECAM1.

To better test this, mice received adoptive cell transfer with NP-specific QM IgHNP Cg1Cre mTmG splenocytes, where antigen-activated B cells can be followed because Cg1Cre induces eGFP expression. On the following day mice were immunised with NP-KLH on the foot and drLN was examined by flow cytometry at 8 days post-immunisation (Fig. 3.17A). This differs from the previous figure as these transferred cells are reporters for B cell activation allowing more accurate determination of BEMs. Expression of CD24 and CD55 were examined by flow cytometry using CD24 to detect activated B cells and CD55 to detect non-GC B cells (Fig. 3.17B). Expression of SLAMF7 and PECAM1 were not shown as they were not as effective at distinguishing BEMs and GC B cells. Co-staining with CD24 and CD55 among all adoptively

transferred B cells was used to detect CD24-CD55+ “nBCs”, CD24+CD55- “GC B cells” and CD24+CD55+ “BEMs” (Fig. 3.17B). The quality of separation of GC and mBC populations was tested by back-gating CD24-CD55+ nBCs, CD24+CD55- GC B cells and CD24+CD55+ BEMs gates against CD38 and Fas; markers commonly used to identify GC and mBCs (Fig. 3.17C). This revealed that CD24-CD55+ cells were CD38+Fas-. One would expect a population of CD38+Fas- B cells to contain nBCs and non-activated B cells. CD24+CD55- were CD38-Fas+, similar to GC B cells. CD24+CD55+ cells were CD38+Fas+, so they were non-GC B cells that still exhibited some GC characteristics similar to BEMs (Zhang et al., 2022). This was more apparent among adoptively transferred cells.

One of the main differences identified in the GSEA comparing BEMs and GC B cells was that GC B cells were more proliferative than BEMs. To test proliferation of the populations defined by CD55 and CD24, EdU uptake was tested in nBCs, GC B cells and BEMs defined by these markers (Fig. 3.17D-E). EdU is incorporated into DNA during the S phase of cell cycle. About 20% of GC B cells took up EdU, while most naïve B cells defined by CD55 and CD24 did not (about 2%). Within BEMs defined by CD55 and CD24, only about 10% took up EdU (Fig. 3.17E). This suggested that some BEMs still proliferate after being generated from the GC or differentiated from GC B cells within 2 hours before tissue collection. LZ CCR6+ pre-memory B cells have been previously reported to exit cell cycle, this may explain why this heterogenous population of BEMs had lower EdU uptake than GC B cells as the BEM population may include pre-memory B cells (Suan et al., 2017). GC and BEM populations defined by CD55 and CD24 contained more IgG1+ cells than the naïve donor B cells, and BEMs contained slightly fewer IgG1 switched cells than the GC B cell population (Fig. 3.17F-G).

Cg1 germline RNA transcription is induced by signals that induce Ig class switch recombination: i.e. antigen-induced BCR stimulation and CD40-ligation plus IL-4 from Tfh cells (Toellner et al., 1998). Therefore, GFP+ donor cells should be antigen-experienced GC B or BEMs. When gating on GFP+ cells, the naïve CD24-CD55+ B cell population was absent, and only the BEMs (CD55+CD24+) and GC B cells (CD55-CD24+) were found. dTomato+ nBCs within the donor population are likely to be B cells that have lost NP-specificity due to secondary VDJ recombination (Cascalho et al., 1996). These were compared to naïve B cells from the endogenous population, which were gated as CD55+CD24- (Fig. 3.18A). These cells are a mix of naïve and antigen-activated cells from the host and naïve dTomato+ non-activated donor B cells; most of these cells were dTomato-. Antigen-experienced donor BEMs (GFP+B220+CD55+CD24+) and GC B cells (GFP+B220+CD55-CD24+) were back-gated onto a CD38 vs FAS plot. BEMs appeared where expected as CD38+Fas+ and GC B cells appeared as CD38-Fas+, whereas nBCs appeared as CD38+Fas- (Fig. 3.18B). As expected, BEMs and GC B cells compared with nBCs showed increased EdU uptake (Fig. 3.18C). IgG1 expression was examined; a larger proportion of donor BEMs and GC B cells had isotype switched to IgG1 compared with CD55/24 gated nBCs (Fig. 3.18D). The IgG1- population of BEMs and GC B cells had slightly higher IgG1 expression than nBCs. These IgG1- BEMs and GC B cells populations may include cells that do not express immunoglobulin (such as DZ B cells) or reflect passive absorption of IgG1 through Fc receptors. B cells from all live lymphocytes, including endogenous and adoptively transferred cells, were examined to determine how well CD24/55 markers detect activated B cells by examining expression of fluorescent protein (Fig. 3.18E). CD24-CD55+ B cells were mainly comprised of endogenous cells (99.8%) with a small number of GFP+ cells (0.13%) and very few dTomato+ cells (0.017%).

CD24+CD55+ cells were also mainly endogenous cells (91.9%) but with a greater proportion of GFP+ cells (7.61%) and very few dTomato+ cells (0.36%). Around 25% of CD24+CD55- cells were GFP+, with 1.48% dTomato+ cells and the remainder were endogenous (73.6%). When back gating CD24/55 populations against CD38 and Fas the CD24-CD55+ cells appeared as CD38+Fas- which would be expected of non-activated B cells. CD24+CD55- cells were Fas+ GC B cells, however CD24+CD55+ cells had a bimodal expression of Fas (Fig. 3.18F). Fas- CD24+CD55+ cells were almost entirely endogenous cells, but around a quarter of Fas+ CD24+CD55+ cells were GFP+ with the rest mainly endogenous cells (Fig. 3.18G). This suggested that CD24+CD55+Fas+ B cells were comprised of activated B cells. The endogenous population of B cells was also examined for CD24 and CD55 expression (Fig. 3.18H). Endogenous CD24-CD55+ cells were CD38+Fas- non-activated B cells, CD24+CD55- endogenous cells were CD38-Fas+ GC B cells, whereas CD24+CD55+ endogenous cells were CD38+ with bimodal expression of Fas (Fig. 3.18I).

To test the power of the CD24 and CD55 marker combination, a similar analysis was done for activated B cells in popliteal LNs from WT mice immunised in the hind foot without adoptive cell transfer (Fig. 3.19A). Non-activated B cells were gated as CD55+CD24- B cells (Fig. 19B, blue gate), BEMs were gated as CD55+CD24+ B cells (Fig. 3.19B, green gate) and GC B cells as CD55-CD24+ B cells (Fig. 3.19B, orange gate). EdU uptake and IgG1 expression was examined in these groups (Fig. 3.19B). There was an $IgG1^{low}$ population of Fas+ BEMs that had slightly higher IgG1 expression than Fas- BEMs. This may again reflect downregulation of immunoglobulin or passive absorption of IgG1 on Fc receptors on Fas+ BEMs. When backgated against CD38 vs Fas, the CD55+CD24- population represented CD38+Fas- non-activated B cells (blue) and the CD55-CD24+ population represented CD38-Fas+ GC B cells

(red). Interestingly, the CD55+CD24+ BEMs population (green) had a bimodal expression of Fas (Fig. 3.19B-C). Total CD55+ B cells contained a range of Fas+ and Fas- cells. Levels of higher CD24 expression correlated with Fas expression (Fig. 3.19D). The CD55+CD24+ Fas+ BEMs showed greater EdU uptake than its Fas- counterpart (Fig. 3.19E-F) and were as proliferative as GC B cells (Fig. 3.19B & D). More Fas+ BEMs had switched to IgG1 (Fig. 3.19G-H).

These observations suggested that the Fas+CD24+CD55+ population of non-BCR transgenic B cells represented the BEMs. This endogenous CD24+CD55+ BEM bimodal expression of Fas was also observed in endogenous B cells and GFP- B cells in the adoptive cell transfer experiment (Fig. 3.18F & I). This may be because the GFP+CD24+CD55+ B cell population contains activated B cells, but the endogenous CD24+CD55+ BEM population has not been stringently selected for activated B cells. Resultantly, this gate included overlap with CD24-intermediate Fas- non-activated B cells.

When gating on EdU+ B cells from NP-KLH immunised WT mice that did not receive adoptive cell transfers, GC B cells (orange) and BEMs (green) could be identified based on expression of CD55 and CD24, as previously described. EdU+ cells also contained a small population of CD24-CD55+ B cells (Fig. 3.20A, blue gate). This differed from examination of total B cells where a much larger population of CD24-CD55+ B cells was observed (3.19D). These did not express as much Fas as EdU+ CD24-CD55+ B cells (Fig. 3.20B). This suggests that the EdU+ CD24-CD55+ population may consist of recently activated cells transitioning into GC B cells. When the CD24/55 gated populations were back gated on CD38 and Fas the CD24+CD55+ BEMs were CD38+Fas+ and the CD24+CD55- GC B cells were CD38-Fas+ as expected. The

CD24-CD55+ “naïve” B cells expressed more Fas than EdU- non-activated B cells described above (Fig. 3.20B). A similar fraction of GC B cells and BEMs were switched to IgG1 among “naïve” B cells (Fig. 3.20C-D). EdU uptake of IgG1+ and IgG1- CD24+CD55- GC B cells and CD24+CD55+ BEMs was examined to verify if switching to IgG1 affected proliferation (Fig. 3.20E). IgG1- and IgG1+ GC B cells had comparable levels of EdU, whereas IgG1- BEMs had reduced EdU uptake than IgG1+ BEMs, this suggested that IgG1+ BEMs were more proliferative. IgG1+ CD24+CD55+ represented activated BEMs that had undergone class switching.

CD24 and CD55 were identified as markers to distinguish BEMs from GC B cells and nBCs. Reporter mouse models for activated B cells better distinguished BEMs from nBCs than CD24/55 staining alone. These CD24+CD55+ were proliferative and expressed IgG1. In endogenous B cells CD24+CD55+ BEMs bimodally expressed Fas, however, Fas+ BEMs appeared to represent IgG1+ proliferative BEMs. These markers may be used to identify BEMs at 8 days post-immunisation in the LN. It is important to note that this population defined as BEMs are likely a heterogenous population consisting of a different types of activated B cells. BEMs may also be produced in the spleen, consequently the response in this tissue was next examined.

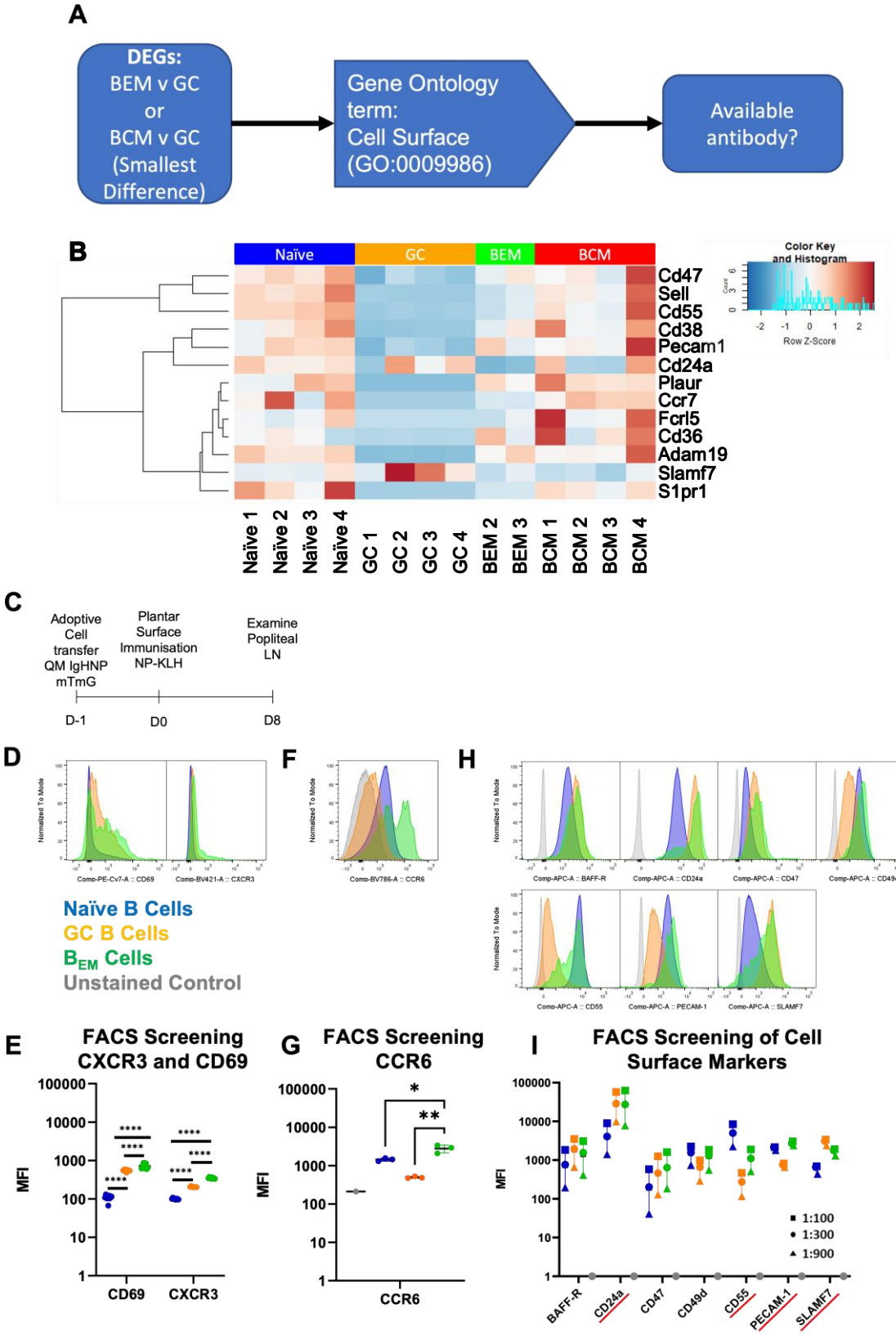

A
DEGs:
BEM v GC
or
BCM v GC
(Smallest
Difference)
Gene Ontology
term:
Cell Surface
(GO:0009986)
Available
antibody?
B
Naïve
GC
BEM
BCM
Color Key
and Histogram
Row Z-Score
Cd47
Sell
Cd55
Cd38
Pecam1
Cd24a
Plaur
Ccr7
Fcrl5
Cd36
Adam19
Slamf7
S1pr1
Naïve 1
Naïve 2
Naïve 3
Naïve 4
GC 1
GC 2
GC 3
GC 4
BEM 2
BEM 3
BCM 1
BCM 2
BCM 3
BCM 4
C
Adoptive
Cell
transfer
QM IgHNP
mTmG
Plantar
Surface
Immunisation
NP-KLH
Examine
Popliteal
LN
D-1
D0
D8
D
F
H
Naïve B Cells
GC B Cells
BEM Cells
Unstained Control
E
FACS Screening
CXCR3 and CD69
MFI
CD69
CXCR3
G
FACS Screening
CCR6
CCR6
I
FACS Screening of Cell
Surface Markers
1:100
1:300
1:900
BAFF-R
CD24a
CD47
CD49d
CD55
PECAM-1
SLAMF7

Figure 3. 16. Identification of potential flow cytometry markers to detect BEMs from RNA-sequencing data

(A) Flow chart describing strategy to obtain potential cell surface markers from RNA-sequencing data to identify BEMs by flow cytometry. See Appendix 1B for baseline adoptive cell transfer input data. (B) Heatmap displaying RNA expression of a selection of cell surface expressed genes.
(C) Schematic for adoptive cell transfer of NP-specific QM IgHNP mTmG splenocytes followed by immunisation with NP-KLH on plantar surface and tissue collection at 8 days post-immunisation. Cell transfers were performed by the University of Birmingham Biomedical Services Unit. (D) Histograms of CD69 (left) and CXCR3 (right) staining from flow cytometry in nBCs (GFP-dTomato+B220+CD138-CD38+), GC B cells (GFP+B220+CD138-CD38-Fas+) and BEMs (GFP+B220+CD138-CD38+). (E) MFIs of CXCR3 and CD69 in nBCs, GC B cells and BEMs, data from 3 separate experiments (n=9). (F) Histogram of CCR6 staining from flow cytometry in nBCs, GC B cells, BEMs and an unstained control. (G) MFIs of CCR6 expression from flow cytometry analysis of nBCs, GC B cells, BEMs (n=3) and an unstained control from one experiment.
(H) Histograms of BAFF-R, CD24a, CD47, CD49d, CD55, PECAM-1 and SLAMF7 staining at a dilution factor of 1:100 from flow cytometry of nBCs, GC B cells, BEMs and unstained control samples. (I) Summary of MFIs in a serial dilution experiment of BEMs markers (BAFF-R, CD24a, CD47, CD49d, CD55, PECAM-1 and SLAMF7) from flow cytometry of nBCs, GC B cells, BEMs and unstained control samples. Data represent 1 biological replicate of pooled lymphocytes from reactive popliteal LNs of 3 mice. Unstained control MFIs were below the minimum threshold so plotted at the threshold. One-Way ANOVA, * $P<0.05$, ** $P<0.01$, *** $P<0.001$, **** $P<0.0001$. Symbols represent individual mice; nBCs (blue), GC B cells (orange), BEMs (green). Horizontal bars show means.

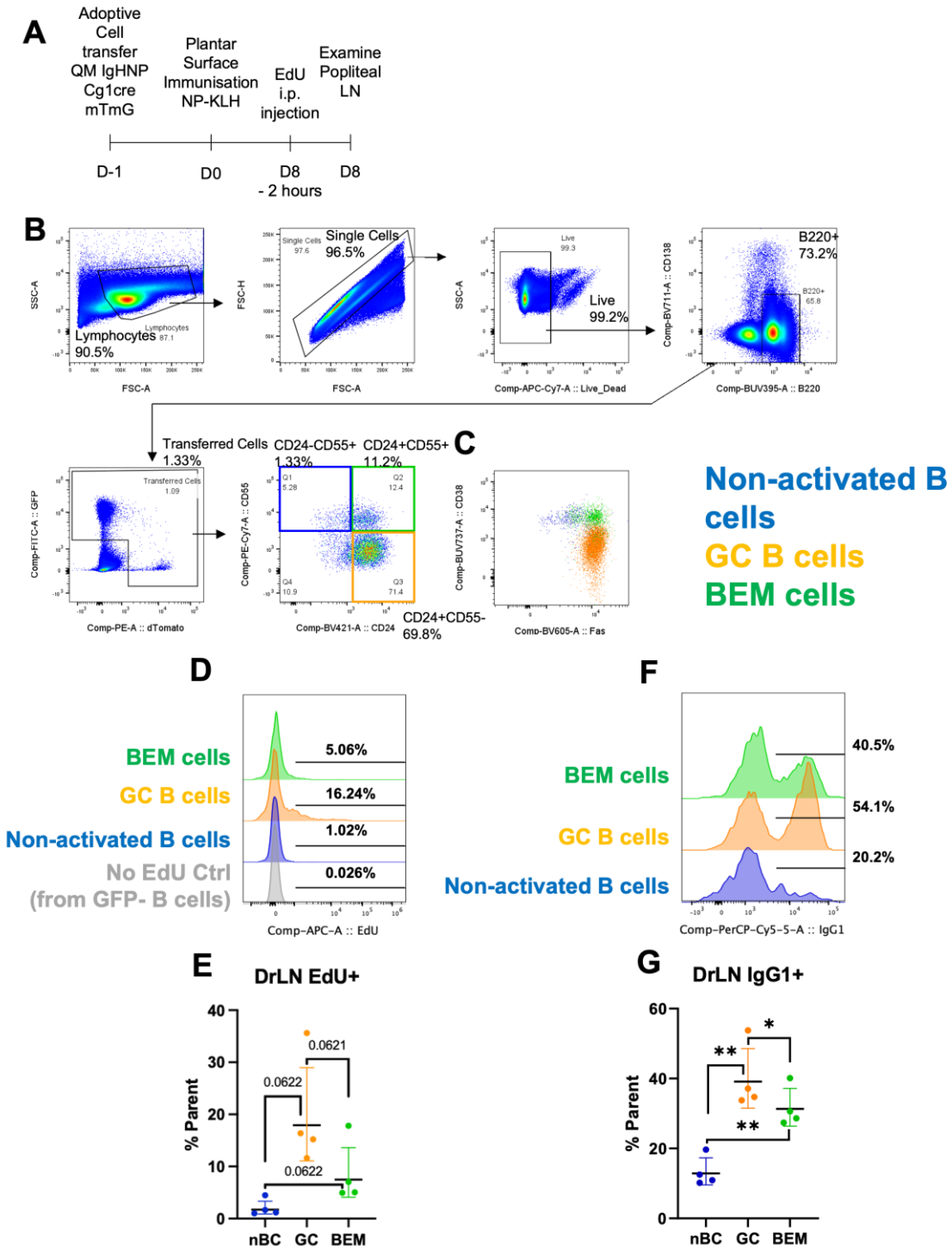


Figure 3. 17. Expression of CD24 and CD55 in BEMs from adoptively transferred cells assists distinguishing them from naive B cells and GC B cells

(A) Schematic of adoptive cell transfer and immunisation protocol. 2mg of EdU was administered 2 hours prior to tissue collection. Cell transfers and EdU administration were performed by the University of Birmingham Biomedical Services Unit. See Appendix 1B for

baseline adoptive cell transfer input data. (B) Gating strategy to isolate naïve B cells (CD55+CD24-), GC B cells (CD55-CSD24+) and BEMs (CD55+CD24+) from adoptively transferred cells (dTomato+ and/or GFP+). (C) Representative flow cytometry plot showing back gating of naïve B cells, GC B cells and BEMs on CD38 v Fas plot. (D) Histogram of EdU incorporation by naïve B cells, GC B cells and BEMs. (E) Expression of EdU in naïve B cells, GC B cells and BEMs as % Parent population (n=4). (F) Histogram of expression of IgG1 by naïve B cells, GC B cells and BEMs. (G) Expression of IgG1 in naïve B cells, GC B cells and BEMs as % Parent population (n=4). One-Way ANOVA, * $P<0.05$, ** $P<0.01$. Symbols represent individual mice; nBCs (blue), GC B cells (orange), BEMs (green).

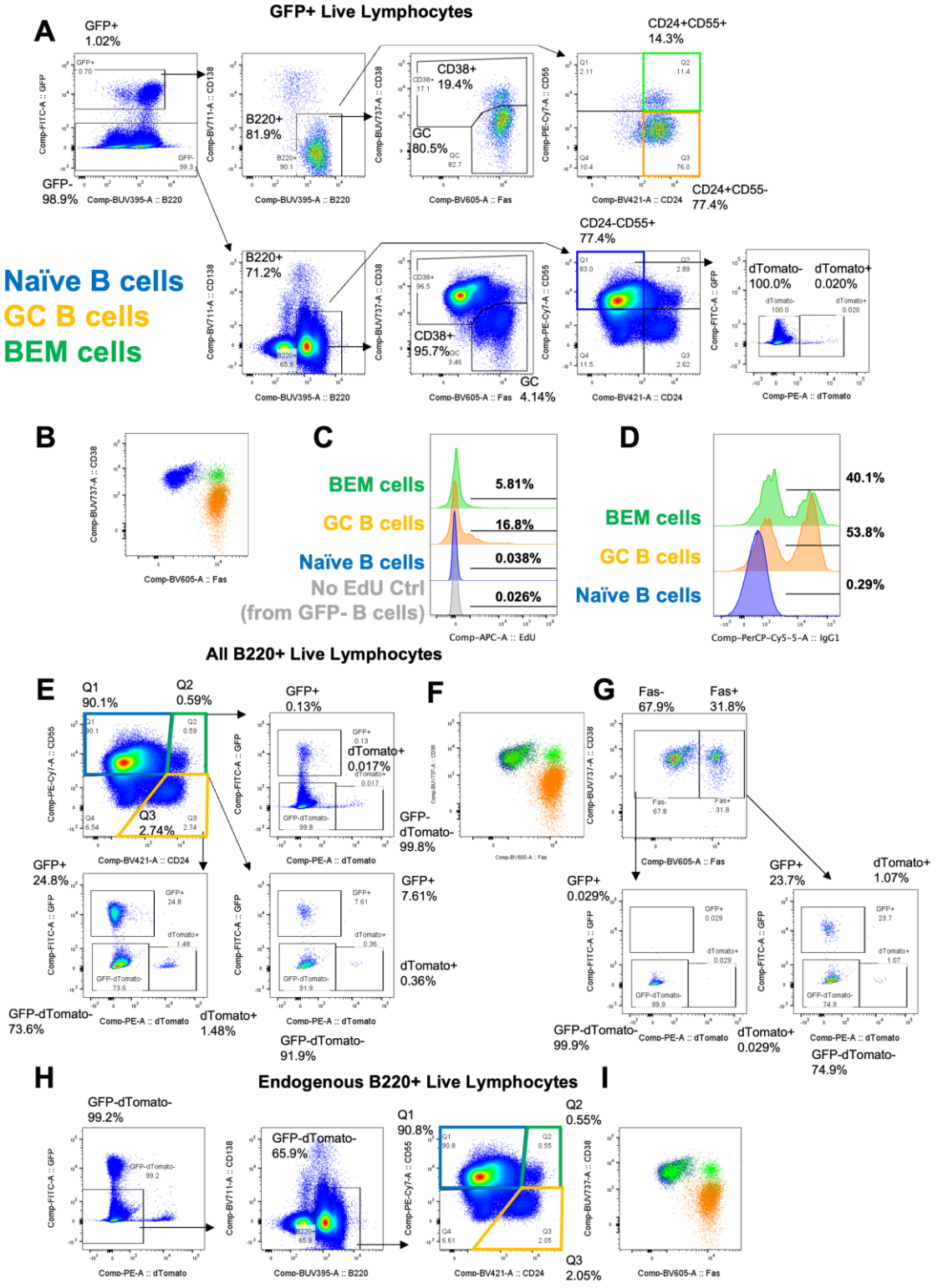


Figure 3. 18. Gating naive B cells, GC B cells and BEMs by CD24/CD55 expression detected cells from both endogenous and adoptively transferred populations

(A) Gating strategy to separate GC B cells from BEMs in GFP+ adoptively transferred cells and B cells from GFP- adoptively transferred and non-BCR transgenic B cells. (B) Representative flow cytometry back gating of “naïve” B cells (blue; GFP-B220+CD138-CD38+), GC B cells (orange; GFP+B220+CD138-CD38-Fas+) and BEMs (green; GFP+B220+CD138-CD38+) on a CD38 v Fas plot. (C) Histogram of EdU uptake in “naïve” B cells, GC B cells and BEMs compared with an unstained FMO control (grey). (D) IgG1 expression of “naïve” B cells, GC B cells and BEMs cells. (E) Representative flow cytometry of CD24 and CD55 staining in all live B220+ lymphocytes and the expression of GFP and dTomato among CD24-CD55+, CD24+CD55+ and CD24+CD55- cells. (F) Back gating of CD24-CD55+, CD24+CD55+ and CD24+CD55- live B220+ lymphocytes against CD38 and Fas. (G) Expression of Fas among CD24+CD55+ live B220+ lymphocytes and the expression of GFP among Fas- and Fas+ cells. (H) Representative flow cytometry showing expression of CD24 and CD55 among endogenous (GFP-dTomato-) B220+ live lymphocytes. (I) Back gating of CD24-CD55+, CD24+CD55+ and CD24+CD55- endogenous B cells against CD38 and Fas.

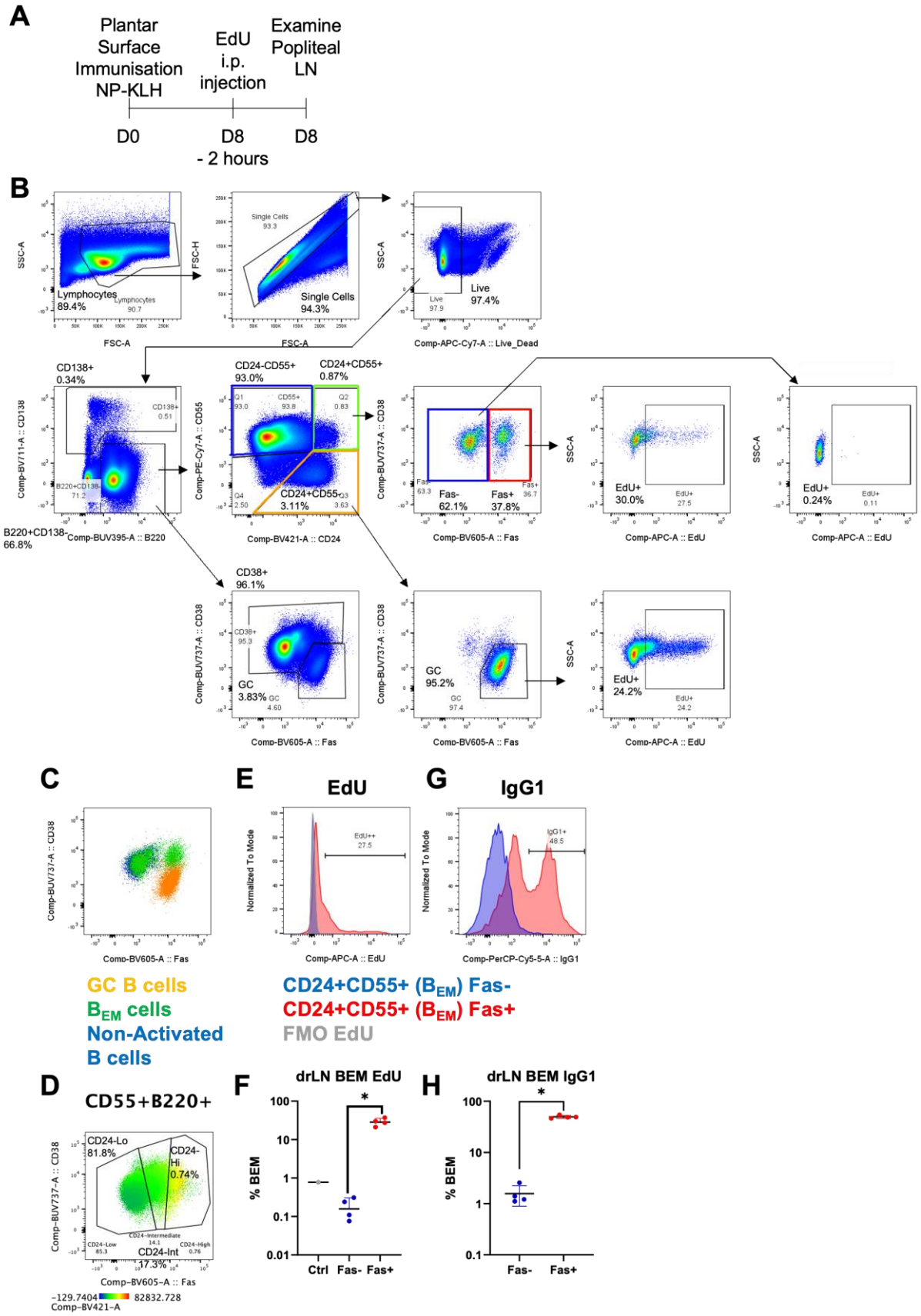

A
Plantar Surface Immunisation NP-KLH
EdU i.p. injection
Examine Popliteal LN
D0
D8 - 2 hours
D8
B
Lymphocytes 89.4%
Single Cells 94.3%
Live 97.4%
CD138+ 0.34%
CD24-CD55+ 93.0%
CD24+CD55+ 0.87%
B220+CD138- 66.8%
CD24+CD55- 3.11%
Fas- 62.1%
Fas+ 37.8%
EdU+ 30.0%
EdU+ 0.24%
CD38+ 96.1%
GC 3.83%
GC 95.2%
EdU+ 24.2%
C
GC B cells
BEM cells
Non-Activated B cells
E
EdU
CD24+CD55+ (BEM) Fas-
CD24+CD55+ (BEM) Fas+
FMO EdU
G
IgG1
D
CD55+B220+
CD24-Lo 81.8%
CD24-Hi 0.74%
CD24-Int 17.3%
F
drLN BEM EdU
% BEM
Ctrl
Fas-
Fas+
H
drLN BEM IgG1
% BEM
Fas-
Fas+

Figure 3. 19. BEMs were detected in WT mice using CD24/CD55 staining

The non-BCR transgenic B cell response in the draining popliteal LN was examined by flow cytometry. (A) Immunisation protocol to detect BEM markers popliteal LN. (B) Gating strategy to isolate naïve B cells (blue; B220+CD138-CD55+CD24-), GC B cells (orange; B220+CD138-CD55-CD24+) and BEMs (green; B220+CD138-CD55+CD24+). (C) Representative FACS showing back-gating of GC B cells and BEMs on CD38 v Fas plot. (D) Representative plot of all CD55+B220+ cells plotted against CD38 and Fas with a heatmap of CD24 expression. Expression of EdU in Fas- (blue) and Fas+ (red) BEMs shown in (E) a representative histogram and (F) presented as MFIs (n=4) compared with an un-stained control (grey). Expression if IgG1 in Fas- and Fas+ BEMs shown in a (G) representative histogram and (H) presented as MFIs (n=4). One-Way ANOVA, * p<0.05. Symbols represent individual mice; Fas- BEMs (blue), Fas+ BEMs (red). Horizontal bars show means.

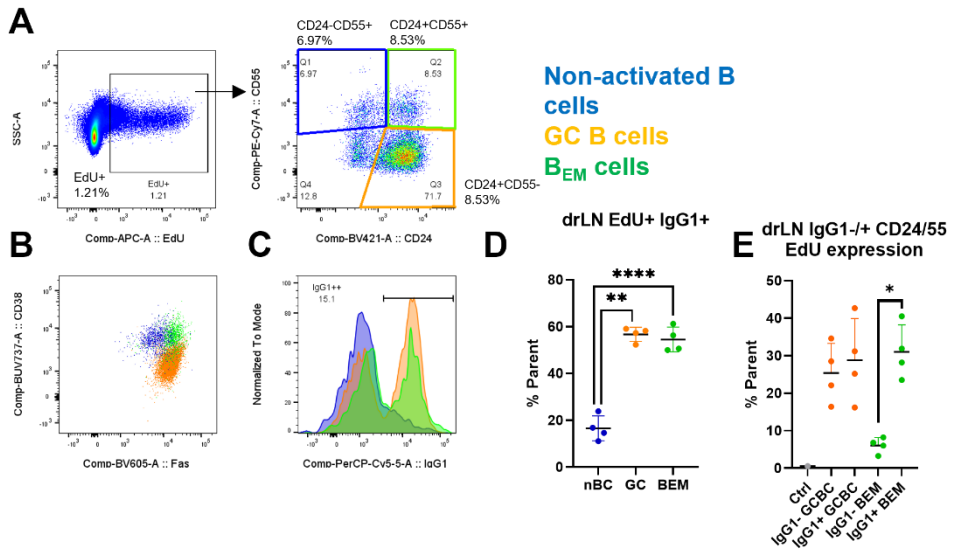


Figure 3. 20. Among EdU+ cells GC B cells and BEMs detected by CD24/CD55 staining were increased

(A) Mice were immunised as in Fig. 3.19 were gated using CD24 and CD55 to identify non-activated "naïve" B cells (blue; B220+CD138-CD55+CD24-), GC B cells (orange; B220+CD138-CD55-CD24+) and BEMs (green; B220+CD138-CD55+CD24+) from EdU+ B cells. (B) Representative flow cytometry plot showing back gating of naïve B cells, GC B cells and BEMs on CD38 v Fas plot. (C) Representative histograms from showing IgG1 expression of naïve B cells, GC B cells and BEMs. (D) IgG1 expression in EdU+ non-activated B cells, GC B cells and BEMs as a proportion of these respective populations (n=4). One-Way ANOVA, * p<0.05, ** p<0.01 and **** p<0.0001. (E) EdU uptake in IgG1+ and IgG1- BEMs and GC B cells and an unstained control sample as a proportion of these respective populations (n=4). Mann-Whitney test between IgG1+ and IgG1- BEMs and between IgG1+ and IgG1- GC B cells, * p<.05. Symbols represent individual mice; nBCs (blue), GC B cells (orange), BEMs (green). Horizontal bars show means.

3.2.5 NP-specific B cell response in the spleen

3.2.5.1 NP-specific response in the spleen over time showed a peak GC response at day 5 post-immunisation

The dynamics of the immune response in the spleen was examined to explore the changes in MZ B cells and BEMs over time, using the QM IgHNP Cg1Cre mTmG reporter mouse model. The response to NP in the spleen of C57BL/6 mice has been previously investigated after i.p. injection of NP-KLH or NP-CGG (Jacob et al., 1991). Murine MZ B cells express high levels of IgM BCRs and low levels of IgD BCRs. Upon recognition of antigen MZ B cells can readily differentiate into IgM-secreting PBs (Cerutti et al., 2013). This study showed that the GC response in the spleen to NP-hapten would reach a peak at 8 days after primary exposure to NP. The same adoptively transferred model, as described in Fig. 3.1A, was used to track antigen (NP)-specific B cells.

C57BL/6 mice were primed with i.p. injections of KLH in alum precipitate and 3 weeks later received adoptive cell transfer with IgHNP Cg1-Cre mTmG splenocytes, followed by secondary i.p. injection of soluble NP-KLH 1 day later. Mice were then examined at 0, 5, 8, 10 and 14 days after immunisation (Fig. 3.21A). Mice were primed with KLH to ensure the presence of KLH-specific T cells in the spleen. These facilitate the activation of NP-specific B cells in the boost by providing T cell help via co-stimulatory signals e.g., CD40-CD40L interactions. MZ B cells are located between the white pulp and the marginal sinus of the spleen. This places them in an advantageous position to act as a defence against blood-borne pathogens. MZ B cells were isolated from spleens by flow cytometry, defined as B220+CD138-CD93-CD23-CD21+ (Fig. 3.21B-C). Expression of GFP and dTomato was also examined among putative MZ B cells defined as dTomato+ or GFP+ B220+CD138-CD93-

CD23-CD21+ cells (Fig. 3.21D), these may indicate a proportion of dTomato+ non-activated putative MZ B cells and GFP+ activated putative MZ B cells from adoptively transferred cells.

MZ B cell numbers in the spleen increased over time, peaking at 10 days post-immunisation, and declining by 14 days post-immunisation (Fig. 3.22A-B). Putative GFP+ MZ B cells first appeared at 5 days post-immunisation and increased over time with a peak at 10 days post-immunisation (Fig. 3.22C-E). A small minority were Putative dTomato+ MZ B cells, these were fewer than total MZ B cells but increased over time, with the same peak at 10 days post-immunisation (Fig. 3.22F-H). Overall, MZ B cells increased during the response in the spleen, and a small number may be derived from adoptively transferred cells as they expressed GFP and dTomato. It is unclear whether these are comprised of pre-existing differentiated MZ B cells that were adoptively transferred and/or B cells that differentiated into MZ B cells in the response to antigen. These populations of putative adoptively transferred MZ B cells require further characterisation by examining expression of CD1d, IgM and location within the spleen to confirm their identity.

BEMs and GC B cells were followed by flow cytometry for CD38 and Fas (Fig. 3.23A-B). GC B cells reached a peak at 5 days post-immunisation (Fig. 3.23C). BEMs were defined as GFP+ CD38+ activated B cells in the spleen, some of these also expressed Fas. The assumption was that these were produced from the GC (due to expression of GFP) and may be similar to BEMs in the LN. BEMs reached peak levels at the same time as GC B cells at 5 days post-immunisation (Fig. 3.23D).

IgG1 expression was examined as a marker of Th2-type activated B cells in BEMs and GC B cells by flow cytometry (Fig. 3.23A, Fig. 3.24A-B). Peak IgG1 expression among GC B cells was

observed at 5 days post-immunisation (Fig. 3.24C). Also, peak IgG1 expression was also detected in BEMs at 5 days post-immunisation (Fig. 3.24D). This peak in the spleen is earlier than the GC response in the LN with a peak at 8 days post-immunisation (Fig. 3.1, Fig. 3.2). This was because the spleen was first primed against KLH before exposure to NP-KLH, therefore there was greater T cell help in the spleen due to recognition of KLH.

The prime-boost study of the response in the spleen was not a novel protocol and has been previously used to examine the B cell response in the spleen (Toellner et al., 1996, Cook, 2015). This experiment shows that the peak GC response and production of BEMs was at 8 days post-immunisation. This study of the splenic response involved adoptive cell transfer with the QM IgHNP Cg1-Cre mTmG splenocytes to ensure that there were NP-specific B cells present and these were reporters for B cell activation. One limitation of this investigation of the splenic response was that a lower concentration of antigen than has been previously validated, perhaps resulting in a weaker response than previous studies. The dose used in this present study was 20 µg NP-KLH (i.p.), whereas previous work used 50 µg of NP-CGG (i.p.), this lower dose may have provoked a weaker response (Toellner et al., 1996, Cook, 2015). Axillary and brachial LNs defined as distLNs were inspected for levels of BCMs, these reached a peak at 5 days post-immunisation. However, this data was not shown due to the mitigating factor that the i.p. injection may have stimulated B cells in the “distLN” (Van den Broeck et al., 2006). Van den Broeck et al (2006), showed by injecting mice with Indian ink and adjuvant, the sites draining the i.p. injection included the spleen and the axillary and brachial LNs.

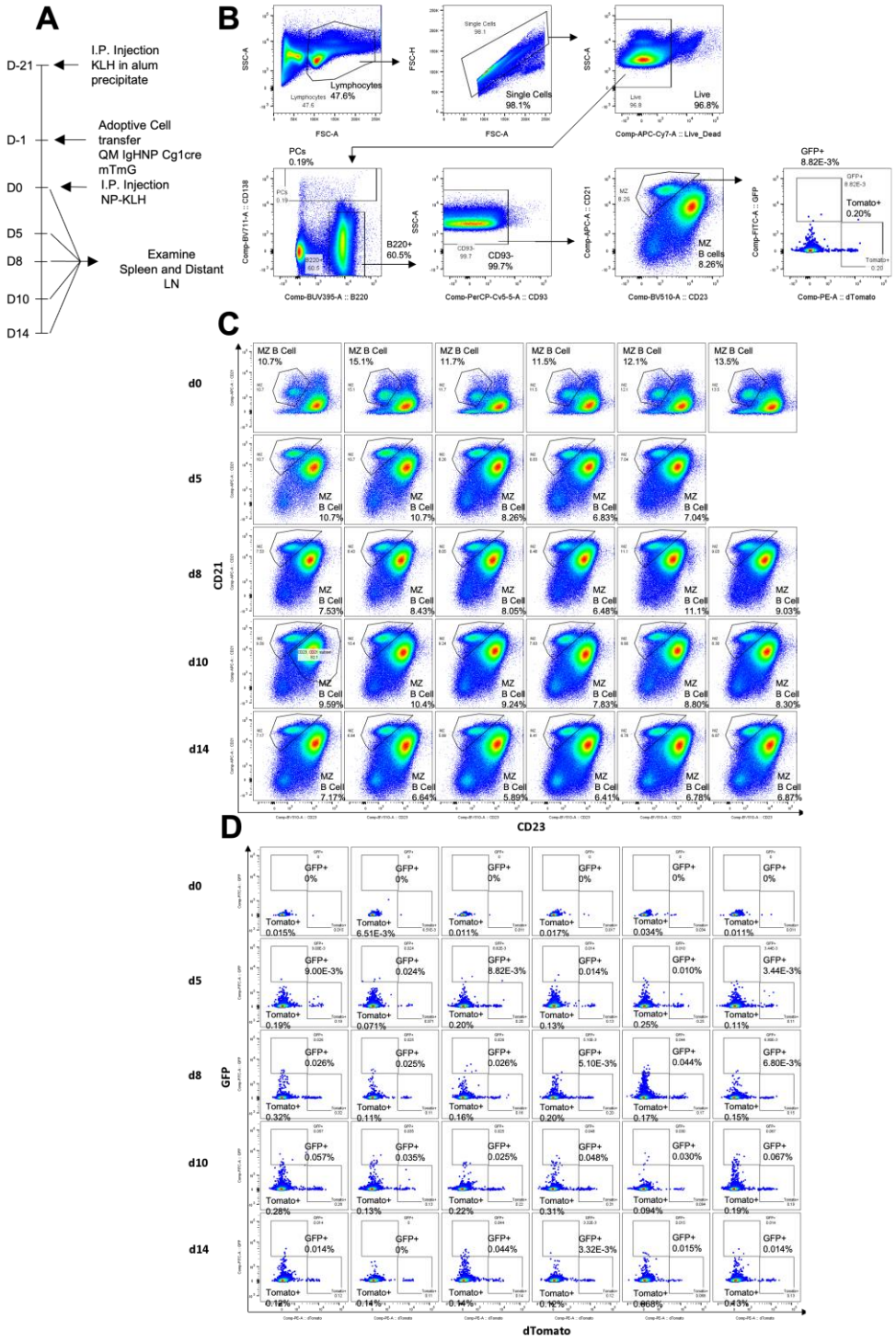


Figure 3. 21. Marginal zone B cells detected in an immunised spleen by flow cytometry over 14 days

(A) Experiment schematic measure response in the spleen over time. Immunisation was performed by the University of Birmingham Biomedical Services Unit. (B) Gating strategy to detect MZ B cells in the spleen. Flow cytometry plots summarising (C) MZ B cells (B220+CD138-CD93-CD21+CD23-) and (D) expression of GFP and dTomato among MZ B cells.

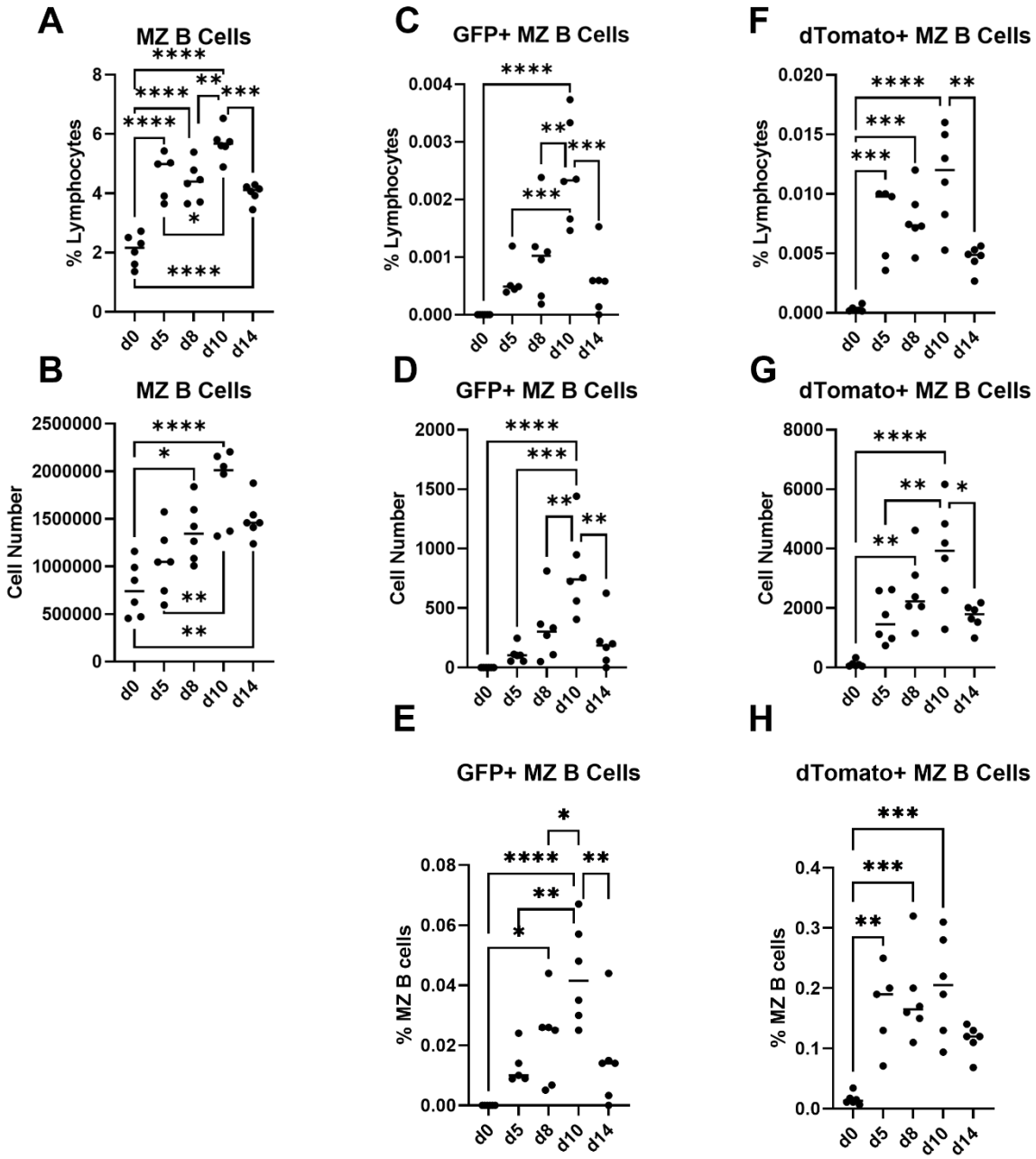


Figure 3. 22. MZ B cells reached a peak at 10 days post-immunisation in the spleen

Graphical summaries of MZ B cells in the spleen over time. Presented are MZ B cells (B220+CD138-CD93-CD21+CD23-) as % lymphocytes (A) and cell number (B). GFP+ MZ B cells as % lymphocytes (C), cell number (D) and % MZ B cells. dTomato+ MZ B cells as % lymphocytes (E), cell number (F) and % MZ B cells (n=5-6). One-way ANOVA, * P<0.05, ** P<0.01, *** P<0.001, **** P<0.0001. Symbols represent individual mice from one experiment. Horizontal bars show means.

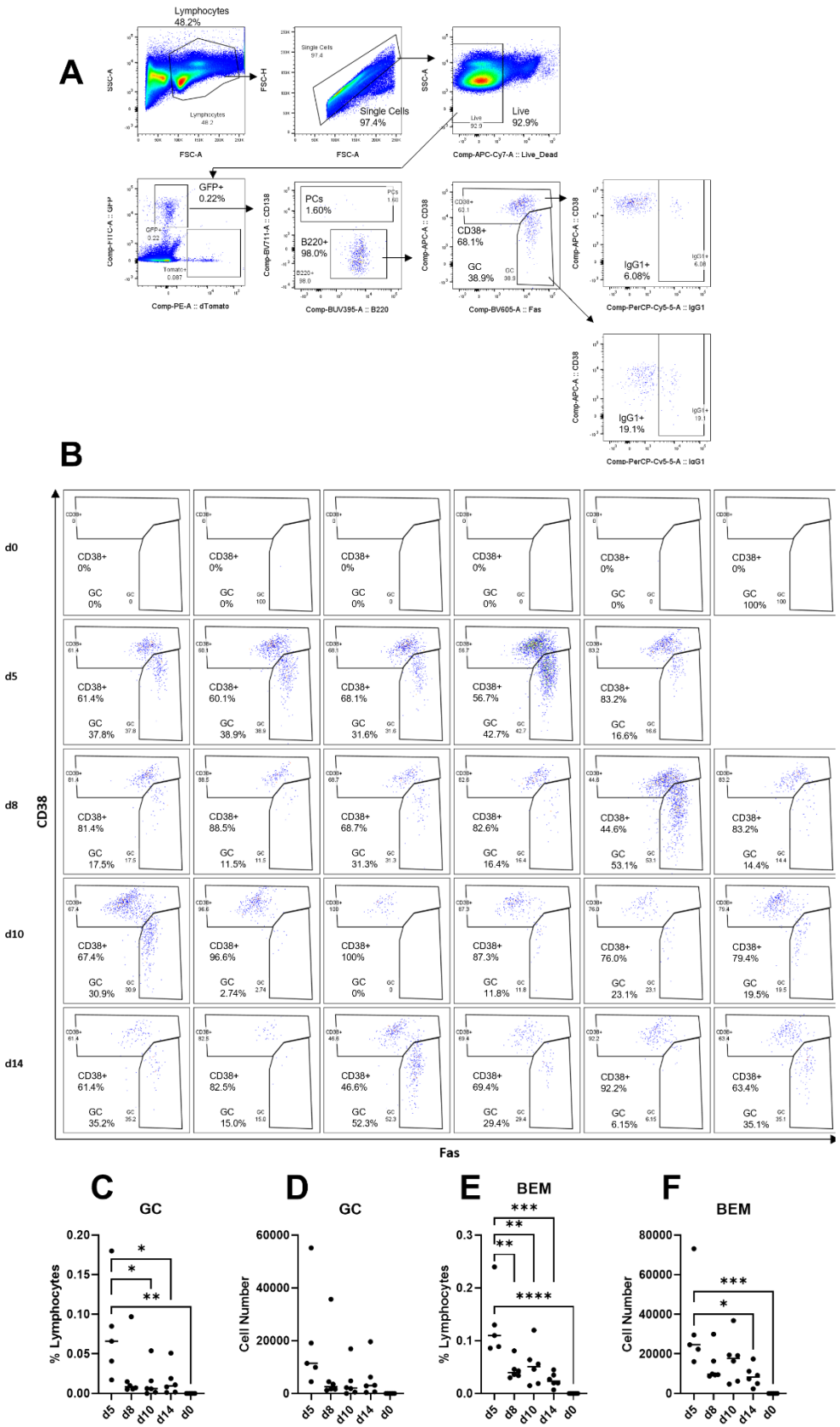


Figure 3. 23. Peak GC response and BEM levels at 5 days post-immunisation in the spleen

(A) Gating strategy to detect GC B cells (GFP+dTomato-B220+CD138-CD38-Fas+), BEMs

(GFP+dTomato-B220+CD138-CD38+), and their expression of IgG1. (B) Flow cytometry plot summaries of BEMs and GC B cells over time. Graphical summaries of GC B cells (C) and BEMs (D) as % lymphocytes (n=5-6). One-way ANOVA, * P<0.05, ** P<0.01, *** P<0.001. Symbols represent individual mice from one experiment. Horizontal bars show means.

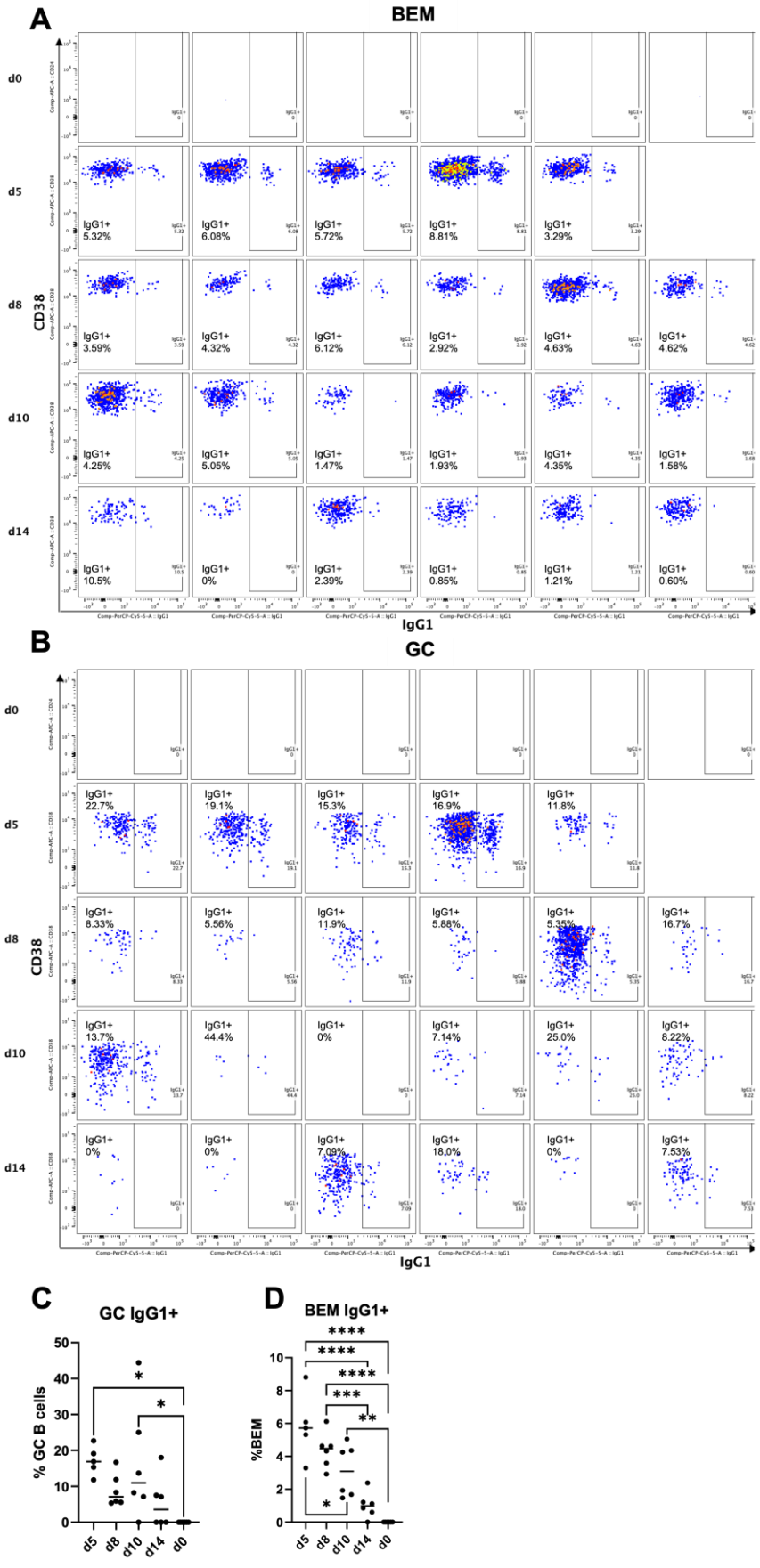

A
BEM
d0
d5
d8
d10
d14
CD38
IgG1
IgG1+ 5.32%
IgG1+ 6.08%
IgG1+ 5.72%
IgG1+ 8.81%
IgG1+ 3.29%
IgG1+ 3.59%
IgG1+ 4.32%
IgG1+ 6.12%
IgG1+ 2.92%
IgG1+ 4.63%
IgG1+ 4.62%
IgG1+ 4.25%
IgG1+ 5.05%
IgG1+ 1.47%
IgG1+ 1.93%
IgG1+ 4.35%
IgG1+ 1.58%
IgG1+ 10.5%
IgG1+ 0%
IgG1+ 2.39%
IgG1+ 0.85%
IgG1+ 1.21%
IgG1+ 0.60%
B
GC
IgG1+ 22.7%
IgG1+ 19.1%
IgG1+ 15.3%
IgG1+ 16.9%
IgG1+ 11.8%
IgG1+ 8.33%
IgG1+ 5.56%
IgG1+ 11.9%
IgG1+ 5.88%
IgG1+ 5.36%
IgG1+ 16.7%
IgG1+ 13.7%
IgG1+ 44.4%
IgG1+ 0%
IgG1+ 7.14%
IgG1+ 25.0%
IgG1+ 8.22%
IgG1+ 0%
IgG1+ 0%
IgG1+ 7.09%
IgG1+ 18.0%
IgG1+ 0%
IgG1+ 7.53%
C
GC IgG1+
% GC B cells
D
BEM IgG1+
%BEM

Figure 3. 24. Peak level of IgG1+ GC B cells and BEMs was at 5 days post-immunisation
Flow cytometry summary of IgG1 expression of (A) BEMs (GFP+dTomato-B220+CD138-CD38+) and (B) GC B cells (GFP+dTomato-B220+CD138-CD38-Fas+) over time. Graphical summaries of IgG1+ GC B cells (C) and IgG1+ BEMs (D) as % Parent. Graphical summaries of IgG1+ GC B cells (E) and IgG1+ BEMs (F) as Cell number (n=5-6). One-way ANOVA, * P<0.05, ** P<0.01, *** P<0.001, **** P<0.0001. Symbols represent individual mice from one experiment. Horizontal bars show means.

3.2.5.2 BEM marker expression in the spleen changed over time

B cells produced in the splenic response to NP-KLH were examined for BEM markers and their expression over time in the same experiment as described in Fig. 3.21A. This was to verify if expression of these markers on BEMs in the spleen was similar to BEMs in LN and to determine if the expression of these markers was retained over time. These markers were identified using RNA sequencing data; flow cytometry detected cell surface expression as shown earlier. In the response in the drLN CD24 and CD55 were found to be good markers to detect BEMs.

Upregulated CD24 transcription was seen in GC B cells. This raised transcription of CD24 was not observed in BEMs and BCMs (Fig. 3.16B). However, BEMs still retained detectable CD24 on cell surface likely due to their recent emergence from GC. As such, CD24 is a valuable marker for detecting BEMs by demarcating cells that have emerged from GCs in the LN. CD24 was examined for its use as a marker for activated B cells in the spleen. CD24 was consistently expressed at higher levels by GC B cells at all time points, whereas it was expressed at very low levels by nBCs. BEMs expressed CD24 at lower levels than GC B cells at all time points. CD24 expression was raised in BEMs compared with nBCs at 5 days (8-fold) and 8 days (11.5-fold) post-immunisation, but not as much on 10 days and 14 days (6-fold) post-immunisation. However, there was a slight resurgence of CD24 at 14 days post-

immunisation (Fig. 3.25A). This suggested that BEM expression of CD24 in the spleen was transient and decreased over time. CD24 may be used as a marker to detect GC B cells, but in the spleen, it could only detect BEMs at 5 days post-immunisation. CD24 was a far better marker for BEMs in the drLN. There were also some outlying CD24- GC B cells from 10 days post-immunisation onwards.

CD55 transcription and cell surface expression in the LN was lost in GC B cells but re-expressed in BEMs, therefore it was used to detect non-GC B cells (Fig. 3.16H and Fig. 3.16B). This is because BCL-6 expressed by GC B cells represses CD55 (Cumpelik et al., 2021). CD55 expression in the splenic GC response was monitored over time. In the spleen CD55 expression was lower in GC B cells compared with nBCs (8-fold) and BEMs (5-fold) at all time points. CD55 was expressed at high levels by nBCs and slightly lower levels by BEMs at all time points (Fig. 3.25B). Histograms showed that CD55 was highly expressed by nBCs; this expression was lost in GC B cells but recovered by BEMs in the spleen at all time points (Fig. 3.25C). Additionally, in a CD38 v Fas plot of GFP+ B cells in the spleen CD55 was typically highly expressed by CD38+ B cells and weakly expressed in CD38-Fas+ GC B cells at all time points (Fig. 3.25D). This showed that CD55 was an effective marker for non-GC B cells in the spleen.

BAFF-R is a crucial receptor for pro-survival signals for B cells and mBCs (Müller-Winkler et al., 2021). BAFF-R expression was examined in nBCs, GC B cells and BEMs to verify its importance in promoting survival of these subsets. BAFF-R was highly expressed by GC B cells at all time points, at about 3-fold higher than nBCs at 5 days post-immunisation. However, the level of GC B cell BAFF-R expression appeared to reduce over time to just

under 2-fold higher in GC B cells by 14 days post-immunisation. BEMs highly expressed BAFF-R compared with nBCs during the peak of the GC response in the spleen at 5 days post-immunisation (around 2.5-fold). However, BEM expression of BAFF-R reduced drastically by 14 days post-immunisation (around 1.25-fold). nBCs expressed very low levels of BAFF-R at all time points (Fig. 3.25E). PECAM1 was identified as a potential marker for non-GC B cells. PECAM1 was expressed at very low levels by GC B cells at all time points. PECAM1 expression by nBCs was consistent at all time points (Fig. 3.25F). PECAM1 was expressed at high levels by BEMs at 5 days post-immunisation (around 2-fold) compared with GC B cells and nBCs. Expression of PECAM1 in BEMs was reduced over time; by 14 days post-immunisation BEM expression was comparable with nBCs but still raised over GC B cells (around 2-fold).

SLAMF7 is used as a robust marker for PCs, and it was selected for use as a potential marker to identify activated B cells due to its upregulation in GC B cells and BEMs in the drLN (Fig. 3.16H). SLAMF7 expression in the splenic GC response over time was evaluated. At 5 days post-immunisation SLAMF7 was expressed at high levels by GC B cells and BEMs (around 3.6-fold) compared with nBCs. BEM SLAMF7 expression decreased by 14 days post-immunisation (around 2-fold) compared with nBCs. SLAMF7 expression by GC B cells was relatively constant at all time points, whereas expression by nBCs was low and remained at this level at all time points (Fig. 3.25G). CXCR3 is a chemokine receptor that is known to be expressed by IgG1+ mBCs (Muehlinghaus et al., 2005). CXCR3 expression in the splenic GC response over time was evaluated. CXCR3 was expressed at high levels by BEMs at 5 days post-immunisation compared with both nBCs (5-fold) and GC B cells (2.5-fold). Expression was reduced by 8 days post-immunisation but was still higher than GC B cells (1.6-fold) and nBCs

(3.5-fold). At 10- and 14-days post-immunisation BEMs and GC B cells expressed high levels of CXCR3 compared with nBCs (BEMs: 3.5-fold, GC B cells: 2.5-fold) (Fig. 3.25H).

CCR6 has previously been identified as a marker for pre-memory B cells and may have some relevance in identifying BEMs (Suan et al., 2017). CCR6 was consistently highly expressed by BEMs at all time points compared with GC B cells (160-230-fold) and was expressed slightly higher in BEMs compared with nBCs at all time points (3-5-fold). However, BEM CCR6 expression reduced slightly after 5 days post-immunisation (Fig. 3.25I). Histogram plots from flow cytometry of the spleen showed that CCR6 was strongly expressed in BEMs compared with GC B cells at all time points. Additionally, to a lesser extent CCR6 was also raised in BEMs compared with nBCs (Fig. 3.25J). Among GFP+ B cells in the spleen CCR6 was typically expressed more by CD38+ BEMs compared with CD38-Fas+ GC B cells at all time points (Fig. 3.25K). This showed that CCR6 may be an effective marker for distinguishing BEMs from GC B cells in the spleen. Whether CCR6 may effectively distinguish BEMs from nBCs is less clear as there was increased overlap of BEMs CCR6 expression with nBCs over time. Another marker for activated B cells in the spleen may be required to better detect BEMs.

BEM markers were observed in the splenic response to NP-hapten. At the peak of the splenic GC response nBCs, GC B cells and BEMs showed a similar pattern of expression to their counterparts in the peak GC response in the LN. BAFF-R, PECAM1, SLAMF7 and CXCR3 expression diminished over time, whereas CD24, CD55 and CCR6 expression remained relatively constant.

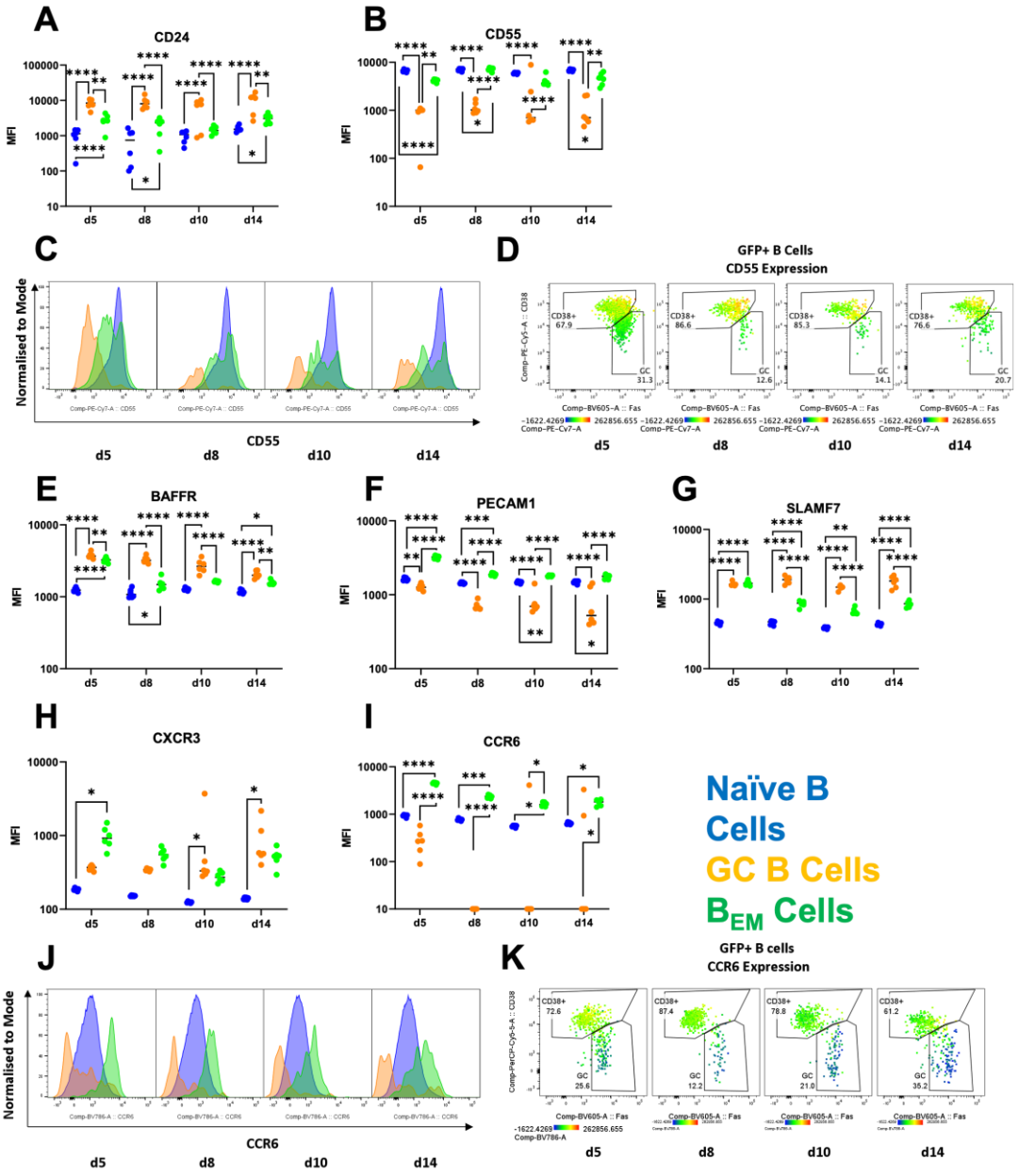


Figure 3. 25. Markers distinguishing BEM from GC B cells and naive B cells were detected in the immunised spleen and BEM marker expression was tracked over time

Summaries of BEM markers CD24 (A) and CD55 (B) of naïve B cells (blue; GFP- B220+CD138-CD38+), GC B cells (orange; GFP+B220+CD138-CD38-Fas+) and BEMs (green; GFP+B220+CD138-CD38+) at 5-, 8-, 10- and 14-days post-immunisation in the spleen displayed as MFIs from flow cytometry data (n=5-6). (C) Representative histograms of CD55 expression in in the spleen. (D) Coloured heatmap statistic of CD55 expression in GFP+ B cells plotted against CD38 and Fas.

Summarised MFIs of BEM markers (E) BAFFR, (F) PECAM1, (G) SLAMF7, (H) CXCR3 and (I) CCR6 from flow cytometry of naïve B cells, GC B cells and BEMs in the spleen at days 5-, 8-,

10- and 14-days post-immunisation. Data points on the X-axis represent samples with an MFI below a threshold of 10 (n=5-6). (J) Representative histograms of CCR6 expression in in the spleen. (K) Coloured heatmap statistic of CCR6 expression in GFP+ B cells plotted against CD38 and Fas. Two-Way ANOVA, * p<0.05, ** p<0.01, *** p<0.001 and **** p<0.0001. Symbols represent individual mice from one experiment. Horizontal bars show means.

3.3 Discussion

The peak of the GC response of QM Cg1-Cre mTmG lymphocytes in the drLN to NP-CGG or NP-KLH was at around 8 days post-immunisation because levels of GFP+ B cells, PCs, GC B cells and BEMs were at their highest. This concurred with previous work which showed a peak GC response and BEM production at 8 days post-immunisation. Additionally, BCMs could be detected in distant LN and spleen from this time point onwards (Zhang et al., 2022, Toellner et al., 1998). At this time point light sheet microscopy showed BEMs migrating between the SCS and GC. This corroborated previous work showing that BEMs "recycle" between the SCS and the GC (Zhang et al., 2022).

The response of QM Cg1-Cre mTmG cells in the spleen to NP-KLH in a prime-boost immunisation was examined over time to track the response of adoptively transferred cells. Endogenous MZ B cells reached a peak at 10 days post-immunisation. This suggested that later in the splenic response to NP-KLH there may be a recruitment of MZ B cells. A small number of GFP+ and Tomato+ "MZ" B cells were also detected; these may be comprised of pre-existing MZ B cells that were present in the adoptive cell transfer solution. This could also represent MZ B cells that developed from adoptively transferred B cells during the response. T1 and T2 transitional B cells can differentiate into MZ B cells by ADAM10-mediated cleavage and activation of Notch2 (Hammad et al., 2017). Therefore, the small number of adoptively transferred MZ B cells detected could also be derived from T2

transitional B cells that differentiated into MZ B cells in the host spleen. This could be verified by quantifying the levels of T2 transitional B cells and MZ B cells in the adoptive cell transfer donor spleen in future work. The prime-boost GC response in the spleen reached peak levels of GC B cells, BEMs and at 5 days post-immunisation. There was also an IgG1 response, however this was not the main response in this protocol.

At the peak of the response in the drLN the RNA expression of B cell subsets was examined. GSEA of GC B cells showed that they typically enriched for gene sets associated with cell cycle progression. This reiterated that GC B cells are highly proliferative. Like GC B cells, GSEA of BEMs suggested that they were proliferative compared with BCMs as they were enriched for gene sets associated with cell cycle progression in GSEA. GSEA suggested that BCMs might better placed for response to antigen than the other B cell subsets due to enrichment for gene sets involved in immune response and antigen presentation. However, this may simply reflect that BCMs have already gone through these processes of immune response and antigen processing/presentation during their initial activation, resulting in higher levels of gene expression than nBCs. BCMs may be more mobile than BEMs and GC B cells due to enrichment for gene sets involving interaction with ECM and water reabsorption.

RNA sequencing also showed that BEMs upregulated *Ccr6*, *Ccr7*, *Cd62l* (*Sell*), *S1pr1* and *Cd38*. This gene expression profile of BEMs was similar to a B cell subset described as pre-memory B cells that upregulated CCR6, Bach2 and Ephrin B1 (Suan et al., 2017, Shinnakasu et al., 2016, Laidlaw et al., 2017). This suggested that they may be similar groups - potentially the same population or there is an overlap in the gating strategy. Due to the position of BEMs

within the LN as outputs from the GC, they may be more mature than pre-memory B cells as they have exited the GC. However, the pre-memory B cells in the LZ may also represent BEMs that have returned from the SCS.

Expression of chemokine receptors may provide clues as to why BEMs migrate towards the SCS. The ligand for CCR6 is CCL20 which is expressed by floor LECs (Grasso et al., 2021). There may be a CCL20 gradient leading to the SCS for CCR6-expressing cells to follow. S1PR1-expressing lymphocytes in the LN can respond S1P which is at high levels in the blood and lymph, facilitating a gradient across the LN where the follicles represent an S1P-low region (Arnon et al., 2011, Hwang et al., 2019). This may facilitate entry of lymphocytes to cortical and medullary sinuses, and perhaps the SCS, allowing egress via the efferent lymphatics (Zhang et al., 2016, Park et al., 2012). This may also facilitate migration of BEMs that express *S1pr1*. BEMs also upregulated *Ebi2* (*Gpr183*). The EBI2 (GPR183) receptor facilitates B cell migration to the SCS and interfollicular areas by following 7a,25-dihydroxycholesterol gradients (Gatto et al., 2011).

RNA sequencing helped to identify CD24 and CD55 as potential cell surface markers to distinguish BEMs from GC B cells. This was confirmed by flow cytometry to determine protein level expression. CD24 is a cell adhesion molecule that is first expressed during B cell development in Pre-Pro-B cells and is expressed at high levels from pro-B cells up until transitional B cells (Hardy, 2013). CD24 is also expressed by GC B cells in mice (Shinall et al., 2000). Transcription of Cd24 was decreased in the BEMs compared to GC B cells. Unexpectedly protein expression of CD24 was detected on the cell surface of BEMs by flow cytometry. Cell surface CD24 expression between GC B cells and BEMs was comparable. This

suggested that, although CD24 was transcribed in the GC B cell, the BEM stage stopped CD24 transcription but still expressed it at the protein level. CD55 was downregulated in GC B cells and because CD55 is repressed by BCL-6 (Cumpelik et al., 2021). CD55 repression in GCs prevented degradation of C3 and C5 convertases which allowed production of C3a and C5a. These products of C3 and C5 convertases contribute to positive selection in the GC (Cumpelik et al., 2021). BEMs in the drLN also upregulated CCR6. CCR6 is a receptor for CCL20 and is expressed by pre-memory B cells (Suan et al., 2017).

PECAM1 was another marker investigated due to its upregulation on nBCs an BEMs. PECAM1 is an adhesion molecule expressed by endothelial cells, typically at junctions of adjacent cells, and is involved in trans-endothelial migration of leukocytes (Woodfin et al., 2007). SLAMF7 was investigated in the drLN as it was upregulated in GC B cells and BEMs. SLAMF7 is used as a robust marker for PCs. SLAMF7 is also a receptor that recognises self-ligands and induces immunomodulation. SLAMF7 promotes immune activation in the presence of Ewing's sarcoma associated transcript 2 (EAT-2) adaptor protein. Conversely, in the absence of EAT-2, SLAMF7 has an inhibitory effect on the immune response (O'Connell et al., 2019). CXCR3 was also investigated as it was known to be expressed by IgG1+ mBCs (Muehlinghaus et al., 2005). BAFF-R was also examined as it is required for B cell survival and plays an important role in mBC survival (Müller-Winkler et al., 2021). These other markers could not distinguish between B cell subsets in the drLN as accurately as CD24 and CD55 so were not used to detect BEMs.

Uptake of EdU was used to confirm the identity of CD24+CD55+ cells as BEMs - they were proliferative, indicating they may be GC-derived. A good next step would be to verify the

BCR affinity of BEMs as memory B cells and pre-memory B cells are of a lower affinity than PCs (Suan et al., 2017). These BEM markers distinguished BEMs from GC B cells in WT mice, to a limited extent, without using reporter mouse models. Co-staining with CD24 and CD55 allowed identification of BEMs, but a proliferation marker made it more effective as CD24+CD55+ BEMs bimodally expressed Fas. The Fas+ non-BCR transgenic BEMs had similar expression of IgG1 and EdU uptake as BEMs from the adoptive cell transfer model, indicating that they may represent the same population. This may allow detection of BEMs in the peak of the GC response to NP-KLH/NP-CGG in LN without a transgenic mouse model to report B cell activation.

Markers to distinguish BEMs from GC B cells in the LN were also examined in the splenic GC response to NP-KLH, which reached a peak of GC B cells and BEMs at 5 days post-immunisation. In the spleen CD24 was highly expressed by GC B cells and BEMs at 5 days post-immunisation, but expression by BEMs was lost over time. Additionally, CD24 was not expressed as strongly by BEMs in the spleen as in the LN. CD55 was similarly downregulated in splenic GC B cells as in the LN, also this downregulation was consistent in the spleen at all time points. During the peak splenic GC response BAFF-R was upregulated in BEMs and GC B cells compared with nBCs. Conversely, in the LN there was no clear difference in BAFF-R expression between these groups during the peak GC response. Additionally, BEM expression of BAFF-R was decreased from 8 days post-immunisation in the spleen. GC B cells in the spleen also appeared to decrease BAFF-R expression over time. SLAMF7 was upregulated in BEMs and GC B cells compared with nBCs during the peak GC response in both spleen and LN. However, expression of SLAMF7 in the spleen decreased over time in a similar trend to BAFF-R. In the LN GC response CXCR3 was slightly increased in BEMs and

increased to a lesser extent in GC B cells compared with nBCs. The same trend was seen in the peak splenic GC response, but over time BEMs expression of CXCR3 decreased until it was comparable with GC B cells by 10 days post-immunisation. CCR6 was strongly upregulated by BEMs compared with GC B cells and upregulated to a lesser extent compared with nBCs in the peak GC response in the LN. This same trend was seen in the spleen at all time points. CCR6 was a good marker to detect BEMs and CD55 could be used to confirm they are non-GC B cells. Co-staining with CCR6 and CD55 may be a good strategy to detect BEMs in the splenic response to NP-hapten, although this was not done in this present study. The expression of some of these markers in the spleen appeared to change over time, so it would be important to investigate the expression of these markers in the response in the LN over time.

In conclusion, the dynamics of production of BEMs were quantified in the drLN and spleen. RNA sequencing characterised BEMs in the drLN as similar to GC B cells, but still distinct from them. BEMs also had a very similar gene expression profile to pre-memory B cells. Cell surface markers were uncovered to help distinguish BEMs from GC B cells in the drLN and spleen.

4 Emigrating memory B cells within the draining lymph node

4.1 Introduction and Objectives

Many factors can direct the movements of lymphocytes within the LN. CCR7 is a requirement for entry of lymphocytes via the CCL21-rich HEVs (Steen et al., 2014). B cell expression of CCR7 is crucial during activation as it mediates migration of B cells that have recognised antigens to the B-T cell zone interface where they can receive help from CD4+ T cells (Toellner, 2014, Okada et al., 2005). CXCR5 expression ensures localisation of B cells to the CXCL13-rich B cell areas in the follicles of the LN (Pereira et al., 2010). S1PR1 facilitates migration following S1P gradients and is expressed by lymphocytes. In the drLN it plays a role in the migration of lymphocytes towards the outer follicular regions, followed by egress from the LN via the efferent lymphatics by entering cortical sinuses (Pereira et al., 2010). S1PR1 is also involved in cell migration in the spleen as MZ B cells express S1PR1. Other lymphocytes also migrate towards the marginal sinus; unlike MZ B cells they do not express sufficient adhesion molecules to withstand the tear forces of the marginal sinus and enter circulation, leaving the spleen (Pereira et al., 2010). After entering the SLO lymphocytes upregulate expression of S1PR1, this level of expression increased with time and was dependent on their position in the tissue, with increasing expression as they migrate to the follicle which is an S1P-low environment (Park et al., 2012). This may indicate an S1P-mediated desensitisation of S1PR1 in S1P-high environments (e.g., blood and lymph) or conversely S1PR1 re-sensitisation in this S1P-low region of the follicle (Arnon et al., 2011, Hwang et al., 2019). Resultantly, lymphocytes in the S1P-low environment of the follicle had enhanced sensitivity to S1P, promoting egress and weaker chemotactic cues from CCR7, CXCR4 and CXCR5 that promote retention within the tissue (Park et al., 2012).

ACKR4 is a scavenger receptor for CCL19 and CCL21 (which are also ligands of CCR7). It can bind these ligands and internalise them (Matti et al., 2020b). ACKR4 plays a role in regulating the chemokine gradients of CCL21 in the LN SCS as ACKR4 is expressed by ceiling LECs (Ulvmar et al., 2014).

RT-PCR data from our lab confirmed our findings of RNA sequencing data that BEMs upregulated *S1pr1* and *Ebi2*, and downregulated *S1pr2* compared with GC B cells (Zhang et al., 2022). In this chapter the role of S1PR1 in the movements of BEMs within the drLN was investigated. Furthermore, BEMs upregulate *Ccr7* compared with GC B cells (Zhang et al., 2022). CCR7 is required for the entry of DCs from the SCS to the drLN following CCL21 gradients regulated by ACKR4 (Ulvmar et al., 2014). In this chapter the role of ACKR4 in the migration of BEMs in the drLN was also investigated.

In humans, PCs can be retained for decades (Landsverk et al., 2017). If PCs can persist for such a long time and can produce antibodies throughout this time, what role do mBCs play? MBCs tend to be less efficiently selected for high affinity than PCs, are highly variable, and therefore may be more likely to be cross-reactive (Smith, 1997, Shinnakasu et al., 2016, Suan et al., 2017, Viant et al., 2020). MBCs can produce an effective response to antigenic variants of the WNV (Purtha et al., 2011). Thus, lower affinity of mBCs may facilitate cross-reactivity to antigen variants. This chapter investigated whether BEMs have a similar role in response to antigenic variants by examining the response to antigenic variants when movement of BEMs is impaired.

This chapter investigated the following hypotheses:

1. CCR7 ligand gradients direct movement of BEMs from the SCS to the GC in the drLN

2. S1PR1 ligand gradients in the drLN direct BEM migration from the GC to the SCS
3. BEM SCS-GC recycling is required for recognition of antigenic variants

4.2 Results

4.2.1 Investigating the role of ACKR4 and expression of CCL21 in draining lymph nodes

ACKR4 is a scavenger receptor that can bind and internalise the chemokines CCL19 and CCL21 and is involved in maintaining CCL19/21 gradients in the SCS (Ulvmar et al., 2014). BEMs and nBCs express CCR7, which would allow them to follow CCL19/21 gradients generated by ACKR4 (Fig. 4.1A). CCL21a is the isotype of CCL21 expressed in the LN and is a ligand of CCR7 and ACKR4 (Matti et al., 2020a). The aim of this section was to uncover the role of ACKR4 expression by SCS ceiling LECs during the response in the drLN and how it affects the generation of PCs, GC B cells and BEM.

To evaluate the role of ACKR4, ACKR4-KO and a control group consisting of WT and ACKR4-heterozygous mice (WT/ACKR4-Het) received adoptive cell transfers of QM IgHNP Cg1cre mTmG splenocytes, where B cells are specific for the hapten NP; these donors were ACKR4-WT. The following day mice were immunised with alum precipitated NP-CGG on the plantar surface of the hind foot. Popliteal draining lymph node, spleen, blood, and axillary and brachial distant lymph nodes were collected at 8 days post-immunisation (Fig. 4.1B).

In the draining lymph node endogenous B cells, plasma cells, BEMs and GC B cells, and GFP+ adoptively transferred cells were quantified by flow cytometry (Fig. 4.1C-D). This was presented as the normalised ratio The normalised ratio which was calculated by dividing the frequency statistic of an individual sample (e.g. % lymphocytes) by the median of frequency

statistics of all control samples (e.g. WT group) in the following formula:

$$Normalised\ Ratio = \frac{sample\ frequency}{Median\ frequency\ of\ control\ samples}$$

There was no clear difference in B cells, PCs, GC B cells and BEMs between WT/ACKR4-Het and ACKR4-KO drLNs (Fig. 4.1E-H). Expression of IgG1 in GC B cells (Fig. 4.1I) and BEMs (Fig. 4.1J) were examined in WT/ACKR4-Het and ACKR4-KO mice, but there was no clear difference in expression (Fig. 4.1K-L). This suggested that environmental ACKR4-deficiency had no apparent effect on the initial activation and expansion of adoptively transferred ACKR4-sufficient B cells.

Earlier studies have shown increased numbers of BEMs inside the SCS when ACKR4-generated chemokine gradients are removed after deletion of *Ackr4* (Zhang et al., 2022). To test whether ACKR4-deficiency affects the migration of ACKR4-WT BEMs at the SCS, the drLN was observed by light sheet microscopy. WT and ACKR4-KO mice received adoptive cell transfers with QM IgHNP mTmG splenocytes. The following day they were immunised on the plantar surface with NP-KLH in alum. At 8 days post-immunisation drLNs were stained *in vivo* with CD169-Alexa647 30 minutes before drLNs were collected and examined by light sheet microscopy (Fig. 4.2A and Fig. 4.3A). In both WT and ACKR4-KO drLNs dTomato+ GCs could be seen in light sheet microscopy, there were also dTomato+ cells located in the follicles between the GC and the CD169-labelled SCS and some dTomato+ cells could be seen within the SCS (Fig. 4.2B and Fig. 4.3B). This was also observed in maximum intensity projections (Fig. 4.2C and Fig. 4.3C). Manual observation showed no major differences of dTomato+ cells in the SCS between WT and ACKR4-KO drLNs. Digital quantification would be required in

future work to confirm whether ACKR4-KO drLN SCS contained more BEMs than in WT drLN SCS as observed by Zhang et al. (2022) in intravital imaging.

As described above, CCL21 is a ligand for CCR7 and is expressed by HEVs in the LN. It has also been observed in the SCS, in which the chemokine gradient is maintained by ACKR4. CCL21 is a means for entry of lymphocytes into the spleen from circulation via HEVs and is involved in the entry of DCs to the LN via afferent lymphatics through the SCS (Ulvmar et al., 2014). CCL21 can be immobilised by binding heparan sulphate on the ECM making it detectable by histology. However, CCL19, the other CCR7 and ACKR4 ligand, is not immobilised on ECM and is soluble (Haessler et al., 2011). BEMs express CCR7 and are observed in the SCS; CCL21 gradients in the SCS may provide the means for BEM entry into the follicle. In the following experiments non-immunised and immunised popliteal LNs were compared to determine whether immunisation affected the expression of CCL21.

CCL21-RFP heterozygous reporter mice were immunised with NP-KLH in alum in the foot. Draining popliteal LN and non-immunised axillary LNs were collected and examined by flow cytometry (Fig. 4.4A). Stromal cells were detected by flow cytometry. Expression of CCL21 was examined in marginal reticular cells (MRCs) defined as MadCAM1+BP3+CD31-gp38+ stromal cells and T cell zone reticular cells (TRCs) defined as MadCAM1-BP3+CD31-gp38+ stromal cells (Fig. 4.4B). Immunisation reduced the proportion of CD31-gp38+ fibroblastic reticular cells (FRCs) by half (Fig. 4.4C). However, there were almost twice as many FRCs expressing CCL21 in immunised LNs (Fig. 4.4D). Within FRCs there was a significantly greater fraction of MRCs and TRCs in immunised LNs (Fig. 4.4E-F), there were also more CCL21-expressing MRCs and TRCs in immunised LNs as a proportion of FRCs (Fig. 4.4G-H). However,

when examining expression of CCL21 as the proportion of either total MRCs or TRCs there was no significant difference between immunised and non-immunised LNs and no significant difference of CCL21 expression between MRCs and TRCs (Fig. 4.4I). This indicates that the respective numbers of CCL21 expressing MRCs and TRCs did not change after immunisation. Instead, there was an immunisation-induced loss of CCL21-RFP negative cells as a proportion of live cells.

The decreased FRCs and CCL21-RFP-expressing FRCs in immunised LNs was unexpected. The immunised LN *in vivo* would expand as there would be an influx of leukocytes and increased volume. Resultantly, it is likely that FRCs increased in real terms, but not as a proportion of live cells, however absolute numbers were not recorded so this could not be verified. In future work absolute numbers of FRCs should be evaluated to determine whether immunisation induced loss of FRCs was real.

Immunised and non-immunised CCL21-RFP/WT popliteal LNs were sectioned and examined by histology with the aim of investigating the expression of CCL21 in the SCS. LNs were stained with CD169 to mark SCS macrophages lining the floor of the SCS. MADCAM1 was stained to help identify MRCs in the SCS; TRCs are also MADCAM1-expressing cells (Fletcher et al., 2015). Non-immunised popliteal LNs revealed expression of CCL21 by TRCs deep in the tissue. Furthermore, CCL21-expressing reticular cells were detected in the SCS floor that co-localised with CD169+ SCS macrophages. CCL21-expression in the SCS floor also co-expressed MADCAM1 indicating that these CCL21-expressing cells are likely to be MRCs (Fig. 4.5). Immunised popliteal LNs likewise had similar CCL21 expression as non-immunised LNs. CCL21 was expressed on TRCs and highly expressed on HEVs. CCL21-expressing cells were

also detected in the SCS demarcated by CD169 and these co-localised with MADCAM1, indicating that they are likely to be MRCs (Fig. 4.6). Additionally, there was co-localisation of SCS macrophages with CCL21-RFP (Fig. 4.5 and Fig. 4.6). MADCAM1 was also expressed by cells deeper in the LN, these included TRCs (Fletcher et al., 2015). This implies that expression of CCR7 may be relevant to cell migration in both the T cell areas and in the SCS.

There was no difference in CCL21 expression of MRCs and TRCs between immunised and non-immunised LNs but there were more CCL21-expressing FRCs in immunised LNs, as determined by flow cytometry. This revealed an expansion of FRCs during a response in the LN. This increased the number of CCL21-expressing cells but may just be related to the increased volume of the LN during an immune response.

Previous findings by intravital microscopy uncovered that in ACKR4-KO mice BEMs migrated to the SCS but were less able to return back to the follicle and thus accumulated within the SCS (Zhang et al., 2022). Based on this it was expected that the same trend would be shown by light sheet microscopy with more BEMs in the ACKR4-KO SCS. Although there was no obvious difference by manual observation there may be a difference uncovered if these SCS located BEMs were quantified.

Previous work showed that BEMs in the SCS of ACKR4-deficient mice failed to return towards the follicle (Zhang et al., 2022). This was due to a dysregulation of CC19 and CCL21 chemokine gradients under conditions of ACKR4-deficiency. Therefore, there was reduced direction for CCR7-mediated migration of BEMs to follow. We next investigated signals directing BEMs in the other direction, such as towards the outer follicular regions and the SCS.

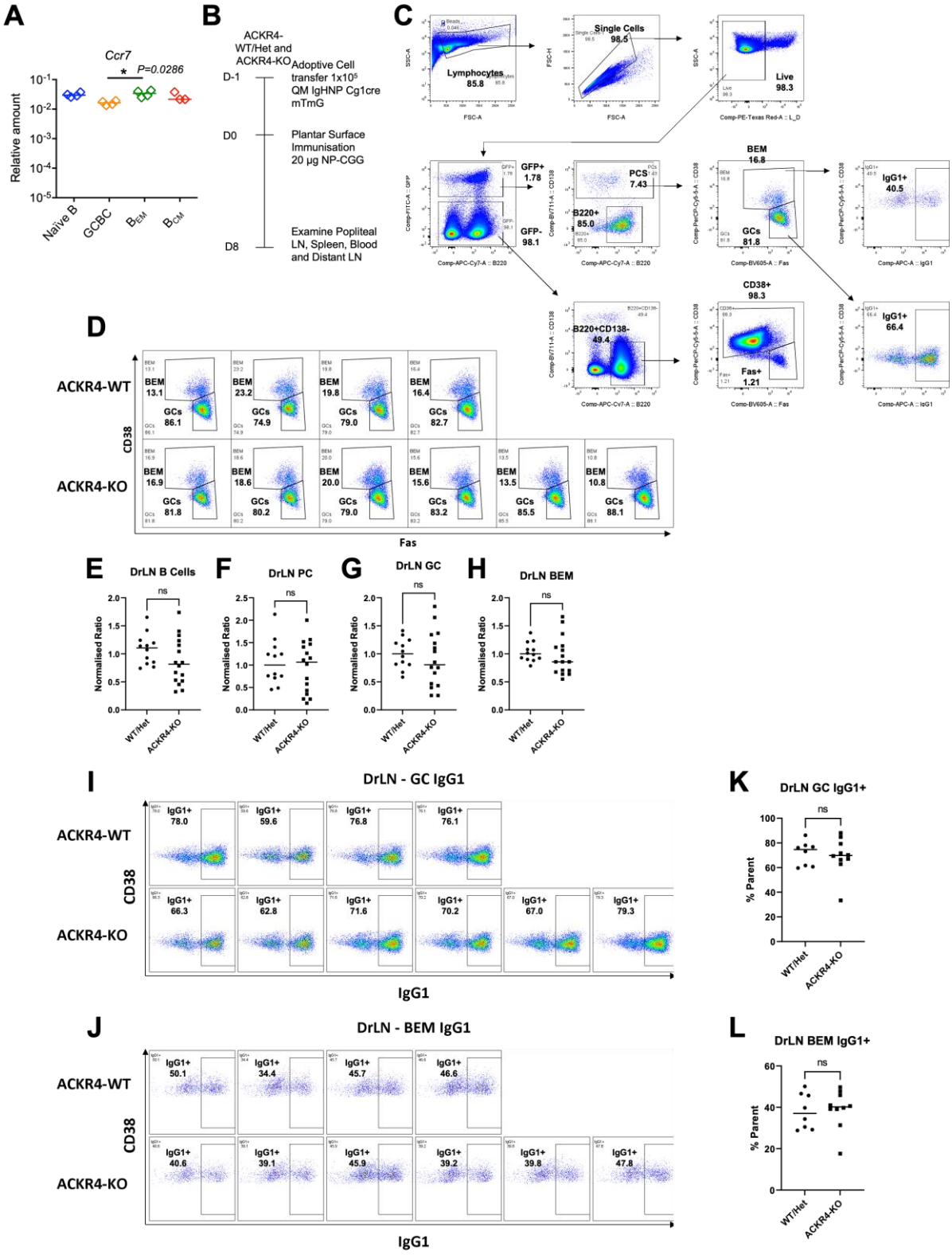
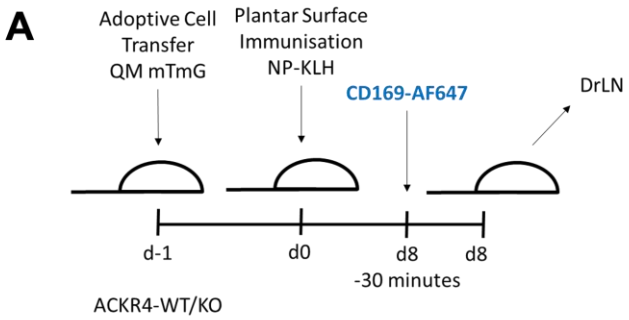


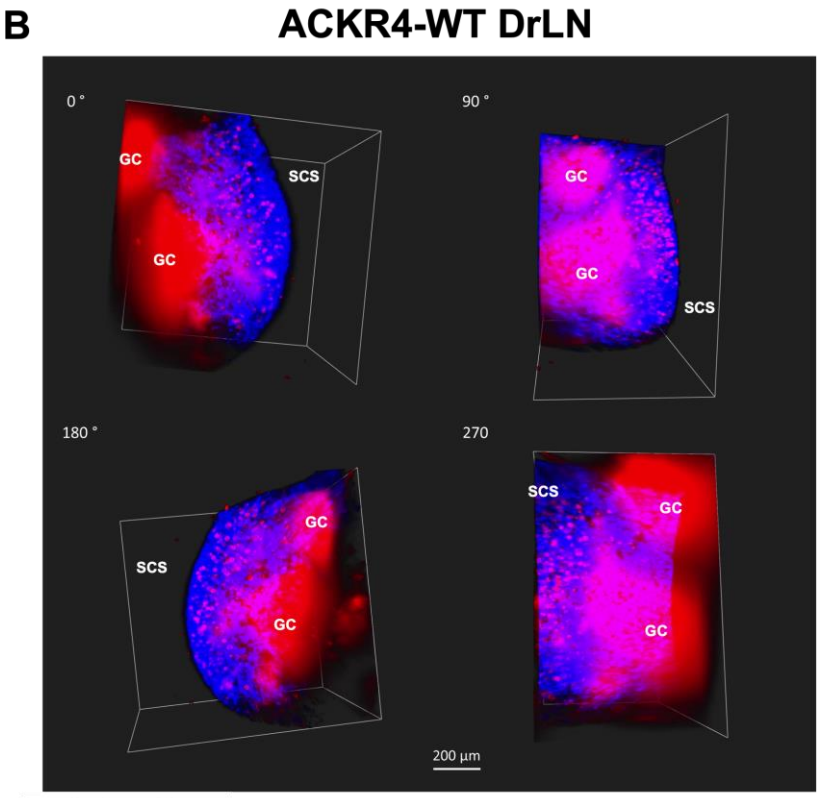
Figure 4. 1. No significant effect on size of GC response and BEM production in ACKR4-deficient drLNs

(A) RT-PCR measuring the mRNA expression of the chemokine receptor CCR7 in nBCs (GFP-B220+CD38+CD138-), GC B cells (GFP+B220+CD138-CD38-Fas+), BEMs (GFP+B220+CD138-CD38+) and BCMs (GFP+B220+CD38+CD138-) in QM Cg1cre mTmG cell transfer recipients (d-1) collected at 8 days post-immunisation. This data was produced by Yang Zhang (Zhang et al., 2022). Each symbol represents pooled LNs (popliteal LNs for GC B cells and distant axillary and brachial LNs for BCMs and nBCs) from 4 mice. All values are relative to levels of *B2m* mRNA. Data representative of 3 independent experiments. Two-tailed Mann-Whitney test, * $p<0.05$.

(B) Schematic of QM Cg1cre mTmG adoptive cell transfer and immunisation protocol into ACKR4-KO and a control group consisting of WT and ACKR4-Heterozygous mice (WT/Het). Cell transfers were performed by the University of Birmingham Biomedical Services Unit. (C) Gating strategy to detect GC B cells (GFP-B220+CD138-CD38-Fas+) and BEMs (GFP-B220+CD138-CD38+) from activated GFP+ adoptively transferred cells. (D) Flow cytometry plots of BEMs and GC B cells from individual WT and ACKR4-KO drLNs from GFP+ B cells. Graphical summaries of % lymphocytes (E) GFP+ B cells (B220+CD138-), (F) GFP+ plasma cells (CD138+), (G) GC B cells and (H) BEMs, data were normalised from 3 separate experiments to the medians of WT samples from each experiment set to 1 (WT n=12, ACKR4-KO n=16). Flow cytometry plots of IgG1 expression in (I) GC B cells and (J) BEMs. Graphical summaries of IgG1+ (K) GC B cells and (L) BEMs, data presented are combined from 2 separate experiments (WT n=8, ACKR4-KO n=10). Symbols represent individual mice. Circles represent WT/Het control group mice, squares represent ACKR4-KO mice. Horizontal bars show means. The normalised ratio was calculated by dividing the frequency statistic of an individual sample (e.g., % lymphocytes) by the median of frequency statistics of all control samples (e.g., WT group) in the formula described below:

$$Normalised\ Ratio = \frac{sample\ frequency}{Median\ frequency\ of\ control\ samples}$$


A
Adoptive Cell Transfer QM mTmG
Plantar Surface Immunisation NP-KLH
CD169-AF647
DrLN
d-1
d0
d8
d8
-30 minutes
ACKR4-WT/KO


B
ACKR4-WT DrLN
0 °
90 °
180 °
270
GC
SCS
200 µm

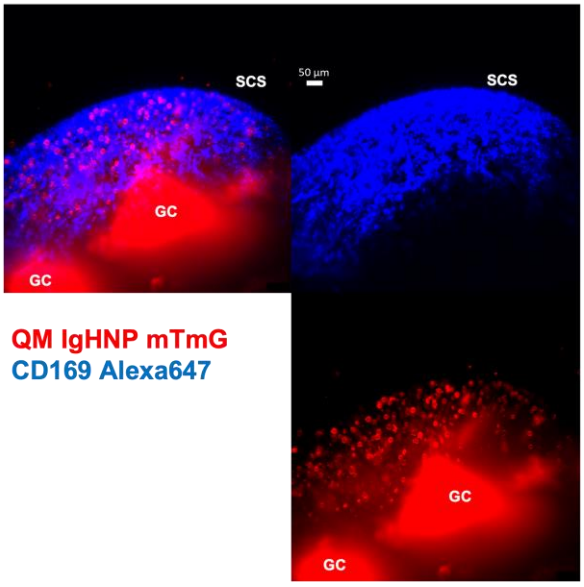

C
SCS
50 µm
GC
QM IgHNP mTmG
CD169 Alexa647

Figure 4. 2. Light sheet microscopy of ACKR4-WT drLN with adoptively transferred QM mTmG cells showed BEM in the SCS

(A) ACKR4-WT mice received adoptive cell transfer of QM mTmG splenocytes one day before immunisation with NP-KLH. Cell transfers were performed by the University of Birmingham Biomedical Services Unit. At 8 days post-immunisation they received *in vivo* staining with CD169-Alexa647 30 minutes before collection of drLN. (B) Snapshots of light sheet microscopy image of GC and SCS taken at 0°, 90°, 180° and 270° rotated along the Y-axis. QR code links to video of light sheet image in the URL: https://youtu.be/Ba74p0PtPYQ. (C) Maximum intensity projection of light sheet microscopy image (top left), with Alexa647-CD169 (top right) and dTomato (bottom right) shown separately.

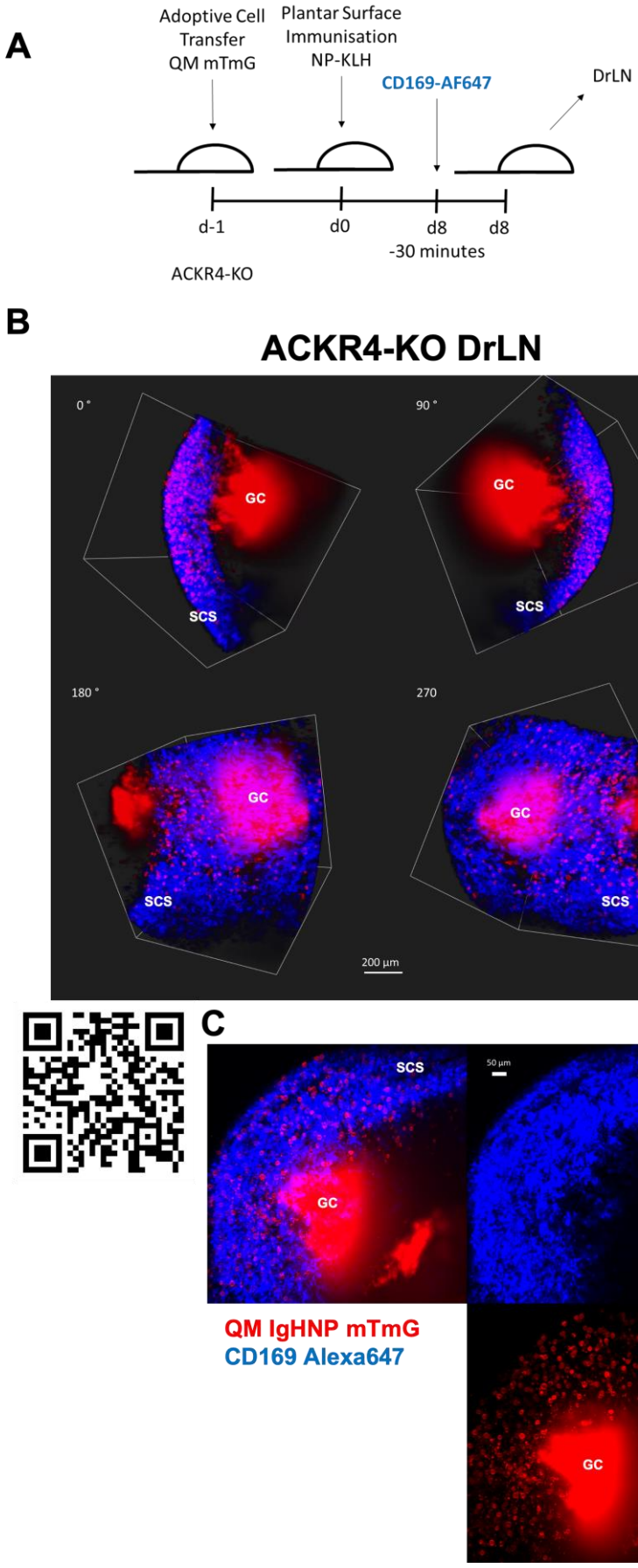

A
Adoptive Cell Transfer QM mTmG
Plantar Surface Immunisation NP-KLH
CD169-AF647
DrLN
d-1
d0
d8
d8
-30 minutes
ACKR4-KO
B
ACKR4-KO DrLN
0 °
90 °
180 °
270
GC
SCS
200 µm
C
SCS
GC
50 µm
QM IgHNP mTmG
CD169 Alexa647

Figure 4. 3. BEM were detected in the SCS of ACKR4-KO drLN by light sheet microscopy

(A) ACKR4-KO mice received adoptive cell transfer of QM mTmG splenocytes one day before immunisation with NP-KLH. Cell transfers were performed by the University of Birmingham Biomedical Services Unit. At 8 days post-immunisation they received *in vivo* staining with CD169-Alexa647 30 minutes before collection of drLN. (B) Snapshots of light sheet microscopy image of GC and SCS taken at 0°, 90°, 180° and 270° rotated along the Y-axis. QR code links to video of light sheet image in the URL: https://youtu.be/WlLWnnk-FaE. (C) Maximum intensity projection of light sheet microscopy image (top left), with Alexa647-CD169 (top right) and dTomato (bottom right) shown separately.

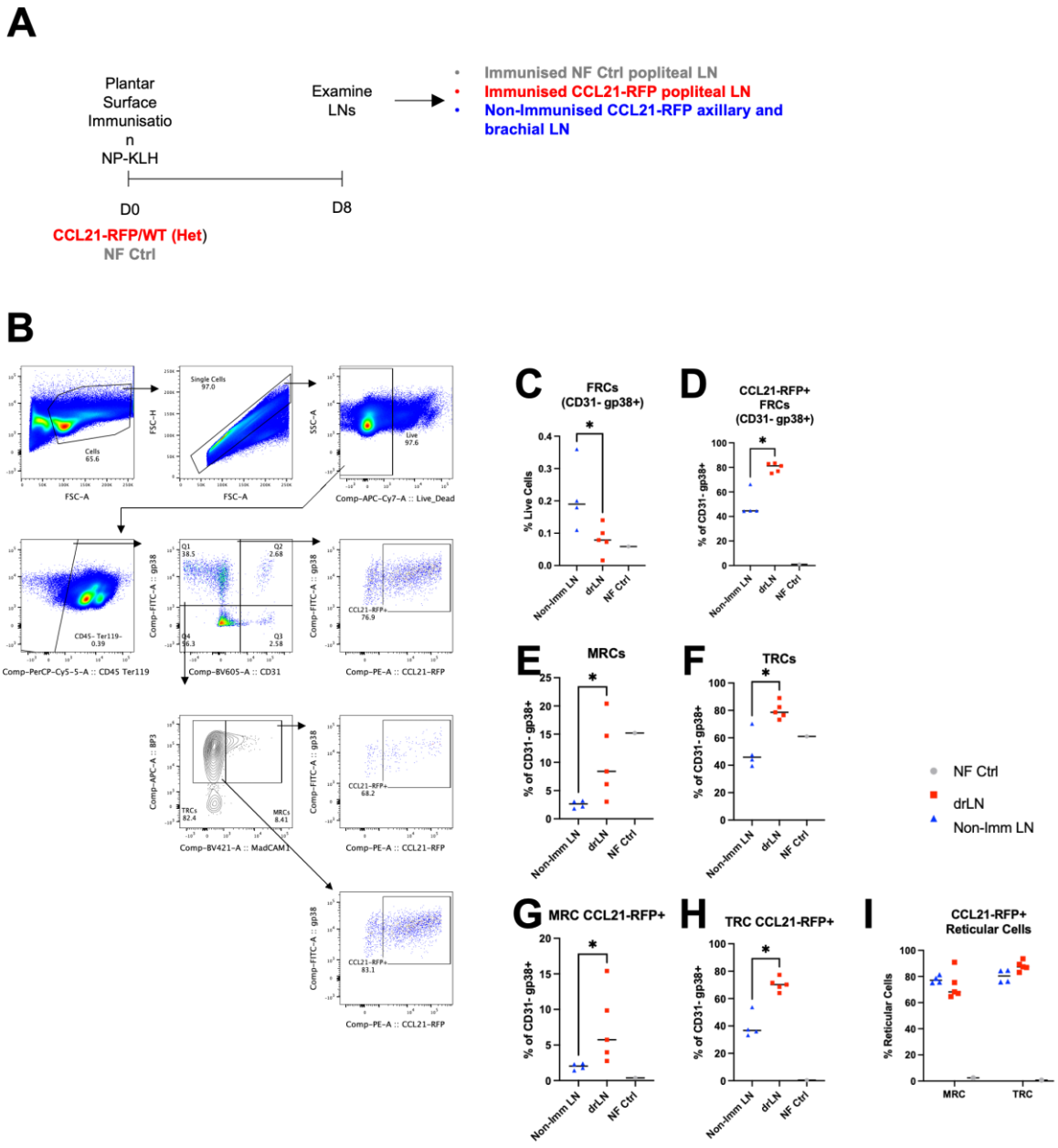


Figure 4. 4. CCL21 expressing MRCs and TRCs detected in the draining and non-immunised LNs

(A) CCL21-RFP heterozygous reporter mice were immunised on plantar surface with NP-KLH in alum precipitate. 8 days post-immunisation drLN and non-immunised popliteal LNs were collected. (B) After digestion these LNs were examined by flow cytometry to detect stromal cells (CD45-Ter119-CD31-gp38+), MRCs (CD45-Ter119-CD31-gp38+BP3+MadCAM1+) and TRCs (CD45-Ter119-CD31-gp38+BP3+MadCAM1-). Tissue digestion was performed by Yang Zhang. (C) Summary of total fibroblastic reticular cells and (D) CCL21-expressing fibroblastic reticular cells. (E) Summaries of MRCs and (F) CCL21-expressing MRCs. (G) Summaries of TRCs and (H) CCL21-expressing TRCs. (I) Summary pf CCL21-expressing MRCs and TRCs as a proportion of total MRCs and TRCs (n=4-5). Mann-Whitney test, * P<0.05. Data are from one

experiment. Symbols represent individual mice. Blue triangles are non-immunised LNs, red squares are immunised popliteal LNs, and grey circles are immunised non-fluorescent popliteal LNs. Horizontal bars show means.

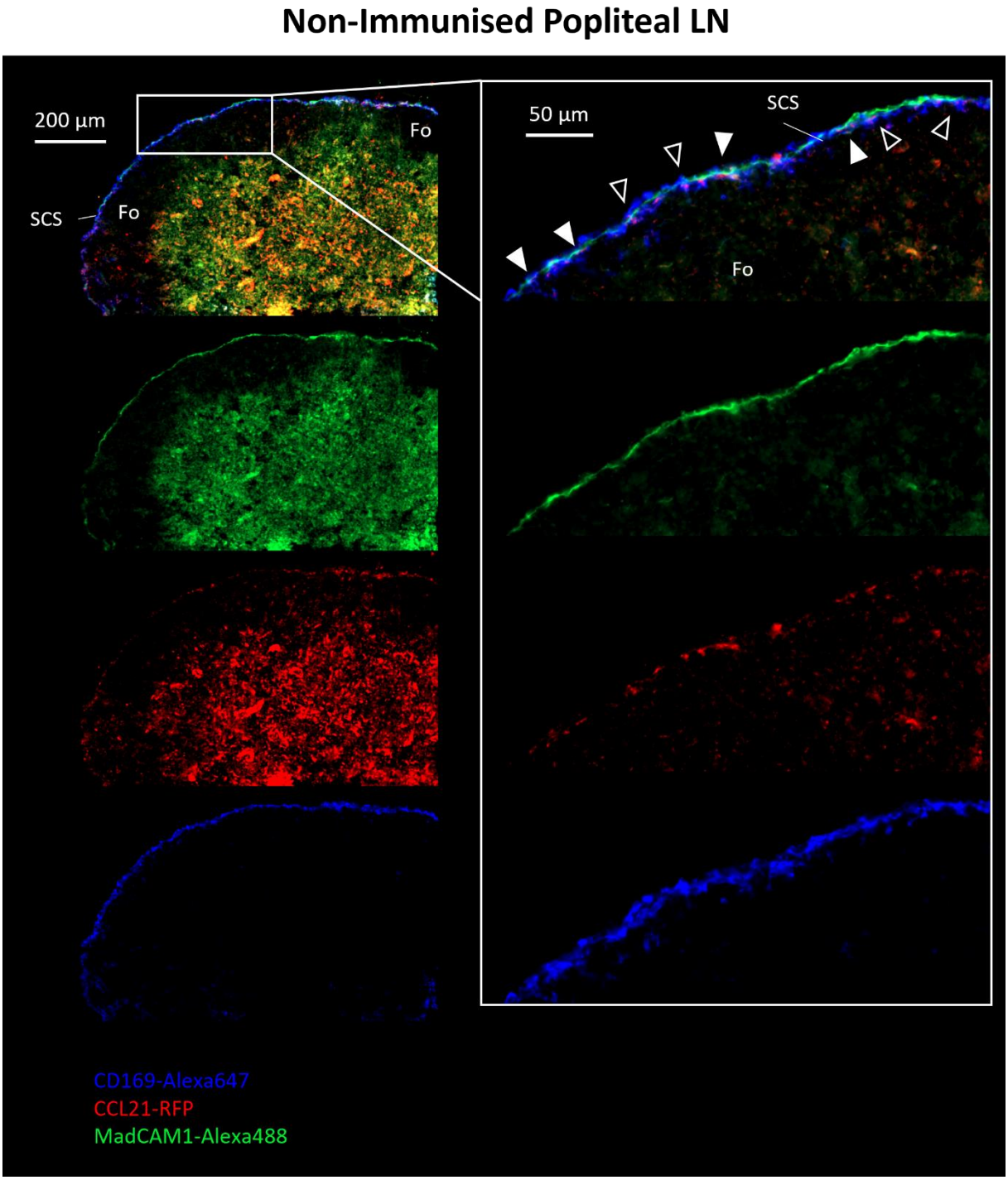


Figure 4. 5. CCL21-RFP expression detected in the SCS floor of non-immunised popliteal LN

Non-immunised CCL21-RFP/WT popliteal LN examined by histology. Stained for MadCAM1 (green), CCL21-RFP (red) and CD169 (blue). White arrowheads mark CCL21-RFP expressing marginal reticular cells and clear arrowheads marks CCL21-RFP co-expressed with SCS macrophages. (SCS = subcapsular sinus, Fo = follicle).

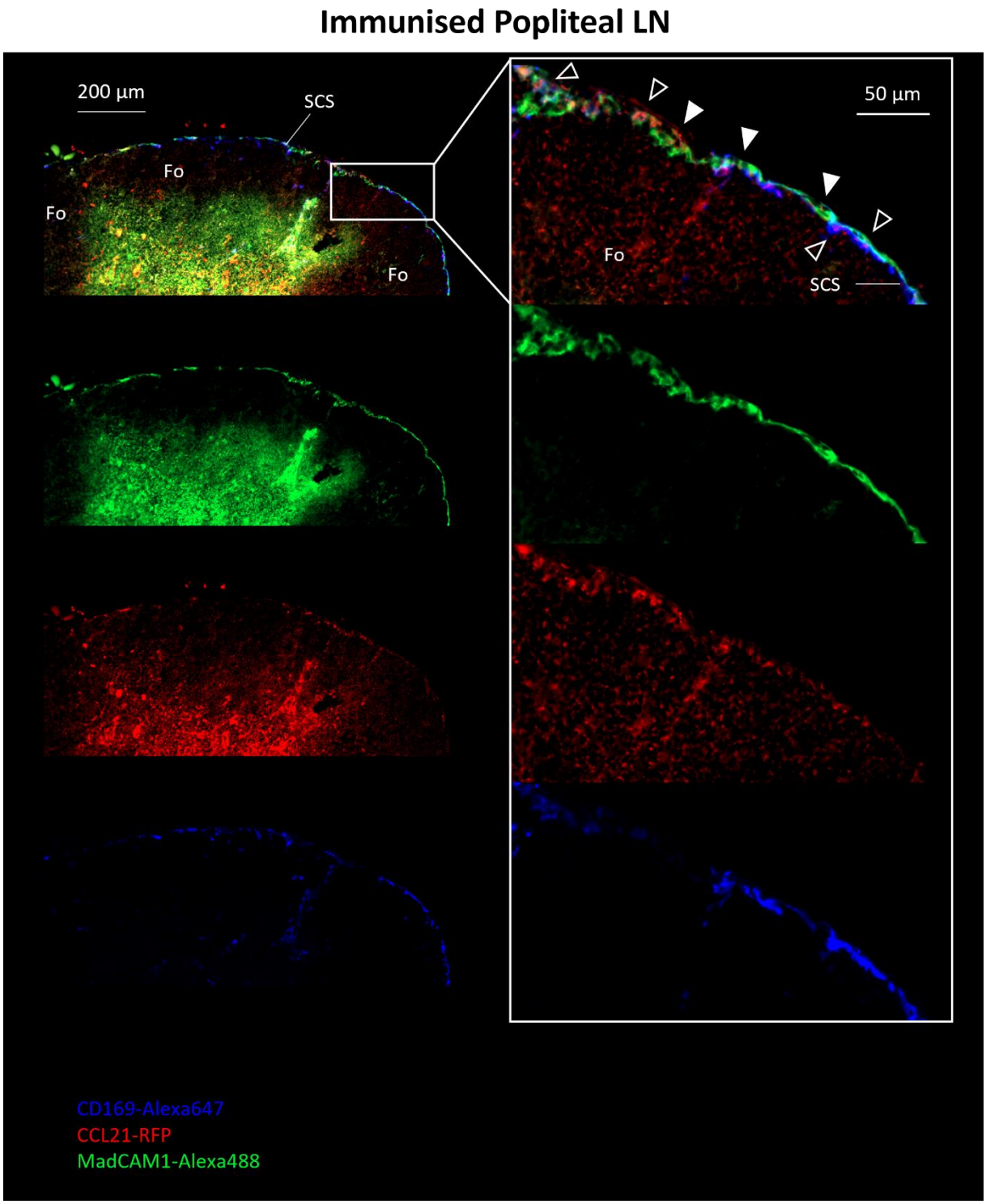


Figure 4. 6. CCL21-expression detected in the SCS floor of immunised popliteal LN

CCL21-RFP/WT draining popliteal LN at 8 days post-immunisation examined by histology. LN was stained for MadCAM1 (green), CCL21-RFP (red) and CD169 (blue). White arrowheads mark CCL21-RFP expressing marginal reticular cells and clear arrowheads marks CCL21-RFP co-expressed with SCS macrophages. (SCS = subcapsular sinus, Fo = follicle).

4.2.2 S1PR1-blockade impaired egress of emigrating memory B cells from the drLN

CCR7 ligands may direct migration of lymphocytes in the LN from SCS to the follicle but the migration of lymphocytes towards the outer follicular regions is dependent upon CCR6, EBI2 and S1PR1 ligands (Zhang et al., 2016, Kelly et al., 2011). CCR6, EBI2 and S1PR1 were expressed at elevated levels among BEMs and GC B cells expressed elevated levels of S1PR2 which acts in opposition to S1PR1 (Fig. 3.12C, Fig. 4.7A-C). The role of S1PR1 in lymphocytes has been effectively studied by treating mice with FTY720 to block S1PR1 which inhibits the egress of lymphocytes from SLOs by preventing migration to the SCS (Zhang et al., 2016). FTY720 also targets S1PR3-5 (Adachi and Chiba, 2007). BAF312 has been used to more specifically target S1PR1 to a similar effect as FTY720 (Gergely et al., 2012). BAF312 can also antagonise S1PR5 (O'Sullivan et al., 2016). B cell subsets examined here did not express S1PR5 (Fig. 3.12C). Given that BEMs expressed elevated levels of S1PR1, mice were treated with FTY720 or BAF312 to evaluate the effect on egress of BEMs from the drLN and appearance in circulation and distant lymphoid tissues.

To investigate the effects of FTY720-mediated S1P receptor blockade, WT mice received adoptive cell transfer of QM IgHNP Cg1Cre mTmG splenocytes. The following day they received immunisation with NP-CGG in alum precipitate on the plantar surface of hind feet. They received i.p. injections of FTY720 or a PBS as an untreated control at 6- and 7-days post-immunisation, and tissues were examined at 8 days post-immunisation (Fig. 4.7D). Flow cytometry was used to detect GFP+ B cells, PCs, GC B cells and BEMs (Fig. 4.7B-G). The FTY720-treated drLN contained slightly fewer GFP+ B cells (Fig. 4.8A) and GC B cells (Fig.

4.8B). There was no major loss of BEMs (Fig. 4.8C) and no difference in PCs in FTY720-treated mice (Fig. 4.8D).

GFP+B220+CD38+CD138- BCMs were quantified from distLN, spleen and blood by flow cytometry (Fig. 4.9A-C). Fewer BCMs were detected in the distLN, spleen and blood of FTY720-treated mice (Fig. 4.9D-E). Some FTY720-treated samples were completely devoid of BCMs, showing the strong effect of blockade of S1PR1. Additionally, GFP- CD3+ T cells and B220+ B cells were examined in distLN, spleen and blood by flow cytometry, to examine the effect of S1PR1-blockade on naïve recirculating lymphocyte egress from SLOs (Fig. 4.9A and 4.10A-C). While there was no difference in T cells in distLN and spleen, very few T cells were present in the blood of FTY720-treated mice (Fig. 4.10D-E). Similarly, B cell numbers in blood from FTY720-treated mice was strongly reduced, while there was a slight, but significant increase in B cells of distLN (Fig. 4.10F-G). This confirms that FTY720 treatment inhibits egress of lymphocytes from SLOs leading to reduction of lymphocytes in the blood. The increased B cells in the distLN of FTY720-treated mice may be due to the production of B cells *in situ* in response to a non-specified antigen. This may be because of animals fighting and/or response to non-specified pathogens in the specific pathogen free conditions of the animal facility. Alternatively, this could be the result of the entry of B cells already present in circulation prior to administration of FTY720. On the other hand, BCMs in distLN were significantly reduced, suggesting that they were produced in drLN but were unable to egress and enter other tissues when exit from drLN was inhibited by S1PR1 blockade.

FTY720 targets multiple S1P receptors. To examine whether the effect observed was due to inhibition of S1PR1, mice were treated with BAF312 which more specifically targets S1PR1.

WT C57BL/6 mice received adoptive cell transfers with QM IgHNP Cg1-Cre mTmG splenocytes followed by immunisation with NP-CGG on the plantar surface the next day, these mice were treated with FTY720 or BAF312 at days 6 and 7 post-immunisation (Fig. 4.11A) Frequency of Lymphocytes and BCMs was examined in distant tissues after treatment at 8 days post-immunisation with NP-KLH (Fig. 4.11AB). B cells and T cells were quantified in blood of FTY720 and BAF312-treated mice (Fig. 4.11C). While there was no significant difference in B cells and T cells of FTY720-treated and BAF312-treated blood, there were fewer B cells and T cells in treated blood compared with untreated PBS controls (Fig. 4.11D-E). BCMs were examined in distLN, spleen and blood (Fig. 4.11F-G). In distLN and blood there was no significant difference in BCMs between FTY720 and BAF312- treatments, whereas, in the BAF312-treated spleen there were significantly fewer BCMs than FTY720-treated. Additionally, when compared with separate PBS controls there were fewer BCMs in the spleen with both treatments (Fig. 4.11H). This indicated an importance for S1P receptors in the egress of BCMs from the drLN, and that BAF312 may more effectively impair this than FTY720. One caveat is that the PBS controls were from separate experiments, nonetheless they appeared as expected showing a larger proportion of B cells and T cells in blood and BCMs in distant tissues compared with samples that received S1PR1 blockade. The important question from these experiments was whether there was a difference between the BAF312 and FTY720 treatment, this was directly compared and answered as shown above.

S1PR1-blockade resulted in fewer BCMs detected in blood and distant tissues suggesting that it may have prevented egress of BEMs from the drLN to become BCMs. Light sheet microscopy was used to verify whether S1PR1 is required to for migration to the SCS prior to

egress via efferent lymphatics. S1PR2-ERT2-Cre x Ai14dTomato mice, which is a reporter for GC-derived B cells and will label BEMs, were immunised with rabbit IgG. At 6 days post-immunisation they were treated with tamoxifen and on the following day they were treated with either PBS as a control or FTY720 by i.p. injection. During the peak of the GC reaction and BEM production at 8 days post-immunisation drLNs were examined. DrLNs were stained *in vivo* with Alexa488-labelled immune complex (IC), 30 minutes after staining, untreated drLN (Fig. 4.12A) and FTY720-treated drLN (Fig. 4.13A) were collected. Untreated (Fig. 4.12B-C) or FTY720-treated (Fig. 4.13B-C) drLNs were then examined by light sheet microscopy. dTomato+ GC could be observed in both drLN, there were also some BEMs present between the GC and the SCS and some present in the SCS labelled by IC. There may be fewer BEMs in the SCS of FTY720-treated drLN, but this was not quantified. This would concur with previous observations of fewer mBCs entering the SCS of drLN to egress towards distant tissues as BCMs.

The above experiments of treating tissues with FTY720 and BAF312 suggested that S1PR1-blockade may have prevented the egress of BEMs from the drLN. This suggests that BEMs emerging from the GC may use S1PR1 to follow S1P gradients towards the SCS. Once in the SCS these BEMs may either undergo egress via efferent lymphatics or return towards the GC-containing follicle. Light sheet microscopy appeared to agree with this observation with fewer BEMs observed in the SCS of FTY720-treated drLN. In the following section I examine the role of this GC-SCS recycling of BEMs mediated by S1PR1 and CCR7 ligands for the antibody response.

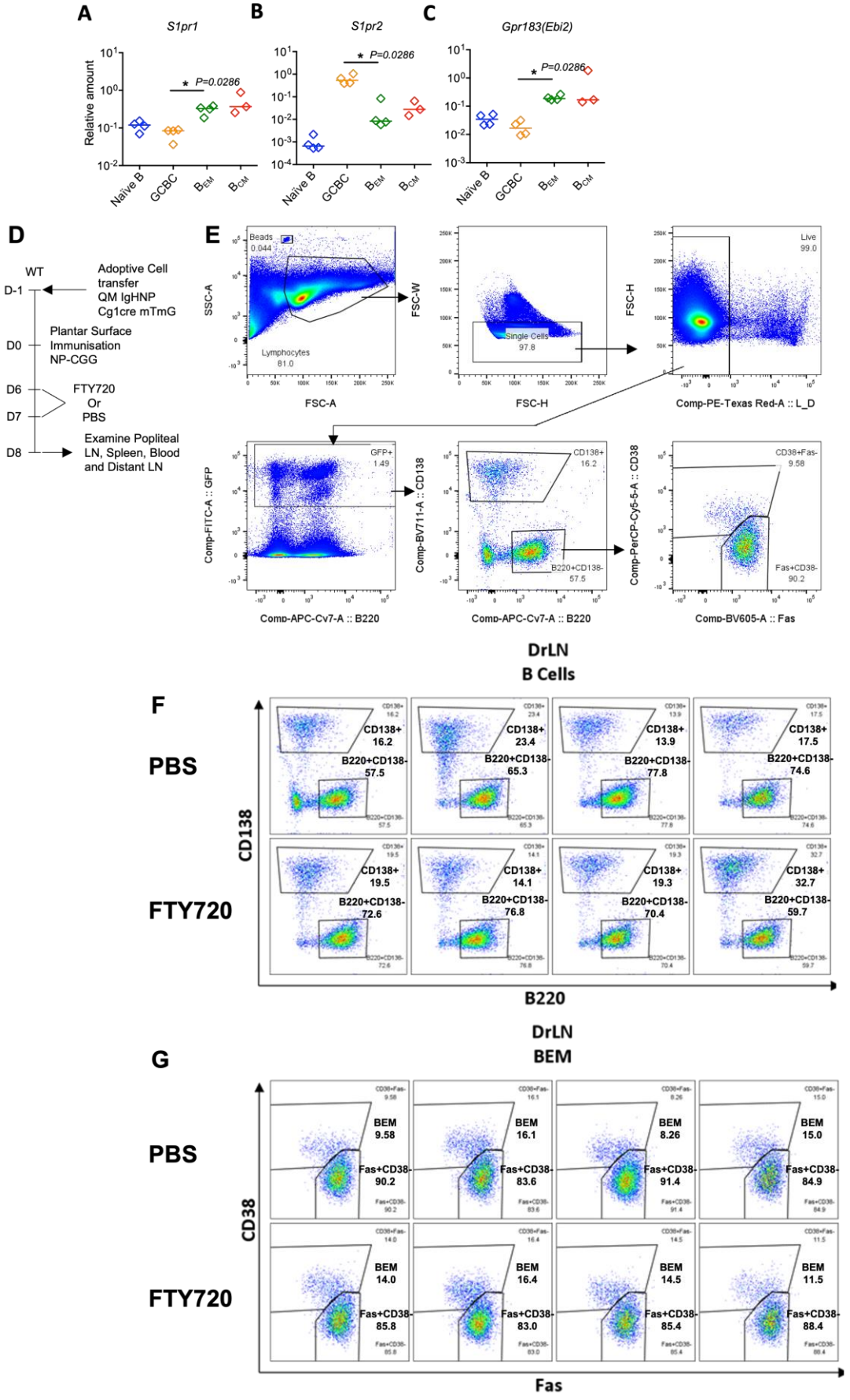

A
S1pr1
B
S1pr2
C
Gpr183(Ebi2)
Relative amount
* P=0.0286
Naïve B
GCBC
BEM
BCM
D
WT
D-1
Adoptive Cell transfer
QM IgHNP Cg1cre mTmG
D0
Plantar Surface Immunisation
NP-CGG
D6
D7
FTY720 Or PBS
D8
Examine Popliteal LN, Spleen, Blood and Distant LN
E
Beads
0.044
Lymphocytes
81.0
SSC-A
FSC-A
FSC-W
FSC-H
Single Cells
97.8
Live
99.0
Comp-PE-Texas Red-A :: L_D
GFP+
1.49
Comp-FITC-A :: GFP
Comp-APC-Cy7-A :: B220
CD138+
16.2
Comp-BV711-A :: CD138
B220+CD138-
57.5
CD38+Fas-
9.58
Comp-PerCP-Cy5-5-A :: CD38
Fas+CD38-
90.2
Comp-BV605-A :: Fas
DrLN
B Cells
F
PBS
FTY720
CD138
B220
CD138+ 16.2
B220+CD138- 57.5
CD138+ 23.4
B220+CD138- 65.3
CD138+ 13.9
B220+CD138- 77.8
CD138+ 17.5
B220+CD138- 74.6
CD138+ 19.5
B220+CD138- 72.6
CD138+ 14.1
B220+CD138- 76.8
CD138+ 19.3
B220+CD138- 70.4
CD138+ 32.7
B220+CD138- 59.7
DrLN
BEM
G
PBS
FTY720
CD38
Fas
BEM 9.58
Fas+CD38- 90.2
BEM 16.1
Fas+CD38- 83.6
BEM 8.26
Fas+CD38- 91.4
BEM 15.0
Fas+CD38- 84.9
BEM 14.0
Fas+CD38- 85.8
BEM 16.4
Fas+CD38- 83.0
BEM 14.5
Fas+CD38- 85.4
BEM 11.5
Fas+CD38- 88.4

Figure 4. 7. FTY720 treated drLNs were evaluated by flow cytometry

RT-PCR measuring the mRNA expression of the chemokine receptors S1pr1 (A), S1pr2 (B) and Gpr183(Ebi2) (C) in nBCs (GFP-B220+CD38+CD138-), GC B cells (GFP+B220+CD138-CD38-Fas+), BEMs (GFP+B220+CD138-CD38+) and BCMs (GFP+B220+CD38+CD138-) in QM Cg1cre mTmG cell transfer recipients (d-1) collected at 8 days post-immunisation. This data was produced by Yang Zhang (Zhang et al., 2022). Each symbol represents pooled LNs (popliteal LNs for GC B cells and distant axillary and brachial LNs for BCMs and nBCs) from 4 mice. All values are relative to levels of *B2m* mRNA. Data representative of 3 independent experiments. Two-tailed Mann-Whitney test, * p<0.05.

(D) Schematic of QM IgHNP Cg1cre mTmG adoptive cell transfer and immunisation protocol into WT mice followed by treatment with FTY720 (i.p.). Cell transfers and administration of FTY720 were performed by Juan Carlos Yam-Puc. (E) Gating strategy to isolate GC B cells and BEMs from GFP+ adoptively transferred cells. (F) Flow cytometry plots of GFP+ B cells and PCs in FTY720-treated and untreated drLNs. (G) Flow cytometry plots of BEMs and GC B cells in FTY720-treated and untreated drLNs from GFP+ B cells.

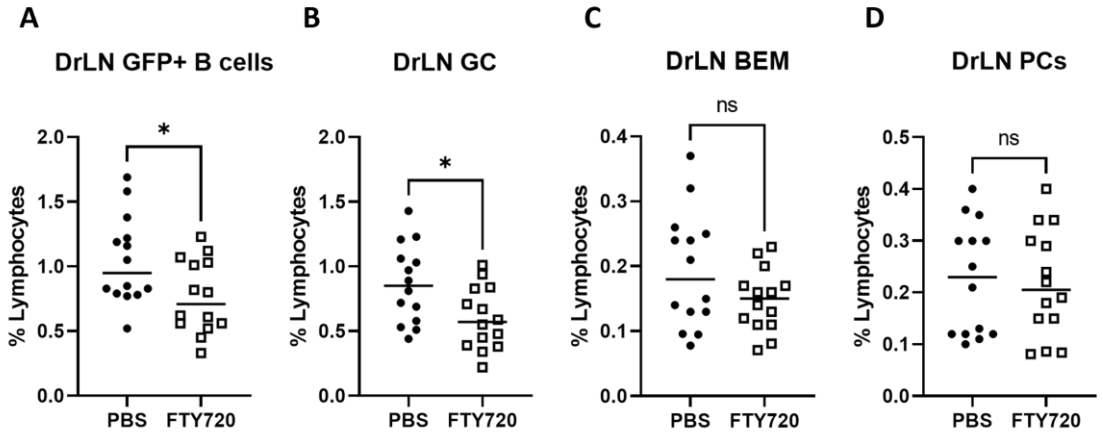
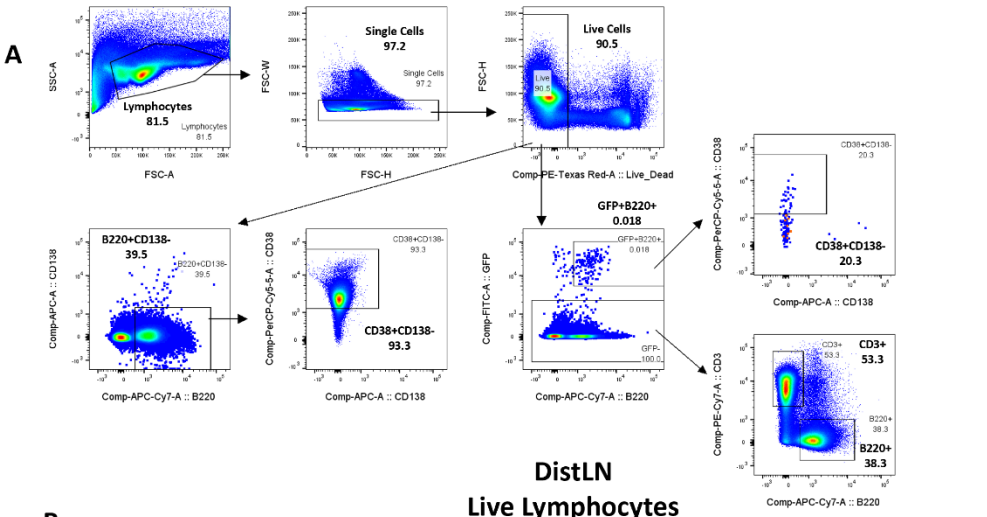
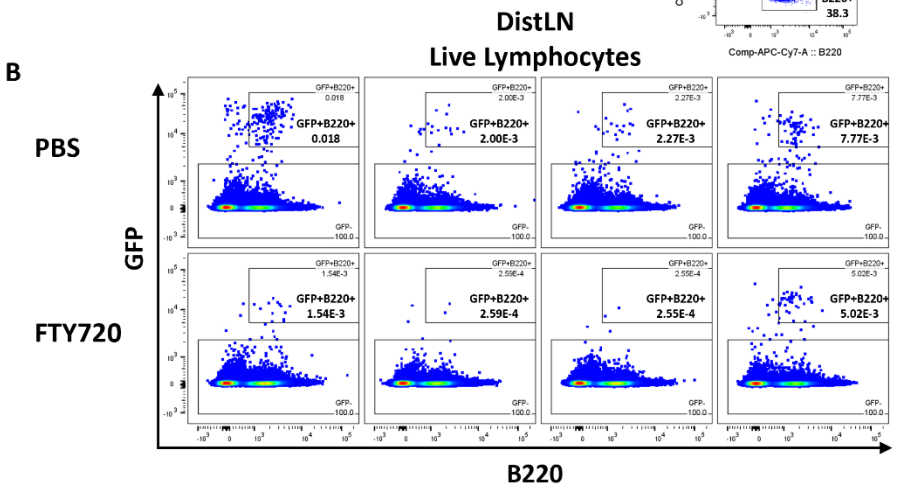
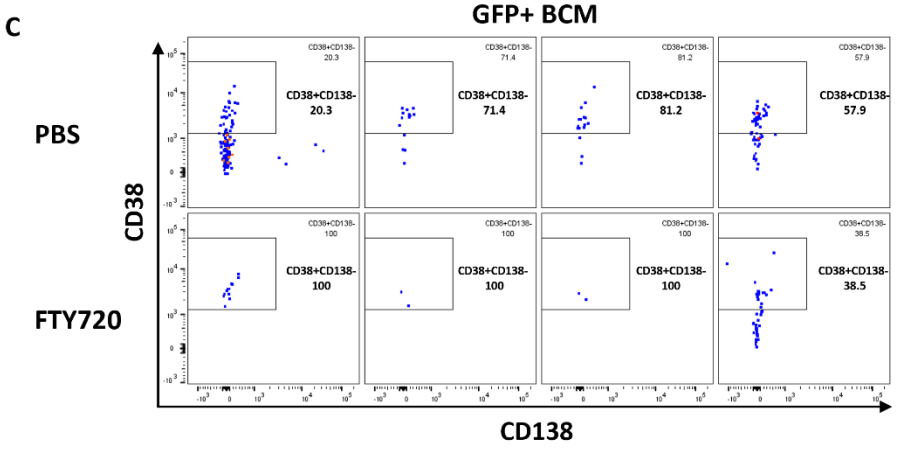


Figure 4. 8. Fewer B cells and GC B cells in FTY720-treated drLNs but no effect on production of BEMs

Summaries of flow cytometry experiments to detect B cell subsets in FTY720-treated and untreated (PBS) drLNs. (A) GFP+ B cells (GFP+B220+CD138-), (B) GC B cells (GFP+B220+CD138-CD38-Fas+), (C) BEMs (GFP+B220+CD138-CD38+) and (D) PCs (GFP+CD138+) in drLN presented as % live lymphocytes. Data presented are combined from 3 separate experiments (WT n=14, CCL19-KO n=16). Unpaired t-test, * p<0.05. Symbols represent individual mice; solid black circles are PBS-treated controls and open squares are FTY720-treated mice. Horizontal bars show means.


A
SSC-A
FSC-A
Lymphocytes
81.5
FSC-W
FSC-H
Single Cells
97.2
FSC-H
Comp-PE-Texas Red-A :: Live_Dead
Live Cells
90.5
Comp-APC-A :: CD138
Comp-APC-Cy7-A :: B220
B220+CD138-
39.5
Comp-PerCP-Cy5-5-A :: CD38
Comp-APC-A :: CD138
CD38+CD138-
93.3
Comp-FITC-A :: GFP
Comp-APC-Cy7-A :: B220
GFP+B220+
0.018
Comp-PerCP-Cy5-5-A :: CD38
Comp-APC-A :: CD138
CD38+CD138-
20.3
Comp-PE-Cy7-A :: CD3
Comp-APC-Cy7-A :: B220
CD3+
53.3
B220+
38.3


B
DistLN
Live Lymphocytes
PBS
FTY720
GFP
B220
GFP+B220+
0.018
GFP+B220+
2.00E-3
GFP+B220+
2.27E-3
GFP+B220+
7.77E-3
GFP+B220+
1.54E-3
GFP+B220+
2.59E-4
GFP+B220+
2.55E-4
GFP+B220+
5.02E-3


C
DistLN
GFP+ BCM
PBS
FTY720
CD38
CD138
CD38+CD138-
20.3
CD38+CD138-
71.4
CD38+CD138-
81.2
CD38+CD138-
57.9
CD38+CD138-
100
CD38+CD138-
38.5

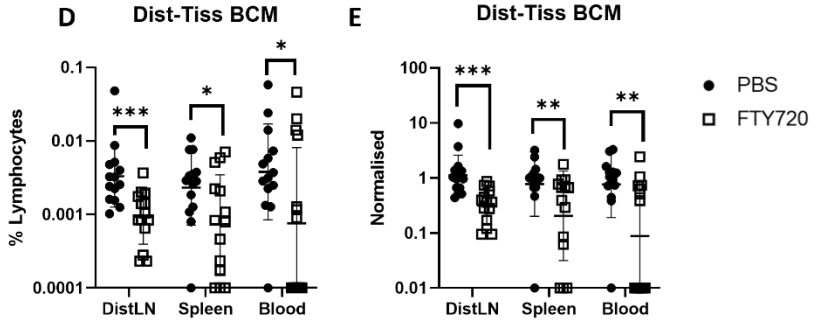

D
Dist-Tiss BCM
% Lymphocytes
0.1
0.01
0.001
0.0001
***
*
*
DistLN
Spleen
Blood
E
Dist-Tiss BCM
Normalised
100
10
1
0.1
0.01
***
**
**
DistLN
Spleen
Blood
PBS
FTY720

Figure 4. 9. Fewer BCMs in distant lymphoid tissues of FTY720-treated mice

(A) Gating strategy to isolate BCMs (GFP+B220+CD138-CD38+) in FTY720-treated and untreated distant tissues, presented is gating strategy for distLN from one representative experiment. (B) Flow cytometry plots to detect GFP+B220+ cells in FTY720-treated and untreated distLN. (C) Flow cytometry plots to detect BCMs in FTY720-treated and untreated distLN. Plots are from one representative experiment. Graphical summaries of BCMs detected in FTY720-treated and untreated distant tissues presented as % live lymphocytes (D) and normalised ratio (E). Data are combined from 3 separate experiments (n=14). Mann-Whitney test, * $p<0.05$, ** $p<0.01$, *** $p<0.001$. Symbols represent individual mice; solid black circles are PBS-treated controls and open squares are FTY720-treated mice. Horizontal bars show means.

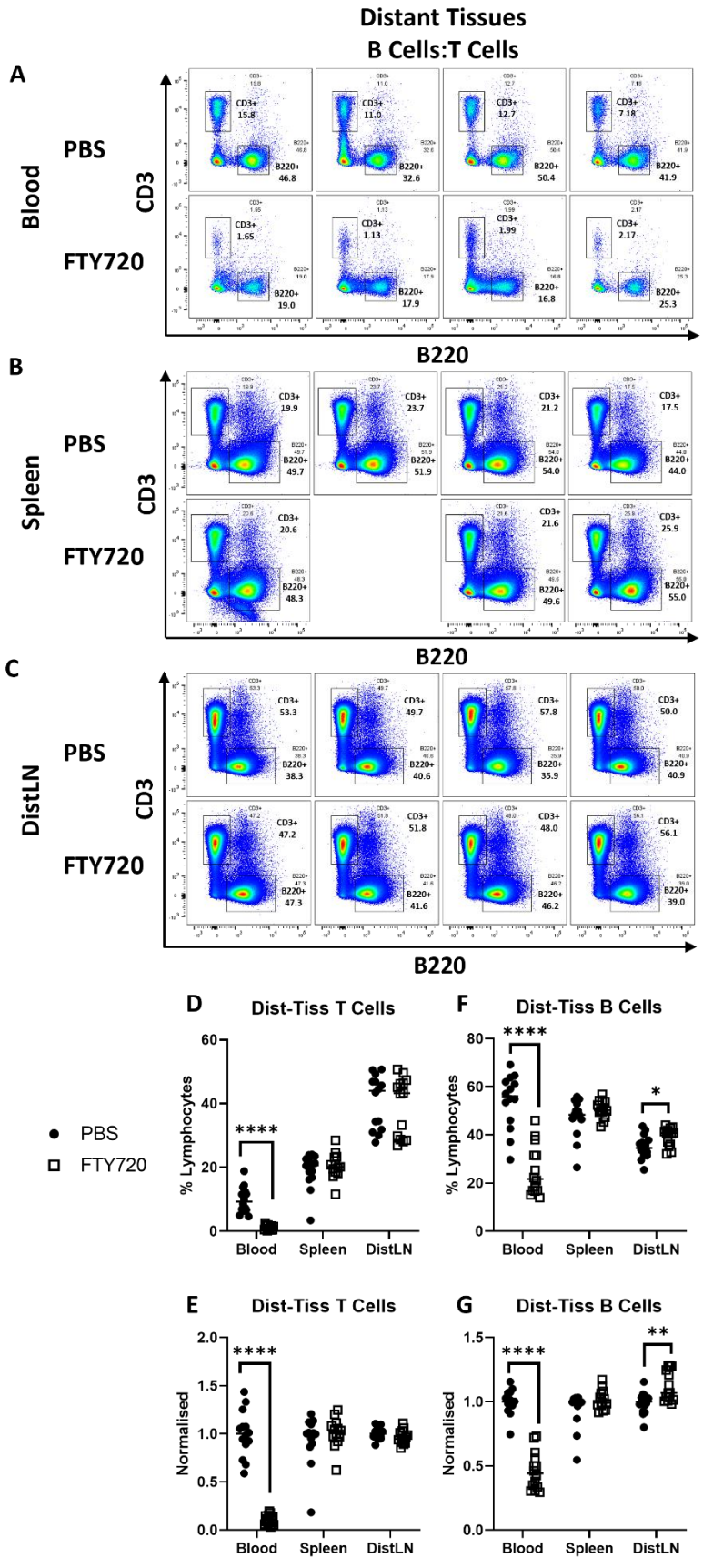

Distant Tissues
B Cells:T Cells
A
Blood
PBS
FTY720
CD3
B220
CD3+ 15.8
B220+ 46.8
CD3+ 11.0
B220+ 32.6
CD3+ 12.7
B220+ 50.4
CD3+ 7.18
B220+ 41.9
CD3+ 1.65
B220+ 19.0
CD3+ 1.13
B220+ 17.9
CD3+ 1.99
B220+ 16.8
CD3+ 2.17
B220+ 25.3
B
Spleen
CD3+ 19.9
B220+ 49.7
CD3+ 23.7
B220+ 51.9
CD3+ 21.2
B220+ 54.0
CD3+ 17.5
B220+ 44.0
CD3+ 20.6
B220+ 48.3
CD3+ 21.6
B220+ 49.6
CD3+ 25.9
B220+ 55.0
C
DistLN
CD3+ 53.3
B220+ 38.3
CD3+ 49.7
B220+ 40.6
CD3+ 57.8
B220+ 35.9
CD3+ 50.0
B220+ 40.9
CD3+ 47.2
B220+ 47.3
CD3+ 51.8
B220+ 41.6
CD3+ 48.0
B220+ 46.2
CD3+ 56.1
B220+ 39.0
PBS
FTY720
D
Dist-Tiss T Cells
% Lymphocytes
****
Blood
Spleen
DistLN
F
Dist-Tiss B Cells
****
*
E
Dist-Tiss T Cells
Normalised
****
G
Dist-Tiss B Cells
****
**

Figure 4. 10. Fewer circulating B cells and T cells in blood of FTY720-treated mice

Flow cytometry plots of B cells (B220+CD3-) and T cells (B220-CD3+) detected in (A) blood, (B) spleen and (C) distLN of FTY720-treated and untreated mice, data presented are from one representative experiment. Graphical summaries of T cells in FTY720-treated and untreated distant tissues presented as % live lymphocytes (D) and normalised ration (E). Graphical summaries of T cells in FTY720-treated and untreated distant tissues presented as % live lymphocytes (F) and normalised ratio (G). Data are combined from 3 separate experiments (n=14). Mann-Whitney test, * $p<0.05$, ** $p<0.01$, *** $p<0.001$, **** $p<0.0001$. Symbols represent individual mice; solid black circles are PBS-treated controls and open squares are FTY720-treated mice. Horizontal bars show means.

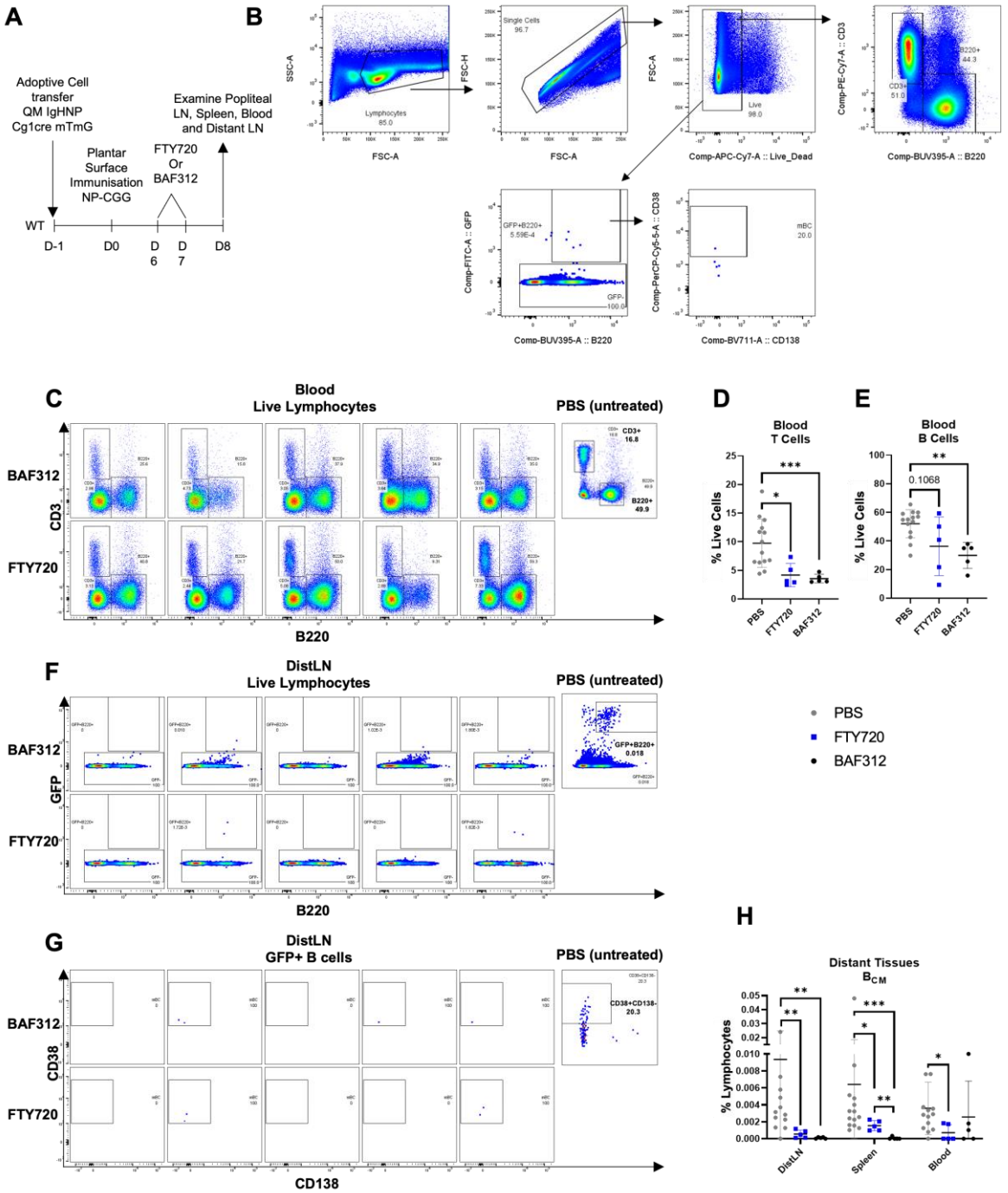
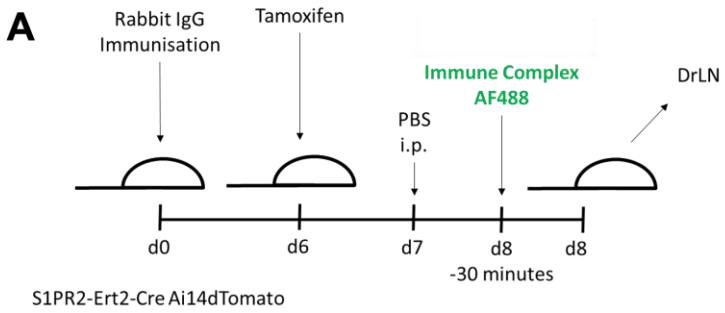
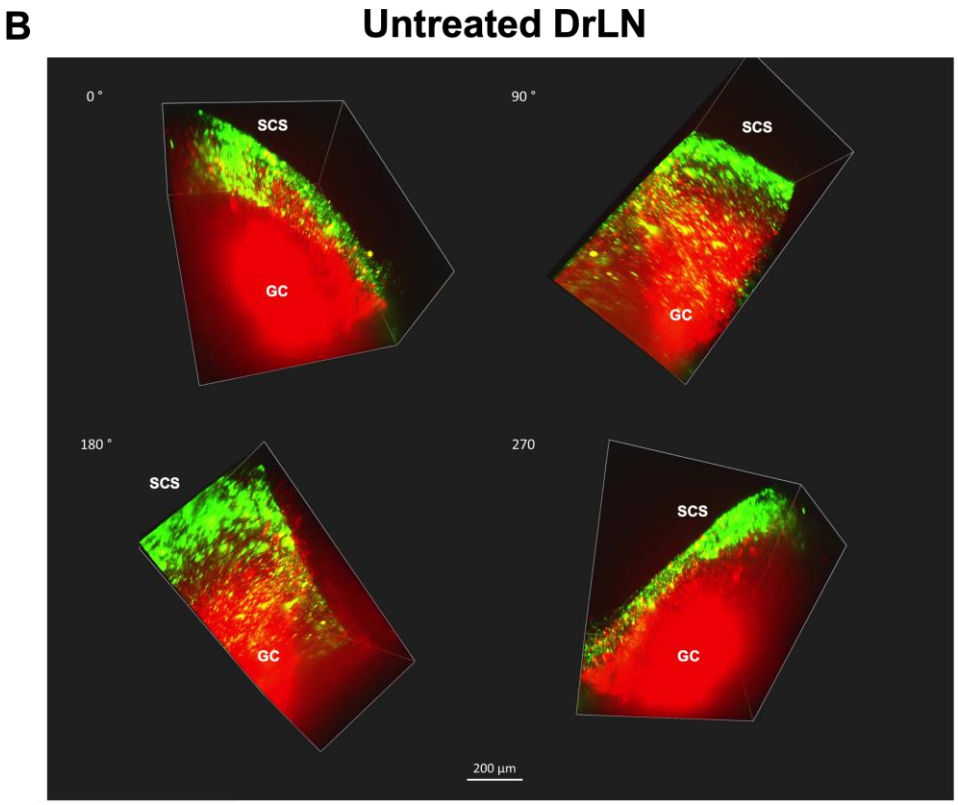


Figure 4. 11. At least as few BCMs in distant lymphoid tissues after BAF312 treatment as after FTY720-treatment

(A) Schematic of QM IgHNP Cg1cre mTmG adoptive cell transfer and immunisation protocol into WT mice followed by treatment with FTY720 or BAF312 (i.p.). Cell transfers were performed by Juan Carlos Yam-Puc. (B) Gating strategy to isolate BCMs (GFP+B220+CD138-CD38+) in distLN at 8 days post-immunisation with NP-KLH. (C) Flow cytometry plots of B cells (B220+CD3-) and T cells (B220-CD3+) in FTY720 and BAF312-treated blood. Graphical summaries of T cells (D) and B cells (E) in blood. Flow cytometry plots of GFP+ B cells (F) and

BCMs (G) in FTY720 and BAF312-treated distLN. (H) Graphical summaries of BCMs in distLN, spleen and blood. FTY720 and BAF312 data are from 1 experiment (n=5), PBS control is combined from 3 separate experiments (n=14). Mann-Whitney test, * $p<0.05$, ** $p<0.01$, *** $p<0.001$. Symbols represent individual mice. Grey circles are PBS controls from a separate experiment, blue squares are FTY720-treated mice and black circles are BAF312-treated mice. Horizontal bars show means.


A
Rabbit IgG
Immunisation
Tamoxifen
Immune Complex
AF488
PBS
i.p.
DrLN
d0
d6
d7
d8
d8
-30 minutes
S1PR2-Ert2-Cre Ai14dTomato


B
Untreated DrLN
0 °
SCS
GC
90 °
SCS
GC
180 °
SCS
GC
270
SCS
GC
200 µm

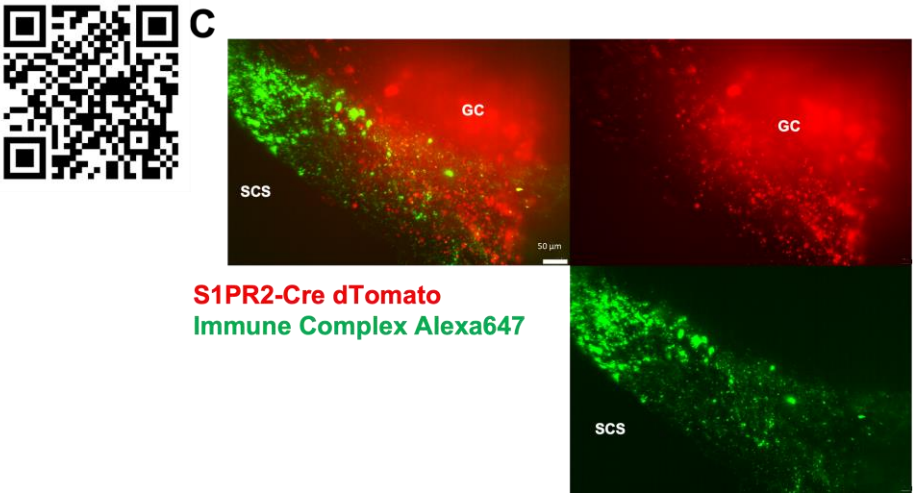
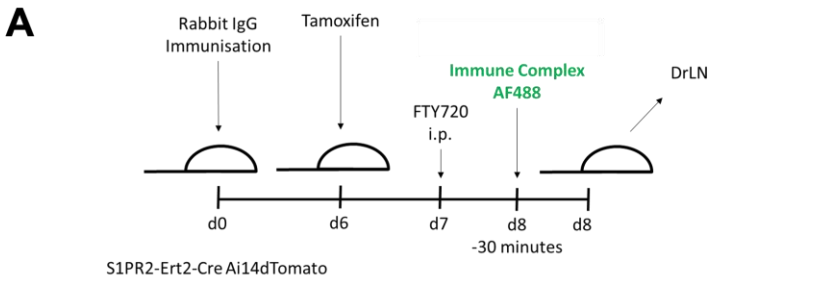
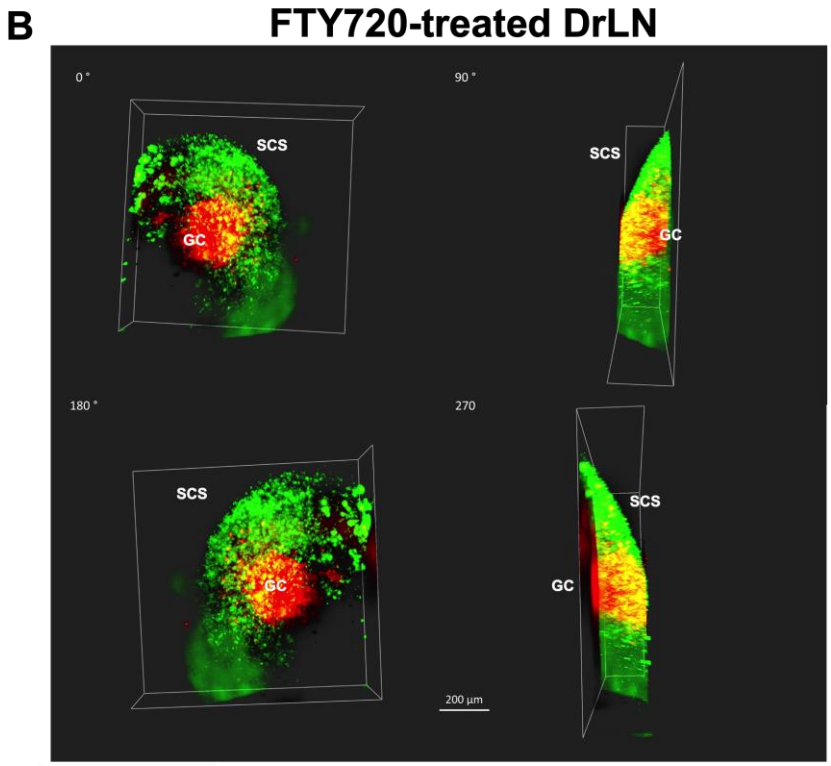

C
GC
SCS
GC
SCS
S1PR2-Cre dTomato
Immune Complex Alexa647

Figure 4. 12. BEMs detected in SCS of FTY720-untreated drLNs

(A) S1PR2-ERT2-Cre Ai14dTomato mice were immunised with rabbit IgG, 48 hours before collection these mice received tamoxifen. 24 hours before collection these mice received injections with i.p. injections with PBS as the experimental control. At day 8 post-immunisation they received *in vivo* staining with Alexa488-labelled immune complex 30 minutes before collection of drLN. (B) Snapshots of light sheet microscopy image of GC and SCS taken at 0°, 90°, 180° and 270° rotated along the Y-axis. QR code links to video of light sheet image in the URL: https://youtu.be/jk9X9wzZ7fI. (C) Maximum intensity projection of light sheet microscopy image (top left), with dTomato (top right) and Alexa488-immune complex (bottom right) shown separately.


A
Rabbit IgG
Immunisation
Tamoxifen
Immune Complex
AF488
FTY720
i.p.
DrLN
d0
d6
d7
d8
d8
-30 minutes
S1PR2-Ert2-Cre Ai14dTomato


B
FTY720-treated DrLN
0 °
90 °
180 °
270
SCS
GC
200 µm

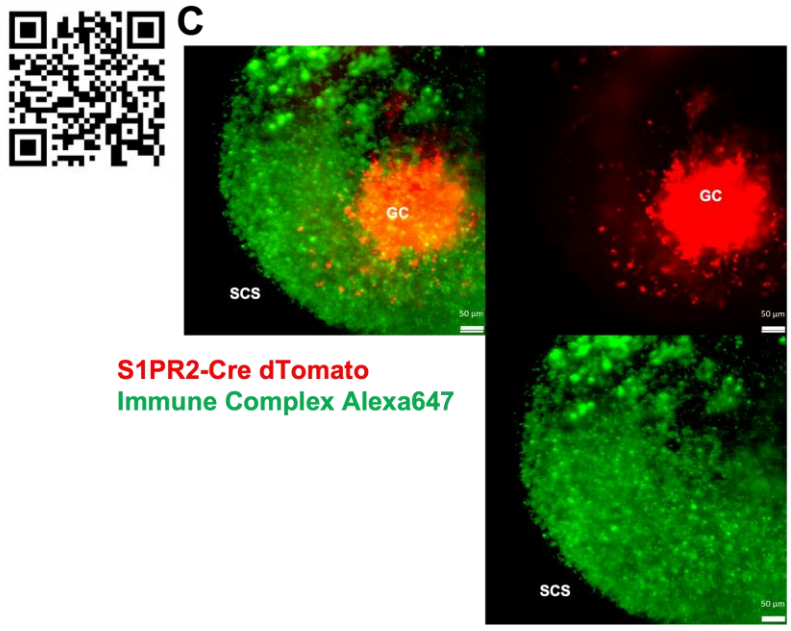

C
GC
SCS
S1PR2-Cre dTomato
Immune Complex Alexa647

Figure 4. 13. Fewer BCMs present in FTY720-treated drLN SCS

(A) S1PR2-ERT2-Cre Ai14dTomato mice were immunised with rabbit IgG, 48 hours before collection these mice received tamoxifen. 24 hours before collection these mice received i.p. injections with FTY720 as the experimental control. At day 8 post-immunisation they received *in vivo* staining with Alexa488-labelled immune complex 30 minutes before collection of drLN. (B) Snapshots of light sheet microscopy image of GC and SCS taken at 0°, 90°, 180° and 270° rotated along the X-axis. QR code links to video of light sheet image in the URL: https://youtu.be/Aq2n90CwBqY. (C) Maximum intensity projection of light sheet microscopy image (top left), with dTomato (top right) and Alexa488-immune complex (bottom right) shown separately.

4.2.3 The role of ACKR4-mediated BEM recycling in response to antigenic variants

The above implies that S1PR1 ligands direct BEMs to the SCS, additionally previous work by our lab showed that CCR7 ligand gradients may direct the return BEMs towards the GC (Zhang et al., 2022). What role does this play in the antibody response? One proposed function of mBCs is in the response to antigenic drift variants; mBCs were reportedly required in the response to WNV variants (Purtha et al., 2011). This may be because mBCs are produced from B cells that are less stringently selected for BCR specificity to the antigen that initiated the response (Suan et al., 2017). This would allow mBCs to be comprised of cells that are more cross-reactive and may allow for BCR variants that better bind variants of the primary antigen.

Although light sheet microscopy did not detect differences in BEM positioning, likely due to lack of quantification (Fig. 4.2 and Fig. 4.3), BEMs were previously observed recycling between the GC-containing follicle and the SCS, and this recycling was dependent upon ACKR4 (Zhang et al., 2022). ACKR4 regulates CCL21 chemokine gradients in the SCS (Ulvmar et al., 2014). Under conditions of ACKR4-deficiency this recycling was not observed: BEMs migrate towards the SCS, but they fail to return towards the follicle (Zhang et al., 2022).

Failure to return to the follicle may be due to a lack of a CCR7 ligand concentration gradient that CCR7-expressing BEMs can follow. This section will investigate the role of ACKR4-dependent SCS-GC BEM recycling and how this relates to the response of BEMs to antigenic variants.

4.2.3.1 ACKR4-defiency resulted in impaired antibody response to hapten antigenic variants

To test the hypothesis that a lack of BEM recycling between SCS and follicle in ACKR4-deficient mice impairs the adaption to antigenic variants, a protocol was established to simulate antigenic drift using a series of haptens. C57BL/6 mice were primed with NIP-KLH. In C57BL/6 mice, B cells triggered to respond to NP typically express a canonical VDJ combination that have highest affinity to NIP, and slightly lower affinity to NP (Reth et al., 1978). The affinity of these BCRs would be lower still to DNP and even further reduced to TNP. After priming with NIP-KLH in alum precipitate, mice received serial boosting injections every 2 days starting from the beginning of BEM recycling at 8 days post-immunisation (Zhang et al., 2022). The first variant antigen NP-KLH, followed by DNP-KLH and lastly TNP-KLH, were injected at days 8, 10 and 12 in soluble form into the foot. 3 days later (15 days post-immunisation) the serum antibody response was examined for affinity to different hapten variants (Fig. 4.14A). The optimal concentration of boosting injections was titrated and was found to be 1 μg per dose, this was the minimum dose to induce a major shift in affinity in serum towards TNP (Fig. 4.14B-C).

To test whether inhibition of BEM recycling affects adaption to antigenic variation, WT/Het (a control group consisting of WT and ACKR4-Heterozygous mice), and ACKR4-KO C57BL/6

mice received the same immunisation protocol as described before but with optimal concentrations. The primary immunisation was with 10 µg NIP-KLH in alum precipitate followed by boosting injections with antigenic variants in PBS at 1 µg (Fig. 4.15A). There was no difference in IgG1 titre and affinity to NIP at 15 days post-immunisation (Fig. 4.15B). NP-specific serum IgG1 at 15 days post-immunisation was examined in WT/Het and ACKR4-KO mice. Relative serum antibody titres were obtained against low valency antigen (left), high valency antigen (middle) and affinity was calculated as a ratio of these (right) - there was no significant difference between WT/Het and ACKR4-KO mice in the affinity to NP antigen at day 15 (Fig. 4.15C). TNP-specific serum IgG1 was examined at 15 days post-immunisation, there was lower relative titre to TNP2; further there was a lower affinity to TNP in ACKR4-KO mice (Fig. 4.15D). This indicated that ACKR4-mediated "recycling" of BEMs between the SCS and the GC may be required for an efficient antibody response to antigenic variants.

4.2.3.2 Reduced generation of Dengue virus envelope protein variant specific antibodies in ACKR4-deficient mice

The role of ACKR4-mediated SCS-GC BEM "recycling" was examined in the context of viral antigen, which may be more clinically relevant due to chronic exposure to antigen. Although Dengue is not known to rapidly mutate to escape variants, seasonal variants provide a good model for studying the response to closely related antigens. Dengue virus envelope protein was selected as the model viral antigen for investigation. Dengue virus has 4 serotypes, these contain a virus enclosed by envelope proteins which play a role in the fusion of viral and endosomal membranes, leading to infection. These envelope (E) proteins are the targets

of neutralising antibodies, they tend to have about 30% sequence variability across all serotypes (Dejnirattisai et al., 2010). The E protein contains 3 domains: DI consisting of a 9-strand β-barrel, DII consisting of 2 loops and the hydrophobic fusion loop at the tip, and DIII consisting of an Ig superfamily fold that is thought to bind cell surface receptors. In the pre-fusion state these are in the form of dimers, 90 of these E dimers encapsulate the dengue virus (Modis et al., 2004). Upon entry to the endosome the acidic conditions induce a conformational change allowing entry into the cell cytoplasm (Modis et al., 2004).

During initial infection with Dengue virus the host develops a lifelong immunity to the infecting serotype, however, in subsequent exposure to virions of differing serotype the infection is enhanced. This is through antibody dependent enhancement - neutralising antibodies to the primary serotype are cross-reactive but not neutralising to the other serotypes. They bind these viruses and are taken up into cells by Fc receptors thus bringing the virus into the endosome where they can undergo membrane fusion and infect the cell (Dejnirattisai et al., 2010). With this pre-established cross-reactivity between serotypes, dengue envelope proteins were considered a good candidate to study the changes in affinity maturation with ACKR4-deficiency in the context of viral proteins.

Dengue virus envelope proteins 1 (E1) and 4 (E4) were compared by sequence alignment using JFATCAT. This test reported a sequence identity of 65% and a similarity of 79% (Fig. 4.16A-B and Fig. 4.17B). WT and ACKR4-KO C57BL/6 mice were primed against E1 in alum precipitate followed by a boost with either E1 or E4 at 8 days post-immunisation - serum IgG1 was examined at 14 days post-immunisation (Fig. 4.17A). To measure affinity maturation towards E4, serum was pre-adsorbed against E1 to remove E1-specific

antibodies, ensuring this serum contained mainly E4 specific antibodies. This was then compared to serum that had not been adsorbed (Fig. 4.17C). As non-adsorbed serum may contain non-specific antibodies, samples with non-adsorbed serum E4-specific IgG1 titres lower than 20 were removed from analysis as they represented baseline levels of specificity. There was no significant difference in E4-specific IgG1 titre between WT and ACKR4-KO mice regardless of whether serum was non-adsorbed (left) or pre-adsorbed (middle). However, there was a slight, non-significant, increase in specificity for E4 in pre-adsorbed antibody in mice that received a boosting injection of E4 compared with mice that received an E1 boost – this was seen in ACKR4-WT mice only (Fig. 4.17D, middle) Furthermore, there was a significant increase in the ratio of pre-adsorbed to non-adsorbed antibody in ACKR4-WT mice when E1 immunisation was followed by E4 immunisation compared with those that received a boost of E1, this was not seen in ACKR4-KO mice (Fig. 4.17D, right). This indicated that BEM recycling may have played a role in affinity maturation towards E4. Although this experiment was replicated twice it should be repeated, maybe with an assay that better tests the fine specificities for antibodies developing or using antigens that are closer related than Dengue antigen variants, e.g., RBD mutants of Coronaviruses or influenza receptor mutants.

This suggested that ACKR4-mediated SCS-GC recycling of BEMs may play a role in the response to variant Dengue viral envelope protein serotypes. There was an improved E4-specific response in serum IgG1 of E1-E4 treated WT mice but not in ACKR4-KO mice, however, it did not reach significance.

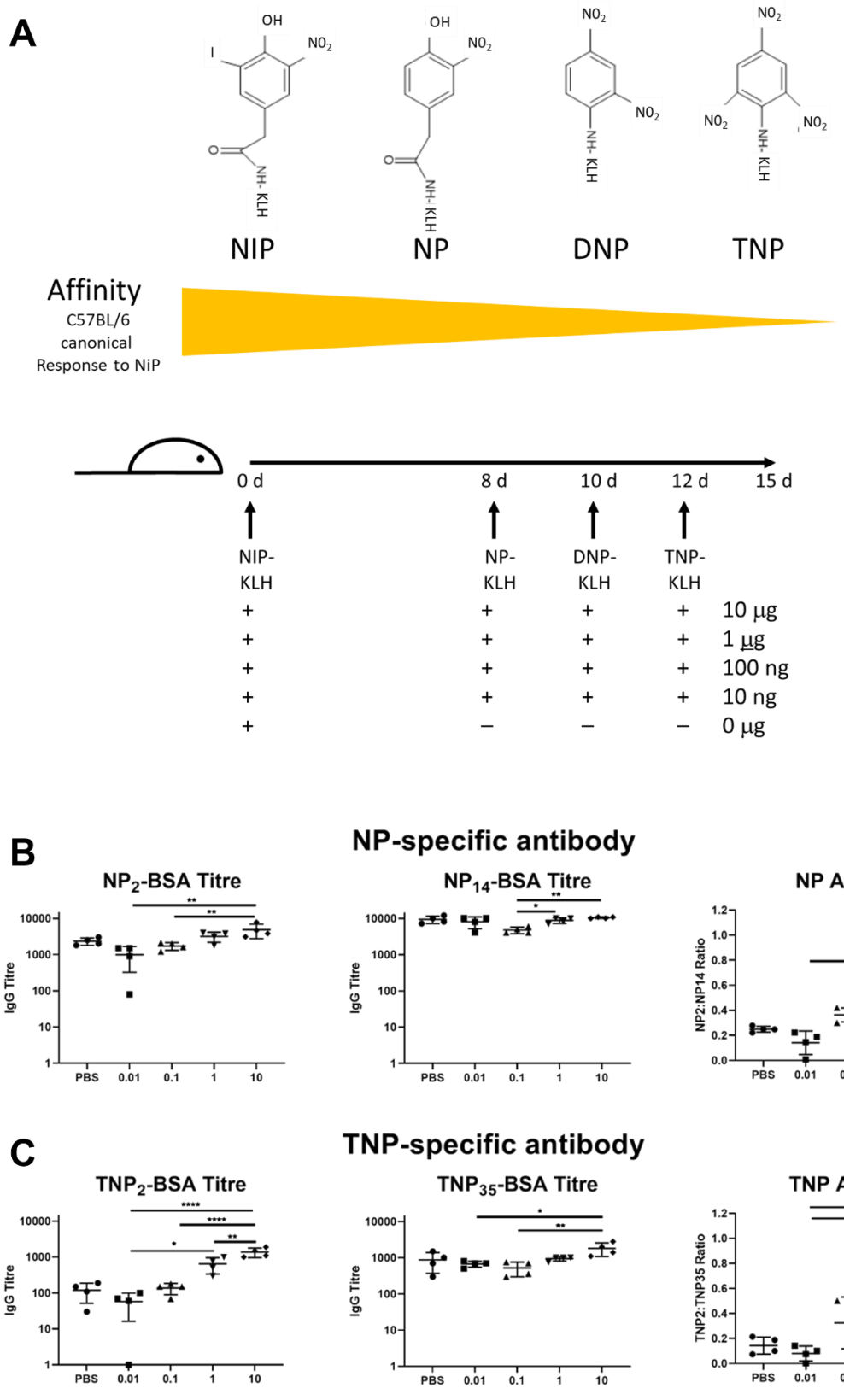


Figure 4. 14. Hapten-based model to simulate antigenic drift

(A) Experimental design to simulate antigenic drift using haptens and serial boosting

injections of increasing variance from the primary hapten injection and titration of optimal concentration. (B) NP-specific serum IgG1 at day 15 post-immunisation, relative titres of serum antibody for low valency antigen (left), high valency antigen (middle) and affinity for NP measured as a ratio between NP2 and NP14 (right). (C) TNP-specific serum IgG1 at day 15 post-immunisation measured serum antibody for low valency antigen (left), high valency antigen (middle) and affinity for TNP measured as a ratio between TNP2 and TNP35 (right). Symbols represent individual mice, circles are PBS controls, squares are recipients of 10 ng of antigen, upward pointing triangles are recipients of 100 ng of antigen, downward pointing triangles are recipients of 1 μg of antigen and diamonds are recipients of 10 μg of antigen. Horizontal bars show geometric means. One-way ANOVA, * $P<0.05$, ** $P<0.01$, *** $P<0.001$, **** $P<0.0001$.

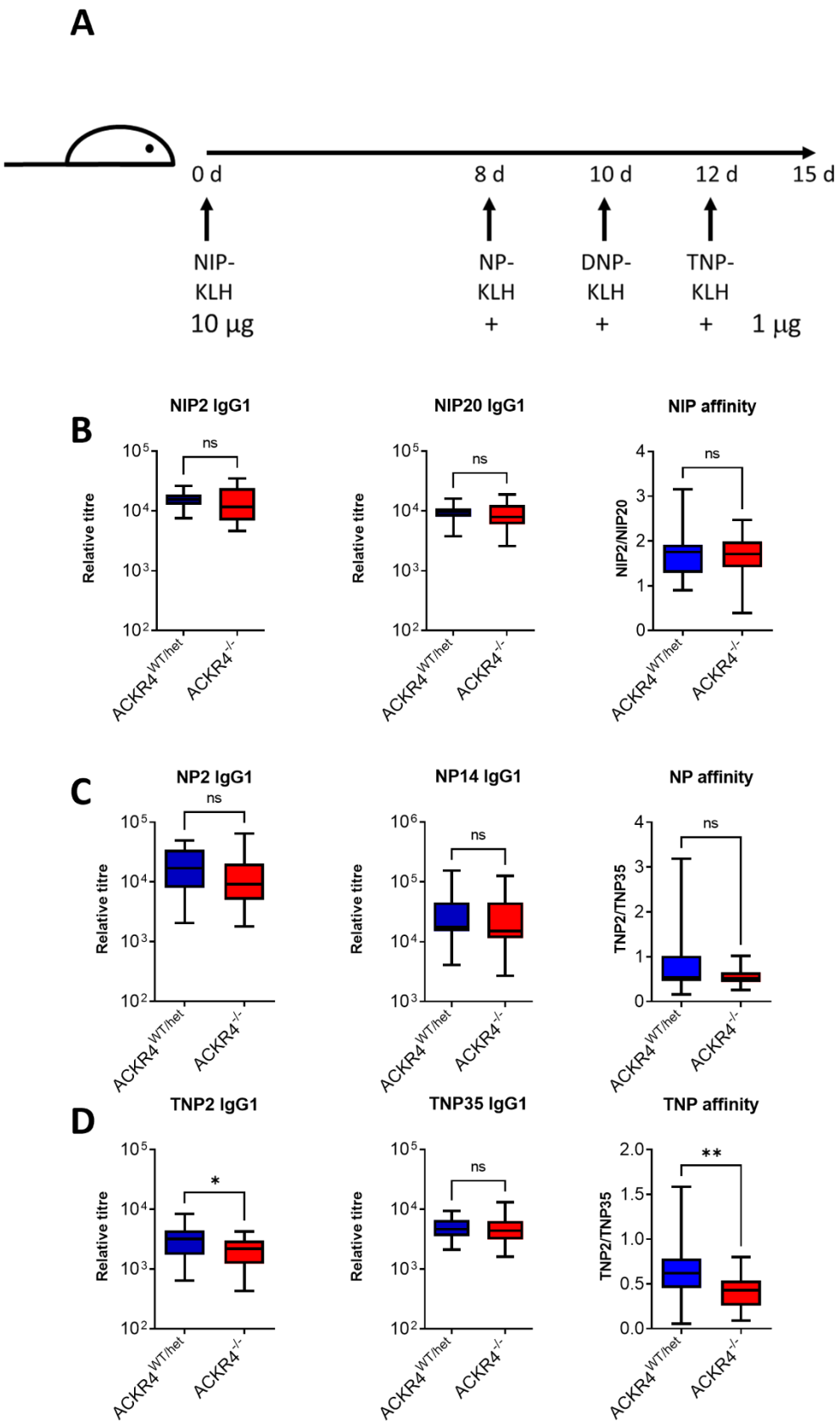

A
0 d
8 d
10 d
12 d
15 d
NIP-KLH 10 µg
NP-KLH +
DNP-KLH +
TNP-KLH + 1 µg
B
NIP2 IgG1
NIP20 IgG1
NIP affinity
Relative titre
NIP2/NIP20
ns
ACKR4 WT/het
ACKR4 -/-
C
NP2 IgG1
NP14 IgG1
NP affinity
TNP2/TNP35
D
TNP2 IgG1
TNP35 IgG1
TNP affinity
*
**

Figure 4. 15. Affinity maturation to TNP was impaired in ACKR4-KO mice that could not recycle BEMs between SCS and follicles

(A) Experiment schematic to simulate antigenic drift using haptens in ACKR4-KO mice and a control group consisting of WT and ACKR4-Heterozygous mice ($ACKR4^{WT/Het}$). (B) Relative titres of NiP-specific IgG1 at day 15 post-immunisation specific to low valency antigen (left), high valency antigen (middle) and affinity measured as the ratio between NiP2 and NiP20 (right). (C) NP-specific IgG1 measured at day 15 post-immunisation. Relative titres of serum antibody binding low valency antigen (left), high valency antigen (middle) and affinity for NP measured as a ratio between NP2 and NP14 (right). (D) TNP-specific IgG1 measured at day 15 post-immunisation. Relative titres of serum antibody binding low valency antigen (left), high valency antigen (middle) and affinity for TNP measured as a ratio between TNP2 and TNP35 (right). Data are normalised and compared within each timepoint. Mann-Whitney test, * $P<0.05$, ** $P<0.01$. NP and TNP data are from 5 separate experiments (n=28). NIP data are from 4 separate experiments (n=24). Bars represent data from multiple mice, horizontal bars are the median and whiskers show standard error. Blue bars represent the control group consisting of WT and ACKR4-Heterozygous mice and the red bars represent ACKR4-KO mice.

A

```
Score:599 bits(1544), Expect:0.0,
Method:Compositional matrix adjust.,
Identities:282/433(65%), Positives:343/433(79%), Gaps:0/433(0%)

Denv-1  1    MRCVGIGNRDFVEGLSGATWVDVVLEHGSCVTTMAKNKPTLDIELLKTEVTNPAVLRKLC  60
             MRCVG+GNRDFVEG+SG  WVD+VLEHG CVTTMA+ KPTLD EL KT     A+LR  C
Denv-4  1    MRCVGVGNRDFVEGVSGGAWVDLVLEHGGCVTTMAQGKPTLDFELTKTTAKEVALLRTYC  60

Denv-1  61   IEAKISNTTTDSRCPTQGEATLVEEQDANFVCRRTVVDRGWGNGCGLFGKGSLLTCAKFK  120
             IEA ISN TT +RCPTQGE  L EEQD  ++CRR VVDRGWGNGCGLFGKG ++TCAKF
Denv-4  61   IEASISNITTATRCPTQGEPYLKEEQDQQYICRRDVVDRGWGNGCGLFGKGGVVTCAKFS  120

Denv-1  121  CVTKLEGKIVQYENLKYSVIVTVHTGDQHQVGNETTEHGTIATITPQAPTSEIQLTDYGT  180
             C  K+ G +VQ ENL+Y+V+VTVH GD H VGN+T+ HG  A ITP++P+ E++L DYG
Denv-4  121  CSGKITGNLVQIENLEYTVVVTVHNGDTHAVGNDTSNHGVTAMITPRSPSVEVKLPDYGE  180

Denv-1  181  LTLDCSPRTGLDFNEMVLLTMKEKSWLVHKQWFLDLPLPWTSGASTSQETWNRQDLLVTF  240
             LTLDC PR+G+DFNEM+L+ MK+K+WLVHKQWFLDLPLPWT+GA TS+  WN ++ +VTF
Denv-4  181  LTLDCEPRSGIDFNEMILMKMKKKTWLVHKQWFLDLPLPWTAGADTSEVHWNYKERMVTF  240

Denv-1  241  KTAHAKKQEVVVLGSQEGAMHTALTGATEIQTSGTTTIFAGHLKCRLKMDKLTLKGMSYV  300
             K  HAK+Q+V VLGSQEGAMH+AL GATE+ +     +FAGHLKC+++M+KL +KGMSY
Denv-4  241  KVPHAKRQDVTVLGSQEGAMHSALAGATEVDSGDGNHMFAGHLKCKVRMEKLRIKGMSYT  300

Denv-1  301  MCTGSFKLEKEVAETQHGTVLVQVKYEGTDAPCKIPFSTQDEKGVTQNGRLITANPIVTD  360
             MC+G F ++KE+AETQHGT +V+VKYEG  APCK+P   +D       GR+I++ P+  +
Denv-4  301  MCSGKFSIDKEMAETQHGTTVVKVKYEGAGAPCKVPIEIRDVNKEKVVGRIISSTPLAEN  360

Denv-1  361  KEKPVNIETEPPFGESYIIVGAGEKALKLSWFKKGGAADDDDKAGWSHPQFEKGGGSGGG  420
                  NIE EPPFG+SYI++G G  AL L WF+KG   DDDDKAGWSHPQFEKGGGSGGG
Denv-4  361  TNSVTNIELEPPFGDSYIVIGVGNSALTLHWFRKGPFEDDDDKAGWSHPQFEKGGGSGGG  420

Denv-1  421  SGGGSWSHPQFEK  433
             SGGGSWSHPQFEK
Denv-4  421  SGGGSWSHPQFEK  433
```

D

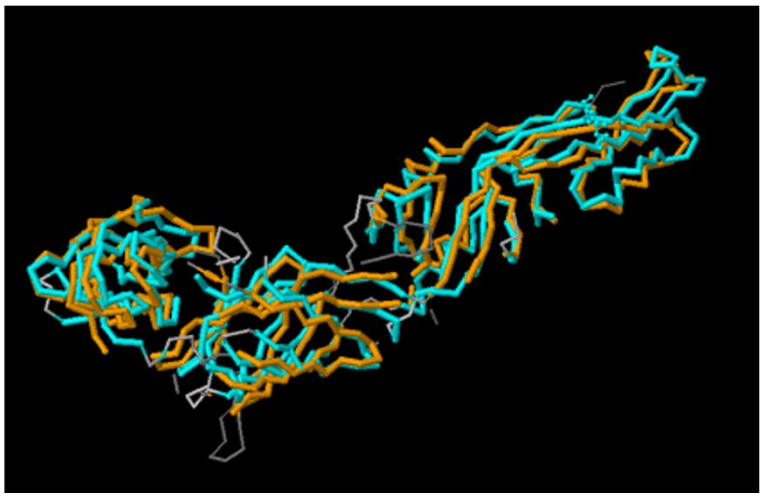


Figure 4. 16. Characterisation of dengue virus envelope proteins

(A) Report for JFATCAT sequence alignment for dengue virus envelope proteins 1 (Denv-1, E1) and 4 (Denv-4, E4) displaying sequence identity, similarity and the matching protein sequence. (B) 3D model of sequence alignment between Denv-1 (orange) and Denv-4 (blue) using protein blast JFATCAT.

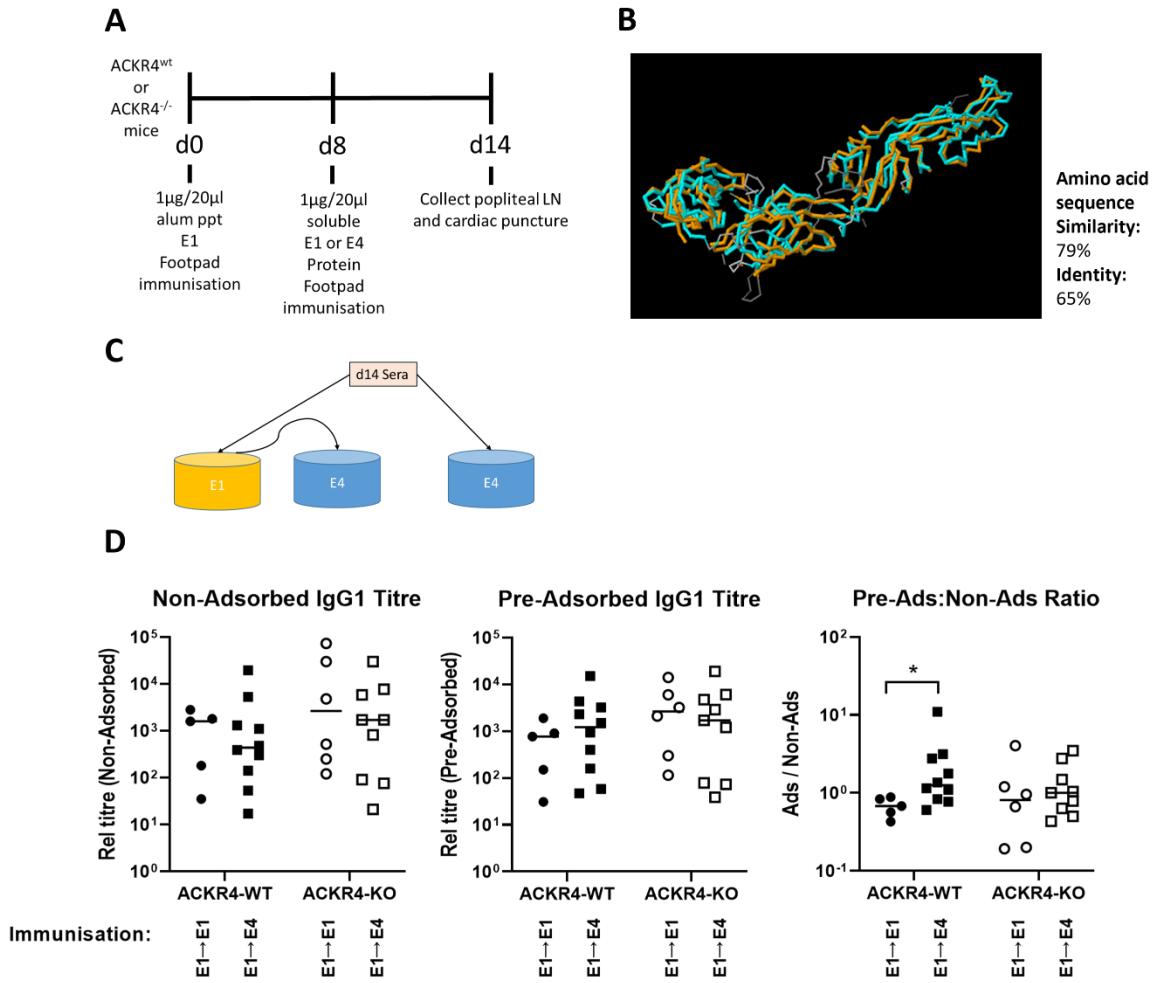


Figure 4. 17. E4-specific serum IgG1 as a ratio to E1-specific serum IgG1 increased in WT but not ACKR4-KO mice after boosting with E4

(A) Experimental schematic to immunise WT and ACKR4-KO mice with Dengue envelope protein-1 (E1) followed by boosting with antigenic variant Dengue envelope protein-4 (E4) and collection of tissues at day 14 post-immunisation. This experiment based on a protocol designed by Juan Carlos Yam-Puc and Raul Maqueda Alfaro. (B) 3D model of sequence alignment of Denv-1 (orange) and Denv-4 (blue). (C) Design to measure affinity for Denv-4 protein by pre-adsorbing E1-specific antibody before measuring serum against E4. (D) E4-specific serum IgG1 at day 14 post-immunisation, relative titres obtained from pre-adsorbed serum (left), non-adsorbed serum (middle) and E4 affinity measured as a ratio between pre-adsorbed and non-adsorbed titres. Samples with a non-adsorbed E4-specific IgG1 titre of

less than 20 were removed from analysis as they represented non-specific baseline serum. Data presented are from 2 separate experiments (n=10). Symbols represent individual mice. Filled symbols represent ACKR4-WT mice and open symbols represent ACKR4-KO mice. Circles represent recipients of E1 followed by a boost with E1 again, whereas squares represent recipients of E1 followed by a boost with E4.

4.3 Discussion

Light Sheet microscopy shown in chapters 3 and 4 and intravital microscopy from a previous study captured the migratory behaviours of BEMs emerging from the GC LZ (Zhang et al., 2022). BEMs "recycled" between the SCS and the GC-containing follicle (Zhang et al., 2022). The migration of lymphocytes in the drLN to the outer follicle and entry to the cortical sinuses was directed by S1P provided by blood and lymph (Pereira et al., 2010, Zhang et al., 2016). This may also play a role in the movements of BEMs during SCS-GC "recycling" as suppression of S1P receptors resulted in reduced egress from the drLN. There were fewer BCMs detected in blood and distant lymphoid tissues in S1PR1-blockade. This may indicate an impairment of BEM entry to the SCS followed by egress of the LN via the efferent lymphatics. This was seen in both FTY20 and BAF312-treated mice. Light sheet microscopy also revealed BEMs in the SCS and there were potentially fewer in the SCS after treatment with FTY720. Quantification of BEMs in the SCS would help to conclusively determine whether S1PR1 blockade prevented BEM migration to the SCS and therefore impaired egress from the drLN.

Return of BEMs from the SCS back towards the GC-containing follicle during "recycling" was impaired by ACKR4-deficiency (Zhang et al., 2022). ACKR4 is expressed by floor LECs and regulates CCL21 gradients in the SCS of the LN (Ulvmar et al., 2014). ACKR4 scavenges and degrades CCL19, CCL21 and CCL25, CCL20 has also been shown to be a ligand for ACKR4 but

whether it is internalised and degraded is as yet unclear (Matti et al., 2020b, Matti et al., 2020a). Moreover, ACKR4 is expressed weakly by DZ GC B cells (Fig. 4.1) (Eckert et al., 2020). ACKR4 may still be expressed by BEMs at the protein level if not the RNA level. This may also help to direct migration, perhaps by scavenging nearby CCL19 and CCL21 to produce localised micro-gradients of chemokines to increase the sensitivity of CCR7 to its ligands. ACKR4 might help to facilitate the greater chemotactic index of CCL19 at shallower concentration gradients (Zidar et al., 2009). CCL20 is furthermore targeted by ACKR4, as there is a concentration gradient of CCL20 leading to the SCS that facilitated migration of innate-like lymphocytes (Zhang et al., 2016). Perhaps in ACKR4-KO mice there was a reduced sensitivity of CCR6 expressed by BEMs to its ligand, resulting in impaired migration to the SCS and subsequent egress from the LN. The effects of ACKR4-deficiency in the drLN suggested that the CCR7-CCL19/21 axis is important for the return of BEMs from the SCS to the GC-containing follicle. CCL21 expression was examined in the LN to help verify this role. CCL21 expression was observed in both immunised and non-immunised LNs by histology and flow cytometry. CCL21 was expressed by TRCs and was observed around the HEVs of the LN. CCL21 expression was also detected among MadCAM1+ MRCs in the floor of the SCS. CCL21 expression was more apparent among TRCs in histology, but some CCL21-expressing MRCs were still detected; however, this was not quantified. Flow cytometry suggested that MRCs and TRCs may express comparable levels of CCL21, however TRCs outnumbered MRCs in both immunised and non-immunised LNs. The number of MRCs increased in immunised LNs, this may be related to an increase in volume of the reactive popliteal LN due to cell expansion.

BEMs in the SCS were in proximity to CD169+ SCS macrophages. Previous work showed that BEMs directly interacted with SCS macrophages. Calcium signalling was induced among BEMs contacting SCS macrophages and patches of CD169-labelled cell membrane from SCS macrophages were present on BEMs (Zhang et al., 2022). Macrophages on the SCS floor can collect lymph-borne antigen brought in by the afferent lymphatics and present them to B cells leading to a humoral response to antigen (Junt et al., 2007). These SCS macrophages can then present antigen to BEM recycling between an ongoing GC and the SCS. These SCS macrophages readily present antigens as they translocate IC encapsulated antigen from the lymphatics to the follicular side of the cell surface (Phan et al., 2009). These IC encapsulated antigens were then captured by non-cognate B cells which played a role in affinity maturation during an ongoing GC reaction (Phan et al., 2009). M1 or M2 polarisation of SCS macrophages was unclear – they had reduced phagocytosis typically seen in M1 macrophages but could still produce pro-inflammatory cytokines (Louie and Liao, 2019).

During the GC reaction PCs are selected due to their higher BCR affinities, however mBCs are selected from the B cells with more intermediate levels of BCR affinity (Suan et al., 2017). This lower affinity of mBCs towards the primary antigen may allow for cross-reactivity to variants of the primary antigen. In a viral infection the virus can rapidly mutate leading to changes in the epitope resulting in an antigenic drift producing variants of the primary antigen. Response of PCs and mBCs from WNV infected mice were compared and mBCs were better able to respond to escape variants of the primary antigen (Purtha et al., 2011). In humans infected with SARS-CoV-2 initially there was a transient increase in PCs, but mBCs were retained - many of these mBCs possessed some cross-reactivity with other beta-coronaviruses (Sokal et al., 2021). The memory B cells response to influenza can also

produce cross-reactive memory B cells (Li et al., 2012). These mBCs can then become antibody-secreting cells and produce broadly cross-reactive antibodies against influenza (Ellebedy et al., 2020). Dengue viral infections produce highly cross-reactive mBCs which readily differentiate into PCs upon encounter with antigen (Priyamvada et al., 2016). However, cross-reactivity but poor neutralisation of cross-reactive Dengue virus-specific antibodies facilitated antibody-dependent enhancement of infection (Whitehead et al., 2007).

Cross-reactivity of mBCs to antigenic variants and the antigen presentation of SCS macrophages to B cells lead to the investigation of BEM response to antigenic variants. ACKR4-deficiency inhibited BEM "recycling" between SCS and follicle and impaired affinity maturation of serum antibody to hapten antigenic variants. In the ACKR4-deficient response to Dengue virus envelope proteins there was also less affinity maturation to the variant antigen of a different serotype to primary antigen; however, this did not reach significance. This suggested that in Dengue infection under ACKR4-deficiency there may be reduced antibody-dependent enhancement of infection. Impaired affinity maturation in ACKR4-deficiency implied that BEMs migrate to the SCS and sentinel for variants of the primary antigen. Upon recognition of this antigen variant presented by SCS macrophages the BEMs could then return towards the GC carrying antigen. These BEMs may participate in the GC leading to the generation of antibody-secreting cells producing antigen with high affinity towards the antigenic variant. Some of these BEMs could also become activated and differentiate into an antibody-secreting cell, as IgG1+ mBCs have been observed to do (Dogan et al., 2009). This process would be important in viral infections due to chronic exposure to antigen and mutation into escape variants as previously discussed. It would

have been illuminating to investigate the role of BEM recycling in the response to other viral antigens such as influenza or HIV.

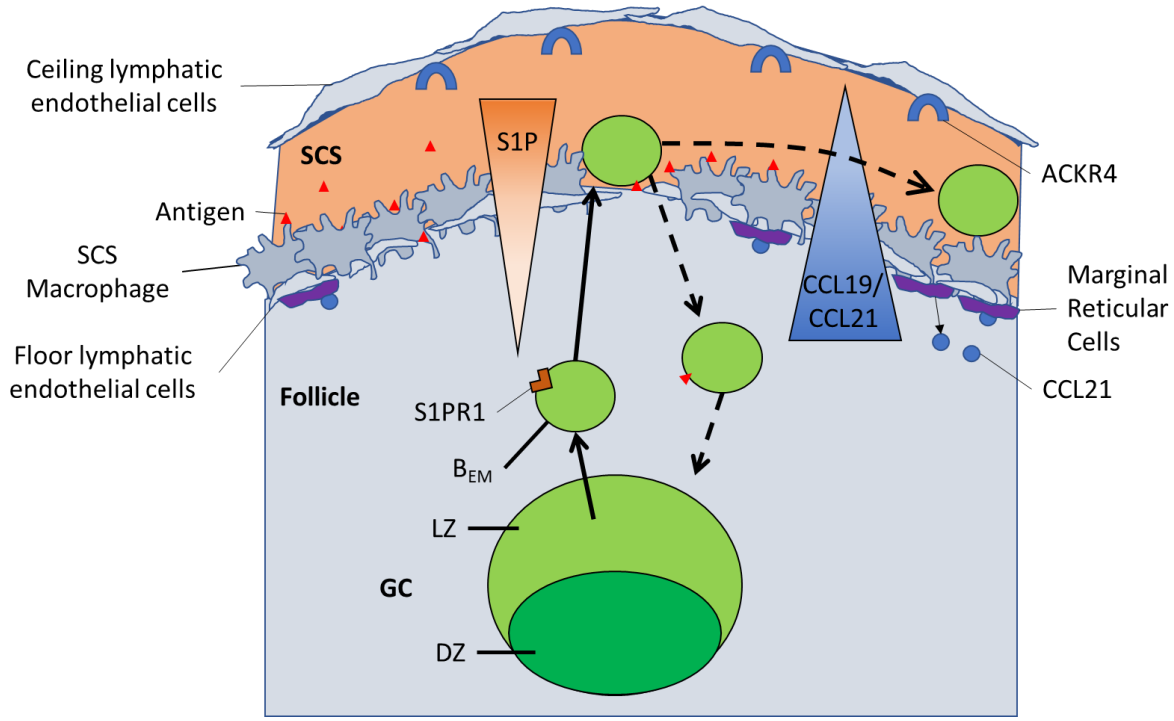


Figure 4. 18. Representative diagram of the migratory behaviours of BEM in the drLN

Diagram of the proposed model of BEM migration. BEMs produced from GC follow S1PR1 ligands to migrate to the SCS. BEMs in the SCS may either egress the LN via efferent lymphatics or migrate back towards the GC following CCR7 ligand gradients regulated by ACKR4.

As described in the above figure during an ongoing GC reaction BEMs are produced, they may exit the GC from the LZ and migrate towards the SCS following S1P gradients. BEMs can then egress the LN via the efferent lymphatics. BEMs can also detect antigen presented by SCS macrophages. They can return to the GC following CCR7 ligands, the gradients of which are regulated by ACKR4 (Fig. 4.18). BEMs can then ferry antigen back to the GC to fuel the

GC reaction. These BEMs could also participate in the GC reaction, contributing their genetic information. This drives the B cell response to antigenic variants.

5 Circulating memory B cells in distant tissues

5.1 Introduction and Objectives

Lymphocyte trafficking is a process that requires chemotaxis to give cells direction. The main chemokines organising entry into the T zone are CCL19 and CCL21 bound by CCR7. For naïve B cells the CXCR5-CXCL13 axis is crucial for entry into follicles. CCR7 is prominently expressed by mature DCs, naïve T cells, regulatory T cells and central memory T cells (Förster et al., 2008). CCR7 is important for lymphocyte entry into the LN via HEVs and is involved in the entry of T cells to draining lymphatics (Förster et al., 2008). B cells also follow this route of entry into LNs through HEVs using CCR7-ligands without requiring CXCR5-ligands (Ebisuno et al., 2003, Okada et al., 2002). For B cells in the bone marrow CCR7 can inhibit retention within its niche by downregulating CXCR4 (McHeik et al., 2019). CCR7 is also essential for DC mobilisation and homing to drLNs via afferent lymphatics. CCR7-deficient DCs are less able to follow CCL21 gradients and enter draining tissues (Förster et al., 1999).

CCR7-deficient mice have smaller spleens and Peyer's patches due to fewer cells migrating to these SLOs. CCR7-deficient B cells in a WT host have been shown by Forster et al (1999) to be better retained in the outer follicles of the spleen as fewer are seen in the PALS due to an inability to follow CCR7 ligands to this area.

The ligands of CCR7 share some expression patterns but also show some differences in the cells that produce them. Both CCL19 and CCL21 are expressed by HEVs and stromal cells of the drLN and spleen. CCL19 is also expressed by mature DCs whereas CCL21 is expressed by the endothelium of the afferent lymphatics. The genes for CCL19 and CCL21 are encoded in chromosome 4 of the mouse (Vassileva et al., 1999, Nakano and Gunn, 2001). The CCL21a

isoform of CCL21 contains a Serine on residue 65 is mainly expressed in lymphoid tissues such as LN and thymus. (Kozai et al., 2017, Lo et al., 2003). This may reflect the difference in function, for example CCL19 has the unique capability to promote internalisation of CCR7 by recruiting β-arrestins and GRK3 in addition to GRK6 resulting in desensitisation of CCR7 (Zidar et al., 2009). This might be a mechanism to regulate responsiveness of the cell to CCR7 ligands depending on concentration and may act in an autocrine manner on mature DCs. CCL21 can signal through β-arrestins and GRK6 but cannot achieve desensitisation of CCR7 (Zidar et al., 2009). CCL21 has been shown to be secreted by afferent lymphatics in a circadian manner. This facilitates a circadian trafficking of CCR7-expressing DCs to the drLN (Holtkamp et al., 2021). This would ensure provision of antigen to the lymph node during the peak of the immune function when there is plenty of energy available reflected by feeding cycles. CCL21, but not CCL19, plays a role in thymocyte development. It is expressed by epithelial cells in the medullary thymus and is required for egress of thymocytes from the thymus into circulation (James et al., 2021). Another key difference between CCL19 and CCL21 is that at shallow concentration gradients CCL19 had a greater capacity to guide chemotaxis than CCL21, but at steeper concentration gradients CCL21 was better able to induce chemotaxis (Ricart et al., 2011). This may be because at higher concentrations of CCL19 there is more internalisation of CCR7 thereby reducing sensitivity to these stronger gradients. CCL21 is immobilised on the surface of the extracellular matrix whereas CCL19 is not immobilised (Haessler et al., 2011).

ACKR4 is part of a family of scavenger receptors that has been found to scavenge CCL19, CCL21 and CCL25 (Ulvmar et al., 2014). CCL20 is also a ligand for ACKR4 (Matti et al., 2020a). ACKR4 is expressed by LECs of the SCS ceiling of the LN (Ulvmar et al., 2014). ACKR4 is

expressed by the peri-marginal sinus in the spleen, which is a distinct layer of the splenic vasculature surrounding the white pulp that is neither part of the red pulp nor the marginal sinus (Werth et al., 2021).

ACKR4 is thought to generate and maintain chemokine gradients of CCL19 and CCL21 by scavenging and taking in these chemokines (Ulvmar et al., 2014). ACKR4 may be involved in increasing receptor sensitivity to chemokine as it may create local micro-gradients by scavenging nearby chemokines to help direct cell migration. ACKR4 may also act to reduce CCL19-mediated desensitisation of CCR7 as described by Zidar et al. (2009) by scavenging CCL19, this may help to maintain responses of CCR7 to CCL19. In the spleen ACKR4-expressing cells of the peri-marginal sinus were able to take in CCL19 and may regulate serum CCL19. They were also posited to control CCL19 gradients locally in the MZ microenvironment (Werth et al., 2021).

B cell expression of CCR7 is required for entry into the LN through HEVs (Ebisuno et al., 2003). This CCR7 expression was specific to B cells in the paracortical cords of the LN rather than the inter-follicular areas (Park et al., 2012). Expression of CXCR5 allows migration to the CXCL13-rich B cell follicles of the LN (Ansel et al., 2000). B cells entering the spleen also express CXCR5 to facilitate homing to the CXCL13-rich follicles. These B cells also express CCR7 allowing them to move through the T cell zones of the PALS (Pereira et al., 2010). Entry of lymphocytes into the spleen was classically thought to occur through the marginal sinus (Bajenoff et al., 2008). However there is mounting evidence that lymphocyte entry to the spleen occurs through the bridging channels into the PALS (Chauveau et al., 2020). This could

occur initially through the ACKR4-rich peri-marginal sinus via a series of shunts that connect to bridging channels with the marginal sinus (Werth et al., 2021).

Circulating B cells are retained in the B cell follicle for up to a day before they migrate towards the marginal sinus possibly following S1PR1 and EBI2 ligands. Once here the follicular B cell lack the adhesion molecules expressed by MZ B cells to withstand shear forces and re-enter circulation through the splenic vasculature (Pereira et al., 2010). In the LN follicle B cells may follow a similar pattern and migrate towards the outer follicle and intranodal lymphatics following S1PR1 and EBI2 ligands (Pereira et al., 2010). This may occur because B cells in the LN increase expression of S1PR1 over time while sensitivity of CCR7, CXCR4 and CXCR5 is reduced. However, this sensitivity is replenished upon re-entry into the blood (Park et al., 2012). This ensures that with time there is a decreasing responsiveness to chemotactic signals from CCR7 and CXCR5 ligands while increasing sensitivity to S1PR1 and EBI2 ligands resulting in egress.

This chapter seeks to understand the signals from CCR7 ligands for entry of BCMs into distant tissues by examining movements of BCMs in mice deficient for CCL19 and CCL21. This effect was also examined in ACKR4 and CCR7-deficient BCMs.

This chapter will investigate the migratory behaviours of BCMs, to determine in which tissues they may be found, and the chemotactic cues required for their presence there. CCR7 was expressed by BEMs and BCMs as noted by bulk RNA sequences data in Chapter 3. ACKR4 is expressed at low levels by GC B cells (Garcia Ibanez, 2017)(Fig. 4.1) and may also be expressed by BEMs and BCMs or retained expression on the protein level, or at least may contribute to initial migration behaviours. Entry of B cells into LN and spleen requires the

ligands of CCR7: CCL19 and CCL21. These are expressed by LN HEVs or expressed in peri-marginal sinus-bridging channel shunts of the spleen. The hypothesis tested in this chapter is that the CCR7-CCL19/21 axis is important for BCM entry into distant lymphoid tissues.

This chapter investigated the following hypotheses:

1. ACKR4-deficiency impairs entry of BCMs entry into distant lymphoid tissues.
2. CCL19 is required for entry of BCMs into distLN and spleen.
3. BCM expression of CCR7 and ACKR4 is required for entry into distant lymphoid tissues.
4. CCL21-deficiency impairs the generation of BEMs and subsequent migration of BCMs into distant lymphoid tissues.

5.2 Results

5.2.1 ACKR4-deficiency resulted in decreased levels of BCM in distLN but not blood and spleen

ACKR4 is involved in regulation of CCL19/21 gradients in the LN SCS. The ACKR4-KO drLN was examined in chapter 4 (Fig. 4.1). It has previously been shown that under conditions of ACKR4-deficiency where this gradient is not maintained BEMs that migrate to the SCS fail to recycle back to the follicle and a greater proportion egress the LN becoming BCMs (Zhang et al., 2022). To verify this and to determine where these BCMs migrate, distant tissues of ACKR4-KO mice were examined.

Mice received adoptive cell transfers of $1x10^5$ NP+B220+ splenocytes from QM Cg1-Cre mTmG mice, followed by immunisation with 20 µg NP-CGG in alum precipitate with

Bordetella pertussis on foot and examination of tissues at 8 days post-immunisation (Fig. 5.1A). BCMs were observed from the adoptively transferred GFP+ B cells at 8 days post-immunisation in blood (Fig. 5.1B and E), spleen (Fig. 5.1C and F) and distant LN (Fig. 5.1D and G) by flow cytometry in WT/ACKR4-Het (a control group consisting of WT and ACKR4-heterozygous mice) and ACKR4-KO hosts. There was no significant difference in BCMs in blood (Fig. 5.1H) and spleen (Fig. 5.1I) between WT/ACKR4-Het and ACKR4-KO hosts. Fewer BCMs were observed in ACKR4-KO distant LN (Fig. 5.1J). It has previously been observed that BCMs in ACKR4-KO mice are raised in the blood indicating greater egress from the drLN (Zhang et al., 2022). In this present study there was no significant difference in levels of BCMs in WT/ACKR4-Het or ACKR4-KO mice, but this does not disprove the prior observation. A novel observation in this present study is that BCMs were reduced in the distLN. This suggested that ACKR4-deficiency impaired entry of BCMs into the distLN, or that BCMs were poorly retained in the distLN of ACKR4-deficient mice. There were more activated B cells in some WT distLNs, this suggested that there may have been an immune response possibly due to male mice fighting or antigen leaking into other tissues from the foot injection. The data presented here were from transferred QM Cg1cre mTmG cells which report activated NP-specific B cells, this differs from previous work from our lab showing increased transferred QM ACKR4-WT and QM ACKR4-KO B cells (without Cg1cre) in the ACKR4-KO blood (Zhang et al., 2022). Another important consideration for this present data is that some of these mice had germinal centre responses taking place within distLN, this was seen in each of 3 repeats, these were not removed in Fig. 5.1. Removal of samples containing GCs did not disrupt the differences between WT and AKCR4-KO distLNs measured as a normalised ratio of % lymphocytes, but significance was lost as % lymphocytes (Appendix 4).

There was still a trend with and without the presence of GCs in distLN that there were fewer GCs in distLNs of ACKR4-KO hosts. However, it was unclear as to the cause of GCs in distLN which mainly appeared in WT/ACKR4-Het mice. Immunisation on the hind foot should only drain to the popliteal LN and other LNs located around the flank and pelvis of the mouse (Van den Broeck et al., 2006, Kawashima et al., 1964). Perhaps there was some leakage of antigen into other tissues. It is unlikely that there was leakage into the spleen as GCs were not detected here. There is also the chance that there was a non-specific response in distLNs that resulted in expansion of B cells; perhaps the result of mice fighting. However, this would not explain why GFP+ NP-specific B cells were detected in distLN.

ACKR4 is involved in the regulation of CCL19 and CCL21 chemokine gradients, and are known to maintain CCL21 gradients in the SCS to facilitate entry of DCs from afferent lymphatics (Ulvmar et al., 2014). In the ACKR4-KO mice these gradients are no longer maintained, the next step was to investigate the effect of deficiency of CCL19 on the generation of BEMs and migration of BCMs to distant lymphoid tissues.

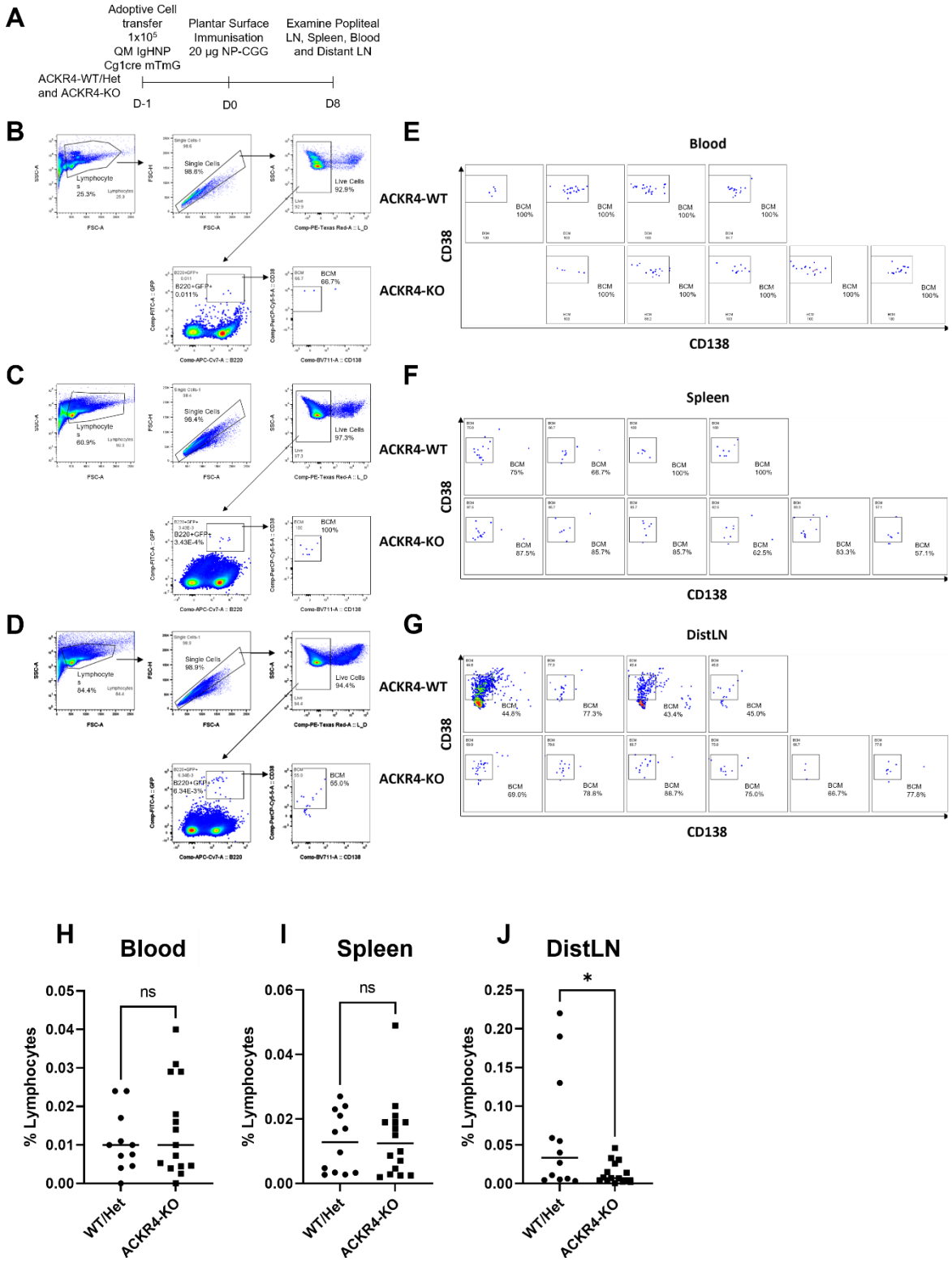


Figure 5. 1. Fewer BCM detected in distLN of ACKR4-deficient mice

(A) Schematic of protocol of adoptive cell transfer and immunisation of a control group of WT and ACKR4-Heterozygous (WT/Het) and ACKR4-KO mice. Cell transfers were performed by the University of Birmingham Biomedical Services Unit. Gating strategy to identify BCMs (GFP+B220+CD138-CD38+) from adoptively transferred activated GFP+ B cells in (B) distant

LN, (C) spleen and (D) blood, presented from one representative experiment. FACS plots displaying BCMs in WT/ACKR4-Het and ACKR4-KO (E) blood, (F) spleen and (G) distant LN, presented from one representative experiment. Graphical summaries of BCMs in (H) blood, (I) spleen and (J) distant LN as % lymphocytes. Summarising statistics are merging data from 3 separate experiments (n=12-18). * p-value <0.05, ** p-value <0.01, Mann-Whitney test. Symbols represent individual mice, circles represent the control group consisting of WT and ACKR4-Heterozygous mice and squares represent ACKR4-KO mice. Horizontal bars show medians. The data presented here are from the same experiments as presented in Figure 4.3.

5.2.2 Generation of BEMs is unchanged but fewer BCMs detected in distant lymphoid tissues in CCL19-deficient mice

ACKR4 is a scavenger receptor for CCL19 and CCL21 that is involved in the maintenance of concentration gradients of these chemokines. In this section the effect of deficiency of CCL19 was examined. CCL19 is a ligand for CCR7 for which the mRNA is expressed in BCMs and BEMs. CCL19 also plays a role in the CCR7-expressing T cell migration. The role of CCL19 in generation of BEMs and migration of BCMs was studied by using of CCL19-deficient mice as a host.

CCL19-KO and WT/CCL19-Het mice (a control group consisting of WT and CCL19-heterozygous mice) received adoptive cell transfer of $1x10^5$ NP+B220+ QM mTmG splenocytes 1 day before immunisation with 20 µg NP-CGG in alum precipitate with *Bordetella pertussis* on foot. Tissues were examined at 8 days post-immunisation (Fig. 5.2A). B cells, plasma cells, GC B cells and BEMs in the drLN were examined by flow cytometry (Fig. 5.2B-C). There were fewer adoptively transferred B cells observed in the drLN from CCL19-KO hosts (Fig. 5.2D). There were clearly significantly fewer GC B cells and IgD- class switched GC B cells detected in CCL19-KO mice (Fig. 5.2E-F). There was a non-significant trend towards reduced PCs observed in CCL19-KO drLNs (Fig. 5.2G), but there was no difference in BEMs in

drLN between CCL19-KO and WT/CCL19-Het mice (Fig. 5.2H-I). The proportion of IgG1+ GC B cells and IgG1+ BEMs were similar between CCL19-KO and WT/CCL19-Het mice (Fig. 5.2L-M). This revealed that CCL19 was involved in B cell activation, but CCL19-deficiency had no effect on IgG1 class switching.

BCMs in distLN, spleen and blood were quantified by flow cytometry (Fig. 5.3A-D). There was a non-significant trend towards fewer BCMs, and class switched IgD- BCMs in CCL19-KO distLNs (Fig. 5.3E-F). There were significantly fewer BCMs (Fig. 5.3G) in the CCL19-KO spleen, this included class-switched IgD- BCMs (Fig. 5.3H). To a lesser extent there were also fewer BCMs in the blood of CCL19-KO hosts: there were significantly fewer total BCMs (Fig. 5.3I) and a non-significant trend towards fewer IgD- BCMs (Fig. 5.3J).

Despite fewer GC B cells detected in the CCL19-deficient drLN the generation of BEMs was comparable between WT and CCL19-KO mice. This may be due to redundancy for CCR7 ligation offered by the presence of CCL21. However, in the CCL19-deficient spleen there were significantly fewer BCMs, this may indicate a potential role for CCL19 in the entry of BCMs to the spleen. This BCM entry to the spleen may be via the ACKR4-rich peri-marginal sinus of the spleen which has been reported as an entry site for circulating T cells to the spleen and support subsequent migration to the PALS (Werth et al., 2021). Reduced levels of BCMs in the blood may suggest fewer BEMs leaving the drLN to become BCMs. However, the trend of fewer BCMs in the CCL19-KO blood was similar to the trend in the CCL19-KO spleen, this suggests that the results in the spleen could instead reflect the effects of CCL19-deficiency on BCM levels in the blood.

CCR7 and ACKR4 are both receptors for CCL19 and CCL21. ACKR4 is expressed weakly by GC B cells and expression may still be retained in BEMs at the protein level even though expression has ceased at the RNA level. CCR7 is expressed by BEMs at the RNA level (Zhang et al., 2022). In the next section the role of ACKR4 and CCR7 on the generation of BEMs and the migration of BCMs to distant lymphoid tissues was explored. Further, the role of CCR7 in the CCL19-mediated entry of BCMs into the spleen was investigated.

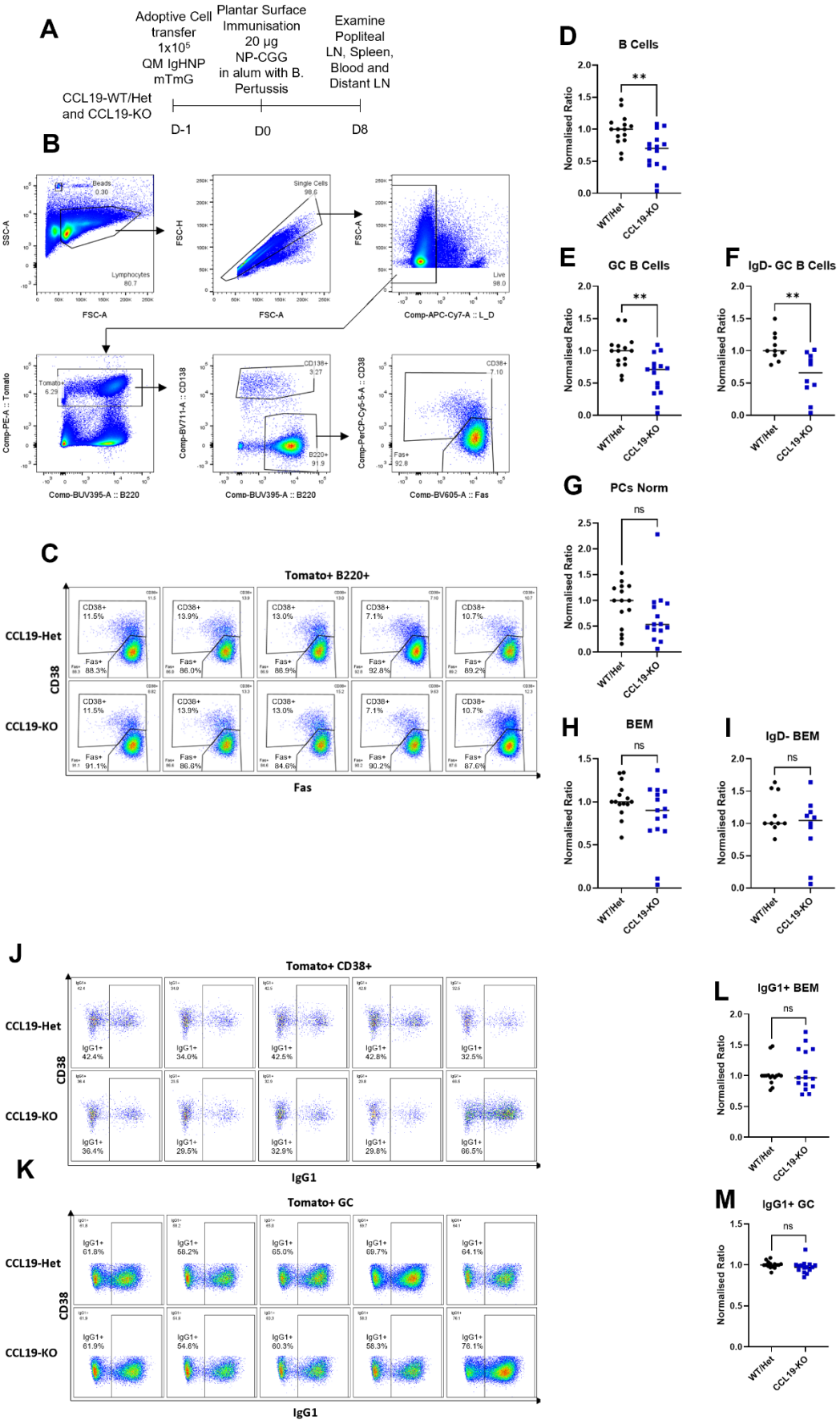

A
Adoptive Cell transfer 1x10^5 QM IgHNP mTmG
Plantar Surface Immunisation 20 µg NP-CGG in alum with B. Pertussis
Examine Popliteal LN, Spleen, Blood and Distant LN
CCL19-WT/Het and CCL19-KO
D-1
D0
D8
B
Beads
Lymphocytes
Single Cells
Live
Tomato+
CD138+
B220+
Fas+
C
Tomato+ B220+
CCL19-Het
CCL19-KO
CD38
Fas
D
B Cells
E
GC B Cells
F
IgD- GC B Cells
G
PCs Norm
H
BEM
I
IgD- BEM
J
Tomato+ CD38+
IgG1
K
Tomato+ GC
L
IgG1+ BEM
M
IgG1+ GC
Normalised Ratio
WT/Het
CCL19-KO
ns

Figure 5. 2. Fewer GC B cells in CCL19-KO drLN but levels of BEMs were unaffected

(A) Schematic of QM mTmG adoptive cell transfer and immunisation protocol into CCL19-KO and a control group of WT and CCL19-Heterozygous (WT/Het). Cell transfers were performed by the University of Birmingham Biomedical Services Unit. (B) Gating strategy to detect GC B cells and BEMs from among dTomato+ adoptively transferred cells. (C) Flow cytometry plots of BEMs (dTomato+B220+CD138-CD38+) and GC B cells (dTomato+B220+CD138-CD38-Fas+) in WT and CCL19-KO drLNs from GFP+ B cells from one representative experiment. Graphical summaries of (D) dTomato+ B cells (dTomato+B220+CD138-), (E) dTomato + plasma cells (dTomato+CD138+), (F) BEMs, (G) IgD- BEMs, (H) GC B cells and (I) IgD- GC B cells, data presented as normalised ratio from 3 separate experiments (WT n=15, CCL19-KO n=15). Flow cytometry plots of IgG1 expression in (J) BEMs and (K) CG B cells from one representative experiment. Graphical summaries of IgG1+ (L) BEMs and (M) GC B cells. Data presented are combined from 3 separate experiments (WT n=15, CCL19-KO n=15). Symbols represent individual mice; black circles represent the control group consisting of WT and CCL19-Heterozygous mice and blue squares represent CCL19-KO mice. Horizontal lines represent means. Mann-Whitney test, ** $p<0.01$.

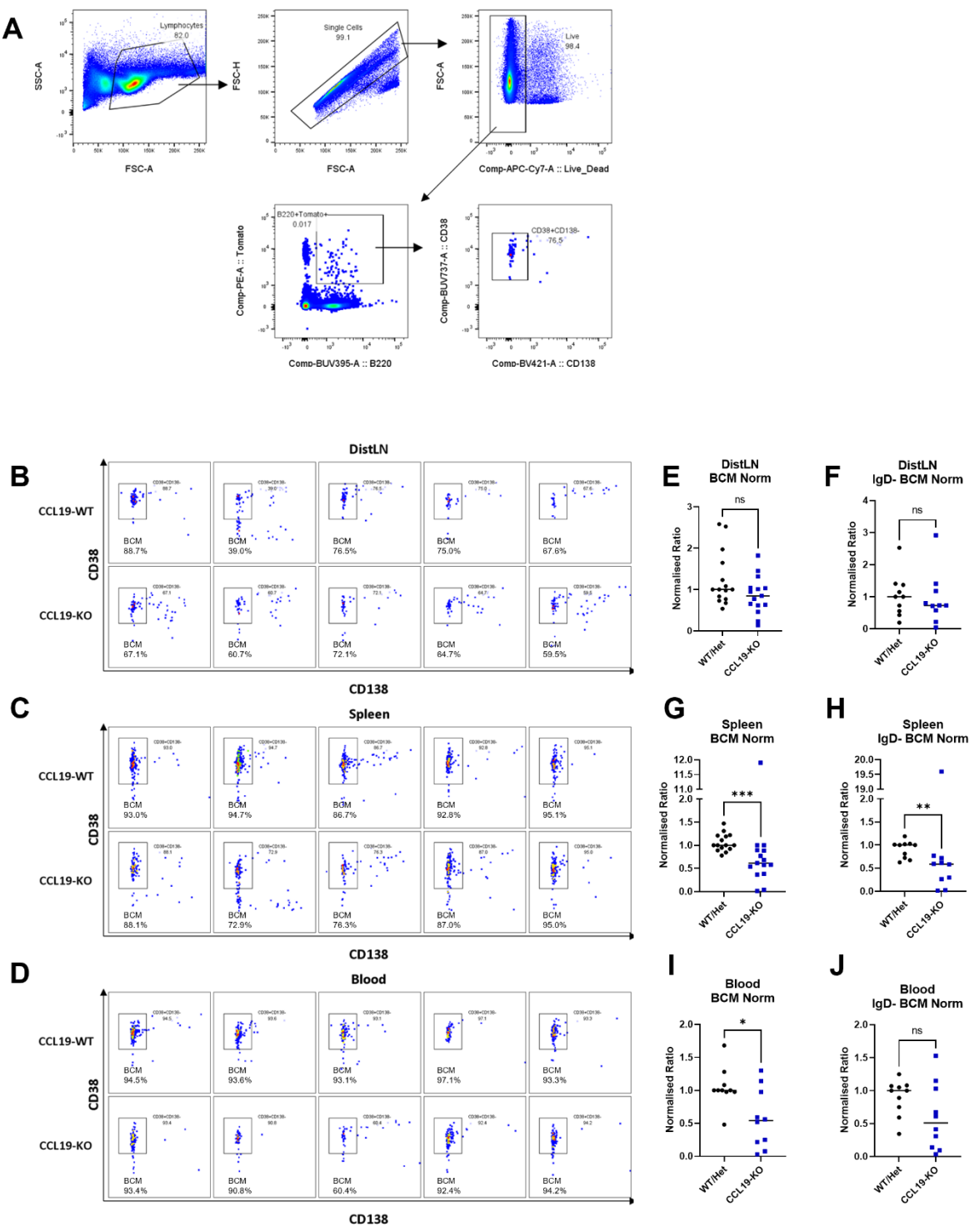


Figure 5. 3. Reduced levels of BCMs in distant lymphoid tissues of CCL19-deficient mice

(A) Gating strategy to detect BCMs in distant lymphoid tissues by flow cytometry. (B-D) Flow cytometry plots of BCMs (dTomato+B220+CD138-CD38+) in WT/Het and CCL19-KO distant LN, spleen and blood from one representative experiment. Graphical summaries of BCMs and IgD- BCMs presented as normalised ratios from % lymphocytes in distant LN (E-F),

spleen (G-H) and blood (I-J), data presented are combined from 3 separate experiments (WT n=15, CCL19-KO n=15). Symbols represent individual mice; black circles represent the control group consisting of WT and CCL19-Heterozygous mice and blue squares represent CCL19-KO mice. Horizontal lines represent means. Mann-Whitney test, * $p<0.05$, ** $p<0.01$, *** $p<0.001$.

5.2.3 Response and migration of ACKR4-KO and CCR7-KO B cells in CCL19-KO mice

5.2.3.1 In an adoptive cell co-transfer ACKR4-KO B cells outcompete CCR7-KO in drLN and in distant lymphoid tissues in both CCL19-WT and CCL19-KO mice

The roles of CCR7 and ACKR4 on BEMs and BCMs (which are receptors for CCL19 and CCL21) were investigated by examining the migration of these cells in the absence of ACKR4 and CCR7. ACKR4 is expressed weakly by GC B cells and may still be expressed on BEMs at the protein level if not the RNA level (Eckert et al., 2020)(Fig. 5.4A). Further, CCR7 is expressed by BEMs and BCMs at the RNA level (Zhang et al., 2022)(Fig. 4.2A). An adoptive cell co-transfer of fluorescently labelled WT, CCR7-deficient and ACKR4-deficient B cells was used to test the competition of these cells for survival in niches in the drLN. The capacity of adoptively transferred cells to compete in the GC reaction and become BEMs was examined. Furthermore, their subsequent entry into distant tissues as BCMs was followed.

The control group, consisting of WT and CCL19-heterozygous mice, and CCL19-KO mice received adoptive cell co-transfer with QM WT eYFP mTmG, QM ACKR4-KO eYFP and QM CCR7-KO mTmG splenocytes at a ratio of 1:1:1 of $1x10^5$ NP-specific B cells. One day later they received immunisations with 20 µg NP-CGG in alum precipitate with *Bordetella pertussis* on foot. Tissues were collected at 8 days post-immunisation (Fig. 5.4B). B cells, BEMs and GC B cells were quantified by flow cytometry (Fig. 5.4C-D).

Competition for B cell survival, which includes by antigen capture and presentation to T cells to receive positive selection signals, was assessed by comparing QM WT, QM ACKR4-KO and QM CCR7-KO B cells within each host. CCR7-KO cells generated fewer B cells, GC B cells and PCs in both WT and CCL19-KO hosts. Conversely, QM WT and QM ACKR4-KO cells competed comparably within both WT and CCL19-KO hosts (Fig. 5.5A-B, Fig. 5.5E-F). There were fewer QM CCR7-KO BEMs than QM WT and QM ACKR4-KO BEMs in both hosts (Fig. 5.5C-D). Additionally, in CCL19-KO hosts there were more QM ACKR4-KO BEMs and NP+ BEMs than their QM WT and CCR7-KO counterparts (Fig. 5.5C-D). This may indicate that ACKR4-deficient B cells had a greater capacity for activation and survival.

In distant lymphoid tissues QM WT, ACKR4-KO and CCR7-KO BCMs were detected by flow cytometry appearing 8 days after immunisation (Fig. 5.6A-B). ACKR4-KO BCMs were raised compared with WT BCMs in distLN among both WT and CCL19-KO hosts, this was statistically significant in WT hosts (Fig. 5.7A). In WT distLNs there was a non-significant trend towards a greater median of CCR7-KO BCMs than WT BCMs. This trend was lost in CCL19-KO distLNs (Fig. 5.7A). There were more ACKR4-KO NP+ BCMs, but fewer CCR7-KO NP+ BCMs, than WT NP+ BCMs in distLNs from both WT and CCL19-KO hosts but this was not statistically significant (Fig. 5.7B). In the spleen there were significantly more ACKR4-KO BCMs than WT BCMs in WT spleens, with a similar non-significant trend in CCL19-KO spleens. The median of WT BCMs was greater than the median of CCR7-KO BCMs in WT spleens but did not reach significance. This trend was not seen in CCL19-KO spleens (Fig. 5.7C). There were more ACKR4-KO NP+ BCMs than WT NP+ BCMs in WT and CCL19-KO spleens. There was a non-significant trend towards fewer CCR7-KO NP+ BCMs than WT NP+ BCMs in both WT and CCL19-KO spleens (Fig. 5.7D).

The data observed in distLN, and spleen were from 2 separate experiments. The trend of CCR7-KO B cells seen in distant lymphoid tissues was unclear. CCR7-KO B cells were expected to be more prominent in distLN, spleen and BM indicating enhanced egress from the drLN, however, depending on the experiment, the results differed somewhat. One experiment observed more CCR7-KO BCMs in distant lymphoid tissues, which was expected due to an inability of BEMs in the drLN SCS to return to the follicle following CCR7-ligands gradients of maintained by ACKR4, although CCR7-deficiency may also impair entry to distLN via HEVs. However, in a repeat experiment there were fewer CCR7-KO BCMs in distant lymphoid tissues. Unfortunately, the poor reproducibility of CCR7-KO BCMs was limiting factor to drawing reliable conclusions from these experiments. Using CCR7-floxed mice to induce CCR7-KO in GC B cells may help to elucidate the role of CCR7 in B cell egress from the drLN.

Adoptively transferred CCR7-KO B cells were outcompeted by WT and ACKR4-KO adoptively transferred B cells in the drLN. There were also fewer CCR7-KO BCMs entering distant lymphoid tissues. The mouse models used for these findings possessed NP-specific BCRs but did not have means for showing activation of B cells. Furthermore, there were no clear differences between WT and CCL19-KO mice with adoptive cell co-transfer. These experiments comparing WT and CCL19-KO mice were repeated using WT and CCR7-KO mice crossed with Cg1-Cre mTmG reporter mice to show activation of B cells as cell transfer donors.

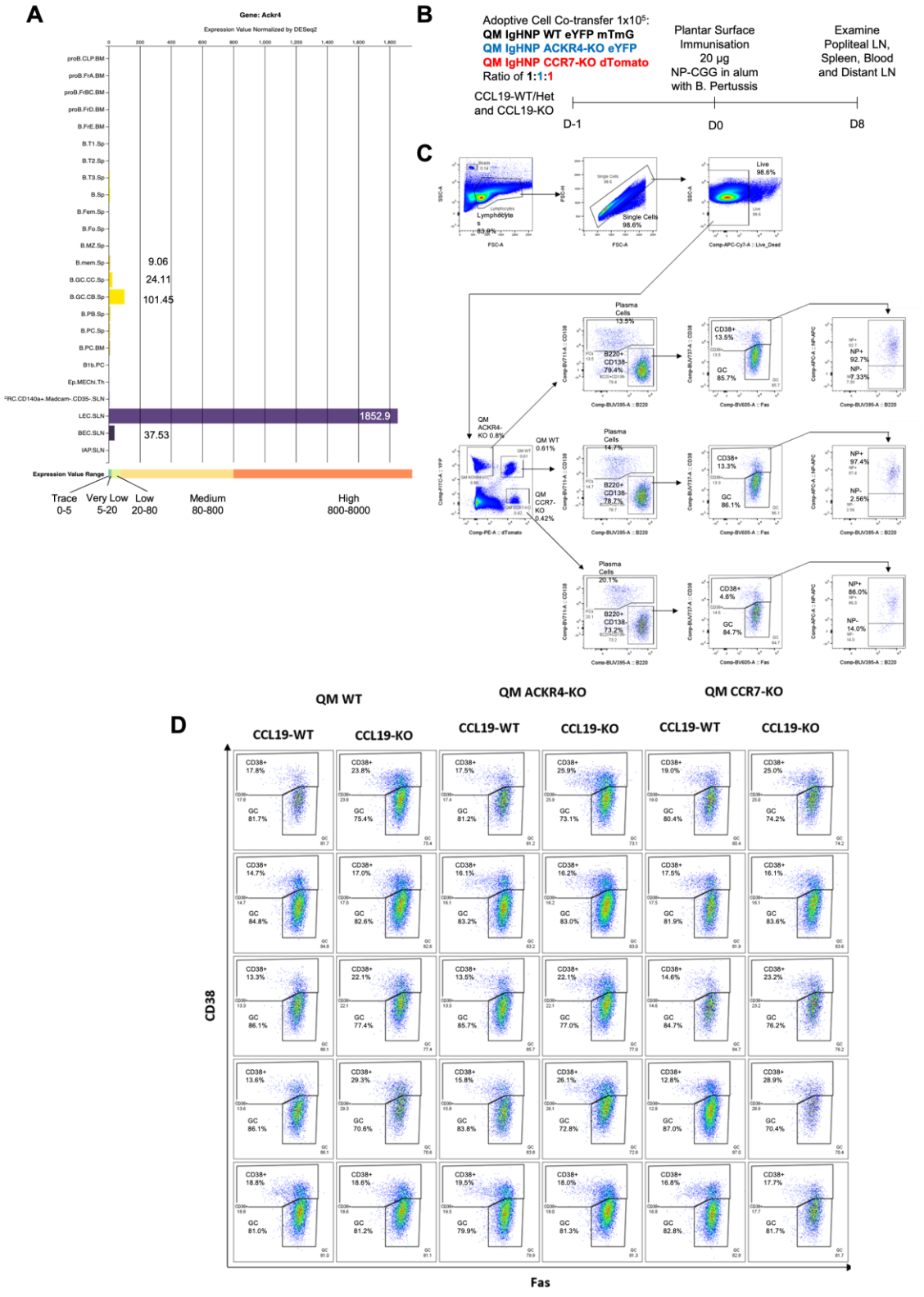

A
Gene: Ackr4
Expression Value Normalized by DESeq2
9.06
24.11
101.45
1852.9
37.53
Expression Value Range
Trace 0-5
Very Low 5-20
Low 20-80
Medium 80-800
High 800-8000
B
Adoptive Cell Co-transfer 1x10⁵:
QM IgHNP WT eYFP mTmG
QM IgHNP ACKR4-KO eYFP
QM IgHNP CCR7-KO dTomato
Ratio of 1:1:1
CCL19-WT/Het and CCL19-KO
Plantar Surface Immunisation 20 µg NP-CGG in alum with B. Pertussis
Examine Popliteal LN, Spleen, Blood and Distant LN
D-1
D0
D8
C
Lymphocyte 83.9%
Single Cells 98.6%
Live 98.6%
Plasma Cells 13.5%
B220+ CD138- 79.4%
CD38+ 13.5%
GC 85.7%
NP+ 92.7%
NP- 7.33%
QM ACKR4-KO 0.8%
QM WT 0.61%
QM CCR7-KO 0.42%
Plasma Cells 14.7%
B220+ CD138- 78.7%
CD38+ 13.3%
GC 86.1%
NP+ 97.4%
NP- 2.56%
Plasma Cells 20.1%
B220+ CD138- 73.2%
CD38+ 4.6%
GC 84.7%
NP+ 86.0%
NP- 14.0%
D
QM WT
QM ACKR4-KO
QM CCR7-KO
CCL19-WT
CCL19-KO
CD38
Fas

Figure 5. 4. CCR7-KO, ACKR4-KO and WT adoptive cell co-transfer and gating strategy

(A) Micro-array gene expression data of ACKR4 in human B cells and stromal cells obtained from the ImmGen consortium (Heng et al., 2008).

(B) Schematic of adoptive co-transfer of a total of 1x10^5 NP+B220+ from QM WT eYFP mTmG, QM ACKR4-KO eYFP and QM CCR7-KO mTmG splenocytes at a ratio of 1:1:1 into WT and CCL19-KO hosts and immunisation protocol. Cell transfers were performed by the University of Birmingham Biomedical Services Unit. (C) Flow cytometry gating strategy to detect B cells (B220+CD138-), PCs (CD138+), BEMs (B220+CD138-CD38+) and GC B cells B220+CD138-CD38-Fas+) among QM WT, QM ACKR4-KO and QM CCR7-KO cells within the host. (D) Flow cytometry plots to detect BEMs and GC B cells from QM WT, QM ACKR4-KO and QM CCR7-KO cells within each host from one representative experiment.

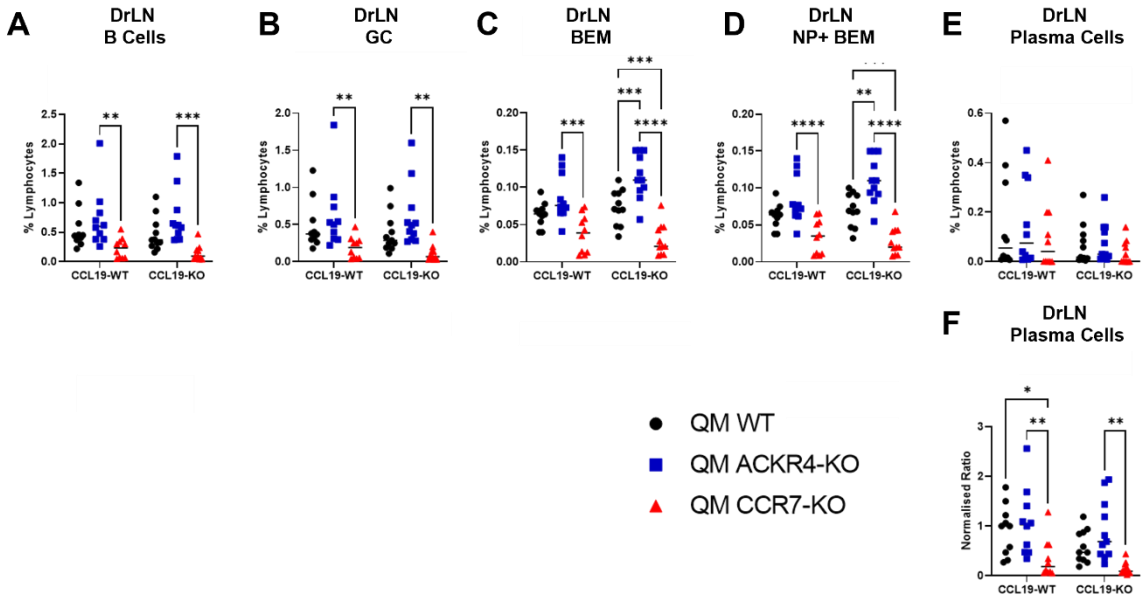
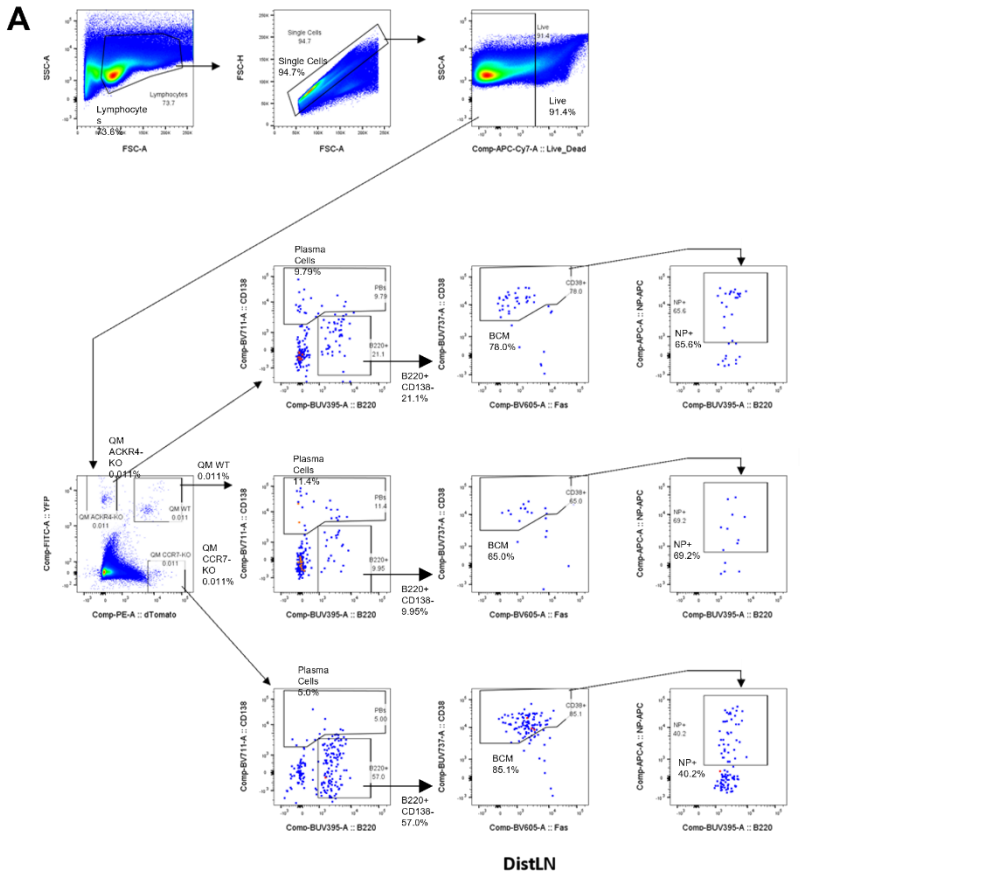


Figure 5. 5. CCR7-KO B cells were outcompeted by WT and ACKR4-KO B cells in WT and CCL19-KO drLN

Summaries of (A) B cells (B220+CD138-), (B) GC B cells B220+CD138-CD38-Fas+), (C) BEMs (B220+CD138-CD38+) and (D) NP+ BEMs in drLN presented as % lymphocytes. Summaries of plasma cells in drLN presented as (E) % lymphocytes and (F) a normalised ratio of % lymphocytes. Data presented are combined from 2 separate experiments (WT n=12, CCL19-KO n=12). Two-Way ANOVA within each host, * p<0.05, ** p<0.01, *** p<0.001, **** p<0.0001. Symbols represent individual mice. Black circles are QM WT cells, blue squares are QM ACKR4-KO cells and red triangles are QM CCR7-KO cells. Horizontal lines represent means.


A
Lymphocyte s
Single Cells 94.7%
Live 91.4%
Plasma Cells 9.79%
B220+ CD138- 21.1%
BCM 78.0%
NP+ 65.6%
QM ACKR4-KO 0.011%
QM WT 0.011%
QM CCR7-KO 0.011%
Plasma Cells 11.4%
B220+ CD138- 9.95%
BCM 85.0%
NP+ 69.2%
Plasma Cells 5.0%
B220+ CD138- 57.0%
BCM 85.1%
NP+ 40.2%
DistLN


B
QM WT
QM ACKR4-KO
QM CCR7-KO
CCL19-WT
CCL19-KO
CD38
Fas
BCM 67.7%
BCM 55.2%
BCM 100%
BCM 96.9%
BCM 85.0%
BCM 99.0%
BCM 88.9%
BCM 78.9%
BCM 100%
BCM 100%
BCM 98.6%
BCM 95.7%
BCM 65.0%
BCM 50.6%
BCM 78.0%
BCM 100%
BCM 85.1%
BCM 96.3%
BCM 76.2%
BCM 52.4%
BCM 98.2%
BCM 100%
BCM 98.8%
BCM 95.5%
BCM 50.0%
BCM 100%
BCM 97.9%

Figure 5. 6. Gating strategy to detect adoptive cell co-transfer BCM in distant lymphoid tissues

(A) Flow cytometry gating strategy to detect QM WT, QM ACKR4-KO and QM CCR7-KO BCMs in distant lymphoid tissues. (B) Flow cytometry plots to detect QM WT, QM ACKR4-KO and QM CCR7-KO BCMs in distant LN from one representative experiment.

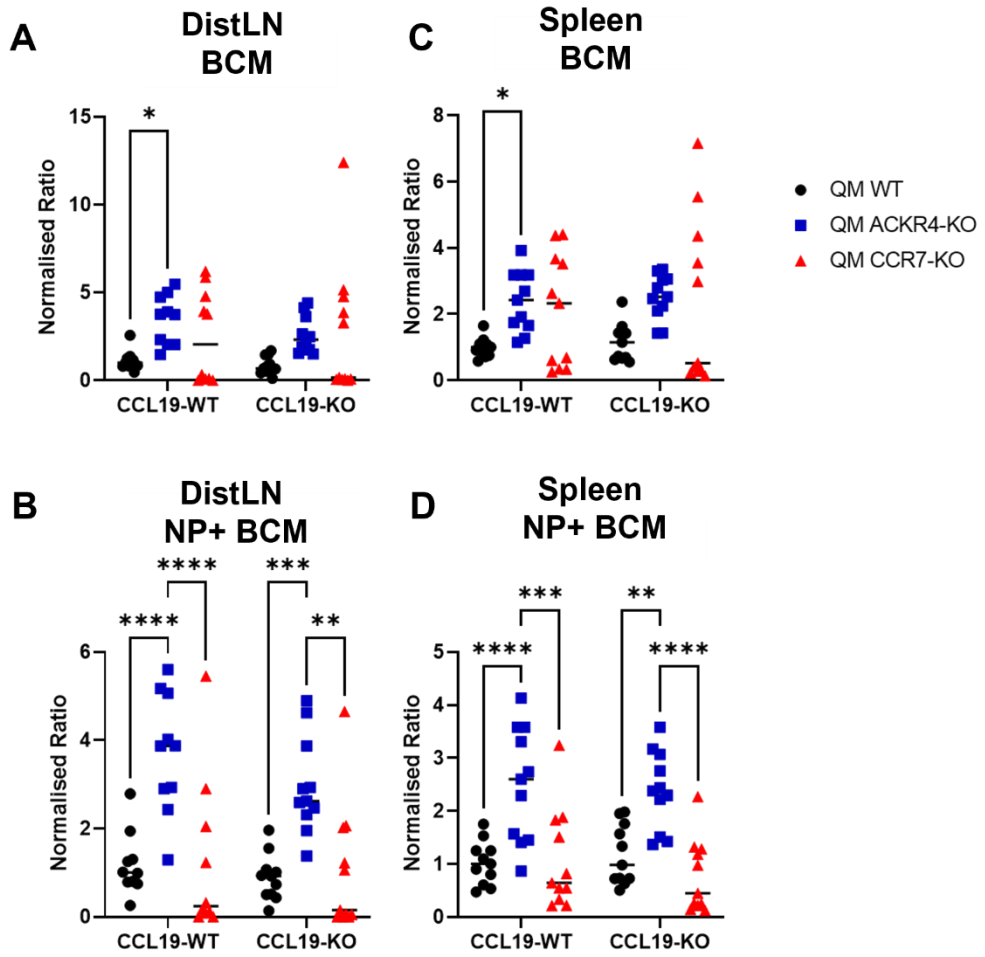


Figure 5. 7. More ACKR4-deficient BCMs detected in distant lymphoid tissues than WT and CCR7-KO BCMs

Graphical summaries of BCMs (B220+CD138-CD38+) and NP-specific BCMs in distLN (A-B) and spleen (C-D) presented as normalised ratios from % lymphocytes. Data presented are combined from 2 separate experiments (distLN WT n=11, CCL19-KO n=12; spleen). Two-Way ANOVA within each host, * p<0.05, ** p<0.01, *** p<0.001, **** p<0.0001. Symbols represent individual mice. Black circles are QM WT cells, blue squares are QM ACKR4-KO cells and red triangles are QM CCR7-KO cells. Horizontal lines represent means.

5.2.3.2 CCR7-deficient B cells were decreased in distant lymph node and fewer circulating CCR7-deficient memory B cells were detected in CCL19-KO spleen

As shown above CCR7-KO B cells were less able to compete with WT and ACKR4-KO B cells for survival niches in the drLN and were less able to enter distant lymphoid tissues in both WT and CCL19-KO hosts. We evaluated whether QM CCR7-deficient B cells also had impaired GC responses and entry into distant lymphoid tissues in WT and CCL19-KO hosts when not competing with QM WT and QM ACKR4-KO B cells. To examine this, splenocytes where adoptive cell transferred that contained a Cre in the IgG1 constant region crossed with mTmG mice, making these reporters for B cell activation as they switched from expression of membrane-bound dTomato to GFP (Casola et al., 2006, Muzumdar et al., 2007). We expected there to be fewer activated B cells among CCR7-KO populations in drLNs and in CCL19-KO drLNs as CCR7 is required for migration of B cells to the T-B border to receive T cell help. Furthermore, as CCR7 is required for lymphocyte entry to distLN via HEVs (Okada et al., 2002) and in entry to spleen via per-marginal sinus (Werth et al., 2021) following CCL19/21 gradients we expected there to be fewer CCR7-KO BCMs in these distant lymphoid tissues. Raised levels of CCR7-deficient activated B cells in drLN and CCR7-deficient BCMs in distant lymphoid tissues would disprove this.

CCL19-KO and CCL19-Het mice received adoptive cell transfers of either $1x10^5$ QM Cg1cre mTmG CCR7-WT or CCR7-KO splenocytes. One day later they were immunised with NP-CGG in alum with *B. pertussis* into the plantar surface, and tissues were examined at 8 days post-immunisation (Fig. 5.8A). B cells, GC B cells and BEMs were quantified in draining lymph nodes by flow cytometry (Fig. 5.8B-C).

There was no clear difference in activated GFP+ B cell numbers regardless of donor CCR7 genotype or host CCL19-expression in drLN (Fig. 5.9A). There was no significant difference in GC B cells from CCR7-WT and CCR7-KO donors in WT and CCL19-KO drLNs (Fig. 5.9B). As a proportion of GC B cells there were somewhat fewer IgG1+ GC B cells in QM CCR7-WT cells in CCL19-KO hosts (p=0.0552) (Fig. 5.9C). Surprisingly, there was a greater proportion of IgG1-expressing GC B cells in CCR7-KO cells in CCL19-KO hosts (Fig. 5.9C). This shows that although fewer GC B cells were detected in CCL19-KO hosts a greater proportion CCR7-KO had undergone class-switching. GC B cells typically downregulate cell surface expression of BCRs compared with follicular B cells (Stewart et al., 2018), in the GC LZ B cells had elevated cell surface BCR expression than DZ B cells (Stewart et al., 2018). Elevated surface BCR expression in CCR7-KO GC B cells may indicate that there were more LZ GC B cells in CCR7-KO mice in CCL19-deficient hosts. CCR7-KO GC B cells may be mainly LZ B cells and may be less able to become DZ B cells, perhaps due to a lack of help from Tfh cells. There may be fewer Tfh cells in CCL19-KO mice as CCR7 ligands are required for entry to the LN via HEVs (Okada et al., 2002). This could be verified by quantifying Tfh cells and examining the LZ/DZ ratios in these mice, but this was not done in this present experiment. Additionally, another group observed increased levels of serum IgG1 from activated B cells in CCR7-KO mice suggesting dysregulated class-switching (Förster et al., 1999), this may be reflected in our CCR7-deficient GC B cells. There was no significant difference in BEMs between either group or host (Fig. 5.9D). A greater proportion of CCR7-KO BEMs expressed IgG1 than WT BEMs in both WT and CCL19-KO drLNs (Fig. 5.9E). This may also reflect the altered class-switching in CCR7-KO mice described by Förster et al. (1999).

There were no significant differences in QM CCR7-WT and CCR7-KO IgM+ GC B cells in CCL19-KO hosts compared with CCL19-WT hosts (Fig. 5.10A). There was no significant difference in NP-binding of these GC B cells as a proportion of GC B cells regardless of donor and host (Fig. 5.10B). IgM expressing BEMs and NP-binding BEMs were comparable regardless of donor and host (Fig. 5.10C-D). IgM expression and NP-binding was unaffected by B cell intrinsic CCR7-deficiency and host CCL19-deficiency in GC B cells and BEMs.

BCMs were quantified in distLN and spleen by flow cytometry (Fig. 5.11A), GFP+ BCMs (Fig. 5.11B) and adoptively transferred GFP+ and/or Tomato+ BCMs (Fig. 5.11C) were examined to evaluate the role of CCR7 and CCL19 in the entry of BCMs to these tissues. In the distLN there was a trend towards increased QM CCR7-WT GFP+ BCMs than QM CCR7-KO GFP+ BCMs in CCL19-WT hosts, further, there were significantly more QM CCR7-WT GFP+ BCMs than QM CCR7-KO GFP+ BCMs in CCL19-KO hosts (Fig. 5.11D). This showed that CCR7 was required for entry to the distLN, and that CCL19-deficiency did not impede this, implying that CCL21 may be more important. There were no significant differences of GFP+ BCMs in spleen comparing QM CCR7-WT and QM CCR7-KO GFP+ BCMs in WT and CCL19-KO hosts (Fig. 5.11E).

GFP+ BCMs did not quite reflect the BCMs examined in CCL19-KO hosts in section 5.2.2; these did not have a fluorescent protein reporter for activation. To more accurately reflect this, BCMs from all adoptively transferred cells were examined by creating a gate to detect both GFP+ and Tomato+ B cells (GFP+/Tomato+) (Fig. 5.11A). In the distLN there were no significant differences but there was a trend towards fewer CCR7-KO GFP+/Tomato+ BCMs compared with CCR7 WT BCMs in WT and CCL19-KO hosts (Fig. 5.11F). In the spleen there

was a trend towards fewer GFP+/Tomato+ BCMs in CCL19-KO hosts among both QM CCR7-WT and QM CCR7-KO BCMs (Fig. 5.11G). A trend for reduced BCMs in CCL19-KO hosts was not among GFP+ BCMs, which represent adoptively transferred B cells that were activated, leading to expression of Cre at the Cg1 locus (Fig. 5.11D-E). However, BCMs in CCL19-KO hosts measured as a fraction of all adoptively transferred cells were reduced in the spleen. This indicated that CCR7-expression of BCMs may be required for entry into the spleen and distLN.

In summary, B cell intrinsic CCR7-deficiency or CCL19-deficiency in hosts did not significantly affect levels of GC B cells or the generation of BEMs. Although, CCL19-deficiency caused no significant difference within the groups of CCR7-WT and CCR7-KO BCMs in distLN, there were fewer CCR7-deficient BCMs in the distLN. This shows that CCR7 is required for the entry of BCMs into distLNs. This concurs with the findings that CCR7 is required for entry of lymphocytes into LNs via HEVs (Okada et al., 2002). Furthermore, there were fewer transferred (GFP+ and/or Tomato+) BCMs in CCL19-KO spleens, particularly among CCR7-KO BCMs. Therefore, while CCL19 may be dispensable for entry to distLN, this section and section 5.2.2 indicate that CCL19 might be involved in BCM entry to the spleen. This is supported by previous work showing that CCL19 was involved in lymphocyte entry to the spleen through the peri-marginal sinus (Werth et al., 2021). We next investigated whether there was also a role for the other CCR7-ligand, CCL21, in the generation of BEMs and migration of BCMs to distLN and spleen.

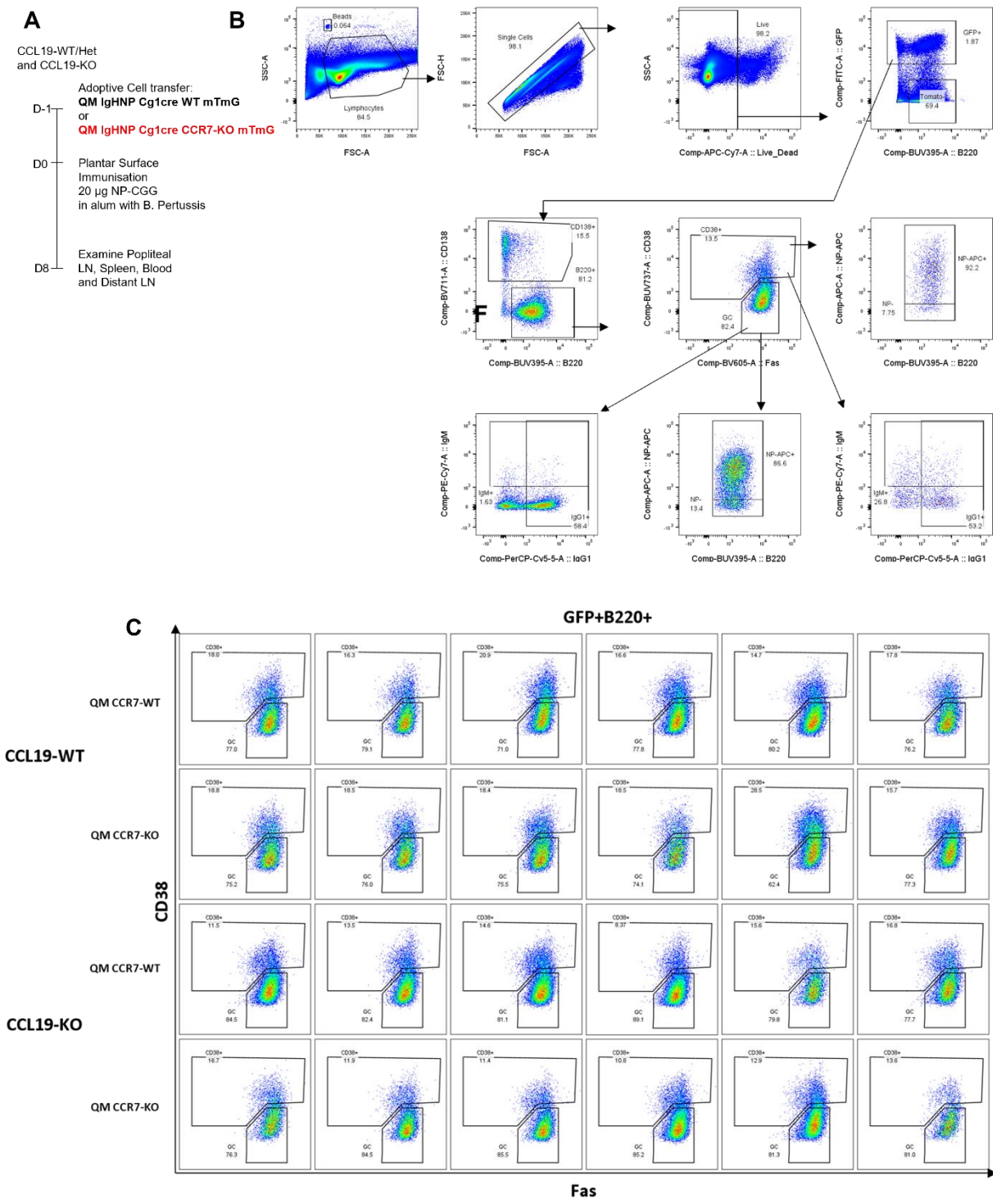


Figure 5. 8. WT and CCR7-KO B cells were detected in WT and CCL19-KO drLN by flow cytometry

(A) Schematic of WT or CCR7-KO QM Cg1Cre mTmG adoptive cell transfer and immunisation protocol into CCL19-KO and WT/CCL19-Het mice. Cell transfers were performed by the University of Birmingham Biomedical Services Unit. (B) Gating strategy to quantify GC B cells

and BEMs from GFP+ adoptively transferred cells. (C) Flow cytometry plots of BEMs and GC B cells in WT and CCL19-KO drLNs from GFP+ B cells from one representative experiment.

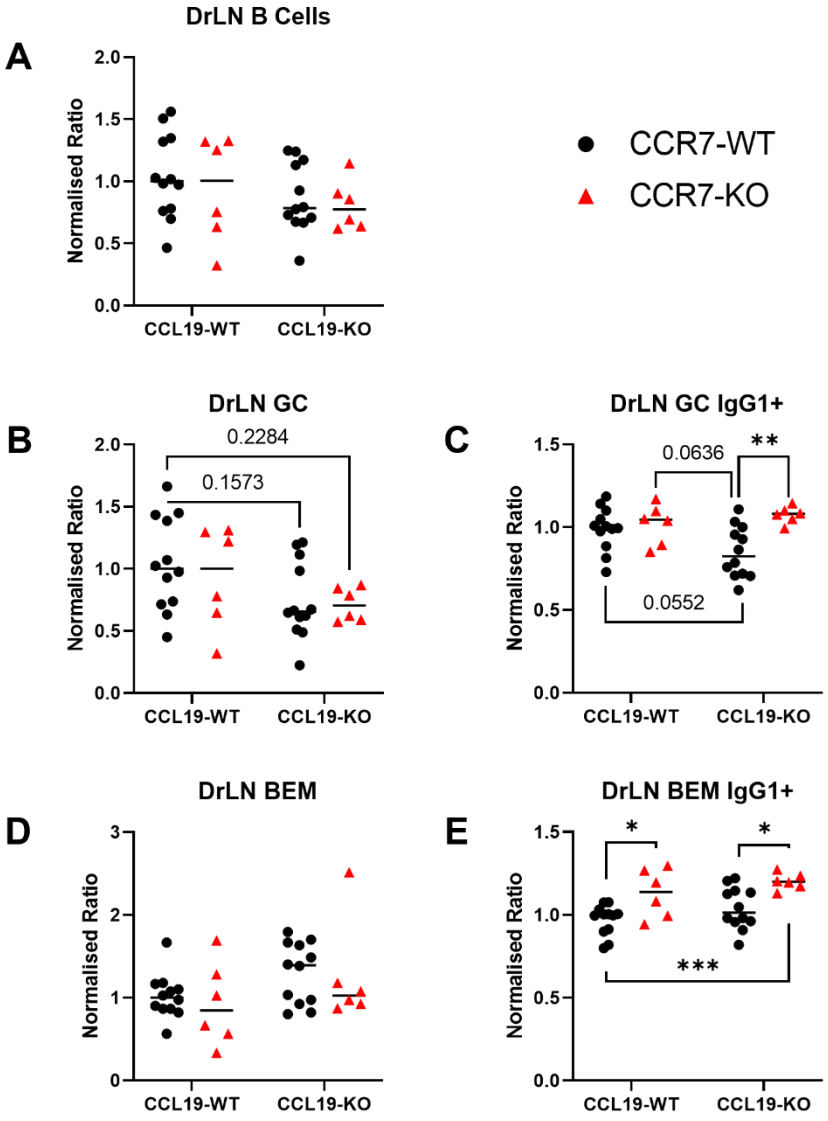


Figure 5. 9. GC response and BEM production in drLN was minimally affected by CCL19-deficiency

Graphical summaries of (A) GFP+ B cells (GFP+B220+CD138-), GFP+ donor (B) GC B cells (GFP+B220+CD138-CD38-Fas+), (C) IgG1+ GC B cells, (D) BEMs (GFP+B220+CD138-CD38+) and (E) IgG1+ BEMs. Data presented are combined from 2 separate experiments (WT n=12, CCL19-KO n=12). Normalised ratios for B cells, GC B cells and BEMs were calculated from % lymphocytes, and normalised ratios for IgG1+ GC B cells and IgG1+ BEMs were calculated from % parent population (GC B cells or BEMs). Two-Way ANOVA, * $p<0.05$, ** $p<0.01$, *** $p<0.001$. Symbols represent individual mice. Black circles are QM Cg1-Cre mTmG CCR7-WT and red triangles are QM Cg1-Cre mTmG CCR7-KO. Horizontal lines represent means.

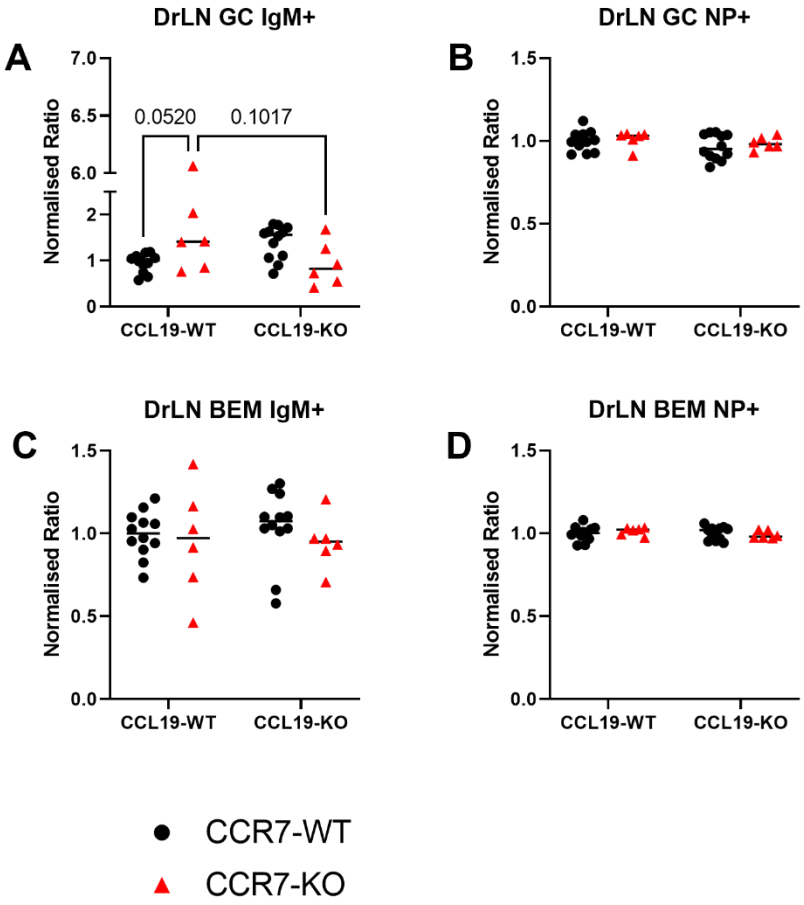


Figure 5. 10. No differences in IgM and NP expression in WT and CCR7-KO GC B cells and BEMs of WT and CCL19-KO drLNs

Graphical summaries of (A) IgM+ GC B cells (GFP+B220+CD138-CD38-Fas+), (B) NP-specific GC B cells, (C) IgM+ BEMs (GFP+B220+CD138-CD38+) and (D) NP-specific BEMs. Data presented are combined from 2 separate experiments (CCR7-WT n=12, QM CCR7-KO n=6). Normalised ratios were calculated from % parent population (GC, BEMs or PCs). Two-Way ANOVA, * $p<0.05$, ** $p<0.01$. Symbols represent individual mice. Black circles are QM Cg1-Cre mTmG CCR7-WT and red triangles are QM Cg1-Cre mTmG CCR7-KO. Horizontal lines represent means.

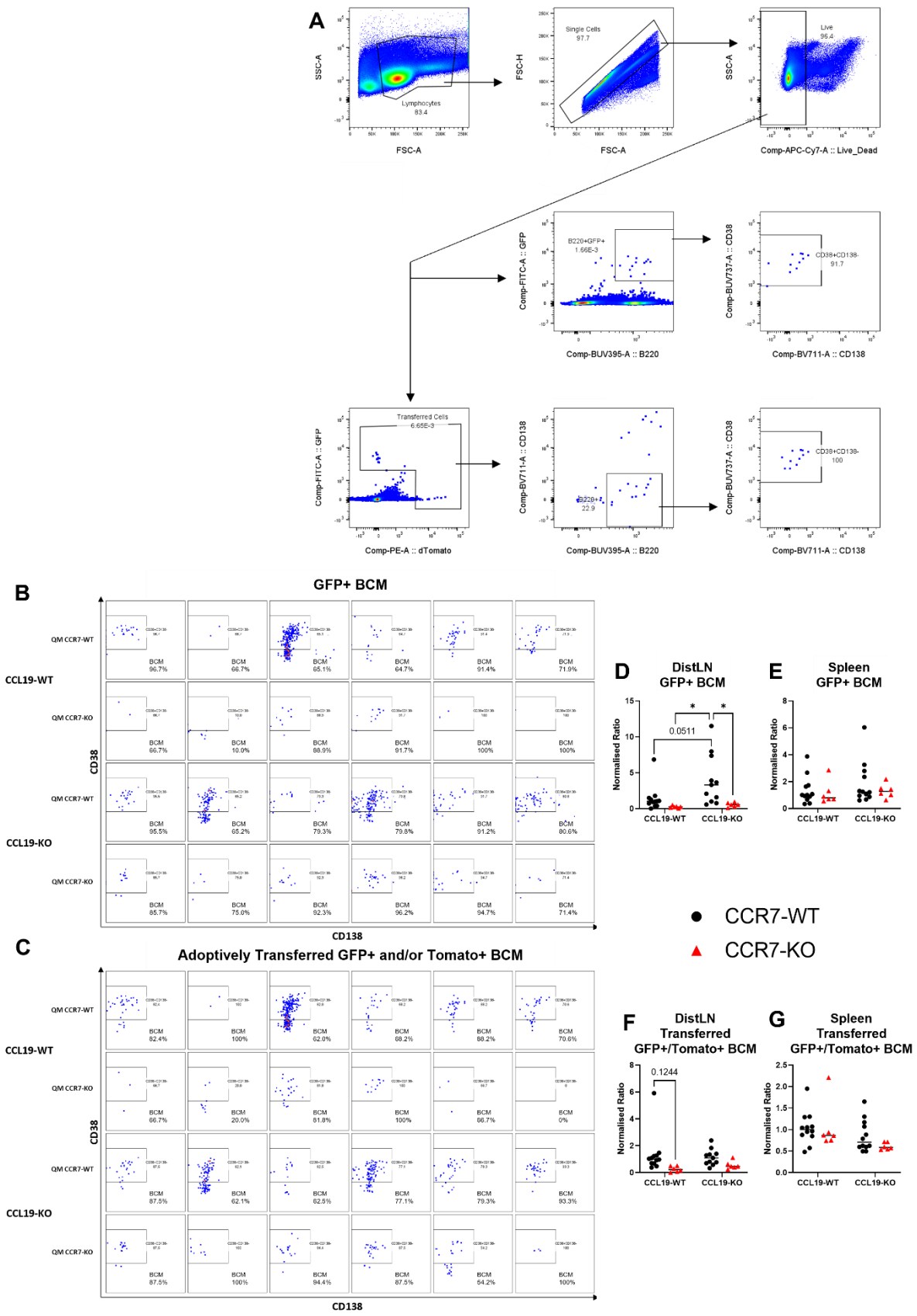

A
SSC-A
FSC-A
Lymphocytes
83.4
FSC-H
FSC-A
Single Cells
97.7
SSC-A
Comp-APC-Cy7-A :: Live_Dead
Live
96.4
Comp-FITC-A :: GFP
Comp-BUV395-A :: B220
B220+GFP+
1.66E-3
Comp-BUV737-A :: CD38
Comp-BV711-A :: CD138
CD38+CD138-
91.7
Comp-FITC-A :: GFP
Comp-PE-A :: dTomato
Transferred Cells
6.65E-3
Comp-BV711-A :: CD138
Comp-BUV395-A :: B220
B220+
22.9
Comp-BUV737-A :: CD38
Comp-BV711-A :: CD138
CD38+CD138-
100
B
GFP+ BCM
CCL19-WT
CCL19-KO
QM CCR7-WT
QM CCR7-KO
CD38
CD138
C
Adoptively Transferred GFP+ and/or Tomato+ BCM
D
DistLN
GFP+ BCM
Normalised Ratio
0.0511
CCL19-WT
CCL19-KO
E
Spleen
GFP+ BCM
CCR7-WT
CCR7-KO
F
DistLN
Transferred
GFP+/Tomato+ BCM
0.1244
G
Spleen
Transferred
GFP+/Tomato+ BCM

Figure 5. 11. A trend was detected towards fewer adoptively transferred BCM in the CCL19-KO spleen and fewer CCR7-KO BCM in the distLN

(A) FACS gating strategy to detect GFP+ BCMs (GFP+B220+CD138-CD38+) and GFP+dTomato+ BCMs (GFP+ and/or dTomato+ B220+CD138-CD38+) in distant lymphoid tissues. FACS plots to detect (B) GFP+ BCMs and (C) GFP+dTomato+ BCMs in distant lymphoid tissues from one representative experiment. Graphical summaries of GFP+ BCMs from distLN (D) and spleen (E) and GFP+dTomato+ BCMs from distLN (F) and spleen (G). Data presented are combined from 2 separate experiments (CCR7-WT n=12, QM CCR7-KO n=6). Normalised ratios were calculated from % lymphocytes. Two-Way ANOVA, * $p<0.05$, ** $p<0.01$. Symbols represent individual mice. Black circles are QM Cg1-Cre mTmG CCR7-WT and red triangles are QM Cg1-Cre mTmG CCR7-KO. Horizontal lines represent means.

5.2.4 Increased BEM generation in drLN and fewer BCM detected in distant lymphoid tissues of CCL21-deficient mice

In the previous section the effect of B cell intrinsic CCR7-deficiency and CCL19-deficiency was investigated revealing that although there was some limited effect on BCM entry to distant tissues there may be some redundancy provided by CCL21. This section examined if CCL21 was required for the generation of BEMs and the entry of BCMs into distant lymphoid tissues. CCL21-RFP mice were used to examine the generation of BEMs and migration of BCMs under conditions of CCL21 deficiency. Homozygous CCL21-RFP mice which lacked expression of CCL21a and expressed RFP instead were used to model CCL21 deficiency (Kozai et al., 2017). The expected result was smaller GCs, reduced BEM generation and fewer BCMs entering distLN and spleen in CCL21-deficient mice. Due to the RFP background of these mice, they received adoptive cell transfers of Cg1-Cre mTmG mice. This allowed distinguishing activated adoptively transferred cells as GFP+. CCL21-KO RFP mice received adoptive cell transfers of $1x10^5$ NP+B220+ QM IgHNP Cg1cre mTmG splenocytes, the following day they were immunised with 20 µg NP-CGG in alum precipitate with *Bordetella pertussis* on foot. Tissues were examined at 8 days post-immunisation (Fig. 5.12A). DrLN was

examined by flow cytometry to quantify GC B cells (GFP+B220+CD138-CD38-Fas+) and BEMs (GFP+B220+CD138-CD38+) (Fig. 5.12B-C).

There was no significant difference in total lymphocytes in CCL21-KO drLN compared with the control group consisting of WT and CCL21-Heterozygous mice (WT/CCL21-Het) (Fig. 5.13A). GFP- cells were examined which constituted a combination of endogenous cells and adoptively transferred cells which did not express Cre, this provided an estimation of B cell entry to the drLN. There was a 25% reduction in GFP- B cell numbers (GFP-B220+CD138-) in CCL21-KO drLNs (Fig. 5.13B), but there was no significant difference between the GFP- host GC B cells in WT/CCL21-Het and CCL21-KO drLNs (Fig. 5.13C). Reduced GFP- B cells in CCL21-KO drLNs indicated that CCL21 was important for their entry to drLN, although CCL21-deficiency did not appear to majorly affect their ability to become GC B cells.

We expected that in CCL21-KO drLNs there would be fewer activated B cells, due to reduced levels of helper T cells to provide co-stimulatory signals during B cell activation because CCL21 is involved in entry of T cells to the LN via HEVs (Förster et al., 1999). Unexpectedly, there were more GFP+ B cells (GFP+B220+CD138-) in CCL21-KO drLNs as a proportion of live lymphocytes (Fig. 5.14A). Conversely, as a proportion of GFP+ transferred cells there were fewer GFP+ B cells in CCL21-KO mice (Fig. 5.14B). There were more PCs (GFP+CD138+) in CCL21-KO drLNs as a proportion of lymphocytes (Fig. 5.14C). There were also more PCs as a proportion GFP+ transferred cells in CCL21-KO drLNs (Fig. 5.14D). Furthermore, detection of fewer B cells as a proportion of GFP+ cells (Fig. 5.14B) showed that a smaller fraction of transferred GFP+ cells were B220+CD138- B cells than were CD138+ PCs in CCL21-deficient recipients. It may be useful to explore whether these PCs were from EF response, but this

was not examined in this present study. There were more GC B cells in CCL21-KO drLNs as a proportion of lymphocytes (Fig. 5.14E) but no difference as a proportion of GFP+ transferred cells (Fig. 5.14F). There were more BEMs in CCL21-KO BEMs as a proportion of lymphocytes (Fig. 5.14G) and no significant difference as a proportion of GFP+ transferred cells (Fig. 5.14H). There were more IgG1+ BEMs in CCL21-KO drLNs as a proportion of BEMs (Fig. 5.14I), showing that along with increased BEMs more of these were class-switched in CCL21-KO drLNs. Raised GFP+ B cells, GC B cells and BEMs as a proportion of lymphocytes in CCL21-KO drLNs was unexpected. CCL21a-deficiency prevents the egress of T cells from the thymus, this can reduce the pool of regulatory T cells (James et al., 2021, Cowan et al., 2016). The raised levels of activated B cells in CCL21-deficiency may be due to inappropriate T cell help as a consequence of a lack of T cell regulation.

The findings in section 5.2.3 suggested that CCR7 may be required for entry of BCMs to the distLN, we tested the hypothesis that there was a role for the CCR7 ligand, CCL21, in the entry of BCMs to distant lymphoid tissues. DistLN, spleen, blood and bone marrow of CCL21-Het and CCL21-KO adoptive cell transfer recipients were examined at 8 days post-immunisation. Adoptively transferred B cells (GFP+B220+) and BCMs (GFP+B220+CD38+CD138-) were quantified by flow cytometry (Fig. 5.15A-C). There was no difference in total adoptively transferred B cells in distLN, blood and bone marrow but there was a trend towards fewer B cells in CCL21-KO spleens (Fig. 5.16A). There were fewer BCMs in distLNs and spleens of CCL21-KO mice, and a trend towards fewer BCMs in CCL21-KO blood as a proportion of lymphocytes (Fig. 5.16B). Despite more BEMs in the CCL21-KO drLN, BCMs were less able to enter distLN and spleen in CCL21-deficiency. This raised the possibility that there was a role for CCL21 in the entry of BCMs into distLN and spleen. Entry

of BCMs to the distLN would be through HEVs (Okada et al., 2002) and entry to the spleen may be through peri-marginal sinus (Werth et al., 2021).

As shown above the role of chemokines in the generation of BEMs in drLN and migration of BCMs to distant lymphoid tissues was investigated in the primary response to antigen. CCR7 and its ligands were required for the entry of BCMs to distLNs and spleen. In the next section the role of mBCs in secondary responses to antigen was investigated for mBCs in drLN or mBCs that had migrated to distLN.

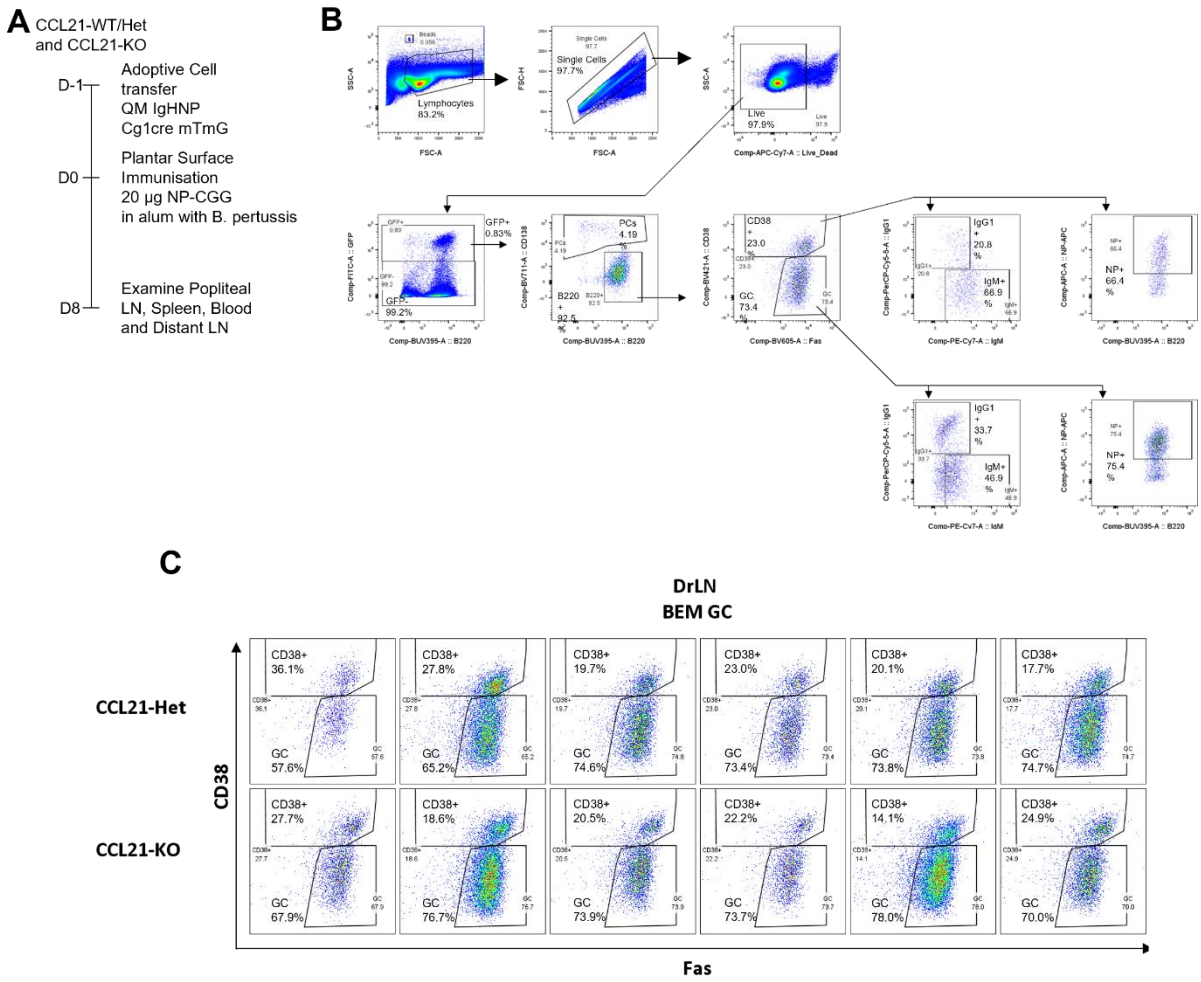


Figure 5. 12. B cell responses were measured in WT and CCL21-KO drLNs by flow cytometry

(A) Schematic of QM IgHNP Cg1cre mTmG adoptive cell transfer and immunisation protocol into CCL21-KO and a control group of WT and CCL21-Heterozygous (WT/Het). Cell transfers were performed by the University of Birmingham Biomedical Services Unit. (B) Gating strategy to detect GC B cells and BEMs among GFP+ adoptively transferred cells. (C) Flow cytometry plots from one representative experiment of BEMs and GC B cells in WT/Het and CCL21-KO drLNs from GFP+ B cells.

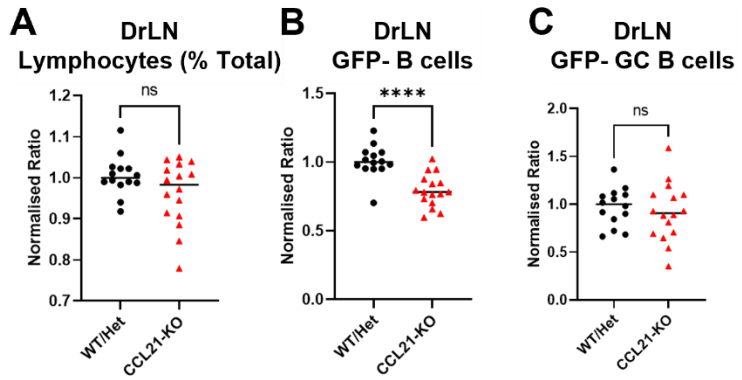


Figure 5. 13. Fewer GFP- B cells present in CCL21-KO drLN compared with WT drLN

(A) Live lymphocytes in a control group of WT and CCL21-Heterozygous (WT/Het) and CCL21-KO drLNs presented as a normalised ratio calculated from % total cells. Summaries of (B) GFP- B cells (GFP-B220+CD138-) and (C) GFP- GC B cells (GFP-B220+CD138-CD38-Fas+) presented as a normalised ratio calculated from % lymphocytes. Data presented are combined from 3 separate experiments (WT/Het n=14, CCL19-KO n=16). Unless otherwise specified normalised ratios were calculated from % lymphocytes. Unpaired t-test, * $p<0.05$, **** $p<0.0001$. Symbols represent individual mice. Black circles are from WT and CCL21-heterozygous mice and red triangles are from CCL21-KO mice. Horizontal bars show means.

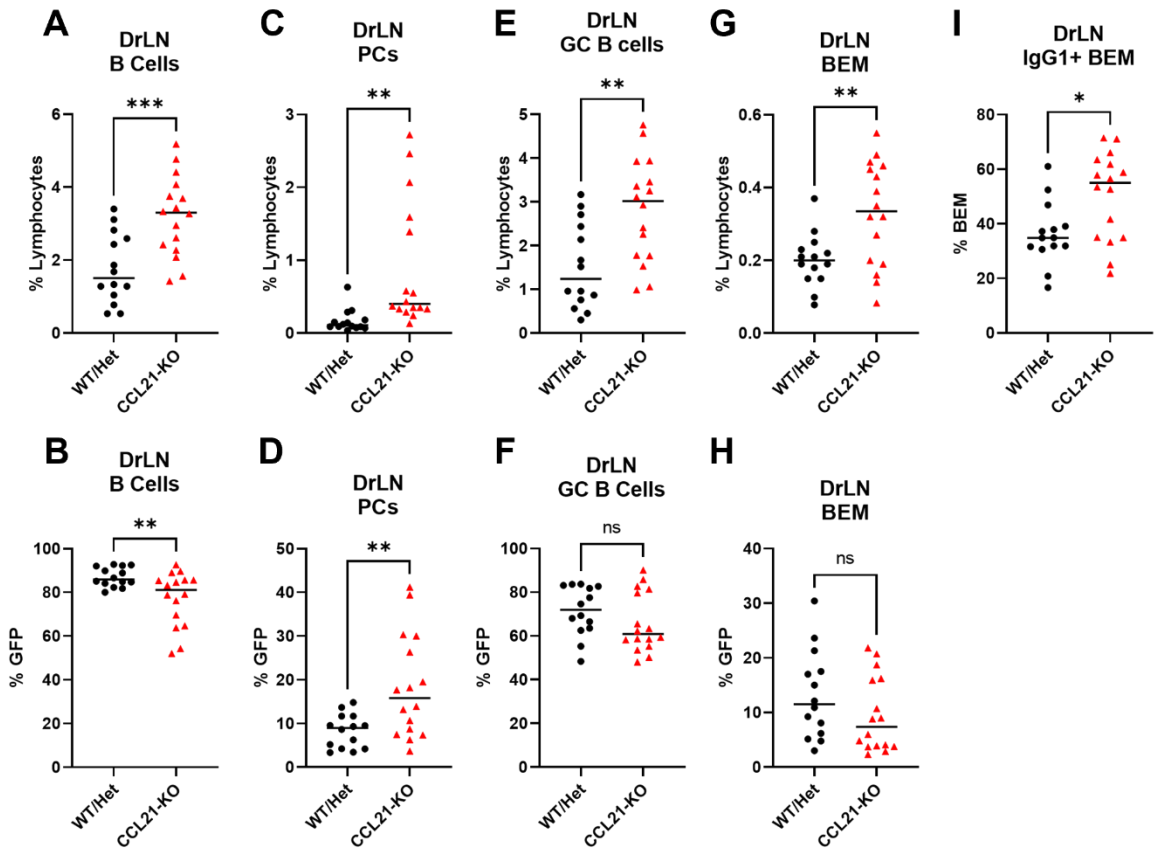


Figure 5. 14. Increased frequency of GFP+ B cells, PCs, GC B cells and BEMs in CCL21-KO mice

Graphical summaries of GFP+ B cells (GFP+B220+CD138-)in drLN as a proportion of (A) lymphocytes and (B) GFP+ transferred cells. Plasma cells (GFP+CD138+) in drLN as a proportion of (C) lymphocytes and (D) GFP+ transferred cells. GC B cells (GFP+B220+CD138-CD38-Fas+) in drLN as a proportion of (E) lymphocytes and (F) GFP+ transferred cells. BEMs (GFP+ B220+CD138-CD38+) in drLN as a proportion of (G) lymphocytes and (H) GFP+ transferred cells. (I) IgG1+ BEMs in drLN as a proportion of BEMs. Data presented as a normalised ratio calculated from % lymphocytes and are combined from 3 separate experiments (WT/Het n=14, CCL19-KO n=16). Unpaired t-test, * $p<0.05$, ** $p<0.01$, *** $p<0.001$, **** $p<0.0001$. Symbols represent individual mice. Black circles are from WT and CCL21-heterozygous mice and red triangles are from CCL21-KO mice. Horizontal bars show means.

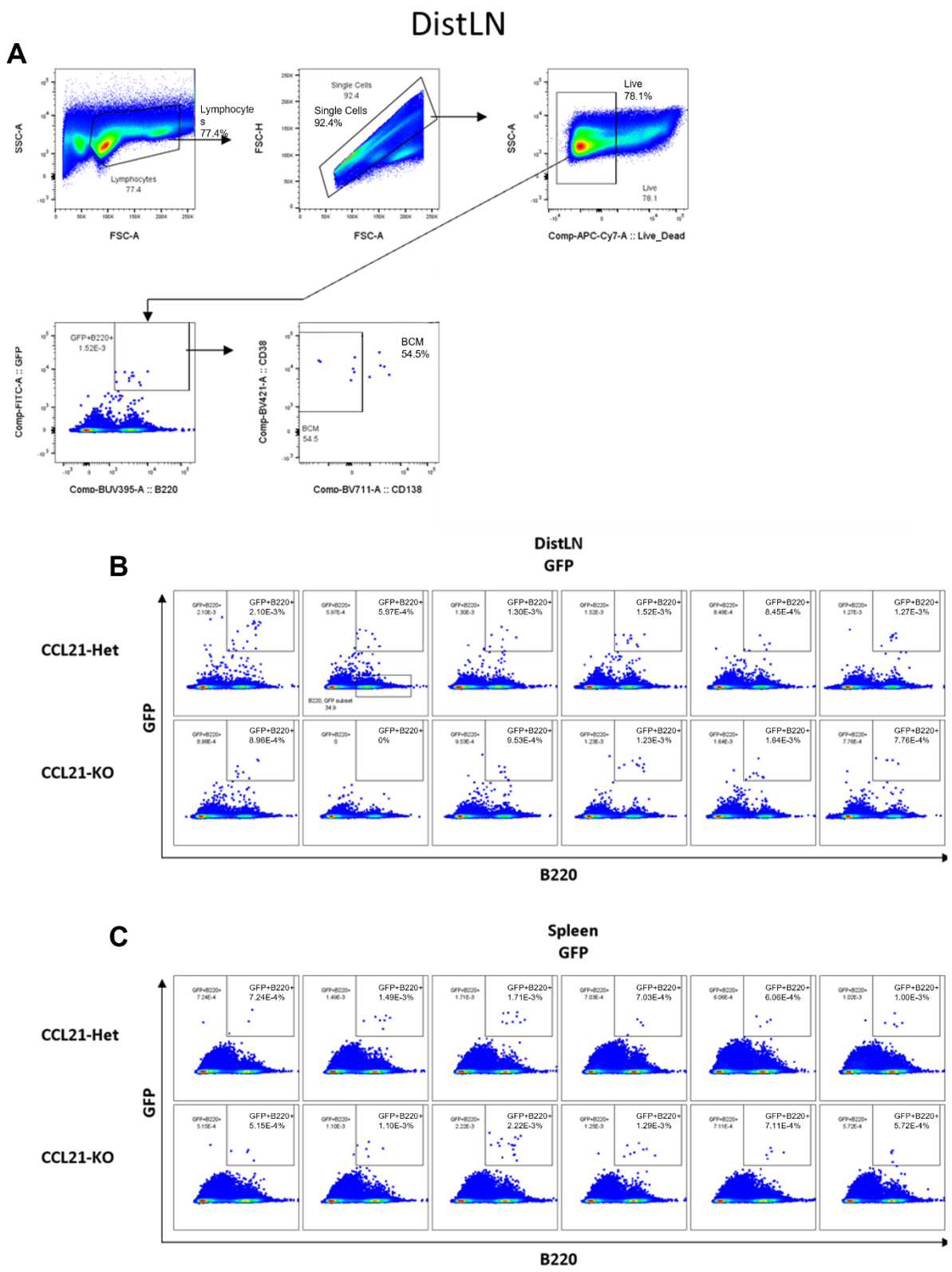


Figure 5. 15. BCM detected in WT and CCL21-KO distant lymphoid tissues by flow cytometry

(A) Gating strategy to detect BCMs in distant lymphoid tissues, presented is gating strategy for distLN from one representative experiment. Flow cytometry plots to detect GFP+B220+ cells in in (B) distLN and (C) spleen. Data are from one representative experiment.

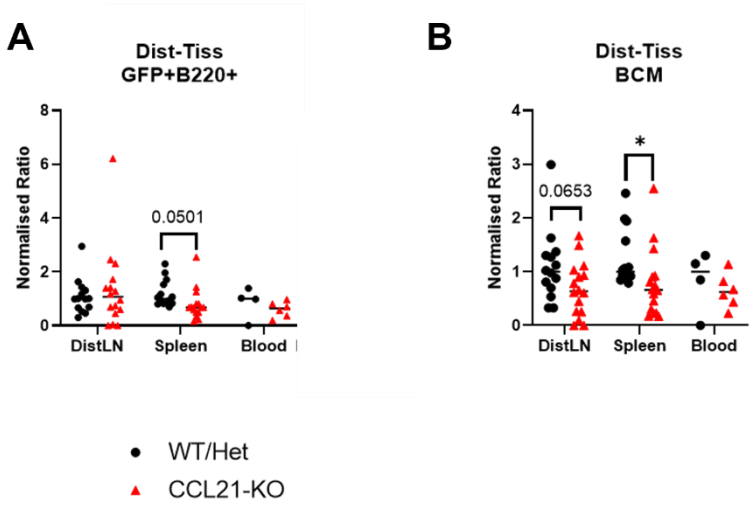


Figure 5. 16. Fewer BCM detected in CCL21-KO distant lymphoid tissues

(A) Graphical summary of GFP+B220+(CD138-) cells detected in distLN, spleen, blood and bone marrow. (B) BCMs (GFP+B220+CD138-CD38+) in distLN, spleen and blood presented as a normalised ratio from the proportion of live lymphocytes. Data presented as a normalised ratio calculated from % lymphocytes and are combined from 3 separate experiments except for blood and bone marrow (WT n=14, CCL19-KO n=16; blood WT n=4, KO n= 6). Unpaired t-test, * $p<0.05$. Symbols represent individual mice. Black circles are from WT and CCL21-heterozygous mice and red triangles are from CCL21-KO mice. Horizontal bars show means.

5.2.5 Differences in GC-derived memory B cell recall responses in drLN and distLN

The findings in the above sections suggested that CCR7 ligands may be required for the generation of BEMs and migration of BCMs to distant lymphoid tissues. In this section the secondary responses of GC-derived mBCs in re-exposed drLN and the response of GC-derived BCMs in antigen exposed naïve distant LN were investigated. During the GC response mBCs are produced, mBCs are long-lived but it is unclear whether they all become tissue resident mBCs in distinct tissues or if some mBCs spend this time in circulation (Palm and Henry, 2019). There may also be evidence of some mBCs remaining resident in the

tissue within which they were produced. A prominent example of these is the lung tissue resident mBCs and some can be observed in the LN just below the SCS (Allie et al., 2019, Moran et al., 2018). Upon secondary exposure to antigen mBCs can be activated and GCs are formed in the drLN, there was a stronger effect in the re-exposed ipsilateral LN compared with contralateral LN (Kuraoka et al., 2022). However, the mBC participation in the secondary GC is limited as the vast majority of GC B cells are derived from nBCs (Mesin et al., 2020). Additionally, upon re-exposure to antigen mBCs can differentiate into PCs (Zuccarino-Catania et al., 2014).

Recall responses were examined after priming S1PR2-Cre x Ai14dTomato mice with 10 µg NP-KLH in alum precipitate by plantar surface injection in one hind leg. Tamoxifen was administered at the peak of the primary response (days 5, 7 and 9 post-immunisation) to induce expression of dTomato among GC-derived cells. In this case tamoxifen acted as a time stamp to demarcate GC-derived cells produced in the primary response. At day 30 mice were boosted with 10 µg soluble NP-KLH on both hind legs and the response in both popliteal LNs was examined at day 34 post-immunisation (Fig. 5.17A). The booster injection increased the total lymphocytes in drLN and distLN (Fig. 5.18B). This is probably due to the induction of cell proliferation in activated B cells, or enhanced homing of lymphocytes to boosted LNs. DrLN (ipsilateral popliteal LN) and distLN (contralateral LN) of mice that received a booster injection of NP-KLH, and non-boosted controls were examined by flow cytometry (Fig. 5.17C-F). This was to detect dTomato+ mBCs, GC B cells and PCs, and quantify them as a proportion of live lymphocytes. dTomato+ mBCs were detected in non-boosted and boosted drLNs but boosting increased levels in drLN. dTomato+ mBCs were

present in non-boosted distLN, albeit at very low levels, conversely, boosted distLN had increased numbers of dTomato+ mBCs (Fig. 5.17G).

Booster immunisation induced no significant change in overall frequency of dTomato+ GC B cells, but markedly increased dTomato+ GC B cells in distLN compared with non-boosted controls (5.17H). Boosted drLNs had raised dTomato+ PCs after booster immunisation (Fig. 5.17I), this would likely be a result of mBC reactivation as mBCs readily differentiate into PCs upon restimulation (Mesin et al., 2020, Zuccarino-Catania et al., 2014). There were very few detectable PCs in distLN after boosting (Fig. 5.17I). The recall response in boosted and non-boosted drLNs and distLNs was also examined by flow cytometry to quantify mBCs, GC B cells and PCs as a proportion of dTomato+ cells, to show the proportion of primary GC progeny-derived cells which includes mBC-derived cells (Fig. 5.18A-D), rather than from dTomato+ cells as a proportion of live lymphocytes described in the previous figure. In the drLN there were few mBCs detected as a proportion of dTomato+ cells, but slightly more were detected after booster immunisation, conversely, in distLN showed a major increase in mBCs as a proportion of dTomato+ cells (Fig. 5.18E). Raised dTomato+ mBCs in distLN may indicate enhanced homing of mBCs to distLN after booster immunisation or the generation of BEMs in the local GC response. Most dTomato+ cells in drLN were GC B cells in non-boosted controls and approximately 50% in boosted drLNs were GC B cells, whereas there were no dTomato+ GCs in non-boosted distLN but 40% dTomato+ cells were GC B cells in boosted distLN (Fig. 5.18F). Very few dTomato+ cells were PCs in non-boosted drLN and both boosted and non-boosted distLN, however, 20% of dTomato+ cells in boosted drLNs were PCs (Fig. 5.18G). This suggests that in distLN, while a small number of mBCs were able to

differentiate into PCs (~1%) they may not have a predisposition to do so, raising the possibility that they instead prefer a GC B cell or mBCs fate.

In the recall response of the ipsilateral drLN, dTomato+ GC B cells derived from mBCs could be observed, however this represented a minority of GC B cells. This concurs with previous observations of recall responses showing that recall GCs were mainly derived from nBCs (Mesin et al., 2020, Arpin et al., 1997, Toellner et al., 1996). The experiments presented here confirm that mBCs in drLN more readily differentiate into PCs upon re-exposure to antigen. In a previous study of the recall response there was a stronger GC reaction in ipsilateral LN compared with response in contralateral LN (Kuraoka et al., 2022), and our experiments support that observation. However, contrary to Kuraoka et al. (2022) in this present study GCs in the contralateral LN were more likely to be mBC-derived and mBCs were less able to differentiate into PCs. Previous work has shown that HIV-1-specific mBCs can participate in recall GCs in contralateral LN, but they represent a minority population of the GC compared with nBCs (Viant et al., 2020). This study used immunisation with the hapten, NP-KLH, and an S1PR2-Cre reporter instead of hemagglutinin immunisation and AID-Cre reporter used by Kuraoka et al. (2022) or HIV-1 antigen with S1PR2-Cre reporter used by Viant et al. (2020). NP-KLH is strongly immunogenic and may very effectively trigger a recall response, possibly leading to the strong recall GC response observed in contralateral LNs observed above. The S1PR2-Cre reporter (used above) demarcates GC-derived cells, whereas, the AID-Cre reporter demarcates activated B cells that have undergone Ig hypermutation or Ig class-switching, which can also be induced in the extrafollicular phase of activation before GCs appear (Roco et al., 2019, Toellner et al., 1996, Marshall et al., 2011). The AID-Cre reporter may mark a larger number of cells to become re-activated in the ipsilateral drLN leading to

the stronger memory-derived GC response seen by Kuraoka et al. (2022). As such these variances may be due to different experimental protocols. In summary, GC-derived mBCs in re-exposed drLNs were more likely to become PCs, whereas GC-derived mBCs in naïve popliteal distLNs were more likely to become GC B cells upon antigen exposure.

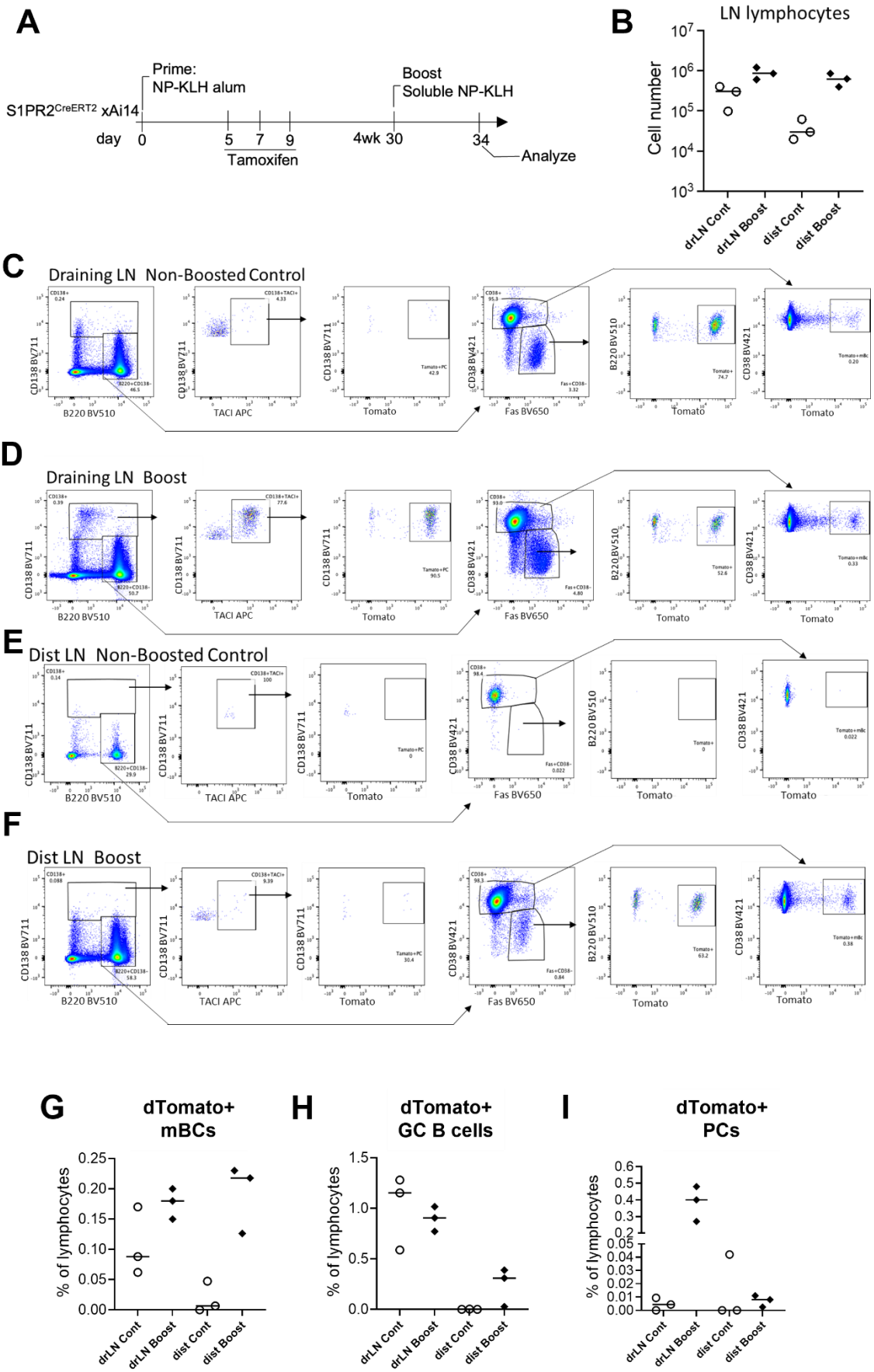

A
Prime:
NP-KLH alum
Boost
Soluble NP-KLH
S1PR2CreERT2 xAi14
day 0
5 7 9
Tamoxifen
4wk 30
34
Analyze
B
LN lymphocytes
Cell number
drLN Cont
drLN Boost
dist Cont
dist Boost
C
Draining LN Non-Boosted Control
D
Draining LN Boost
E
Dist LN Non-Boosted Control
F
Dist LN Boost
CD138 BV711
B220 BV510
TACI APC
Tomato
Fas BV650
CD38 BV421
G
dTomato+
mBCs
% of lymphocytes
H
dTomato+
GC B cells
I
dTomato+
PCs

Figure 5. 18. GC-derived mBCs become PCs in a recall response in the drLN

Experiment schematic to examine memory-derived B cell responses in S1PR2cre-Ert2 x Ai14dTomato mice with a non-boosted control group. (B) Cell numbers of total lymphocytes in drLN and distLN of mice that received boost and the no boost control group. Gating strategy to detect dTomato+ memory-derived GC B cells and PCs produced in secondary response of mice in non-boosted controls and mice that received booster injections of 10 µg NP-KLH, shown are plots for (C) non-boosted drLN, (D) boosted drLN, (E) non-boosted distLN and (F) boosted distLN.

Summary of primary GC-derived dTomato+ (G) mBCs (dTomato+B220+CD138-CD38+), (H) GC B cells (dTomato+B220+CD138-CD38-Fas+) and (I) PCs (dTomato+CD138+) in the drLN and distLN of mice that received boost or no boost control, presented as % lymphocytes. (E) Summary of dTomato+ PCs produced in the memory response in the drLN of mice that received boost or no boost control, presented as % lymphocytes. Two-tailed Mann-Whitney test between control and boosted groups within their respective tissues (drLN or distLN), unmarked if P>0.05 (n=3). Each symbol represents an individual sample. Open circles represent non-boosted controls and filled black diamonds represent mice that received a boost. Horizontal bars show means. This experiment was performed in full by Yang Zhang.

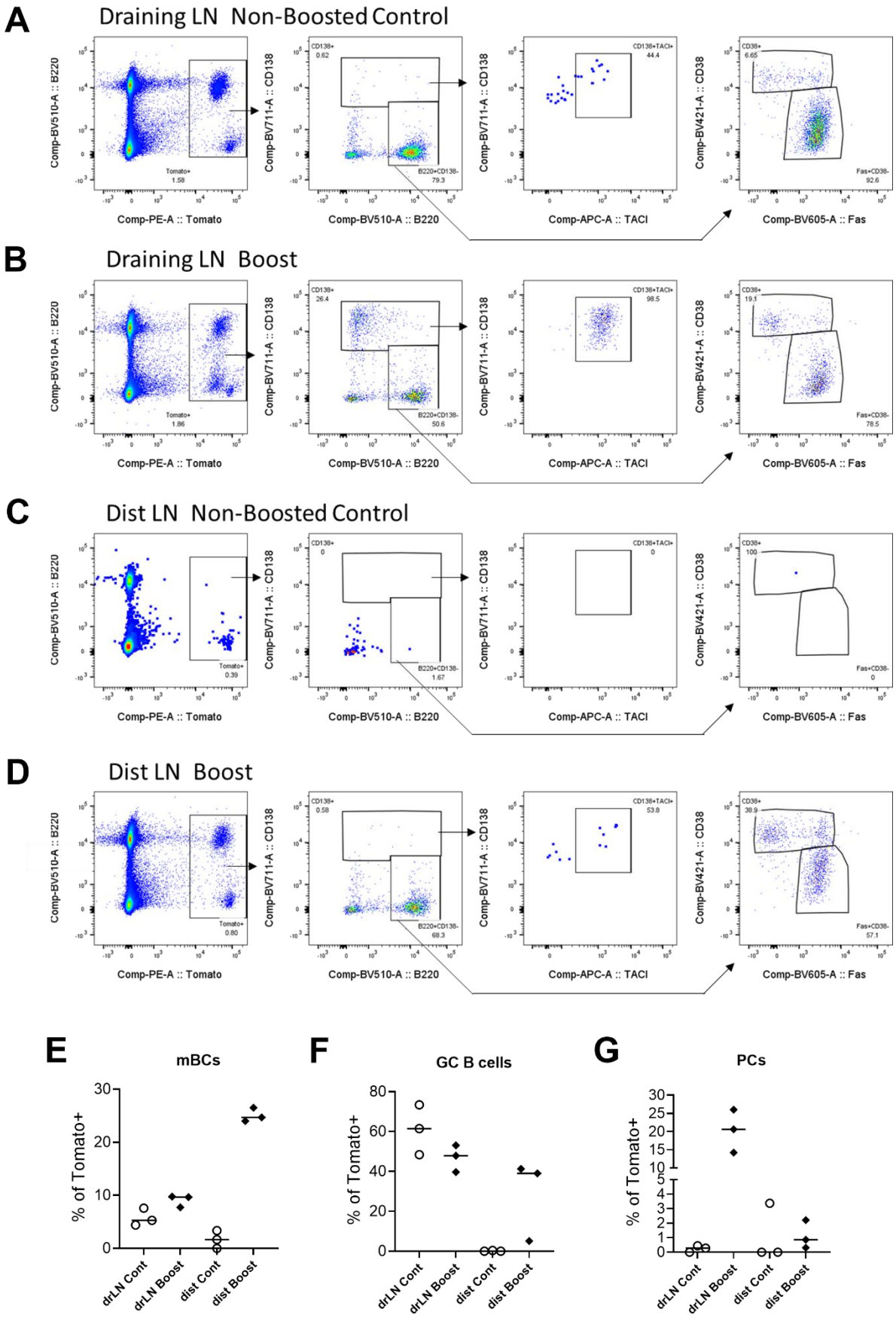

A
Draining LN Non-Boosted Control
B
Draining LN Boost
C
Dist LN Non-Boosted Control
D
Dist LN Boost
Comp-BV510-A :: B220
Comp-PE-A :: Tomato
Comp-BV711-A :: CD138
Comp-APC-A :: TACI
Comp-BV421-A :: CD38
Comp-BV605-A :: Fas
E
mBCs
F
GC B cells
G
PCs
% of Tomato+
drLN Cont
drLN Boost
dist Cont
dist Boost

Figure 5. 19. Boosting distLNs increased dTomato+ mBCs and dTomato+ GC B cells but not PCs

Gating strategy to detect dTomato+ memory-derived GC B cells and PCs produced in secondary response of mice as a proportion of all dTomato+ cells in non-boosted controls and mice that received booster injections of 10 µg NP-KLH, shown are plots for (A) non-boosted drLN, (B) boosted drLN, (C) non-boosted distLN and (D) boosted distLN. Summary of primary GC-derived dTomato+ (E) mBCs (dTomato+B220+CD138-CD38+), (F) GC B cells (dTomato+B220+CD138-CD38-Fas+) and (G) PCs (dTomato+Cd138+) in the drLN and distLN of mice that received boost or no boost control, presented as % Tomato+. (E) Summary of dTomato+ PCs produced in the memory response in the drLN of mice that received boost or no boost control, presented as % lymphocytes. Two-tailed Mann-Whitney test between control and boosted groups within their respective tissues (drLN or distLN), unmarked if P>0.05 (n=3). Each symbol represents an individual sample. Open circles represent non-boosted controls and filled black diamonds represent mice that received a boost. Horizontal bars show means. This experiment was performed in full by Yang Zhang.

5.3 Discussion

In this chapter it was revealed that CCR7 and its ligands play a role in the generation of BEMs and migration of BCMs to distant lymphoid tissues. ACKR4 is a scavenger receptor for CCR7 ligands and is involved in the maintenance of concentration gradients of these chemokines (CCL19 and CCl21) (Ulvmar et al., 2014). ACKR4-deficiency in the host had a different effect than ACKR4-deficiency in B cells. ACKR4-deficient hosts had impaired entry of BCMs to distant lymphoid tissues while in ACKR4-deficient B cells it was enhanced. In the ACKR4-deficient host the regulation of CCL19/21 gradients at the SCS was disrupted (Ulvmar et al., 2014). Intravital microscopy revealed BEM recycling between GC and SCS, but in ACKR4-KO drLNs there were more BEMs in the SCS and fewer returning towards the GC (Zhang et al., 2022). One would expect the disruption of CCL19/21 ligands would enhance egress of CCR7-expressing BEMs. However, fewer BCMs were detected in the ACKR4-deficient distLN, although there was no apparent difference in the spleen and blood. This suggested a role for

ACKR4 in the entry of BCMs into the distLN, but this is counter intuitive as BCM entry to LN is via the HEVs which do not express ACKR4. Perhaps ACKR4 plays a less direct role in entry of BCMs to LN via HEVs. BCMs in ACKR4-deficient mice might be less capable of entry due to the desensitisation of CCR7 via CCL19 (Zidar et al., 2009). This may be a consequence of increased CCL19 in the blood of ACKR4-KO mice (Werth et al., 2021).

CCL19 played a role in the entry of BCMs to the spleen. Although, CCL19-deficiency should not affect the generation of CD4+ T cells (James et al., 2021), there may be a lack of expression of CCL19 around the HEVs which may impede entry of B cells (and T cells) into the drLN. CCL19-deficiency also may cause B cells to be less able to move towards the T cell areas to receive co-stimulatory signals from CD4+ T cells. Additionally, there may be fewer CD4+ T cells present in the drLN to provide T cell help. This would mean that during initial encounter with antigen B cells are less able to become activated in a T cell-dependent manner. This may be the cause of the observation that CCL19-deficient drLN contained fewer B cells and smaller GCs.

The fewer BCMs seen in distant lymphoid tissues and blood of CCL19-KO mice may reflect reduced GC responses, however, production of BEMs in the drLN was not affected by CCL19-deficiency. The reduced numbers of BCMs seen in CCL19-deficient spleen may reflect the lack of BCMs detected in the blood of CCL19-KO hosts. An alternative explanation is that CCL19 gradients, which may be regulated by ACKR4 expressed in the splenic peri-marginal sinus (Werth et al., 2021), may not be present to facilitate entry of BCM into the spleen. As such, CCL19 may play a role in entry of lymphocytes to the spleen, however, the reduced number seen in the CCL19-KO blood may just as well explain smaller numbers in the CCL19-

deficient spleen. Although not significant, there was a trend towards fewer BCMs in CCL19-KO distLN. This may reflect that entry into distLN is through the HEVs which also produce CCL21 (Steen et al., 2014), which may mitigate the effects of CCL19-deficiency on entry into the LN. There were reduced BCMs in CCL19-KO mice, but the question remains as to where the remainder of BCMs go under CCL19-KO conditions if not the spleen, do they undergo apoptosis or migrate to other tissues?

In CCL21-deficient drLNs we expected to see the same trends detected in CCL19-deficient drLNs. This would be due to a lack of T cells available to provide T cell help as CCL21 is required for egress of thymocytes from the thymus during their development (James et al., 2021). Instead, there were increased levels of activated B cells in drLNs. This may be due to the disruption of tolerance and a reduced pool of regulatory T cells in CCL21a-deficient mice (James et al., 2021, Cowan et al., 2016), leading to inappropriate T cell help activating B cells. CCL21-deficiency also affected BCM migration to distant lymphoid tissues as there was a clear reduction in BCMs in CCL21-KO distLN and to a lesser extent to the spleen. CCL21 likely played a role in entry of BCMs to distLN via HEVs, but since CCL19 is still available in the spleen it may be more important to promote entry which may explain the lessened effect in the CCL21-deficient spleen.

A lack of ACKR4 on B cells coupled with a lack of CCL19 in the host resulted in increased BEMs in the drLN, they were able to outcompete WT and CCR7-KO BEMs, the reason for this is unclear (Fig. 5.19A). ACKR4 is weakly expressed by DZ GC B cells (Eckert et al., 2020, Garcia Ibanez, 2017). Nonetheless, AKCR4-deficient GCs have larger DZ and smaller LZs (Garcia Ibanez, 2017), perhaps this affects selection pressures of GC B cells enhancing differentiation

to BEMs. ACKR4 scavenges CCL19, CCL21 and CCL21, and may also scavenge CCL20 (Matti et al., 2020b, Matti et al., 2020a). ACKR4-mediated scavenging may help to prevent CCL19-mediated desensitisation of CCR7 (Zidar et al., 2009) and promote shallower concentration gradients at which CCL19 is more effective (Ricart et al., 2011). ACKR4 may work by generating local micro-gradients of its ligands to enhance chemokine receptor sensitivity. In the drLN B cell intrinsic CCR7-deficiency prevented competition with CCR7-sufficient and ACKR4-deficient B cells. CCR7-deficient B cells were likely less able to enter the drLN via HEVs (Okada et al., 2002), so there were fewer CCR7-deficient B cells present in the drLN. Furthermore, CCR7-deficient B cells would also less able to move to the T-B border to receive CD4+ T cell help during activation (Garside et al., 1998), resulting in the fewer activated CCR7-deficient B cells and smaller GCs observed in the drLN. CCR7-deficient BEMs may also be less able to recycle between SCS and GC due to an inability to follow CCR7 ligand gradients back to the GC (Zhang et al., 2022), although this was not investigated in this study.

In the distLN and spleen there were increased ACKR4-deficient BCMs. This may be due an inability of ACKR4-deficent BEMs in the SCS to follow CCR7 ligand gradients back to the follicle, resulting in enhanced egress and appearance in distant lymphoid tissues. Perhaps there is an inability to generate micro-gradients of CCR7 ligands and that ACKR4 may not have a strong role in preventing CCL19-mediated desensitisation of CCR7. There were fewer NP-specific CCR7-deficient BCMs in distLN and spleen. This suggests that CCR7 is important for the entry of BCMs into distLN via HEVs, as seen with other B cells (Okada et al., 2002)(Fig. 5.19B), and in the entry of BCMs to the spleen, possibly via the peri-marginal sinus (Werth et al., 2021)(Fig. 5.19C). CCR7 was also implicated in the seeding of BALTs in the lung by B cells,

and also played a role in the egress of lymphocytes and DCs from BALTs (Fleige et al., 2018). CCR7 certainly plays a role in the egress of BEMs from drLN and entry of BCMs into distant tissues, however, precise nature of these roles has yet to be elucidated in firm detail. This study showed that CCR7-KO B cells were consistently outcompeted for survival niches by WT and ACKR4-KO B cells.

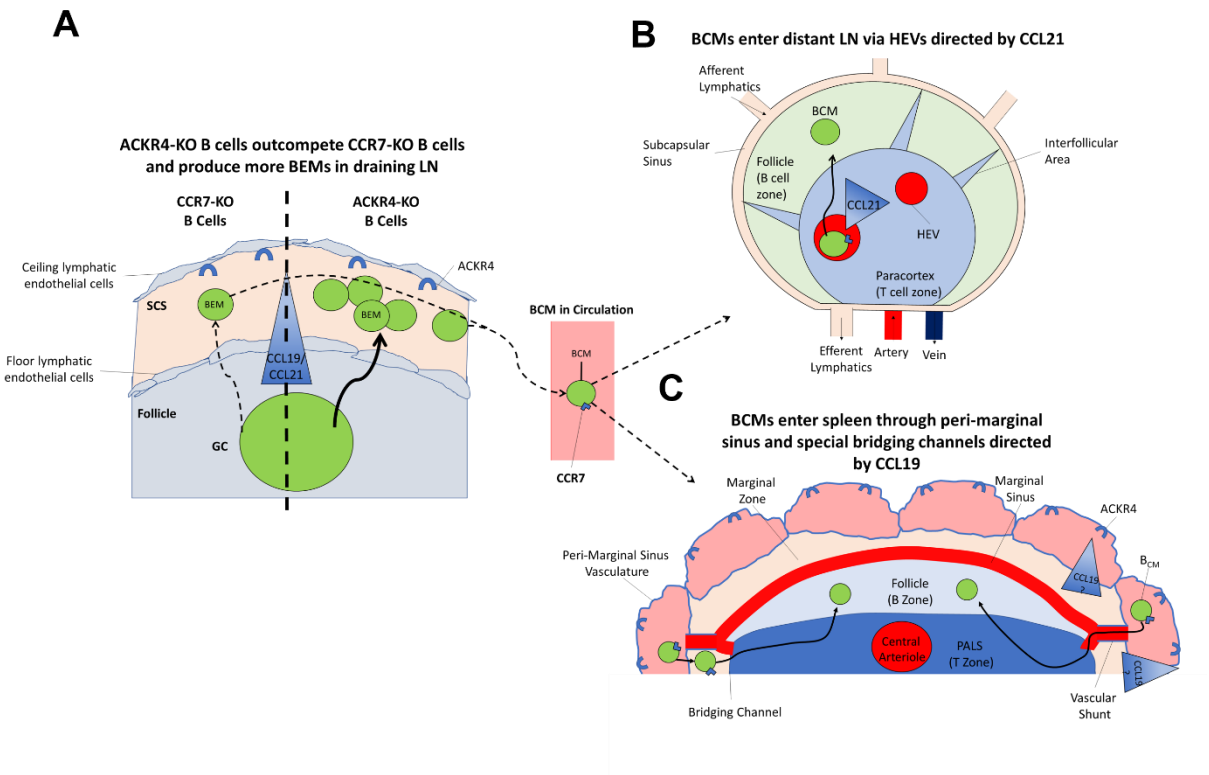


Figure 5. 20. CCR7 and its ligands direct migration of BCMs to distant lymphoid tissues

(A) Summary diagram of CCR7-KO and ACKR4-KO B cells in the drLN. ACKR4-KO B cells outcompete CCR7-KO B cells resulting in more ACKR4-KO GC B cells and the production of more BEMs. BEMs migrate to the SCS and then enter circulation to become BCMs. (B) BCMs enter distant LNs through HEVs. BCMs express CCR7 which allows them to follow CCL21 expressed by endothelial cells of the HEV and enter the LN (Okada et al., 2002). (C) BCMs may enter the spleen through the peri-marginal sinus (Werth et al., 2021). CCL19 gradients may direct entry of BCMs into the spleen.

During the recall response in the drLN fewer dTomato+ mBCs differentiated into GC B cells but more dTomato+ mBCs became PCs. This implies that mBCs in the drLN are more prone to differentiate into PCs upon re-exposure to antigen. This has been previously described as IgG1+ mBCs are prone to become PCs (Dogan et al., 2009). The clonality of GCs in a recall response has been recorded as mainly nBC-derived with only a minority of GC B cells derived from mBCs (Mesin et al., 2020).

The recall response in the distLN resulted in increased mBCs, this could be a consequence of improved homing of mBCs to the distLN during the recall response. Alternatively, there may be a generation of BEMs from a limited number of dTomato+ mBCs participating in the early GC response (Viant et al., 2020, Mesin et al., 2020). There were also more mBC-derived PCs, however, overall numbers of PCs in the distLN were very small. This suggests a difference in response between antigen experienced and naïve LNs. Similar studies have claimed that primary GC B cell outputs were more efficiently recruited into secondary GCs in pre-activated LNs leading to a stronger GC response (Kuraoka et al., 2022). They also recorded no difference in production of PCs in both ipsilateral and contralateral LNs (Kuraoka et al., 2022). Kuraoka et al. (2022) also showed that the reactivation of mBCs in the ipsilateral LN was not majorly impaired by treatment with anti-CD40L suggesting that co-stimulation from helper T cells may not be so important for re-activation. However, they did not show the effect of this on recall responses in the contralateral LN (Kuraoka et al., 2022). This present study concurs with the finding of enhanced secondary GC B cell response in pre-activated LN, however, this study found differing results in contralateral LNs as GCs were more likely to be derived from mBCs. Furthermore, we found very few PCs derived from mBCs in boosted contralateral LNs, suggesting that these mBCs were less likely to become PCs upon

activation. This may reflect differences in the immunisation protocol between both studies and that Kuraoka et al, (2022) mainly focused on responses to influenza hemagglutinin and not hapten.

This chapter shows that CCR7 and its ligands are required for the generation of BEMs and migration of BCMs to distant lymphoid tissues. An ACKR4-deficient host, in which maintenance of CCL19/21 ligands is impaired, had fewer BCMs in the distLN, showing a role for regulation of these ligand gradients in BCM entry to this tissue. CCL19-deficiency impairs GC response but does not affect production of BEMs. Counterintuitively, CCL21-deficiency enhances GC responses and generation of BEMs. Nonetheless, both CCL19 and CCL21-deficiency reduced numbers of BCMs into distant lymphoid tissues, particularly in the spleen, suggesting that they direct migration of BCMs to these tissues. In the recall response in ipsilateral popliteal LN BEMs were predisposed to differentiate into PCs. Conversely, in the contralateral popliteal LN recall response BCMs were prone to become GC B cells.

6 Conclusions

The main event investigated in this thesis is the migration of a small number of GC-derived antigen-activated memory-like B cells observed migrating between the SCS and the GC. These were defined as BEMs due to their emigration from GC LZ. The GC response of reactive LNs (drLNs) and spleen was evaluated. In the drLN response to NP-CGG and NP-KLH the peak GC reaction is at around 8 days post-immunisation. This coincides with the peak production of BEM. In the spleen using a prime-boost protocol in which mice are primed with KLH in alum, followed by immunisation against soluble NP-KLH, the peak GC response and BEM production was 5 days post-immunisation with NP-KLH.

To characterise the B cells produced during the peak of the GC reaction in drLN nBCs, GC B cells, BEMs and BCMs were isolated for RNA-sequencing. PCA and unsupervised clustering revealed relative distances of these B cell subsets from one another. BEMs and GC B cell samples clustered proximal to one another but could still be distinguished, whereas BCMs and nBCs clustered closely together and were difficult to distinguish. There was considerable distance between the BCM/nBC and BEM/GC clusters. The roles of these B cell subsets were investigated by GSEA. GC B cells and BEMs enriched for gene sets associated with cell cycle progression, BCMs were enriched for gene sets associated with immune response and antigen presentation. This confirms that GC B cells are proliferative. BEMs only recently differentiated from GC B cells, and therefore still maintained some GC characteristics, as they had recently turned off some proliferative capacity yet still retained more than nBCs and BCMs. GSEA also suggested that BCMs are better placed to respond to stimulus than the other B cell subsets as they were enriched for gene sets associated with cell signal transduction, antigen processing and antigen presentation. To examine these B cell subsets

in more detail DEGs were investigated. Among the DEGs distinguishing B cell subsets genes associated with chemotaxis were differentially expressed. GC B cells upregulate *S1pr2*, while BEMs upregulate *S1pr1*, *Ebi*2 (*Gpr183*), *Ccr6*, *Ccr7* and *Cd62l*. *Ki67* and *Aicda* were upregulated in both GC B cells and BEM, indicating cell proliferation and SHM, respectively. BEMs shared a similar gene expression profile to Ephrin B1+ S1PR2^{low} pre-memory B cells (Laidlaw et al., 2017). This suggests that the cell sorted BEM population contains many pre-memory B cells. Cell surface markers were identified to help distinguish BEMs from GC B cells and nBCs in the drLN at the peak of the GC response. These were CD24, which was upregulated in activated B cells (GC B cells and BEM), and CD55, which was downregulated in GC B cells. Co-staining allowed detection of BEMs by flow cytometry as CD24+CD55+ cells. These BEM markers were also tested in the spleen during the peak of the GC response at 5 days post-immunisation. CD24 expression by BEMs during the GC response was lower compared to BEMs in the drLN. However, CD55 still marked non-GC B cells and CCR6 could identify BEM. This shows that markers for BEMs differ between spleen and drLN, because CD24 is not as effective at detecting activated B cells in the spleen but CD55 can be used to detect non-GC B cells in both spleen and drLN. CD24 is not a necessary marker in the spleen because CCR6 distinguished BEMs from GC B cells and BCMs at all time points. A time course of BEM marker expression in drLN should be investigated in future work.

The role of S1P receptors for the migration of BEMs to the SCS was investigated by treatment of mice with S1PR inhibitors FTY720 and BAF312. S1PR1 is known to be involved in the egress of lymphocytes from LN and spleen by facilitating migration towards the SCS and marginal sinus, in their respective tissues (Zhang et al., 2016, Pereira et al., 2010, Ramos-Perez et al., 2015). We showed that S1PR1 is required for BEM migration from the GC

to the SCS in the drLN and subsequent egress from the LN via afferent lymphatics. The oxysterol receptor, EBI2, is reportedly involved in directing the migration of lymphocytes in the LN to the outer follicle and interfollicular areas (Kelly et al., 2011), so it may help direct lymphocyte migration to the SCS. There is also a role for CCR6 in the migration of lymphocytes towards the SCS of the LN (Zhang et al., 2016), which is notable as BEMs express elevated levels of CCR6. CCR6-deficient B cells were previously investigated by our lab to determine the role of CCR6 in egress of BEMs from the drLN, however, there was no obvious effect on the generation of BEMs or appearance of BCMs in spleen and distLN (Zhang et al., 2022). The return of BEMs from the SCS to the GC in the drLN was examined in ACKR4-deficient mice in which CCR7 ligand gradients near the SCS were not maintained (Ulvmar et al., 2014). CCR7 ligand gradients, maintained by ACKR4, are required for the return from the SCS to the GC in the drLN. This allows BEMs to "recycle" between the GC and the SCS (Zhang et al., 2022). BEMs in the SCS may collect antigen from SCS macrophages before returning to the GC in an ACKR4-dependent manner, here the BEMs may contribute not only collected antigen but also its genome as it may participate in the GC reaction (Fig. 6.1A). This facilitates the response to antigenic variants as shown by hapten-based antigens and Dengue envelope proteins. In ACKR4-deficient conditions the humoral response to these antigenic variants was diminished.

In previous studies, more BCMs were detected in the blood of ACKR4-deficient mice, showing that when BEMs cannot recycle back to the GC they egress the LN via afferent lymphatics (Zhang et al., 2022). Factors directing the migration of BCMs to distant lymphoid tissues were examined. In distant lymphoid tissues of ACKR4-deficient host mice there were fewer BCMs detected in distLN, but no significant difference was observed in spleen and

blood, however previous studies by our lab suggest that there are increased BCMs in blood and distLN (Zhang et al., 2022). ACKR4-deficient hosts have increased CCL19 in the blood (Werth et al., 2021). This may facilitate desensitisation of CCR7 (Zidar et al., 2009) which may impair entry to the distLN via HEVs. Investigation of CCL19-deficient hosts revealed that there were fewer BCMs in the spleen and blood, and a non-significant trend towards fewer BCMs in distLN. This suggests that CCL19 may play a role in entry of BCMs into the spleen, perhaps via the ACKR4-expressing peri-marginal sinus (Werth et al., 2021)(Fig. 6.1B). B cell intrinsic expression of ACKR4 appeared to play a role in the migration to distant lymphoid tissues as levels of BCMs from ACKR4-deficient transferred B cells in WT and CCL19-KO mice were increased in distant lymphoid tissues. This confirmed previous work in our lab which showed that ACKR4-deficient BEMs had enhanced egress from the drLN (Garcia Ibanez, 2017, Zhang et al., 2022). This may be the result of increased egress of ACKR4-deficient BEMs from the drLN SCS due to an impaired capacity to return to the follicle following CCR7 ligands. ACKR4 may generate local micro-gradients of CCR7 ligands which enhance migration or influence CCR7 sensitivity as CCL19-ligation can cause internalisation (Zidar et al., 2009), so scavenging this ligand would reduce its affects. Conversely, CCR7-deficient B cells were less able to form GCs and BEMs and had even fewer CCR7-deficient BCMs arriving in distant lymphoid tissues. This may be due to impaired production of BCMs and/or the inability to follow CCR7 ligands for entry into distant lymphoid tissues. This would be because CCR7 is required for lymphocytes to enter the LN and for B cells to migrate towards the T cell zone to receive T cell help (Okada et al., 2002, Okada et al., 2005). CCR7-deficiency resulted in fewer BEMs produced due to an impaired GC reaction and CCR7-deficient BCMs derived from these BEMs were less able to enter distant lymphoid tissues. CCL21-deficiency resulted

in fewer lymphocytes and B cells in the drLN as it is a ligand for CCR7, the CCR7-CCL21 chemokine axis is required for egress of T cells from the thymus and entry of lymphocytes into LNs via HEVs (James et al., 2021, Okada et al., 2002). CCL21-deficiency resulted in fewer GC B cells and reduced generation of BEMs in the drLN. There were fewer BCMs in CCL21-deficient distant lymphoid tissues as CCL21 may be required for entry of BCM, particularly in the distLN (Fig. 6.1C). Reduced BCMs in CCL21-deficient distLNs is likely the result of both impaired generation of BEMs, which become BCMs, and impaired entry to distant lymphoid tissues via the CCR7-CC21 axis.

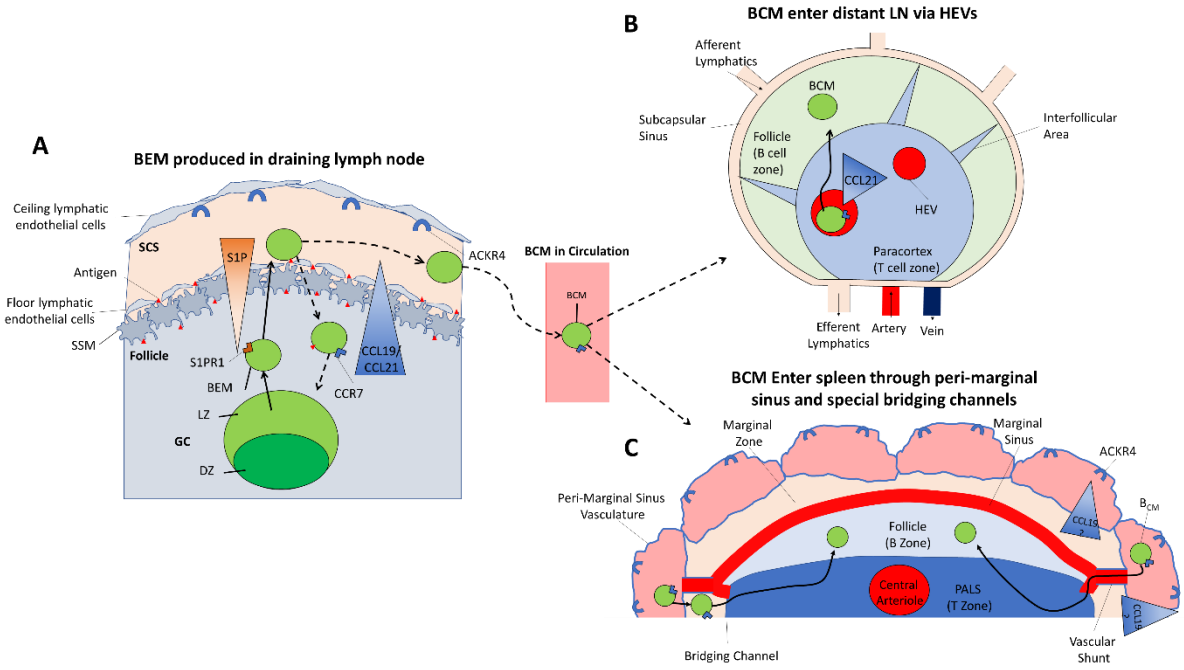


Figure 6. 1. Schematic of generation and migration of BEM in the draining LN and migration of BCM to distant LN and spleen

(A) BEMs in the drLN recycle between the B cell follicles and the SCS following S1P and CCL19-21 ligand gradients. BEMs in the SCS may egress the LN via afferent lymphatics. (B) BCMs enter distant lymph nodes through HEVs, this is directed by expression of CCL21 by endothelial cells of the HEV. (C) BCMs may enter the spleen via the peri-marginal sinus. This BCM entry may be directed by CCL19.

The role of memory B cells in secondary responses was examined using S1PR2-ERT2-Cre x ai14dTomato mice which reported GC-derived B cells including mBCs. In the recall response to antigen when the ipsilateral popliteal LN (drLN) was immunised there were fewer GC B cells derived from primary GC progeny, which includes mBCs, compared with non-boosted controls. Tamoxifen was delivered to S1PR2-ERT2-Cre mice at days 7-9 post-immunisation ensuring labelling of only primary GCs. The reactivated cells in the ipsilateral side may derive from a mixture of primary GC-derived mBCs and persistent GC B cells. There were more PCs in the ipsilateral LN after secondary exposure to antigen, these are likely to be mainly mBC-derived as mBCs readily differentiate to PCs upon re-activation and GC-derived PCs are produced later in the GC response (Mesin et al., 2020, Florian et al., 2016). When the contralateral popliteal LN (distLN) received the booster injection there were more mBCs and mBC-derived GC B cells compared with non-boosted controls. There were very few detectable PCs, but the majority of these were mBC-derived. There were also more total lymphocytes in both boosted drLN and distLN. This showed that mBCs in antigen experienced and naïve LNs responded differently to recall antigen. In experienced LNs there was a preference for differentiation to PCs whereas in naïve LNs the preference was towards GC B cell differentiation. Kuraoka and colleagues also showed that in a re-stimulated antigen-experienced LN there was a stronger GC response than in distant naïve LNs (Kuraoka et al., 2022). They also concluded that secondary GCs in re-stimulated LNs were comprised of memory B cells or persistent GC B cells which provided a head-start for the GC reaction before activated naïve B cells begin to participate in GC (Kuraoka et al., 2022). This differs from the present study as we did not directly compare GCs in re-stimulated drLN and distLN. Instead, we focused on the proportion of primary GC progeny-derived B cells within drLN or

distLN. It is likely that there was a greater number of primary GC progeny-derived GC B cells (including restimulated persistent GCs) in the re-stimulated drLN than distLN. There also appeared to be considerably more primary GC progeny-derived PCs, which are likely to derive mainly from mBCs, in re-stimulated drLN than distLN.

In a B cell response primary antigen exposure leads to activation of naive B cells specific to the antigen, these form GCs or undergo the EF pathway to produce PCs that secrete low affinity antigen-specific antibodies. mBCs are also produced which tend to have lower affinity towards antigen than the PCs emerging from GCs (Suan et al., 2017). Upon re-exposure to the same antigen there is a rapid response by B cells: GC B cells and PCs specific to the antigen are formed. In this context the GC B cells mainly consist of recently activated naive B cells with a minority derived from mBCs (Mesin et al., 2020, Kuraoka et al., 2022, Toellner et al., 1996). IgG1+ mBCs can readily differentiate into PCs after re-exposure to antigen (Dogan et al., 2009), this may be due to strong BCR signal transduction of IgG1 BCRs (Song et al., 2016). These IgG1+ mBCs may have undergone affinity maturation to develop a higher affinity to antigen which upon re-exposure promotes PC differentiation (Suan et al., 2017). Highly motile mature resting mBCs have been observed in the SCS up to 70 days post-immunisation, upon re-exposure to antigen they underwent proliferation and could differentiate into Blimp1-expressing PCs with reduced motility and Blimp1-negative PCs that retained some motility (Moran et al., 2018). This study by Moran et al., (2018) showed that these mBC-derived PCs in SCS had greater antigen affinity, but they did not test their longevity. Blimp1+ mBC-derived PCs near the SCS may be short-lived extrafollicular PCs. This suggests that mBCs may contribute to antibody feedback by becoming PCs that facilitate more rapid affinity maturation of activated B cells to produce higher affinity clones (Zhang et

al., 2013). MBC re-exposure to antigen can differ between whether re-exposed locally to or distant from the site of primary exposure (Kuraoka et al., 2022). Although distant or local re-exposure did not affect the magnitude of the antibody response, local exposures had greater levels of antigen-specific antibodies, more SHM mutations and a greater participation of mBCs and persistent GC B cells in the secondary GC. Additionally local re-exposure led to the production of more cross-reactive BCRs (Kuraoka et al., 2022) (Fig. 6.2).

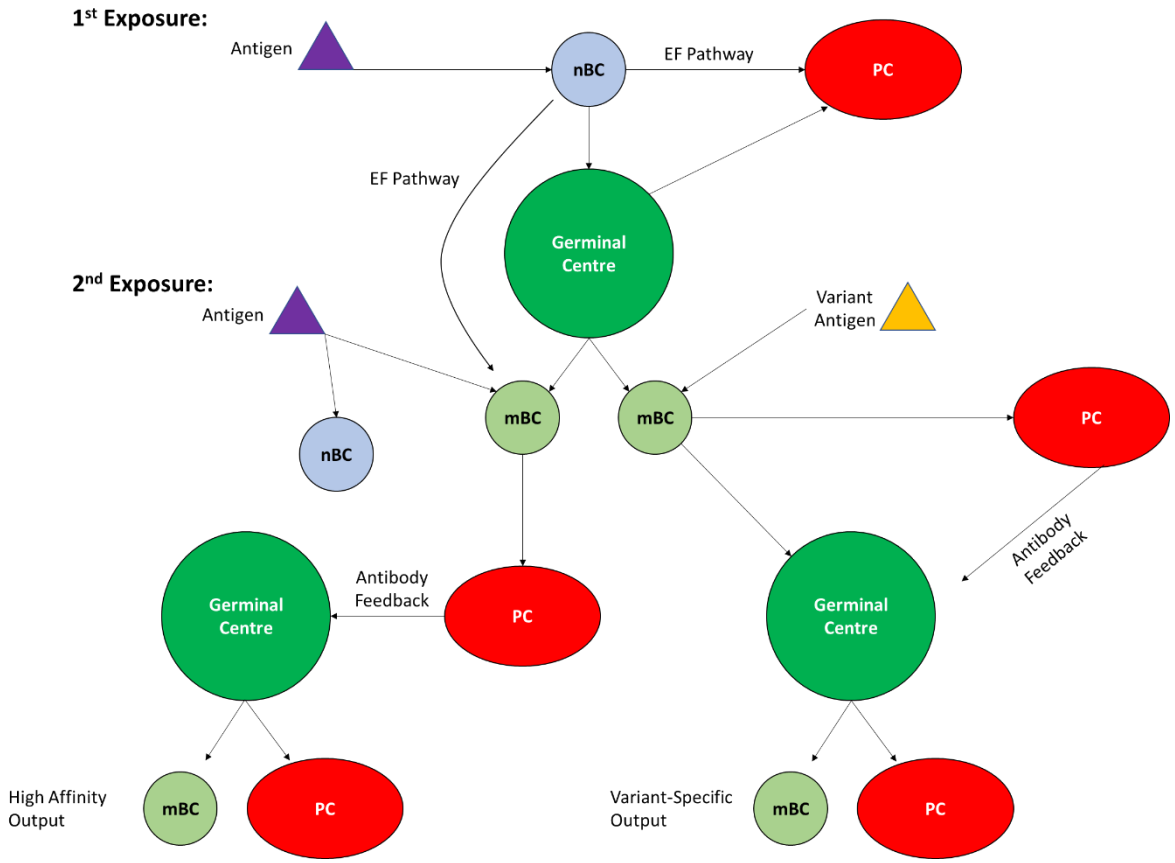


Figure 6. 2. A proposed model for the role of mBCs in secondary responses to antigen: re-exposure to primary antigen or exposure to a variant of the primary antigen

In the primary exposure to antigen nBCs recognise antigen, they can produce mBCs and PCs through the extrafollicular pathway, they can also enter the GC reaction. This primary GC produces PCs and mBCs. Upon secondary exposure to the same antigen mBCs can become re-activated and become PCs which produce antibodies that can influence the nBC-derived GC response, possibly assisting the high affinity output of the GC. Upon exposure to a variant of the primary antigen mBCs may participate in the GC response. Additionally, mBC-derived

PCs may produce variant-specific antibodies to provide antibody feedback to the GC. Leading to the generation of high affinity variant-specific GC output.

A future direction for this project may be to examine the mBC response to antigen in more detail. This would involve investigating the recall response in antigen experienced and naïve LNs and evaluating the role of variant and recall antigen in secondary GC responses in these tissues. Evaluating the role of antibody feedback by mBC-derived PCs in secondary GC responses may also be a future avenue of research. The role of BCM migration would be assessed by investigating the recall response in naïve LNs in mouse models where migration of BCMs to distant lymphoid tissues is impaired, such as in CCL19-KO hosts, CCL21-KO hosts and CCR7-KO B cells. Also models of ACKR4-KO B cells where migration of BCMs to distant lymphoid tissues is enhanced would be investigated. This would help determine whether BCMs participate in secondary GC reactions in distant lymphoid tissues and the role they might play in this. This may have an impact on vaccine design as it may provide insights into how best to deliver a response to antigenic variants, which would be relevant in response to viruses with high rates of mutation to escape variants such as influenza and HIV.

7 References

ADACHI, K. & CHIBA, K. 2007. FTY720 story. Its discovery and the following accelerated development of sphingosine 1-phosphate receptor agonists as immunomodulators based on reverse pharmacology. *Perspectives in medicinal chemistry,* 1**,** 1177391X0700100002.

ALLIE, S. R., BRADLEY, J. E., MUDUNURU, U., SCHULTZ, M. D., GRAF, B. A., LUND, F. E. & RANDALL, T. D. 2019. The establishment of resident memory B cells in the lung requires local antigen encounter. *Nat Immunol,* 20**,** 97-108.

ALLMAN, D. M., FERGUSON, S. E. & CANCRO, M. P. 1992. PERIPHERAL B-CELL MATURATION .1. IMMATURE PERIPHERAL B-CELLS IN ADULTS ARE HEAT-STABLE ANTIGEN(HI) AND EXHIBIT UNIQUE SIGNALING CHARACTERISTICS. *Journal of Immunology,* 149**,** 2533-2540.

ANDREANI, V., RAMAMOORTHY, S., FÄSSLER, R. & GROSSCHEDL, R. 2023. Integrin β1 regulates marginal zone B cell differentiation and PI3K signaling. *Journal of Experimental Medicine,* 220.

ANSEL, K. M., NGO, V. N., HYMAN, P. L., LUTHER, S. A., FÖRSTER, R., SEDGWICK, J. D., BROWNING, J. L., LIPP, M. & CYSTER, J. G. 2000. A chemokine-driven positive feedback loop organizes lymphoid follicles. *Nature,* 406**,** 309-14.

ARNON, T. I., XU, Y., LO, C., PHAM, T., AN, J., COUGHLIN, S., DORN, G. W. & CYSTER, J. G. 2011. GRK2-Dependent S1PR1 Desensitization Is Required for Lymphocytes to Overcome Their Attraction to Blood. *Science,* 333**,** 1898-1903.

ARPIN, C., BANCHEREAU, J. & LIU, Y.-J. 1997. Memory B Cells Are Biased Towards Terminal Differentiation: A Strategy That May Prevent Repertoire Freezing. *Journal of Experimental Medicine,* 186**,** 931-940.

BAGGIOLINI, M., DEWALD, B. & MOSER, B. 1997. Human chemokines: an update. *Annual review of immunology,* 15**,** 675-705.

BAIN, G., MAANDAG, E. C. R., RIELE, H. P. J. T., FEENEY, A. J., SHEEHY, A., SCHLISSEL, M., SHINTON, S. A., HARDY, R. R. & MURRE, C. 1997. Both E12 and E47 Allow Commitment to the B Cell Lineage. *Immunity,* 6**,** 145-154.

BAJENOFF, M., GLAICHENHAUS, N. & GERMAIN, R. N. 2008. Fibroblastic reticular cells guide T lymphocyte entry into and migration within the splenic T cell zone. *Journal of Immunology,* 181**,** 3947-3954.

BANKOVICH, A. J., SHIOW, L. R. & CYSTER, J. G. 2010. CD69 suppresses sphingosine 1-phosophate receptor-1 (S1P1) function through interaction with membrane helix 4. *J Biol Chem,* 285**,** 22328-37.

BANNARD, O., ROBERT, CHRISTOPHER, AN, J., NAGASAWA, T. & JASON 2013. Germinal Center Centroblasts Transition to a Centrocyte Phenotype According to a Timed Program and Depend on the Dark Zone for Effective Selection. *Immunity,* 39**,** 912-924.

BÉGUELIN, W., RIVAS, M. A., CALVO FERNÁNDEZ, M. T., TEATER, M., PURWADA, A., REDMOND, D., SHEN, H., CHALLMAN, M. F., ELEMENTO, O., SINGH, A. & MELNICK, A. M. 2017. EZH2 enables germinal centre formation through epigenetic silencing of CDKN1A and an Rb-E2F1 feedback loop. *Nature Communications,* 8.

BEISHUIZEN, C. R. L., KRAGTEN, N. A. M., BOON, L., NOLTE, M. A., VAN LIER, R. A. W. & VAN GISBERGEN, K. P. J. M. 2009. Chronic CD70-Driven Costimulation Impairs IgG Responses by Instructing T Cells to Inhibit Germinal Center B Cell Formation through FasL-Fas Interactions. *The Journal of Immunology,* 183**,** 6442-6451.

BELLOMO, A., GENTEK, R., BAJENOFF, M. & BARATIN, M. 2018. Lymph node macrophages: Scavengers, immune sentinels and trophic effectors. *Cellular Immunology,* 330**,** 168-174.

BHATTACHARYA, D., CHEAH, M. T., FRANCO, C. B., HOSEN, N., PIN, C. L., WILLIAM, C. S. & WEISSMAN, I. L. 2007. Transcriptional profiling of antigen-dependent murine B cell differentiation and memory formation. *The Journal of Immunology,* 179**,** 6808-6819.

BOTHWELL, A. L., PASKIND, M., RETH, M., IMANISHI-KARI, T., RAJEWSKY, K. & BALTIMORE, D. 1981. Heavy chain variable region contribution to the NPb family of antibodies: somatic mutation evident in a γ2a variable region. *Cell,* 24**,** 625-637.

BUTCHER, E. C. 1991. Leukocyte-endothelial cell recognition: three (or more) steps to specificity and diversity. *Cell,* 67**,** 1033-1036.

BUTT, D., CHAN, T. D., BOURNE, K., HERMES, J. R., NGUYEN, A., STATHAM, A., O'REILLY, L. A., STRASSER, A., PRICE, S., SCHOFIELD, P., CHRIST, D., BASTEN, A., MA, C. S., TANGYE, S. G., PHAN, T. G., RAO, V. K. & BRINK, R. 2015. FAS Inactivation Releases Unconventional Germinal Center B Cells that Escape Antigen Control and Drive IgE and Autoantibody Production. *Immunity,* 42**,** 890-902.

CANNONS, J. L., QI, H., LU, K. T., DUTTA, M., GOMEZ-RODRIGUEZ, J., CHENG, J., WAKELAND, E. K., GERMAIN, R. N. & SCHWARTZBERG, P. L. 2010. Optimal Germinal Center Responses Require a Multistage T Cell:B Cell Adhesion Process Involving Integrins, SLAM-Associated Protein, and CD84. *Immunity,* 32**,** 253-265.

CARRASCO, Y. R. & BATISTA, F. D. 2007. B cells acquire particulate antigen in a macrophage-rich area at the boundary between the follicle and the subcapsular sinus of the lymph node. *Immunity,* 27**,** 160-71.

CASCALHO, M., MA, A., LEE, S., MASAT, L. & WABL, M. 1996. A quasi-monoclonal mouse. *Science,* 272**,** 1649-52.

CASOLA, S., CATTORETTI, G., UYTTERSPROT, N., KORALOV, S. B., SEGAL, J., HAO, Z. Y., WAISMAN, A., EGERT, A., GHITZA, D. & RAJEWSKY, K. 2006. Tracking germinal center B cells expressing germ-line immunoglobulin gamma 1 transcripts by conditional gene targeting. *Proceedings of the National Academy of Sciences of the United States of America,* 103**,** 7396-7401.

CERUTTI, A., COLS, M. & PUGA, I. 2013. Marginal zone B cells: virtues of innate-like antibody-producing lymphocytes. *Nature Reviews Immunology,* 13**,** 118-132.

CHAN, T. D., WOOD, K., HERMES, J. R., BUTT, D., JOLLY, C. J., BASTEN, A. & BRINK, R. 2012. Elimination of Germinal-Center-Derived Self-Reactive B Cells Is Governed by the Location and Concentration of Self-Antigen. *Immunity,* 37**,** 893-904.

CHAUVEAU, A., PIRGOVA, G., CHENG, H.-W., DE MARTIN, A., ZHOU, F. Y., WIDEMAN, S., RITTSCHER, J., LUDEWIG, B. & ARNON, T. I. 2020. Visualization of T Cell Migration in the Spleen Reveals a Network of Perivascular Pathways that Guide Entry into T Zones. *Immunity,* 52**,** 794-807.e7.

CHEVRIER, S., KRATINA, T., EMSLIE, D., TARLINTON, D. M. & CORCORAN, L. M. 2017. IL4 and IL21 cooperate to induce the high Bcl6 protein level required for germinal center formation. *Immunology and Cell Biology,* 95**,** 925-932.

CHUNG, Y., TANAKA, S., CHU, F., NURIEVA, R. I., MARTINEZ, G. J., RAWAL, S., WANG, Y.-H., LIM, H., REYNOLDS, J. M. & ZHOU, X.-H. 2011. Follicular regulatory T cells expressing Foxp3 and Bcl-6 suppress germinal center reactions. *Nature medicine,* 17**,** 983-988.

CINAMON, G., ZACHARIAH, M. A., LAM, O. M., FOSS, F. W. & CYSTER, J. G. 2008. Follicular shuttling of marginal zone B cells facilitates antigen transport. *Nature Immunology,* 9**,** 54-62.

COMERFORD, I., HARATA-LEE, Y., BUNTING, M. D., GREGOR, C., KARA, E. E. & MCCOLL, S. R. 2013. A myriad of functions and complex regulation of the CCR7/CCL19/CCL21 chemokine axis in the adaptive immune system. *Cytokine & Growth Factor Reviews,* 24**,** 269-283.

COMERFORD, I., MILASTA, S., MORROW, V., MILLIGAN, G. & NIBBS, R. 2006. The chemokine receptor CCX-CKR mediates effective scavenging of CCL19 in vitro. *European Journal of Immunology,* 36**,** 1904-1916.

COMERFORD, I., NIBBS, R. J., LITCHFIELD, W., BUNTING, M., HARATA-LEE, Y., HAYLOCK-JACOBS, S., FORROW, S., KORNER, H. & MCCOLL, S. R. 2010. The atypical chemokine receptor CCX-CKR

scavenges homeostatic chemokines in circulation and tissues and suppresses Th17 responses. *Blood,* 116**,** 4130-40.
COOK, S. L. 2015. *The role of CC-chemokine receptor-like 2 in the B cell response.* University of Birmingham.
COWAN, J. E., MCCARTHY, N. I. & ANDERSON, G. 2016. CCR7 controls thymus recirculation, but not production and emigration, of Foxp3+ T cells. *Cell reports,* 14**,** 1041-1048.
CROUCH, E. E., LI, Z. Y., TAKIZAWA, M., FICHTNER-FEIGL, S., GOURZI, P., MONTANO, C., FEIGENBAUM, L., WILSON, P., JANZ, S., PAPAVASILIOU, F. N. & CASELLAS, R. 2007. Regulation of AID expression in the immune response. *Journal of Experimental Medicine,* 204**,** 1145-1156.
CUMPELIK, A., HEJA, D., HU, Y., VARANO, G., ORDIKHANI, F., ROBERTO, M. P., HE, Z., HOMANN, D., LIRA, S. A., DOMINGUEZ-SOLA, D. & HEEGER, P. S. 2021. Dynamic regulation of B cell complement signaling is integral to germinal center responses. *Nature Immunology,* 22**,** 757-768.
D'SOUZA, L., GUPTA, S. L., BAL, V., RATH, S. & GEORGE, A. 2017. CD73 expression identifies a subset of IgM(+) antigen-experienced cells with memory attributes that is T cell and CD40 signalling dependent. *Immunology,* 152**,** 602-612.
DAL PORTO, J. M., HABERMAN, A. M., SHLOMCHIK, M. J. & KELSOE, G. 1998. Antigen drives very low affinity B cells to become plasmacytes and enter germinal centers. *The Journal of Immunology,* 161**,** 5373-5381.
DE BOER, L. L., MELGRATI, S., VANES, L., O'MAY, J. B., HAYWARD, D., KÖCHL, R. & TYBULEWICZ, V. L. J. 2022. T cell migration requires ion and water influx to regulate actin polymerization. Cold Spring Harbor Laboratory.
DE VINUESA, C. G., COOK, M. C., BALL, J., DREW, M., SUNNERS, Y., CASCALHO, M., WABL, M., KLAUS, G. G. B. & MACLENNAN, I. C. M. 2000. Germinal centers without T cells. *Journal of Experimental Medicine,* 191**,** 485-493.
DEJNIRATTISAI, W., JUMNAINSONG, A., ONSIRISAKUL, N., FITTON, P., VASANAWATHANA, S., LIMPITIKUL, W., PUTTIKHUNT, C., EDWARDS, C., DUANGCHINDA, T., SUPASA, S., CHAWANSUNTATI, K., MALASIT, P., MONGKOLSAPAYA, J. & SCREATON, G. 2010. Cross-reacting antibodies enhance dengue virus infection in humans. *Science,* 328**,** 745-8.
DERUDDER, E., CADERA, E. J., VAHL, J. C., WANG, J., FOX, C. J., ZHA, S., VAN LOO, G., PASPARAKIS, M., SCHLISSEL, M. S., SCHMIDT-SUPPRIAN, M. & RAJEWSKY, K. 2009. Development of immunoglobulin lambda-chain-positive B cells, but not editing of immunoglobulin kappa-chain, depends on NF-kappa B signals. *Nature Immunology,* 10**,** 647-U118.
DING, C., CHEN, X., DASCANI, P., HU, X., BOLLI, R., ZHANG, H.-G., MCLEISH, K. R. & YAN, J. 2016. STAT3 Signaling in B Cells Is Critical for Germinal Center Maintenance and Contributes to the Pathogenesis of Murine Models of Lupus. *The Journal of Immunology,* 196**,** 4477-4486.
DOBIN, A., DAVIS, C. A., SCHLESINGER, F., DRENKOW, J., ZALESKI, C., JHA, S., BATUT, P., CHAISSON, M. & GINGERAS, T. R. 2013. STAR: ultrafast universal RNA-seq aligner. *Bioinformatics,* 29**,** 15-21.
DOGAN, I., BERTOCCI, B., VILMONT, V., DELBOS, F., MEGRET, J., STORCK, S., REYNAUD, C. A. & WEILL, J. C. 2009. Multiple layers of B cell memory with different effector functions. *Nature Immunology,* 10**,** 1292-U9.
DUNKELBERGER, J. R. & SONG, W.-C. 2010. Complement and its role in innate and adaptive immune responses. *Cell Research,* 20**,** 34-50.
DUNON, D., PIALI, L. & IMHOF, B. A. 1996. To stick or not to stick: the new leukocyte homing paradigm. *Current opinion in cell biology,* 8**,** 714-723.
EBISUNO, Y., KATAGIRI, K., KATAKAI, T., UEDA, Y., NEMOTO, T., INADA, H., NABEKURA, J., OKADA, T., KANNAGI, R. & TANAKA, T. 2010. Rap1 controls lymphocyte adhesion cascade and interstitial migration within lymph nodes in RAPL-dependent and-independent manners. *Blood, The Journal of the American Society of Hematology,* 115**,** 804-814.

EBISUNO, Y., TANAKA, T., KANEMITSU, N., KANDA, H., YAMAGUCHI, K., KAISHO, T., AKIRA, S. & MIYASAKA, M. 2003. Cutting Edge: The B Cell Chemokine CXC Chemokine Ligand 13/B Lymphocyte Chemoattractant Is Expressed in the High Endothelial Venules of Lymph Nodes and Peyer's Patches and Affects B Cell Trafficking Across High Endothelial Venules. *The Journal of Immunology,* 171**,** 1642-1646.

ECKERT, N., WERTH, K., WILLENZON, S., TAN, L. & FÖRSTER, R. 2020. B cell hyperactivation in an Ackr4 -deficient mouse strain is not caused by lack of ACKR4 expression. *Journal of Leukocyte Biology,* 107**,** 1155-1166.

ED RAINGER, G., CHIMEN, M., HARRISON, M. J., YATES, C. M., HARRISON, P., WATSON, S. P., LORDKIPANIDZÉ, M. & NASH, G. B. 2015. The role of platelets in the recruitment of leukocytes during vascular disease. *Platelets,* 26**,** 507-520.

ELLEBEDY, A. H., NACHBAGAUER, R., JACKSON, K. J. L., DAI, Y.-N., HAN, J., ALSOUSSI, W. B., DAVIS, C. W., STADLBAUER, D., ROUPHAEL, N., CHROMIKOVA, V., MCCAUSLAND, M., CHANG, C. Y., CORTESE, M., BOWER, M., CHENNAREDDY, C., SCHMITZ, A. J., ZARNITSYNA, V. I., LAI, L., RAJABHATHOR, A., KAZEMIAN, C., ANTIA, R., MULLIGAN, M. J., WARD, A. B., FREMONT, D. H., BOYD, S. D., PULENDRAN, B., KRAMMER, F. & AHMED, R. 2020. Adjuvanted H5N1 influenza vaccine enhances both cross-reactive memory B cell and strain-specific naive B cell responses in humans. *Proceedings of the National Academy of Sciences,* 117**,** 17957-17964.

ELSNER, R. A. & SHLOMCHIK, M. J. 2019. IL-12 Blocks Tfh Cell Differentiation during Salmonella Infection, thereby Contributing to Germinal Center Suppression. *Cell Reports,* 29**,** 2796-2809.e5.

ELSNER, R. A. & SHLOMCHIK, M. J. 2020. Germinal Center and Extrafollicular B Cell Responses in Vaccination, Immunity, and Autoimmunity. *Immunity,* 53**,** 1136-1150.

FEIL, R., WAGNER, J., METZGER, D. & CHAMBON, P. 1997. Regulation of Cre recombinase activity by mutated estrogen receptor ligand-binding domains. *Biochemical and biophysical research communications,* 237**,** 752-757.

FLEIGE, H., BOSNJAK, B., PERMANYER, M., RISTENPART, J., BUBKE, A., WILLENZON, S., SUTTER, G., LUTHER, S. A. & FÖRSTER, R. 2018. Manifold roles of CCR7 and its ligands in the induction and maintenance of bronchus-associated lymphoid tissue. *Cell reports,* 23**,** 783-795.

FLETCHER, A. L., ACTON, S. E. & KNOBLICH, K. 2015. Lymph node fibroblastic reticular cells in health and disease. *Nature Reviews Immunology,* 15**,** 350-361.

FLORIAN, GRISELDA, CHIKINA, M. & MARK 2016. A Temporal Switch in the Germinal Center Determines Differential Output of Memory B and Plasma Cells. *Immunity,* 44**,** 116-130.

FÖRSTER, R., DAVALOS-MISSLITZ, A. C. & ROT, A. 2008. CCR7 and its ligands: balancing immunity and tolerance. *Nature Reviews Immunology,* 8**,** 362-371.

FÖRSTER, R., SCHUBEL, A., BREITFELD, D., KREMMER, E., RENNER-MÜLLER, I., WOLF, E. & LIPP, M. 1999. CCR7 Coordinates the Primary Immune Response by Establishing Functional Microenvironments in Secondary Lymphoid Organs. *Cell,* 99**,** 23-33.

FUELLER, F. & KUBATZKY, K. F. 2008. The small GTPase RhoH is an atypical regulator of haematopoietic cells. *Cell Communication and Signaling,* 6**,** 6.

GARCIA IBANEZ, L. 2017. *Decision events in the germinal centre: the role of ACKR4.* University of Birmingham.

GARSIDE, P., INGULLI, E., MERICA, R. R., JOHNSON, J. G., NOELLE, R. J. & JENKINS, M. K. 1998. Visualization of specific B and T lymphocyte interactions in the lymph node. *Science,* 281**,** 96-9.

GATTO, D. & BRINK, R. 2013. B cell localization: regulation by EBI2 and its oxysterol ligand. *Trends in immunology,* 34**,** 336-341.

GATTO, D., WOOD, K. & BRINK, R. 2011. EBI2 Operates Independently of but in Cooperation with CXCR5 and CCR7 To Direct B Cell Migration and Organization in Follicles and the Germinal Center. *Journal of Immunology,* 187**,** 4621-4628.

GENESTIER, L., TAILLARDET, M., MONDIERE, P., GHEIT, H., BELLA, C. & DEFRANCE, T. 2007. TLR agonists selectively promote terminal plasma cell differentiation of B cell subsets specialized in thymus-independent responses. *The Journal of Immunology,* 178**,** 7779-7786.

GERGELY, P., NUESSLEIN-HILDESHEIM, B., GUERINI, D., BRINKMANN, V., TRAEBERT, M., BRUNS, C., PAN, S., GRAY, N., HINTERDING, K., COOKE, N., GROENEWEGEN, A., VITALITI, A., SING, T., LUTTRINGER, O., YANG, J., GARDIN, A., WANG, N., CRUMB JR, W., SALTZMAN, M., ROSENBERG, M. & WALLSTRÖM, E. 2012. The selective sphingosine 1-phosphate receptor modulator BAF312 redirects lymphocyte distribution and has species-specific effects on heart rate. *British Journal of Pharmacology,* 167**,** 1035-1047.

GITLIN, A. D., MAYER, C. T., OLIVEIRA, T. Y., SHULMAN, Z., JONES, M. J. K., KOREN, A. & NUSSENZWEIG, M. C. 2015. T cell help controls the speed of the cell cycle in germinal center B cells. *Science,* 349**,** 643-646.

GOOD, K. L., AVERY, D. T. & TANGYE, S. G. 2009. Resting human memory B cells are intrinsically programmed for enhanced survival and responsiveness to diverse stimuli compared to naive B cells. *The Journal of Immunology,* 182**,** 890-901.

GRASSO, C., PIERIE, C., MEBIUS, R. E. & VAN BAARSEN, L. G. M. 2021. Lymph node stromal cells: subsets and functions in health and disease. *Trends in Immunology,* 42**,** 920-936.

GREEN, J. A. & CYSTER, J. G. 2012. S1PR2 links germinal center confinement and growth regulation. *Immunological Reviews,* 247**,** 36-51.

GREEN, J. A., SUZUKI, K., CHO, B., WILLISON, L. D., PALMER, D., ALLEN, C. D. C., SCHMIDT, T. H., XU, Y., PROIA, R. L., COUGHLIN, S. R. & CYSTER, J. G. 2011. The sphingosine 1-phosphate receptor S1P(2) maintains the homeostasis of germinal center B cells and promotes niche confinement. *Nature Immunology,* 12**,** 672-U128.

GUNN, M. D., TANGEMANN, K., TAM, C., CYSTER, J. G., ROSEN, S. D. & WILLIAMS, L. T. 1998. A chemokine expressed in lymphoid high endothelial venules promotes the adhesion and chemotaxis of naive T lymphocytes. *Proceedings of the National Academy of Sciences,* 95**,** 258-263.

HABIB, T., PARK, H., TSANG, M., DE ALBORÁN, I. M., NICKS, A., WILSON, L., KNOEPFLER, P. S., ANDREWS, S., RAWLINGS, D. J., EISENMAN, R. N. & IRITANI, B. M. 2007. Myc stimulates B lymphocyte differentiation and amplifies calcium signaling. *J Cell Biol,* 179**,** 717-31.

HAESSLER, U., PISANO, M., WU, M. & SWARTZ, M. A. 2011. Dendritic cell chemotaxis in 3D under defined chemokine gradients reveals differential response to ligands CCL21 and CCL19. *Proceedings of the National Academy of Sciences,* 108**,** 5614-5619.

HAMMAD, H., VANDERKERKEN, M., POULIOT, P., DESWARTE, K., TOUSSAINT, W., VERGOTE, K., VANDERSARREN, L., JANSSENS, S., RAMOU, I., SAVVIDES, S. N., HAIGH, J. J., HENDRIKS, R., KOPF, M., CRAESSAERTS, K., DE STROOPER, B., KEARNEY, J. F., CONRAD, D. H. & LAMBRECHT, B. N. 2017. Transitional B cells commit to marginal zone B cell fate by Taok3-mediated surface expression of ADAM10. *Nature Immunology,* 18**,** 313-320.

HARDY, R. R. 2013. B-lymphocyte Development and Biology. *In:* PAUL, W. E. (ed.) *Fundamental Immunology.* 7 ed. Philadelphia: Wolters Kluwer Health.

HARDY, R. R. & HAYAKAWA, K. 2001. B Cell Development Pathways. *Annual Review of Immunology,* 19**,** 595-621.

HEALY, J. I. & GOODNOW, C. C. 1998. POSITIVE VERSUS NEGATIVE SIGNALING BY LYMPHOCYTE ANTIGEN RECEPTORS. *Annual Review of Immunology,* 16**,** 645-670.

HENG, T. S., PAINTER, M. W., ELPEK, K., LUKACS-KORNEK, V., MAUERMANN, N., TURLEY, S. J., KOLLER, D., KIM, F. S., WAGERS, A. J. & ASINOVSKI, N. 2008. The Immunological Genome Project: networks of gene expression in immune cells. *Nature immunology,* 9**,** 1091-1094.

HERLANDS, R. A., CHRISTENSEN, S. R., SWEET, R. A., HERSHBERG, U. & SHLOMCHIK, M. J. 2008. T Cell-Independent and Toll-like Receptor-Dependent Antigen-Driven Activation of Autoreactive B Cells. *Immunity,* 29**,** 249-260.

HERTZ, M. & NEMAZEE, D. 1997. BCR Ligation Induces Receptor Editing in IgM+IgD− Bone Marrow B Cells In Vitro. *Immunity,* 6**,** 429-436.

HOLTKAMP, S. J., INCE, L. M., BARNOUD, C., SCHMITT, M. T., SINTUREL, F., PILORZ, V., PICK, R., JEMELIN, S., MÜHLSTÄDT, M., BOEHNCKE, W.-H., WEBER, J., LAUBENDER, D., PHILIPPOU-MASSIER, J., CHEN, C.-S., HOLTERMANN, L., VESTWEBER, D., SPERANDIO, M., SCHRAML, B. U., HALIN, C., DIBNER, C., OSTER, H., RENKAWITZ, J. & SCHEIERMANN, C. 2021. Circadian clocks guide dendritic cells into skin lymphatics. *Nature Immunology,* 22**,** 1375-1381.

HÖPKEN, U. E., DROESE, J., LI, J. P., JOERGENSEN, J., BREITFELD, D., ZERWES, H. G. & LIPP, M. 2004. The chemokine receptor CCR7 controls lymph node-dependent cytotoxic T cell priming in alloimmune responses. *European journal of immunology,* 34**,** 461-470.

HUANG, C., GONZALEZ, D. G., COTE, C. M., JIANG, Y., HATZI, K., TEATER, M., DAI, K., HLA, T., HABERMAN, A. M. & MELNICK, A. 2014. The BCL6 RD2 domain governs commitment of activated B cells to form germinal centers. *Cell Rep,* 8**,** 1497-508.

HWANG, I.-Y., PARK, C., HARRISON, K. & KEHRL, J. H. 2019. Biased S1PR1 signaling in B cells subverts responses to homeostatic chemokines, severely disorganizing lymphoid organ architecture. *The Journal of Immunology,* 203**,** 2401-2414.

ISE, W., FUJII, K., SHIROGUCHI, K., ITO, A., KOMETANI, K., TAKEDA, K., KAWAKAMI, E., YAMASHITA, K., SUZUKI, K., OKADA, T. & KUROSAKI, T. 2018. T Follicular Helper Cell-Germinal Center B Cell Interaction Strength Regulates Entry into Plasma Cell or Recycling Germinal Center Cell Fate. *Immunity,* 48**,** 702-715.e4.

ISHII, M., KIKUTA, J., SHIMAZU, Y., MEIER-SCHELLERSHEIM, M. & GERMAIN, R. N. 2010. Chemorepulsion by blood S1P regulates osteoclast precursor mobilization and bone remodeling in vivo. *Journal of Experimental Medicine,* 207**,** 2793-2798.

JACOB, J., KASSIR, R. & KELSOE, G. 1991. In situ studies of the primary immune response to (4-hydroxy-3-nitrophenyl) acetyl. I. The architecture and dynamics of responding cell populations. *The Journal of experimental medicine,* 173**,** 1165-1175.

JACOB, J. & KELSOE, G. 1992. In situ studies of the primary immune response to (4-hydroxy-3-nitrophenyl)acetyl. II. A common clonal origin for periarteriolar lymphoid sheath-associated foci and germinal centers. *Journal of Experimental Medicine,* 176**,** 679-687.

JAMES, K. D., LEGLER, D. F., PURVANOV, V., OHIGASHI, I., TAKAHAMA, Y., PARNELL, S. M., WHITE, A. J., JENKINSON, W. E. & ANDERSON, G. 2021. Medullary stromal cells synergize their production and capture of CCL21 for T-cell emigration from neonatal mouse thymus. *Blood advances,* 5**,** 99-112.

JANČÍK, S., DRÁBEK, J., RADZIOCH, D. & HAJDÚCH, M. 2010. Clinical Relevance of KRAS in Human Cancers. *Journal of Biomedicine and Biotechnology,* 2010**,** 1-13.

JOHNSON, J. L., ROSENTHAL, R. L., KNOX, J. J., MYLES, A., NARADIKIAN, M. S., MADEJ, J., KOSTIV, M., ROSENFELD, A. M., MENG, W. & CHRISTENSEN, S. R. 2020. The transcription factor T-bet resolves memory B cell subsets with distinct tissue distributions and antibody specificities in mice and humans. *Immunity,* 52**,** 842-855. e6.

JOHNSON, L. A. & JACKSON, D. G. 2010. Inflammation-induced secretion of CCL21 in lymphatic endothelium is a key regulator of integrin-mediated dendritic cell transmigration. *International immunology,* 22**,** 839-849.

JOHNSTON, R. J., CHOI, Y. S., DIAMOND, J. A., YANG, J. A. & CROTTY, S. 2012. STAT5 is a potent negative regulator of TFH cell differentiation. *Journal of Experimental Medicine,* 209**,** 243-250.

JUNT, T., MOSEMAN, E. A., IANNACONE, M., MASSBERG, S., LANG, P. A., BOES, M., FINK, K., HENRICKSON, S. E., SHAYAKHMETOV, D. M., DI PAOLO, N. C., VAN ROOIJEN, N., MEMPEL, T. R., WHELAN, S. P. & VON ANDRIAN, U. H. 2007. Subcapsular sinus macrophages in lymph nodes clear lymph-borne viruses and present them to antiviral B cells. *Nature,* 450**,** 110-+.

KANSAS, G. S. 1996. Selectins and their ligands: current concepts and controversies.

KAWASHIMA, Y., SUGIMURA, M., HWANG, Y.-C. & KUDO, N. 1964. The lymph system in mice. *Japanese Journal of Veterinary Research,* 12**,** 69-78.
KELLER, A. M., XIAO, Y., PEPERZAK, V., NAIK, S. H. & BORST, J. 2009. Costimulatory ligand CD70 allows induction of CD8+ T-cell immunity by immature dendritic cells in a vaccination setting. *Blood,* 113**,** 5167-5175.
KELLY, L. M., PEREIRA, J. P., YI, T. S., XU, Y. & CYSTER, J. G. 2011. EBI2 Guides Serial Movements of Activated B Cells and Ligand Activity Is Detectable in Lymphoid and Nonlymphoid Tissues. *Journal of Immunology,* 187**,** 3026-3032.
KIKUCHI, Y., YASUE, T., MIYAKE, K., KIMOTO, M. & TAKATSU, K. 1995. CD38 ligation induces tyrosine phosphorylation of Bruton tyrosine kinase and enhanced expression of interleukin 5-receptor alpha chain: synergistic effects with interleukin 5. *Proc Natl Acad Sci U S A,* 92**,** 11814-8.
KIRSTETTER, P., THOMAS, M., DIERICH, A., KASTNER, P. & CHAN, S. 2002. Ikaros is critical for B cell differentiation and function. *European Journal of Immunology,* 32**,** 720.
KITAURA, K., YAMASHITA, H., AYABE, H., SHINI, T., MATSUTANI, T. & SUZUKI, R. 2017. Different somatic hypermutation levels among antibody subclasses disclosed by a new next-generation sequencing-based antibody repertoire analysis. *Frontiers in immunology,* 8**,** 389.
KOIKE, T., HARADA, K., HORIUCHI, S. & KITAMURA, D. 2019. The quantity of CD40 signaling determines the differentiation of B cells into functionally distinct memory cell subsets. *Elife,* 8**,** 25.
KOMETANI, K., NAKAGAWA, R., SHINNAKASU, R., KAJI, T., RYBOUCHKIN, A., MORIYAMA, S., FURUKAWA, K., KOSEKI, H., TAKEMORI, T. & KUROSAKI, T. 2013. Repression of the Transcription Factor Bach2 Contributes to Predisposition of IgG1 Memory B Cells toward Plasma Cell Differentiation. *Immunity,* 39**,** 136-147.
KOMORI, T., OKADA, A., STEWART, V. & ALT, F. W. 1993. LACK OF N-REGIONS IN ANTIGEN RECEPTOR VARIABLE REGION GENES OF TDT-DEFICIENT LYMPHOCYTES. *Science,* 261**,** 1171-1175.
KOZAI, M., KUBO, Y., KATAKAI, T., KONDO, H., KIYONARI, H., SCHAEUBLE, K., LUTHER, S. A., ISHIMARU, N., OHIGASHI, I. & TAKAHAMA, Y. 2017. Essential role of CCL21 in establishment of central self-tolerance in T cells. *J Exp Med,* 214**,** 1925-1935.
KRAUSE, R., SNYMAN, J., SHI-HSIA, H., MUEMA, D., KARIM, F., GANGA, Y., NGOEPE, A., ZUNGU, Y., GAZY, I. & BERNSTEIN, M. 2022. HIV skews the SARS-CoV-2 B cell response towards an extrafollicular maturation pathway. *Elife,* 11**,** e79924.
KÜPPERS, V., VESTWEBER, D. & SCHULTE, D. 2013. Locking endothelial junctions blocks leukocyte extravasation, but not in all tissues. *Tissue Barriers,* 1**,** e23805.
KURAOKA, M., YEH, C. H., BAJIC, G., KOTAKI, R., SONG, S. L., WINDSOR, I., HARRISON, S. C. & KELSOE, G. 2022. Recall of B cell memory depends on relative locations of prime and boost immunization. *Science Immunology,* 7**,** 11.
LAIDLAW, B. J., SCHMIDT, T. H., GREEN, J. A., ALLEN, C. D., OKADA, T. & CYSTER, J. G. 2017. The Eph-related tyrosine kinase ligand Ephrin-B1 marks germinal center and memory precursor B cells. *J Exp Med,* 214**,** 639-649.
LANDSVERK, O. J., SNIR, O., CASADO, R. B., RICHTER, L., MOLD, J. E., RÉU, P., HORNELAND, R., PAULSEN, V., YAQUB, S. & AANDAHL, E. M. 2017. Antibody-secreting plasma cells persist for decades in human intestine. *Journal of Experimental Medicine,* 214**,** 309-317.
LAWRENCE, M. B. & SPRINGER, T. A. 1991. Leukocytes roll on a selectin at physiologic flow rates: distinction from and prerequisite for adhesion through integrins. *Cell,* 65**,** 859-873.
LECHNER, M., ENGLEITNER, T., BABUSHKU, T., SCHMIDT-SUPPRIAN, M., RAD, R., STROBL, L. J. & ZIMBER-STROBL, U. 2021. Notch2-mediated plasticity between marginal zone and follicular B cells. *Nature Communications,* 12.
LEE, S. K., RIGBY, R. J., ZOTOS, D., TSAI, L. M., KAWAMOTO, S., MARSHALL, J. L., RAMISCAL, R. R., CHAN, T. D., GATTO, D., BRINK, R., YU, D., FAGARASAN, S., TARLINTON, D. M., CUNNINGHAM,

A. F. & VINUESA, C. G. 2011. B cell priming for extrafollicular antibody responses requires Bcl-6 expression by T cells. *Journal of Experimental Medicine,* 208**,** 1377-1388.
LEY, K., LAUDANNA, C., CYBULSKY, M. I. & NOURSHARGH, S. 2007. Getting to the site of inflammation: the leukocyte adhesion cascade updated. *Nature Reviews Immunology,* 7**,** 678-689.
LI, G.-M., CHIU, C., WRAMMERT, J., MCCAUSLAND, M., ANDREWS, S. F., ZHENG, N.-Y., LEE, J.-H., HUANG, M., QU, X. & EDUPUGANTI, S. 2012. Pandemic H1N1 influenza vaccine induces a recall response in humans that favors broadly cross-reactive memory B cells. *Proceedings of the National Academy of Sciences,* 109**,** 9047-9052.
LI, Y. F., OU, X. J., XU, S. L., JIN, Z. B., IWAI, N. & LAM, K. P. 2016. Loss of miR-182 affects B-cell extrafollicular antibody response. *Immunology,* 148**,** 140-149.
LINK, A., VOGT, T. K., FAVRE, S., BRITSCHGI, M. R., ACHA-ORBEA, H., HINZ, B., CYSTER, J. G. & LUTHER, S. A. 2007. Fibroblastic reticular cells in lymph nodes regulate the homeostasis of naive T cells. *Nat Immunol,* 8**,** 1255-65.
LINTERMAN, M. A., BEATON, L., YU, D., RAMISCAL, R. R., SRIVASTAVA, M., HOGAN, J. J., VERMA, N. K., SMYTH, M. J., RIGBY, R. J. & VINUESA, C. G. 2010. IL-21 acts directly on B cells to regulate Bcl-6 expression and germinal center responses. *Journal of Experimental Medicine,* 207**,** 353-363.
LINTERMAN, M. A., PIERSON, W., LEE, S. K., KALLIES, A., KAWAMOTO, S., RAYNER, T. F., SRIVASTAVA, M., DIVEKAR, D. P., BEATON, L., HOGAN, J. J., FAGARASAN, S., LISTON, A., SMITH, K. G. C. & VINUESA, C. G. 2011. Foxp3+ follicular regulatory T cells control the germinal center response. *Nature Medicine,* 17**,** 975-982.
LIU, Y., SHAW, S. K., MA, S., YANG, L., LUSCINSKAS, F. W. & PARKOS, C. A. 2004. Regulation of leukocyte transmigration: cell surface interactions and signaling events. *The Journal of Immunology,* 172**,** 7-13.
LIU, Y. J., JOSHUA, D. E., WILLIAMS, G. T., SMITH, C. A., GORDON, J. & MACLENNAN, I. C. M. 1989. Mechanism of antigen-driven selection in germinal centres. *Nature,* 342**,** 929-931.
LIU, Y. J., MASON, D. Y., JOHNSON, G. D., ABBOT, S., GREGORY, C. D., HARDIE, D. L., GORDON, J. & MACLENNAN, I. C. 1991. Germinal center cells express bcl-2 protein after activation by signals which prevent their entry into apoptosis. *European journal of immunology,* 21**,** 1905-1910.
LO, J. C., CHIN, R. K., LEE, Y., KANG, H.-S., WANG, Y., WEINSTOCK, J. V., BANKS, T., WARE, C. F., FRANZOSO, G. & FU, Y.-X. 2003. Differential regulation of CCL21 in lymphoid/nonlymphoid tissues for effectively attracting T cells to peripheral tissues. *Journal of Clinical Investigation,* 112**,** 1495-1505.
LOUIE, D. A. P. & LIAO, S. 2019. Lymph node subcapsular sinus macrophages as the frontline of lymphatic immune defense. *Frontiers in immunology,* 10**,** 347.
LOVE, M., ANDERS, S. & HUBER, M. 2014. Differential gene expression analysis based on the negative binomial distribution. *Genome Biol,* 15**,** 550.
LUO, W., WEISEL, F. & SHLOMCHIK, M. J. 2018. B Cell Receptor and CD40 Signaling Are Rewired for Synergistic Induction of the c-Myc Transcription Factor in Germinal Center B Cells. *Immunity,* 48**,** 313-+.
LUU, N., RAINGER, G. & NASH, G. B. 2000. Differential ability of exogenous chemotactic agents to disrupt transendothelial migration of flowing neutrophils. *The Journal of Immunology,* 164**,** 5961-5969.
MACKAY, C. 1995. Lymphocyte Migration: A new spin on lymphocyte homing. *Current Biology,* 5**,** 733-736.
MACLEAN, A. J., RICHMOND, N., KONEVA, L., ATTAR, M., MEDINA, C. A. P., THORNTON, E. E., GOMES, A. C., EL-TURABI, A., BACHMANN, M. F., RIJAL, P., TAN, T. K., TOWNSEND, A., SANSOM, S. N., BANNARD, O. & ARNON, T. I. 2022. Secondary influenza challenge triggers resident memory

B cell migration and rapid relocation to boost antibody secretion at infected sites. *Immunity,* 55**,** 718-733.e8.
MACLENNAN, I. C. 1994. Germinal centers. *Annu Rev Immunol,* 12**,** 117-39.
MACLENNAN, I. C. M., TOELLNER, K. M., CUNNINGHAM, A. F., SERRE, K., SZE, D. M. Y., ZUNIGA, E., COOK, M. C. & VINUESA, C. G. 2003. Extrafollicular antibody responses. *Immunological Reviews,* 194**,** 8-18.
MADISEN, L., ZWINGMAN, T. A., SUNKIN, S. M., OH, S. W., ZARIWALA, H. A., GU, H., NG, L. L., PALMITER, R. D., HAWRYLYCZ, M. J., JONES, A. R., LEIN, E. S. & ZENG, H. 2010. A robust and high-throughput Cre reporting and characterization system for the whole mouse brain. *Nat Neurosci,* 13**,** 133-40.
MAEDA, K., MEHTA, H., DREVETS, D. A. & COGGESHALL, K. M. 2010. IL-6 increases B-cell IgG production in a feed-forward proinflammatory mechanism to skew hematopoiesis and elevate myeloid production. *Blood,* 115**,** 4699-4706.
MAMANI-MATSUDA, M., COSMA, A., WELLER, S., FAILI, A., STAIB, C., GARÇON, L., HERMINE, O., BEYNE-RAUZY, O., FIESCHI, C., PERS, J.-O., ARAKELYAN, N., VARET, B., SAUVANET, A., BERGER, A., PAYE, F., ANDRIEU, J.-M., MICHEL, M., GODEAU, B., BUFFET, P., REYNAUD, C.-A. & WEILL, J.-C. 2008. The human spleen is a major reservoir for long-lived vaccinia virus–specific memory B cells. *Blood,* 111**,** 4653-4659.
MANZO, A., BUGATTI, S., CAPORALI, R., PREVO, R., JACKSON, D. G., UGUCCIONI, M., BUCKLEY, C. D., MONTECUCCO, C. & PITZALIS, C. 2007. CCL21 Expression Pattern of Human Secondary Lymphoid Organ Stroma Is Conserved in Inflammatory Lesions with Lymphoid Neogenesis. *The American Journal of Pathology,* 171**,** 1549-1562.
MARSHALL, J. L., ZHANG, Y., PALLAN, L., HSU, M. C., KHAN, M., CUNNINGHAM, A. F., MACLENNAN, I. C. M. & TOELLNER, K. M. 2011. Early B blasts acquire a capacity for Ig class switch recombination that is lost as they become plasmablasts. *European Journal of Immunology,* 41**,** 3506-3512.
MARTIN, F., OLIVER, A. M. & KEARNEY, J. F. 2001. Marginal zone and B1 B cells unite in the early response against T-independent blood-borne particulate antigens. *Immunity,* 14**,** 617-29.
MATTI, C., D'UONNOLO, G., ARTINGER, M., MELGRATI, S., SALNIKOV, A., THELEN, S., PURVANOV, V., STROBEL, T. D., SPANNAGEL, L., THELEN, M. & LEGLER, D. F. 2020a. CCL20 is a novel ligand for the scavenging atypical chemokine receptor 4. *Journal of Leukocyte Biology,* 107**,** 1137-1154.
MATTI, C., SALNIKOV, A., ARTINGER, M., D'AGOSTINO, G., KINDINGER, I., UGUCCIONI, M., THELEN, M. & LEGLER, D. F. 2020b. ACKR4 Recruits GRK3 Prior to beta-Arrestins but Can Scavenge Chemokines in the Absence of beta-Arrestins. *Frontiers in Immunology,* 11**,** 16.
MCHEIK, S., VAN EECKHOUT, N., DE POORTER, C., GALES, C., PARMENTIER, M. & SPRINGAEL, J. Y. 2019. Coexpression of CCR7 and CXCR4 During B Cell Development Controls CXCR4 Responsiveness and Bone Marrow Homing. *Frontiers in Immunology,* 10**,** 14.
MCHEYZER-WILLIAMS, M. G., NOSSAL, G. J. & LALOR, P. A. 1991. Molecular characterization of single memory B cells. *Nature,* 350**,** 502-5.
MEBIUS, R. E. & KRAAL, G. 2005. Structure and function of the spleen. *Nat Rev Immunol,* 5**,** 606-16.
MELAMED, D., BENSCHOP, R. J., CAMBIER, J. C. & NEMAZEE, D. 1998. Developmental Regulation of B Lymphocyte Immune Tolerance Compartmentalizes Clonal Selection from Receptor Selection. *Cell,* 92**,** 173-182.
MESIN, L., SCHIEPERS, A., ERSCHING, J., BARBULESCU, A., CAVAZZONI, C. B., ANGELINI, A., OKADA, T., KUROSAKI, T. & VICTORA, G. D. 2020. Restricted Clonality and Limited Germinal Center Reentry Characterize Memory B Cell Reactivation by Boosting. *Cell,* 180**,** 92-+.
MILLÁN, J., HEWLETT, L., GLYN, M., TOOMRE, D., CLARK, P. & RIDLEY, A. J. 2006. Lymphocyte transcellular migration occurs through recruitment of endothelial ICAM-1 to caveola- and F-actin-rich domains. *Nature Cell Biology,* 8**,** 113-123.

MODIS, Y., OGATA, S., CLEMENTS, D. & HARRISON, S. C. 2004. Structure of the dengue virus envelope protein after membrane fusion. *Nature,* 427**,** 313-319.

MORAN, I., NGUYEN, A., KHOO, W. H., BUTT, D., BOURNE, K., YOUNG, C., HERMES, J. R., BIRO, M., GRACIE, G., MA, C. S., MUNIER, C. M. L., LUCIANI, F., ZAUNDERS, J., PARKER, A., KELLEHER, A. D., TANGYE, S. G., CROUCHER, P. I., BRINK, R., READ, M. N. & PHAN, T. G. 2018. Memory B cells are reactivated in subcapsular proliferative foci of lymph nodes. *Nature Communications,* 9.

MOUTSOPOULOS, I., MAISCHAK, L., LAUZIKAITE, E., VASQUEZ URBINA, S. A., WILLIAMS, E. C., DROST, H.-G. & MOHORIANU, I. I. 2021. noisyR: enhancing biological signal in sequencing datasets by characterizing random technical noise. *Nucleic acids research,* 49**,** e83-e83.

MUEHLINGHAUS, G., CIGLIANO, L., HUEHN, S., PEDDINGHAUS, A., LEYENDECKERS, H., HAUSER, A. E., HIEPE, F., RADBRUCH, A., ARCE, S. & MANZ, R. A. 2005. Regulation of CXCR3 and CXCR4 expression during terminal differentiation of memory B cells into plasma cells. *Blood,* 105**,** 3965-3971.

MUELLER, S. N. & GERMAIN, R. N. 2009. Stromal cell contributions to the homeostasis and functionality of the immune system. *Nature Reviews Immunology,* 9**,** 618-629.

MÜLLER-WINKLER, J., MITTER, R., RAPPE, J. C., VANES, L., SCHWEIGHOFFER, E., MOHAMMADI, H., WACK, A. & TYBULEWICZ, V. L. 2021. Critical requirement for BCR, BAFF, and BAFFR in memory B cell survival. *Journal of Experimental Medicine,* 218.

MUZUMDAR, M. D., TASIC, B., MIYAMICHI, K., LI, L. & LUO, L. 2007. A global double-fluorescent Cre reporter mouse. *Genesis,* 45**,** 593-605.

NAGIRA, M., IMAI, T., HIESHIMA, K., KUSUDA, J., RIDANPAA, M., TAKAGI, S., NISHIMURA, M., KAKIZAKI, M., NOMIYAMA, H. & YOSHIE, O. 1997. Molecular cloning of a novel human CC chemokine secondary lymphoid-tissue chemokine that is a potent chemoattractant for lymphocytes and mapped to chromosome 9p13. *Journal of Biological Chemistry,* 272**,** 19518-19524.

NAKANO, H. & GUNN, M. D. 2001. Gene duplications at the chemokine locus on mouse chromosome 4: multiple strain-specific haplotypes and the deletion of secondary lymphoid-organ chemokine and EBI-1 ligand chemokine genes in the plt mutation. *The Journal of Immunology,* 166**,** 361-369.

NIBBS, R. J. & GRAHAM, G. J. 2013. Immune regulation by atypical chemokine receptors. *Nat Rev Immunol,* 13**,** 815-29.

NISHIMURA, M., MURAKAMI, A., HARA, Y. & AZUMA, T. 2011. Characterization of memory B cells responsible for affinity maturation of anti- (4-hydroxy-3-nitrophenyl)acetyl (NP) antibodies. *International Immunology,* 23**,** 271-285.

NUTT, S. L., HEAVEY, B., ROLINK, A. G. & BUSSLINGER, M. 1999. Commitment to the B-lymphoid lineage depends on the transcription factor Pax5. *Nature,* 402**,** 14-20.

O'CONNELL, AMALFITANO & ALDHAMEN 2019. SLAM Family Receptor Signaling in Viral Infections: HIV and Beyond. *Vaccines,* 7**,** 184.

O'SULLIVAN, C., SCHUBART, A., MIR, A. K. & DEV, K. K. 2016. The dual S1PR1/S1PR5 drug BAF312 (Siponimod) attenuates demyelination in organotypic slice cultures. *Journal of Neuroinflammation,* 13.

OETTINGER, M. A., SCHATZ, D. G., GORKA, C. & BALTIMORE, D. 1990. RAG-1 AND RAG-2, ADJACENT GENES THAT SYNERGISTICALLY ACTIVATE V(D)J RECOMBINATION. *Science,* 248**,** 1517-1523.

OKADA, T., MILLER, M. J., PARKER, I., KRUMMEL, M. F., NEIGHBORS, M., HARTLEY, S. B., O'GARRA, A., CAHALAN, M. D. & CYSTER, J. G. 2005. Antigen-Engaged B Cells Undergo Chemotaxis toward the T Zone and Form Motile Conjugates with Helper T Cells. *PLoS Biology,* 3**,** e150.

OKADA, T., NGO, V. N., EKLAND, E. H., FÖRSTER, R., LIPP, M., LITTMAN, D. R. & CYSTER, J. G. 2002. Chemokine requirements for B cell entry to lymph nodes and Peyer's patches. *J Exp Med,* 196**,** 65-75.

OTT, T. R., LIO, F. M., OLSHEFSKI, D., LIU, X. J., LING, N. & STRUTHERS, R. S. 2006. The N-terminal domain of CCL21 reconstitutes high affinity binding, G protein activation, and chemotactic activity, to the C-terminal domain of CCL19. *Biochemical and Biophysical Research Communications,* 348**,** 1089-1093.

OYAMA, T., HARIGAYA, K., MURADIL, A., HOZUMI, K., HABU, S., OGURO, H., IWAMA, A., MATSUNO, K., SAKAMOTO, R. & SATO, M. 2007. Mastermind-1 is required for Notch signal-dependent steps in lymphocyte development in vivo. *Proceedings of the National Academy of Sciences,* 104**,** 9764-9769.

PALM, A. E. & HENRY, C. 2019. Remembrance of Things Past: Long-Term B Cell Memory After Infection and Vaccination. *Front Immunol,* 10**,** 1787.

PARK, C., HWANG, I. Y., SINHA, R. K., KAMENYEVA, O., DAVIS, M. D. & KEHRL, J. H. 2012. Lymph node B lymphocyte trafficking is constrained by anatomy and highly dependent upon chemoattractant desensitization. *Blood,* 119**,** 978-989.

PEREIRA, J. P., KELLY, L. M. & CYSTER, J. G. 2010. Finding the right niche: B-cell migration in the early phases of T-dependent antibody responses. *International Immunology,* 22**,** 413-419.

PETER, ALISON, SCOTT & ARLENE 2014. The Coinhibitory Receptor CTLA-4 Controls B Cell Responses by Modulating T Follicular Helper, T Follicular Regulatory, and T Regulatory Cells. *Immunity,* 41**,** 1026-1039.

PHAM, T. H. M., BALUK, P., XU, Y., GRIGOROVA, I., BANKOVICH, A. J., PAPPU, R., COUGHLIN, S. R., MCDONALD, D. M., SCHWAB, S. R. & CYSTER, J. G. 2010. Lymphatic endothelial cell sphingosine kinase activity is required for lymphocyte egress and lymphatic patterning. *Journal of Experimental Medicine,* 207**,** 17-27.

PHAN, R. T. & DALLA-FAVERA, R. 2004. The BCL6 proto-oncogene suppresses p53 expression in germinal-centre B cells. *Nature,* 432**,** 635-9.

PHAN, T. G., GREEN, J. A., GRAY, E. E., XU, Y. & CYSTER, J. G. 2009. Immune complex relay by subcapsular sinus macrophages and noncognate B cells drives antibody affinity maturation. *Nature Immunology,* 10**,** 786-U153.

PILZECKER, B. & JACOBS, H. 2019. Mutating for good: DNA damage responses during somatic hypermutation. *Frontiers in immunology,* 10**,** 438.

PRIYAMVADA, L., CHO, A., ONLAMOON, N., ZHENG, N.-Y., HUANG, M., KOVALENKOV, Y., CHOKEPHAIBULKIT, K., ANGKASEKWINAI, N., PATTANAPANYASAT, K. & AHMED, R. 2016. B cell responses during secondary dengue virus infection are dominated by highly cross-reactive, memory-derived plasmablasts. *Journal of virology,* 90**,** 5574-5585.

PURTHA, W. E., TEDDER, T. F., JOHNSON, S., BHATTACHARYA, D. & DIAMOND, M. S. 2011. Memory B cells, but not long-lived plasma cells, possess antigen specificities for viral escape mutants. *J Exp Med,* 208**,** 2599-606.

R-CORE-TEAM 2022. R: A language and environment for statistical computing. Vienna, Austria: R Foundation for Statistical Computing.

RADTKE, F., FASNACHT, N. & MACDONALD, H. R. 2010. Notch signaling in the immune system. *Immunity,* 32**,** 14-27.

RAHMAN, Z. S., SHAO, W. H., KHAN, T. N., ZHEN, Y. & COHEN, P. L. 2010. Impaired apoptotic cell clearance in the germinal center by Mer-deficient tingible body macrophages leads to enhanced antibody-forming cell and germinal center responses. *J Immunol,* 185**,** 5859-68.

RAMOS-PEREZ, W. D., FANG, V., ESCALANTE-ALCALDE, D., CAMMER, M. & SCHWAB, S. R. 2015. A map of the distribution of sphingosine 1-phosphate in the spleen. *Nature Immunology,* 16**,** 1245-1252.

RAUCH, M., TUSSIWAND, R., BOSCO, N. & ROLINK, A. G. 2009. Crucial role for BAFF-BAFF-R signaling in the survival and maintenance of mature B cells. *PLoS One,* 4**,** e5456.

RETH, M., HÄMMERLING, G. & RAJEWSKY, K. 1978. Analysis of the repertoire of anti-NP antibodies in C57BL/6 mice by cell fusion. I. Characterization of antibody families in the primary and hyperimmune response. *European journal of immunology,* 8**,** 393-400.

REYA, T., O'RIORDAN, M., OKAMURA, R., DEVANEY, E., WILLERT, K., NUSSE, R. & GROSSCHEDL, R. 2000. Wnt Signaling Regulates B Lymphocyte Proliferation through a LEF-1 Dependent Mechanism. *Immunity,* 13**,** 15-24.

RICART, B. G., JOHN, B., LEE, D., HUNTER, C. A. & HAMMER, D. A. 2011. Dendritic Cells Distinguish Individual Chemokine Signals through CCR7 and CXCR4. *Journal of Immunology,* 186**,** 53-61.

RIEDEL, R., ADDO, R., FERREIRA-GOMES, M., HEINZ, G. A., HEINRICH, F., KUMMER, J., GREIFF, V., SCHULZ, D., KLAEDEN, C., CORNELIS, R., MENZEL, U., KRÖGER, S., STERVBO, U., KÖHLER, R., HAFTMANN, C., KÜHNEL, S., LEHMANN, K., MASCHMEYER, P., MCGRATH, M., NAUNDORF, S., HAHNE, S., SERCAN-ALP, Ö., SIRACUSA, F., STEFANOWSKI, J., WEBER, M., WESTENDORF, K., ZIMMERMANN, J., HAUSER, A. E., REDDY, S. T., DUREK, P., CHANG, H.-D., MASHREGHI, M.-F. & RADBRUCH, A. 2020. Discrete populations of isotype-switched memory B lymphocytes are maintained in murine spleen and bone marrow. *Nature Communications,* 11.

ROBERTO, LEE, S.-J., JASON, REBECCA, TRIVEDI, N., JASON, NAMITA, STEVEN, VIGNEAULT, F., TAMARA, MEFFRE, E., STEPHEN & MARK 2015. Salmonella Infection Drives Promiscuous B Cell Activation Followed by Extrafollicular Affinity Maturation. *Immunity,* 43**,** 120-131.

ROCO, J. A., MESIN, L., BINDER, S. C., NEFZGER, C., GONZALEZ-FIGUEROA, P., CANETE, P. F., ELLYARD, J., SHEN, Q., ROBERT, P. A., CAPPELLO, J., VOHRA, H., ZHANG, Y., NOWOSAD, C. R., SCHIEPERS, A., CORCORAN, L. M., TOELLNER, K. M., POLO, J. M., MEYER-HERMANN, M., VICTORA, G. D. & VINUESA, C. G. 2019. Class-Switch Recombination Occurs Infrequently in Germinal Centers. *Immunity,* 51**,** 337-350.e7.

RODDA, L. B., BANNARD, O., LUDEWIG, B., NAGASAWA, T. & CYSTER, J. G. 2015. Phenotypic and morphological properties of germinal center dark zone Cxcl12-expressing reticular cells. *The Journal of Immunology,* 195**,** 4781-4791.

ROLINK, A., TENBOEKEL, E., MELCHERS, F., FEARON, D. T., KROP, I. & ANDERSSON, J. 1996. A subpopulation of B220(+) cells in murine bone marrow does not express CD19 and contains natural killer cell progenitors. *Journal of Experimental Medicine,* 183**,** 187-194.

RSTUDIOTEAM 2020. RStudio: Integrated Development for R. 2022.02.02+485 ed. Boston, MA: RStudio, PBC.

RYG-CORNEJO, V., LISA, LY, A., CHRIS, TELLIER, J., DANIKA, SIMON, PELLEGRINI, M., YU, D., STEPHEN, KALLIES, A. & DIANA 2016. Severe Malaria Infections Impair Germinal Center Responses by Inhibiting T Follicular Helper Cell Differentiation. *Cell Reports,* 14**,** 68-81.

SAGE, P. T., ALVAREZ, D., GODEC, J., VON ANDRIAN, U. H. & SHARPE, A. H. 2014. Circulating T follicular regulatory and helper cells have memory-like properties. *Journal of Clinical Investigation,* 124**,** 5191-5204.

SAGE, P. T., RON-HAREL, N., JUNEJA, V. R., SEN, D. R., MALERI, S., SUNGNAK, W., KUCHROO, V. K., HAINING, W. N., CHEVRIER, N., HAIGIS, M. & SHARPE, A. H. 2016. Suppression by TFR cells leads to durable and selective inhibition of B cell effector function. *Nature Immunology,* 17**,** 1436-1446.

SCHILHAM, M. W., OOSTERWEGEL, M. A., MOERER, P., YA, J., DE BOER, P. A. J., VAN DE WETERING, M., VERBEEK, S., LAMERS, W. H., KRUISBEEK, A. M., CUMANO, A. & CLEVERS, H. 1996. Defects in cardiac outflow tract formation and pro-B-lymphocyte expansion in mice lacking Sox-4. *Nature,* 380**,** 711-714.

SCHIMMEL, L., HEEMSKERK, N. & VAN BUUL, J. D. 2017. Leukocyte transendothelial migration: a local affair. *Small GTPases,* 8**,** 1-15.

SCHLISSEL, M. S. & BALTIMORE, D. 1989. ACTIVATION OF IMMUNOGLOBULIN KAPPA GENE REARRANGEMENT CORRELATES WITH INDUCTION OF GERMLINE KAPPA GENE-TRANSCRIPTION. *Cell,* 58**,** 1001-1007.

SCHWAB, S. R. & CYSTER, J. G. 2007. Finding a way out: lymphocyte egress from lymphoid organs. *Nature Immunology,* 8**,** 1295-1301.
SHINALL, S. M., GONZALEZ-FERNANDEZ, M., NOELLE, R. J. & WALDSCHMIDT, T. J. 2000. Identification of Murine Germinal Center B Cell Subsets Defined by the Expression of Surface Isotypes and Differentiation Antigens. *The Journal of Immunology,* 164**,** 5729-5738.
SHINNAKASU, R., INOUE, T., KOMETANI, K., MORIYAMA, S., ADACHI, Y., NAKAYAMA, M., TAKAHASHI, Y., FUKUYAMA, H., OKADA, T. & KUROSAKI, T. 2016. Regulated selection of germinal-center cells into the memory B cell compartment. *Nat Immunol,* 17**,** 861-9.
SIDOROVA, E., LI-SHENG, L., DEVLIN, B., CHERNISHOVA, I. & GAVRILOVA, M. 2003. Role of different B-cell subsets in the specific and polyclonal immune response to T-independent antigens type 2. *Immunology letters,* 88**,** 37-42.
SINGH, H., MEDINA, K. L. & PONGUBALA, J. M. R. 2005. Contingent gene regulatory networks and B cell fate specification. *Proceedings of the National Academy of Sciences of the United States of America,* 102**,** 4949-4953.
SINHA, R. K., PARK, C., HWANG, I.-Y., DAVIS, M. D. & KEHRL, J. H. 2009. B lymphocytes exit lymph nodes through cortical lymphatic sinusoids by a mechanism independent of sphingosine-1-phosphate-mediated chemotaxis. *Immunity,* 30**,** 434-446.
SMITH, K. G. C. 1997. The extent of affinity maturation differs between the memory and antibody-forming cell compartments in the primary immune response. *The EMBO Journal,* 16**,** 2996-3006.
SMITH, M. & FORD, W. 1983. The recirculating lymphocyte pool of the rat: a systematic description of the migratory behaviour of recirculating lymphocytes. *Immunology,* 49**,** 83.
SOKAL, A., CHAPPERT, P., BARBA-SPAETH, G., ROESER, A., FOURATI, S., AZZAOUI, I., VANDENBERGHE, A., FERNANDEZ, I., MEOLA, A., BOUVIER-ALIAS, M., CRICKX, E., BELDI-FERCHIOU, A., HUE, S., LANGUILLE, L., MICHEL, M., BALOUL, S., NOIZAT-PIRENNE, F., LUKA, M., MÉGRET, J., MÉNAGER, M., PAWLOTSKY, J.-M., FILLATREAU, S., REY, F. A., WEILL, J.-C., REYNAUD, C.-A. & MAHÉVAS, M. 2021. Maturation and persistence of the anti-SARS-CoV-2 memory B cell response. *Cell,* 184**,** 1201-1213.e14.
SONG, H. F., NIE, X. B., BASU, S. & CERNY, J. 1998. Antibody feedback and somatic mutation in B cells: regulation of mutation by immune complexes with IgG antibody. *Immunological Reviews,* 162**,** 211-218.
SONG, J., UYTTERSPROT, N., CLASSEN, S. & WAISMAN, A. 2016. The IgG1 B-cell receptor provides survival and proliferative signals analogue to the Igα but not the Igβ co-receptor. *European Journal of Immunology,* 46**,** 1878-1886.
SPRINGER, T. A. 1994. Traffic signals for lymphocyte recirculation and leukocyte emigration: the multistep paradigm. *Cell,* 76**,** 301-314.
STAVNEZER, J., GUIKEMA, J. E. & SCHRADER, C. E. 2008. Mechanism and regulation of class switch recombination. *Annu Rev Immunol,* 26**,** 261-92.
STEEN, A., LARSEN, O., THIELE, S. & ROSENKILDE, M. M. 2014. Biased and G protien-indepedent signalling of chemokine receptors. *Frontiers in Immunology,* 5**,** 13.
STEWART, I., RADTKE, D., PHILLIPS, B., MCGOWAN, S. J. & BANNARD, O. 2018. Germinal Center B Cells Replace Their Antigen Receptors in Dark Zones and Fail Light Zone Entry when Immunoglobulin Gene Mutations are Damaging. *Immunity,* 49**,** 477-489.e7.
SUAN, D., KRAUTLER, N. J., MAAG, J. L. V., BUTT, D., BOURNE, K., HERMES, J. R., AVERY, D. T., YOUNG, C., STATHAM, A., ELLIOTT, M., DINGER, M. E., BASTEN, A., TANGYE, S. G. & BRINK, R. 2017. CCR6 Defines Memory B Cell Precursors in Mouse and Human Germinal Centers, Revealing Light-Zone Location and Predominant Low Antigen Affinity. *Immunity,* 47**,** 1142-+.
SWEET, R. A., OLS, M. L., CULLEN, J. L., MILAM, A. V., YAGITA, H. & SHLOMCHIK, M. J. 2011. Facultative role for T cells in extrafollicular Toll-like receptor-dependent autoreactive B-cell

responses in vivo. *Proceedings of the National Academy of Sciences of the United States of America,* 108**,** 7932-7937.

SZE, D. M.-Y., TOELLNER, K.-M., DE VINUESA, C. G., TAYLOR, D. R. & MACLENNAN, I. C. 2000. Intrinsic constraint on plasmablast growth and extrinsic limits of plasma cell survival. *The Journal of experimental medicine,* 192**,** 813-822.

TAKEMORI, T., KAJI, T., TAKAHASHI, Y., SHIMODA, M. & RAJEWSKY, K. 2014. Generation of memory B cells inside and outside germinal centers. *Eur J Immunol,* 44**,** 1258-64.

TANIGAKI, K., HAN, H., YAMAMOTO, N., TASHIRO, K., IKEGAWA, M., KURODA, K., SUZUKI, A., NAKANO, T. & HONJO, T. 2002. Notch–RBP-J signaling is involved in cell fate determination of marginal zone B cells. *Nature immunology,* 3**,** 443-450.

TARLINTON, D. M. & SMITH, K. G. C. 2000. Dissecting affinity maturation: a model explaining selection of antibody-forming cells and memory B cells in the germinal centre. *Immunology Today,* 21**,** 436-441.

TESSELAAR, K., XIAO, Y. L., ARENS, R., VAN SCHIJNDEL, G. M. W., SCHUURHUIS, D. H., MEBIUS, R. E., BORST, J. & VAN LIER, R. A. W. 2003. Expression of the murine CD27 ligand CD70 in vitro and in vivo. *Journal of Immunology,* 170**,** 33-40.

TOELLNER, K.-M., JENKINSON, W. E., TAYLOR, D. R., KHAN, M., SZE, D. M.-Y., SANSOM, D. M., VINUESA, C. G. & MACLENNAN, I. C. 2002. Low-level hypermutation in T cell–independent germinal centers compared with high mutation rates associated with T cell–dependent germinal centers. *The Journal of experimental medicine,* 195**,** 383-389.

TOELLNER, K.-M., LUTHER, S. A., SZE, D. M.-Y., CHOY, R. K.-W., TAYLOR, D. R., MACLENNAN, I. C. & ACHA-ORBEA, H. 1998. T helper 1 (Th1) and Th2 characteristics start to develop during T cell priming and are associated with an immediate ability to induce immunoglobulin class switching. *The Journal of experimental medicine,* 187**,** 1193-1204.

TOELLNER, K. M. 2014. Cognate interactions: Extrafollicular IL-4 drives germinal-center reactions, a new role for an old cytokine. *European Journal of Immunology,* 44**,** 1917-1920.

TOELLNER, K. M., GULBRANSON-JUDGE, A., TAYLOR, D. R., SZE, D. M. & MACLENNAN, I. C. 1996. Immunoglobulin switch transcript production in vivo related to the site and time of antigen-specific B cell activation. *Journal of Experimental Medicine,* 183**,** 2303-2312.

TOMAYKO, M. M., STEINEL, N. C., ANDERSON, S. M. & SHLOMCHIK, M. J. 2010. Cutting Edge: Hierarchy of Maturity of Murine Memory B Cell Subsets. *Journal of Immunology,* 185**,** 7146-7150.

TULL, T. J., PITCHER, M. J., GUESDON, W., SIU, J. H., LEBRERO-FERNÁNDEZ, C., ZHAO, Y., PETROV, N., HECK, S., ELLIS, R. & DHAMI, P. 2021. Human marginal zone B cell development from early T2 progenitors. *Journal of Experimental Medicine,* 218**,** e20202001.

ULVMAR, M. H., HUB, E. & ROT, A. 2011. Atypical chemokine receptors. *Exp Cell Res,* 317**,** 556-68.

ULVMAR, M. H., WERTH, K., BRAUN, A., KELAY, P., HUB, E., ELLER, K., CHAN, L., LUCAS, B., NOVITZKY-BASSO, I., NAKAMURA, K., RÜLICKE, T., NIBBS, R. J., WORBS, T., FÖRSTER, R. & ROT, A. 2014. The atypical chemokine receptor CCRL1 shapes functional CCL21 gradients in lymph nodes. *Nat Immunol,* 15**,** 623-30.

VAN DEN BROECK, W., DERORE, A. & SIMOENS, P. 2006. Anatomy and nomenclature of murine lymph nodes: Descriptive study and nomenclatory standardization in BALB/cAnNCrl mice. *Journal of immunological methods,* 312**,** 12-19.

VAN ZELM, M. C., SZCZEPAŃSKI, T., VAN DER BURG, M. & VAN DONGEN, J. J. M. 2007. Replication history of B lymphocytes reveals homeostatic proliferation and extensive antigen-induced B cell expansion. *Journal of Experimental Medicine,* 204**,** 645-655.

VASSILEVA, G., SOTO, H., ZLOTNIK, A., NAKANO, H., KAKIUCHI, T., HEDRICK, J. A. & LIRA, S. A. 1999. The Reduced Expression of 6ckine in the plt Mouse Results from the Deletion of One of Two 6ckine Genes. *Journal of Experimental Medicine,* 190**,** 1183-1188.

VIANT, C., WEYMAR, G. H. J., ESCOLANO, A., CHEN, S., HARTWEGER, H., CIPOLLA, M., GAZUMYAN, A. & NUSSENZWEIG, M. C. 2020. Antibody Affinity Shapes the Choice between Memory and Germinal Center B Cell Fates. *Cell,* 183**,** 1298-1311.e11.

VICTORA, G. D. & NUSSENZWEIG, M. C. 2012. Germinal centers. *Annu Rev Immunol,* 30**,** 429-457.

VICTORA, G. D., SCHWICKERT, T. A., FOOKSMAN, D. R., KAMPHORST, A. O., MEYER-HERMANN, M., DUSTIN, M. L. & NUSSENZWEIG, M. C. 2010. Germinal center dynamics revealed by multiphoton microscopy with a photoactivatable fluorescent reporter. *Cell,* 143**,** 592-605.

WALLACE, M. E. 1950. Locus of the Gene 'Fidget' in the House Mouse. *Nature,* 166**,** 407-407.

WEISEL, F., WELLMANN, U. & WINKLER, T. H. 2007. Autoreactive B cells get activated in extrafollicular sites. *European Journal of Immunology,* 37**,** 3330-3333.

WEISEL, F. J., MULLETT, S. J., ELSNER, R. A., MENK, A. V., TRIVEDI, N., LUO, W., WIKENHEISER, D., HAWSE, W. F., CHIKINA, M., SMITA, S., CONTER, L. J., JOACHIM, S. M., WENDELL, S. G., JURCZAK, M. J., WINKLER, T. H., DELGOFFE, G. M. & SHLOMCHIK, M. J. 2020. Germinal center B cells selectively oxidize fatty acids for energy while conducting minimal glycolysis. *Nature Immunology,* 21**,** 331-+.

WERTH, K., HUB, E., GUTJAHR, J. C., BOSJNAK, B., ZHENG, X., BUBKE, A., RUSSO, S., ROT, A. & FÖRSTER, R. 2021. Expression of ACKR4 demarcates the "peri-marginal sinus," a specialized vascular compartment of the splenic red pulp. *Cell Reports,* 36**,** 109346.

WESTERMANN, J., PUSKAS, Z. & PABST, R. 1988. Blood transit and recirculation kinetics of lymphocyte subsets in normal rats. *Scandinavian journal of immunology,* 28**,** 203-210.

WHITEHEAD, S. S., BLANEY, J. E., DURBIN, A. P. & MURPHY, B. R. 2007. Prospects for a dengue virus vaccine. *Nature Reviews Microbiology,* 5**,** 518-528.

WICKHAM, H. 2016. *ggplot2: Elegant Graphics for Data Analysis*, Springer-Verlag New York.

WOLLENBERG, I., AGUA-DOCE, A., HERNÁNDEZ, A., ALMEIDA, C., OLIVEIRA, V. G., FARO, J. & GRACA, L. 2011. Regulation of the germinal center reaction by Foxp3+ follicular regulatory T cells. *The Journal of Immunology,* 187**,** 4553-4560.

WOODFIN, A., VOISIN, M.-B. & NOURSHARGH, S. 2007. PECAM-1: A Multi-Functional Molecule in Inflammation and Vascular Biology. *Arteriosclerosis, Thrombosis, and Vascular Biology,* 27**,** 2514-2523.

WU, L., MAILLARD, I., NAKAMURA, M., PEAR, W. S. & GRIFFIN, J. D. 2007. The transcriptional coactivator Maml1 is required for Notch2-mediated marginal zone B-cell development. *Blood, The Journal of the American Society of Hematology,* 110**,** 3618-3623.

XU, S., WONG, S.-C. & LAM, K.-P. 2000. Cutting Edge: B Cell Linker Protein Is Dispensable for the Allelic Exclusion of Immunoglobulin Heavy Chain Locus But Required for the Persistence of CD5+ B Cells. *The Journal of Immunology,* 165**,** 4153-4157.

YI, T., WANG, X., LISA, AN, J., XU, Y., ANDREAS, GUSTAFSSON, J.-A., DAVID & JASON 2012. Oxysterol Gradient Generation by Lymphoid Stromal Cells Guides Activated B Cell Movement during Humoral Responses. *Immunity,* 37**,** 535-548.

YU, Q., QUINN, W. J., SALAY, T., CROWLEY, J. E., CANCRO, M. P. & SEN, J. M. 2008. Role of β-catenin in B cell development and function. *The Journal of Immunology,* 181**,** 3777-3783.

ZHANG, Y., GARCIA-IBANEZ, L., ULBRICHT, C., LOK, L. S. C., PIKE, J. A., MUELLER-WINKLER, J., DENNISON, T. W., FERDINAND, J. R., BURNETT, C. J. M., YAM-PUC, J. C., ZHANG, L., ALFARO, R. M., TAKAHAMA, Y., OHIGASHI, I., BROWN, G., KUROSAKI, T., TYBULEWICZ, V. L. J., ROT, A., HAUSER, A. E., CLATWORTHY, M. R. & TOELLNER, K.-M. 2022. Recycling of memory B cells between germinal center and lymph node subcapsular sinus supports affinity maturation to antigenic drift. *Nature Communications,* 13.

ZHANG, Y., MEYER-HERMANN, M., GEORGE, L. A., FIGGE, M. T., KHAN, M., GOODALL, M., YOUNG, S. P., REYNOLDS, A., FALCIANI, F., WAISMAN, A., NOTLEY, C. A., EHRENSTEIN, M. R., KOSCO-VILBOIS, M. & TOELLNER, K. M. 2013. Germinal center B cells govern their own fate via antibody feedback. *Journal of Experimental Medicine,* 210**,** 457-464.

ZHANG, Y., ROTH, T. L., GRAY, E. E., CHEN, H., RODDA, L. B., LIANG, Y., VENTURA, P., VILLEDA, S., CROCKER, P. R. & CYSTER, J. G. 2016. Migratory and adhesive cues controlling innate-like lymphocyte surveillance of the pathogen-exposed surface of the lymph node. *Elife,* 5.

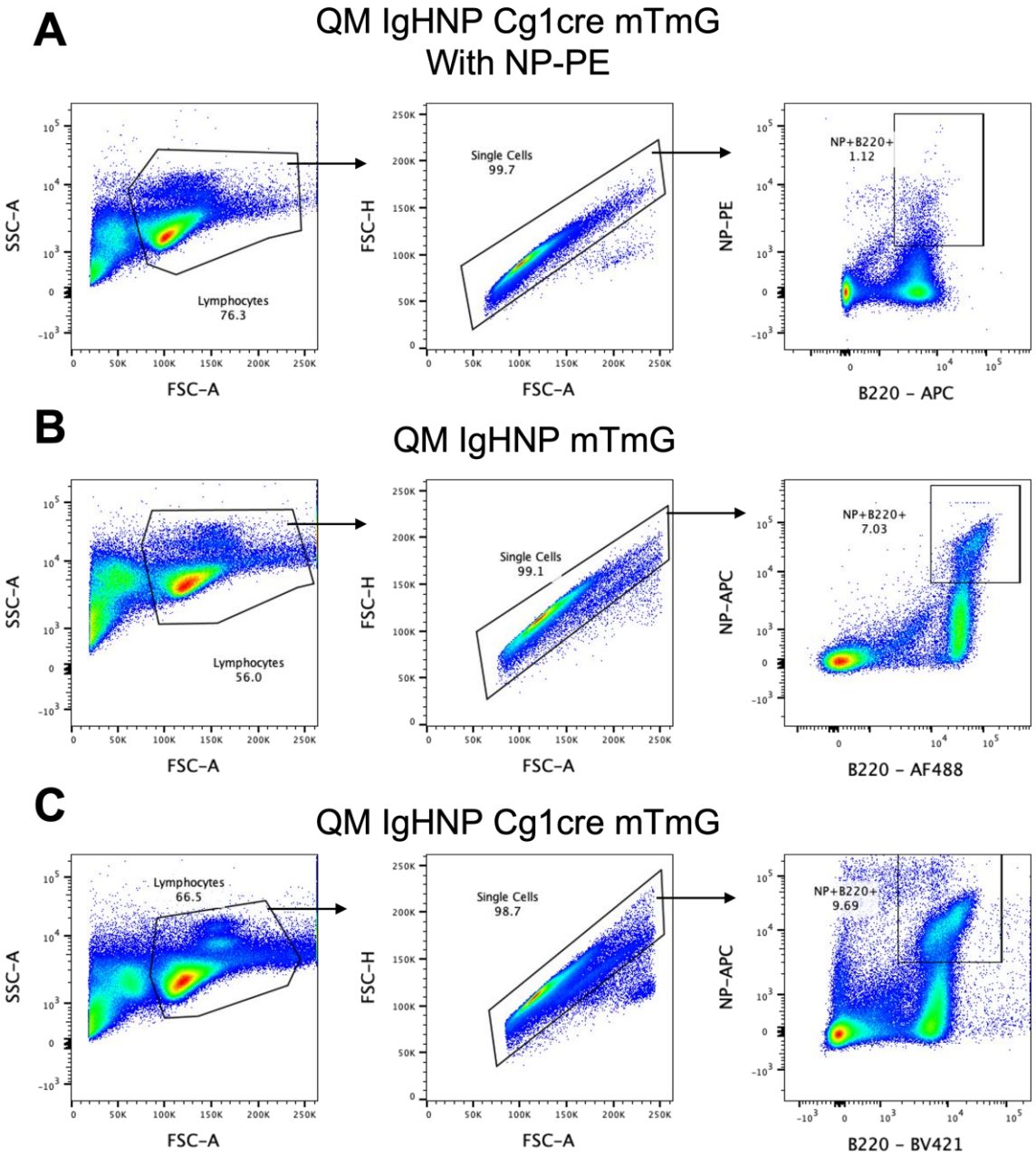
ZHANG, Y., TECH, L., GEORGE, L. A., ACS, A., DURRETT, R. E., HESS, H., WALKER, L. S. K., TARLINTON, D. M., FLETCHER, A. L., HAUSER, A. E. & TOELLNER, K. M. 2018. Plasma cell output from germinal centers is regulated by signals from Tfh and stromal cells. *Journal of Experimental Medicine,* 215**,** 1227-1243.

ZIDAR, D. A., VIOLIN, J. D., WHALEN, E. J. & LEFKOWITZ, R. J. 2009. Selective engagement of G protein coupled receptor kinases (GRKs) encodes distinct functions of biased ligands. *Proceedings of the National Academy of Sciences,* 106**,** 9649-9654.

ZLOTNIK, A. & YOSHIE, O. 2000. Chemokines. *Immunity,* 12**,** 121-127.

ZUCCARINO-CATANIA, G. V., SADANAND, S., WEISEL, F. J., TOMAYKO, M. M., MENG, H. L., KLEINSTEIN, S. H., GOOD-JACOBSON, K. L. & SHLOMCHIK, M. J. 2014. CD80 and PD-L2 define functionally distinct memory B cell subsets that are independent of antibody isotype. *Nature Immunology,* 15**,** 631-637.

Appendices



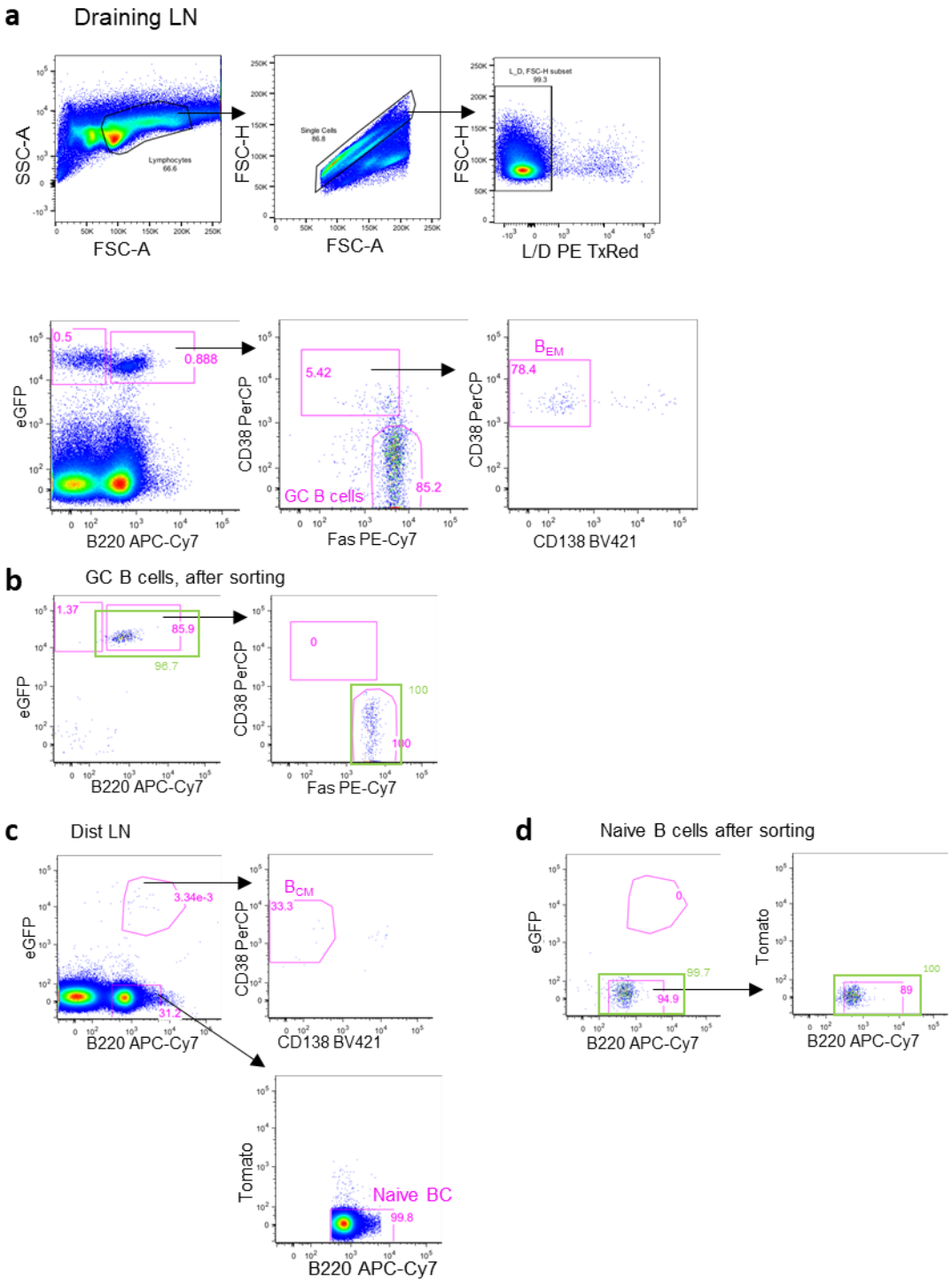
Appendix 1: Baseline input data detecting NP+B220+ splenocytes for adoptive cell transfers

Flow cytometry plots to detect NP+B220+ splenocytes from in which spleens were depleted of RBCs using ACK lysis buffer and number of lymphocytes were counted using a hemacytometer and Trypan Blue dye. The proportion of NP+B220+ cells was used to calculate the total number within the whole spleen allowing calculation of the optimal concentration of splenocytes for adoptive cell transfer.

(A) Representative flow cytometry plot of NP+B220+ splenocytes from a QM IgHNP Cg1cre mTmG mouse. NP-specific cells were detected using NP-PE. PE was detected using a blue (488 nm) laser and a 575/25 filter. dTomato was detected for compensation purposes using the yellow-green (561 nm) laser and a 630/30 filter.

(B) Representative flow cytometry plot of NP+B220+ splenocytes from a QM IgHNP mTmG mouse in which NP-binding cells were detected using NP-APC.

(C) Representative flow cytometry plot of NP+B220+ splenocytes from a QM IgHNP Cg1cre mTmG mouse in which NP-binding cells were detected using NP-APC.



Appendix 2: Gating scheme for qRT-PCR, RNA-sequencing library preparation

FACS sorted cells from popliteal lymph node in C57BL/6J mice that had received NP+ B cells from Cγ1Cre QM mTomato/mGFP, 8 d after foot injection. (A) eGFP+B220+Fas+CD38- as GC B cells, and eGFP+ B220+ CD38+Fasint CD138- as BEMs in drLN. (B) GC B cell reanalysis was run on an

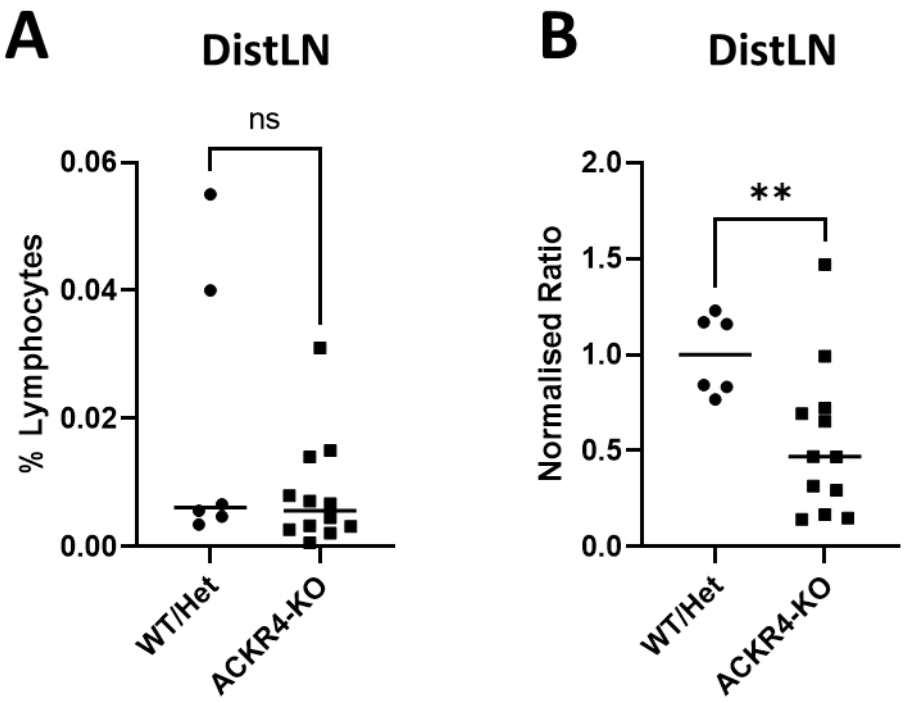
independent FACS sorter. (C) eGFP+ B220+ CD38+ Fas- CD138- as BCMs, and eGFP- Tomato- B220+ as naive B cells in distLN. (D) Naive B cells after the sorting was run on an independent FACS sorter. Pink boxes and numbers: sorting gates and population size in %. Green boxes: reanalysis gates with purities in % of parent population. This strategy was used in the study by Zhang et al., (2022).

Gene	Log2 FC	Fold Change	P-value	Max Count	Comparison	BD Biosciences	BioLegend	Miltenyi	Bio-Techne	Antibody Available
Ccr7	6.15	71.01245	8.31E-06	1082.13	BEM v GC	✓	✓	✓	✓	✓
Adam19	5.49	44.94224	3.45E-05	1433.56	BCM v GC	✗	✗	✗	✗	✗
Ighd	5	32	7.88E-06	59156.76	BEM v GC	✓	✗	✓	✓	✓
Cd38	4.34	20.25211	0.000258	4627.89	BEM v GC	✓	✓	✓	✗	✓
Dpp4	3.91	15.03236	5.55E-05	1103.99	BEM v GC	✓	✓	✓	✓	✓
S1pr1	3.82	14.12325	0.000132	2089.54	BEM v GC	✗	✗	✗	✓	✓
Nrros	3.57	11.87619	0.009546	1900.03	BEM v GC	✗	✗	✗	✗	✗
Igkc	3.53	11.55143	0.000303	20235.51	BEM v GC	✓	✗	✗	✗	✓
Cd55	2.89	7.412704	1.75E-06	12446.55	BEM v GC	✗	✓	✓	✓	✓
Ccr6	2.84	7.160201	0.02709	1759.94	BCM v GC	✓	✓	✓	✓	✓
Sdc4	1.97	3.917681	0.010308	1961.53	BEM v GC	✗	✗	✗	✗	✗
Cd47	1.78	3.434262	0.00414	6476.76	BCM v GC	✓	✗	✓	✓	✓
Cd2	1.41	2.657372	0.009211	1126.82	BCM v GC	✓	✗	✓	✓	✓
Pecam1	1.33	2.514027	5.23E-05	3227.73	BCM v GC	✓	✗	✓	✓	✓
Iglc3	1.25	2.378414	0.00491	3210.07	BEM v GC	✗	✗	✗	✗	✗
B2m	1.15	2.219139	0.049128	26138.49	BEM v GC	✓	✗	✗	✗	✓
Fcmr	1.1	2.143547	0.017578	5717.75	BEM v GC	✓	✗	✗	✓	✓
Tmem123	1.09	2.12874	0.02245	3330.73	BEM v GC	✗	✗	✗	✗	✗
Msn	0.7	1.624505	0.004534	14369.91	BCM v GC	✗	✗	✗	✗	✗
Iglc1	0.69	1.613284	3.15E-07	23390.7	BCM v GC	✗	✗	✗	✗	✗
Itga4	0.62	1.536875	0.016561	7205.81	BEM v GC	✓	✗	✓	✗	✓
H2-Aa	0.48	1.394744	0.034615	52098.69	BEM v GC	✗	✗	✗	✗	✗
Atp5a1	-0.64	-1.55833	0.01096	3064.9	BEM v GC	✗	✗	✗	✗	✗
Calr	-1.05	-2.07053	0.016742	2142.02	BEM v GC	✗	✗	✗	✓	✓
Slc3a2	-1.13	-2.18859	0.014676	1189.66	BEM v GC	✓	✓	✗	✗	✓
Slamf7	-1.16	-2.23457	3.42E-06	2649.11	BCM v GC	✓	✓	✗	✓	✓

Appendix 3: Table of BEM Markers with available antibody

Data extracted from bulk RNA sequencing data using Partek® Flow® software, version 8.0.19 Copyright ©: 2019 Partek Inc., St. Louis, MO, USA. RNA sequencing was performed on isolated cell subsets as reported in Appendix 1 and RNA-sequencing was performed as described in Chapter 2.6. Reads were aligned to mouse genome mm10 (GRCm38) mouse genome and gene specific analysis (GSA) was performed using Partek Flow to compare BEM v GC B cells and BCM v GC B cells. For each gene the comparison with the lowest absolute difference of the least square mean statistic was selected. The comparison used is presented in the "Comparison" column. Genes were filtered for adjusted P-value <0.05 and for if the gene is present in the gene ontology term "cell surface" (GO:009986). Level of expression of each gene is presented by the fold-change, log2(fold change) and Max Count.

The availability antibodies specific to the cell surface marker was checked from BD Biosciences, BioLegend, Miltenyi Biotec and R&D Systems/Bio-Techne on 24/08/2020.



Appendix 4: BCM in the distant LN after removal of samples containing GCs

WT and ACKR4-KO received adoptive cell transfers with QM Cg1-Cre mTmG splenocytes (i.v.) followed by immunisation with 20 µg NP-CGG in alum precipitate, distant LN was examined on day 8 post-immunisation as described in Figure 5.1. Graphical summaries presented in this figure show BCM in distLN with samples that contained GCs removed from the analysis. (A) With data examined as a % lymphocytes there was no significant difference between distLNs from WT and ACKR4-KO hosts. (B) When data was presented as a normalised ration of % lymphocytes there was still significantly fewer BCMs in the ACKR4-KO distLN as observed in Figure 5.1M. * P<0.05, Mann-Whitney test. Data presented are from 3 separate experiments (WT n=6, KO n=12). Symbols represent individual mice.